Stony Brook University

Metal-Thiolate Complexes as Models for Metal-Cysteine Centers in Metalloproteins: the Role of the Second Coordination Sphere Interactions

A Dissertation Presented

by

Lu Gan

to

The Graduate School

in Partial Fulfillment of the

Requirements

for the Degree of

Doctor of Philosophy

in

Chemistry

Stony Brook University

December 2010

Stony Brook University

The Graduate School

Lu Gan

We, the dissertation committee for the above candidate for the

Doctor of Philosophy degree, hereby recommend

acceptance of this dissertation.

Professor Stephen A. Koch (Dissertation Advisor)

[Professor, Department of Chemistry]

Professor Andreas Mayr (Chair of Academic Committee)

Professor, Department of Chemistry

Professor Joseph W. Lauher (Third Member of Academic Committee)

Professor, Department of Chemistry

Professor Jianfeng Jiang (Outside Member)

Assistant Professor, Department of Chemistry, Yeshiva University

This dissertation is accepted by the Graduate School

Lawrence Martin

Dean of the Graduate School

Abstract of the Dissertation

Metal-Thiolate Complexes as Models for Metal-Cysteine Centers in Metalloproteins: the Role of the Second Coordination Sphere Interactions

by

Lu Gan

Doctor of Philosophy degree

in

Chemistry

Stony Brook University

2010

As a clean energy source, hydrogen is an attractive alternative. Among all the challenges that hydrogen economy has, it is particularly important to develop new ways to generate hydrogen without hydrocarbons. In search of cheap and robust material, we are learning from nature.

Hydrogenase enzymes, which occur in a wide variety of microorganisms, catalyze the oxidization or production of molecular hydrogen ($2H^+ + 2e = H_2$,). In the case of [NiFe]-hydrogenase enzymes, the Ni is coordinated as a [Ni-$(S\text{-}Cys)_4$] center which undergoes a series of redox changes during the catalytic processes. This work is focusing

on the synthesis of model compounds that can provide some insights into the mechanism by which H_2 is consumed or produced.

To mimic the cysteine coordination in metalloezymes, we have used a variety of chelating type ligands with thiolate and phosphine donor atoms: [bis-phenyl-(5-methyl-2-thio-phenyl)phosphine] (abbreviated PS1'), [bis(5-methyl-2-thio-phenyl)phenylphosphine] (abbreviated PS2') and [tris(5-methyl-2-thio-phenyl) phosphine] (abbreviated PS3'), to create new compounds. Herein, we report the synthesis and properties of series of Ni, Pd and Pt complexes of PS2' and/or PS1'. Significantly, a biologically relevant three membered redox series of Ni(II) ↔ Ni(III) ↔ Ni(IV) have been synthesized and the oxidation state of metal center was confirmed by Ni K-edge XAS (X-ray Absorption Spectroscopy).

$[M^{II}(PS2'H)_2]$ and $[M^{II}(PS2')_2]^{2-}$ (M = Ni, Pd and Pt) are square planar complexes with $[MS_2P_2]$ coordination and two non-coordinated pendant thiols and thiolates respectively. These M(II) complexes can be oxidized to form octahedral M(IV) complexes, $[M^{IV}(PS2')_2]$, in which the pendant thiolates have coordinated to the metal. Under certain conditions the M(II) complexes are oxidized without the addition of any external oxidizing agent. The pendant thiol SH's in the $[M^{II}(PS2'H)_2]$ complexes are engaged in hydrogen bonding interactions with the metal. This interaction has been demonstrated by X-ray crystallography and by NMR studies which indicated coupling between the thiol SH and ^{195}Pt. ^{1}H and ^{31}P NMR spectroscopic studies have been used to study the thermal and photochemical induced isomerization of $[Pt^{II}(PS2'H)_2]$ and its

oxidation to $[M^{IV}(PS2')_2]$. All four possible isomers of $[Pt^{II}(PS2'H)_2]$ have been detected in the NMR (Nuclear Magnetic Resonance) spectra, and the structures of three of the isomers have been characterized by X-ray crystallography. The participation of the pendant SH protons in the oxidation of the M(II) complexes has been demonstrated. The pendant thiolate groups of the $[M^{II}(PS2')_2]^{2-}$ (M = Pd, Pt) complexes react with CH_2Cl_2 under very mild condition to give a neutral compound in which the pendant thiolates have become linked by a CH_2 group. A characteristic feature of all these studies is the reactivity of the pendant ligands. In metalloproteins, the reactivity of the metal center is determined by the residues in the second coordination sphere as well as the groups which bind directly to the metal.

In a second study, the reactivity of $[Fe^{II}\ Fe^{II}(PS3)_2]^{2-}$ species with molecular oxygen has been investigated. Using different solvent and temperature conditions, two different binuclear products have been isolated and characterized. One in which the phosphine has been oxidized to a phosphine oxide and a second product in which two atoms of oxygen have been added to a thiolate to generate a RSO_2^- ligand.

Table of Contents

List of Figures

List of Schemes

List of Tables

List of Abbreviations

acac:	Acetyl acetone or 2,4-pentadione
CV:	Cyclic voltammetry
DMF:	N,N-dimethylformaldehyde
DMSO:	dimethyl sulfoxide
EtOH:	ethanol
MeCN:	acetonitrile
MeOH:	methanol
NMR:	nuclear magnetic resonance
PS3:	tris(2-thio-phenyl) phosphine
PS3':	tris(5-methyl-2-thio-phenyl) phosphine
PS2:	bis(2-thio-phenyl)phenylphosphine
PS2:	bis(5-methyl-2-thio-phenyl)phenylphosphine
$TBABF_4$:	tetrabutylammonium tetrafluoroborate
THF:	tetrahydrofuran
UV-vis:	ultraviolet-visible

Acknowledgements

I would like to thank my research advisor Dr. Stephen A. Koch his guidance, advice, wisdom and support through my research. He taught me things beyond PhD with his great passion of chemistry and teaching. I would also like to thank Dr. Michelle Millar not only for her advising in research, but also making our group and the department feels like family.

I would like to thank Dr. Clare P. Grey and Dr. Andreas Mayr for their valuable advices and help during my research and academic meetings. I would like to thank Dr. Joseph Lauher for his suggestions and kindly agreed to be on my committee as a substitution. Especially thanks to Dr. Jim Marecek for his help and advice in the field of NMR spectroscopy.

I would like to thank all the people in Koch and Millar groups: Jianfeng, Gina, Doris, Daniel, Su'aad, Soumya, Eric, Jason, David, Anthony and Brian, for their help and understanding.

I would never forget all the nice and helpful people in the chemistry main office, especially Katherine M. Hughes and Heidi Ciolfi. They've been always helpful and ready for my questions.

Finally, I want to thank my family and my friends, my parents, my sister, my in-laws, all my friend in Stony Brook and especially my husband and my son, for their unconditional love and support.

Chapter 1

Introduction

1. Hydrogen fuel and Hydrogenases

Fossil fuel production and combustion, the current dominating energy infrastructure, is causing massive emission of greenhouse gases. Hydrogen is one of the suggested alternative clean energy resources. Hydrogen is not a fuel, since it is derived from fuels such as methane only with energy input. It is more correct to call hydrogen an energy currency.[1]

The hydrogen economy, which is a whole network of hydrogen production and storage, is still more hypothetical due to several fundamental problems, such as efficiency in generation, price, high-gravimetric hydrogen density for storage and transportation.[2] Among all these challenges, it is particularly important to develop new ways to generate hydrogen without hydrocarbons.[1]

In nature, hydrogenase utilizes/ produces hydrogen efficiently. Hydrogenase is a family of enzymes mediating hydrogen activation, found in a wide variety of microorganisms.[3] These microorganisms, such as photosynthetic, sulfate-reducing, methanogenic, or nitrogen-fixing bacteria, metabolize hydrogen.[4] Hydrogenase catalyzes the simplest chemical reaction:[5]

$$2H^+ + 2e^- \leftrightarrow H_2$$

The reversible oxidation-reduction reaction of the smallest molecule, molecular hydrogen (H_2), and its elementary particle constituents, two electrons and two protons is vital in anaerobic metabolism. The enzymatic activity was first discovered in 1931, when

it was noted that *Escherichia coli* evolves hydrogen in the course of growth under certain conditions.[6]

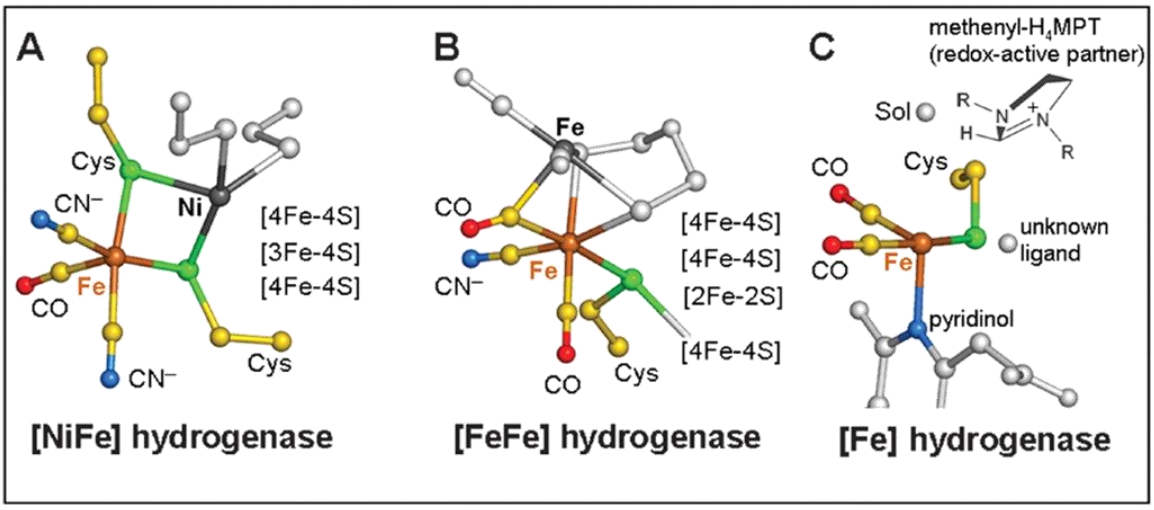

Figure I- 1. Superimposed active-site structure of the three phylogenetically unrelated hydrogenases.
(**A**) [NiFe]-hydrogensase from *Desulfovibrio gigas*. (**B**) [FeFe]-hydrogenase from *Clostridium pasteurianum* and *Desulfovibrio desulfuricans*. (**C**)[Fe]-hydrogenasefrom *Methanocaldococcus jannaschii* (this work). In [Fe]-hydrogenase, the fifth and sixth ligation sites are marked by gray spheres. All three hydrogenase types have in common a low-spin iron (brown) ligated by thiolate(s), CO, and cyanide or pyridinol (considered as cyanide functional analog), which acts together with a redox-active partner (dark gray). The partners—Ni, the distal iron, and methenyl-H_4MPT^+ (modeled), respectively—take over the electrons or the hydride and perhaps play a role in the heterolytic cleavage of H_2.[7]

The hydrogenase enzymes catalyze both uptake and production of hydrogen, depending upon the conditions. H_2 oxidation is coupled to the reduction of electron acceptors such as oxygen, nitrate, sulfate, carbon dioxide, and fumarate,[5] whereas proton reduction is essential in pyruvate fermentation and in the disposal of excess electrons.[3] Due to the very low solubility of hydrogen in water, hydrogenases must have a very high affinity for hydrogen. [1]

All hydrogenases are metalloenzymes, which are classified in three groups: [NiFe]-hydrogenases, [FeFe]-hydrogenases, and [Fe]-hydrogenase. The metal active site structures are shown in **Figure I-1.**[7]

2. Structure and mechanisms of Hydrogenases

2. 1. Structure and mechanisms [NiFe]-hydrogenases

In 1995, the crystallographic studies on the [NiFe]-hydrogenases from the sulfate reducing bacteria *desulfoibrio gigas* showed that the hydrogenase activating site contains a bimetallic center, one nickel and one iron.[8] From this work, the Fe atom, which was previously missed by biochemical and spectroscopic studies, was first revealed to be presented in the active site. The full structure of active site in the inactive forms of enzyme, Ni-A and Ni-B, is shown as in **Figure I-2**.

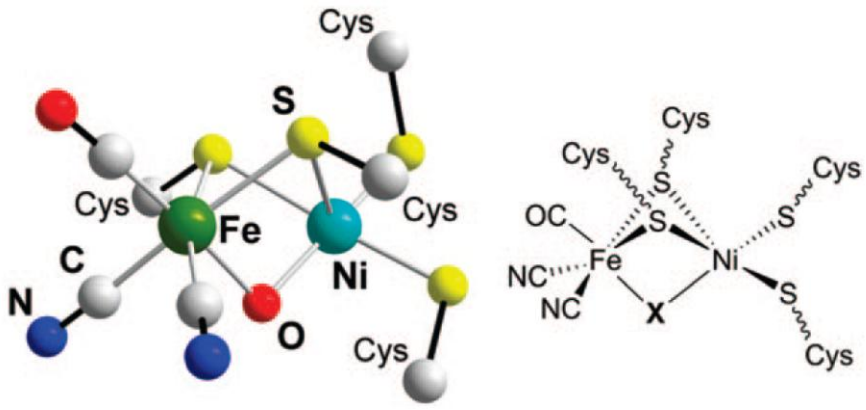

Figure I- 2. X-ray structure and schematic representation of the metallo-center of the aerobically isolated, inactive form of the [NiFe]-hydrogenase.

(X HOO- for Ni-A and HO- for Ni-B).[9]

It was found that, in all [NiFe]-hydrogenases, there is a hetero-metallic cluster in which a Ni ion coordinated by four cysteine thiolates and to a Fe ion by two bridging thiolates. Additional coordination to Fe is supplies by two cyanides, one carbonyl and a bridging species, for which its composition has been proposed to be a μ-oxo, sulfide, hydroxo, peroxide, or sulfoxide group.[10-12] The iron was found to remain the +II oxidation state in a low-spin (S=0) diamagnetic system in the inactive form(Ni-A) and active form(Ni-B) of the enzyme.[8] Besides the Ni-A and Ni-B forms, crystallographic studies reported Ni-C, Ni-CO and Ni-R structures and the potential proton and gas-channel pathways were therefore proposed.[10,13-15]

There are three structural "signature" features in all the crystallographically defined states/forms: (i) the {Ni(μ-SCys)$_2$Fe}-butterfly arrangement formed by the

bridging cysteinyl ligands (ii) a distorted square-planar arrangement of the four cysteinyl ligands about the Ni center (iii) the {Fe(CO)(CN)$_2$}-motif.[9] The distances between the two metals are different, ranging from about 2.9Å to about 2.5Å for the inactive forms Nis-A, Ni-B and the reduced active form Ni-SI respectively.[11,16-17]

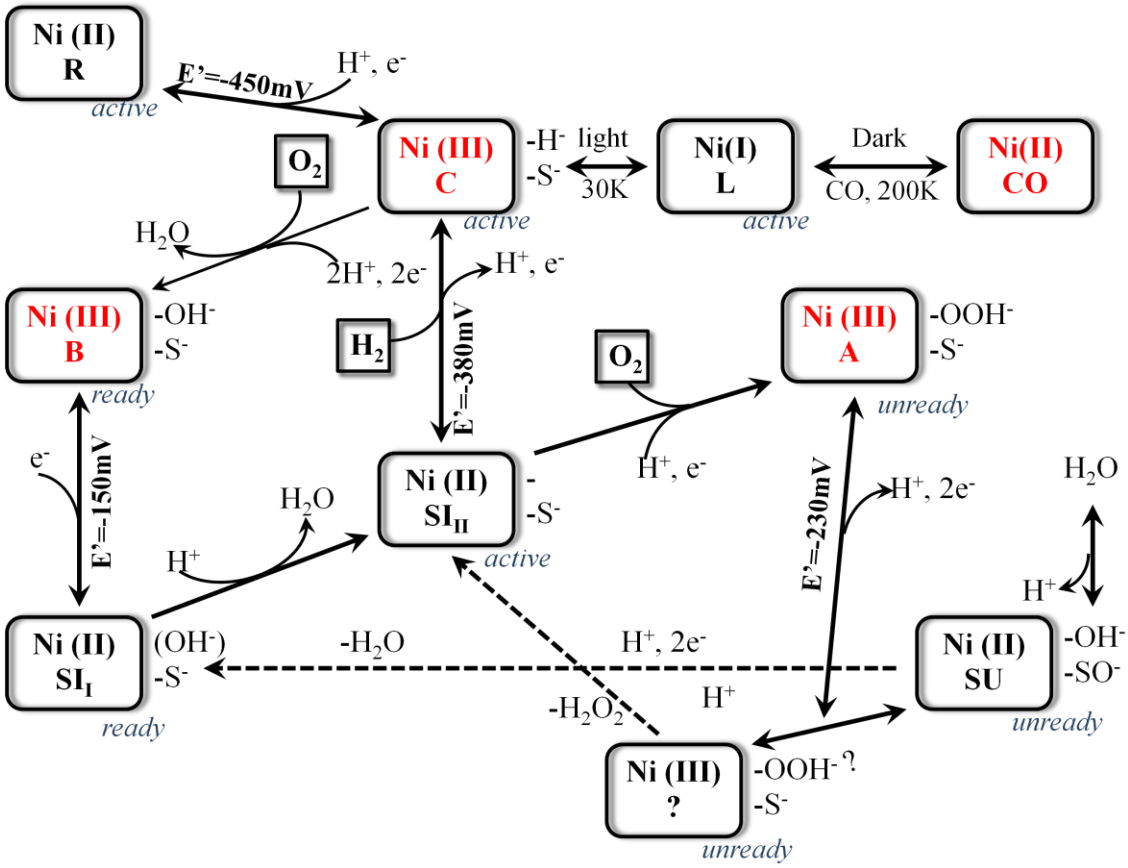

Scheme I- 1. Possible aerobic oxidation that lead to the ready Ni-B state and unready Ni-A stated, as well as all different redox states of active site [NiFe]-hydrogenases.

(inspired and modified from previous publication[11,18]) States that were structurally characterized by X-ray crystallography are labeled in red.

Van der Zwaan et al. reported that, according to their $^{17}O_2$ study, oxygen is bound near Ni iron in both the Ni-A and the Ni-B states.[19] It was also concluded from their work

that there was no direct interaction between Ni and O. Related study implied a rather unexpected conclusion, which is that the bridging ligand in Ni-A state could originate from either O_2 or H_2O.[20-22] Different redox states of [NiFe]-hydrogenases present a complex scheme with inactive and active forms as well as CO-inhibited states, Ni-R states and Ni-L state, as summarized in Scheme1. The possible reaction fragments, such as HOO^-, SO^-, OH^-, H^+, O_2 and S^-, are also labeled in majority states. Not all states are fully structurally characterized. The square-planar Ni(II) is EPR silent while Ni(III) ($S=^1/_2$) and Ni(I) ($S=^1/_2$) are EPR active. Therefore EPR signal is used to probe the redox state of nickel iron in the bimetallic center. The oxidation states of the nickel center of all states are labeled in **Scheme I-1**.

Based on spectroscopic data, detailed mechanisms for hydrogen activation involving hydrides of both Ni and Fe have been proposed. It is generally accepted that the redox states of the active site that correspond to catalytically competent enzyme are Ni-R, Ni-C and Ni-SI.[18] The three-step mechanism which involves these three was supported by kinetic data obtained by spectroscopic redox titrations.[23-25] The shift of the vibrational frequencies observed between the FTIR spectra of Ni-SI_I and Ni-SI_{II} suggests different levels of protonation of one of the terminal cysteines of Ni atom, which is also consistent with the broad pH range in which [NiFe]-hydrogenases are active.[25-26] In any case, it is generally agreed that Ni-C is the key intermediate of the catalytic cycle, because the idea of heterolytic cleavage of H_2 at active site is supported by enormous experimental and theoretical data which show that the Ni-C state contains a bridging hydride.[27-32] The crystal structures indicate that the gas transport channel of enzyme ends at the Ni center, so it is widely believed that Ni is the binding place of the substrate. [13,33]

Conversely, computational studies of the intermediates and transition steps of catalytic cycle favored the Fe atom as the binding place of H_2. Leger et al. calculated the energy barrier for the heterolytic cleavage assisted by a terminal S ligand to be similar to the direct electrochemistry data, 55kh/mol.[34] Siegbahn pointed out by his DFT study that a bridging cysteines may act as a base during the catalytic cycle.[30] With their DFT study, Pardo et al have proposed a catalytic mechanism for H_2 oxidation and production by [NiFe]-hydrogenases (Figure I-3), which favored the Fe atom as the binding place of H_2.[28]

The inner cycle of Figure I-3 corresponds to the H_2 production pathway. The starting point is the Ni-SI_{II} state, which in a one-electron/one-proton step forms the stable intermediate Ni-C. A Ni(I)-Fe(II) transient intermediate might accrued within this first one-electron/one-proton step, which is not detected by spectroscopy during turnover conditions but could be similar to the Ni-L state detected by photodissociation at low temperature.[27,35] The discovery of H_2/D_2 exchange activity of [NiFe]-hydrogenases implied the existence of this transient intermediate in the catalytic mechanism.[36] The Ni-C intermediate, in a second one-electron/one-proton step, forms Ni-R state. The FTIR frequency shifts of the CN/CO diatomic ligands of the active site observed when Ni-C is reduced to the Ni-R state suggest that the latter state retains the bridging hydride ligand.[33] No further direct experimental evidence has been gained concerning the nature of the hydrogen species bound to the Ni-R state. Most DFT calculation proposed the structure of Ni-R as shown in Figure I-3.[18] Formation of a H_2 ligand on the Fe and the release of

hydrogen gas via the gas-transport channel finish the catalytic cycle of H_2-production and returns to Ni-SI_{II} state.

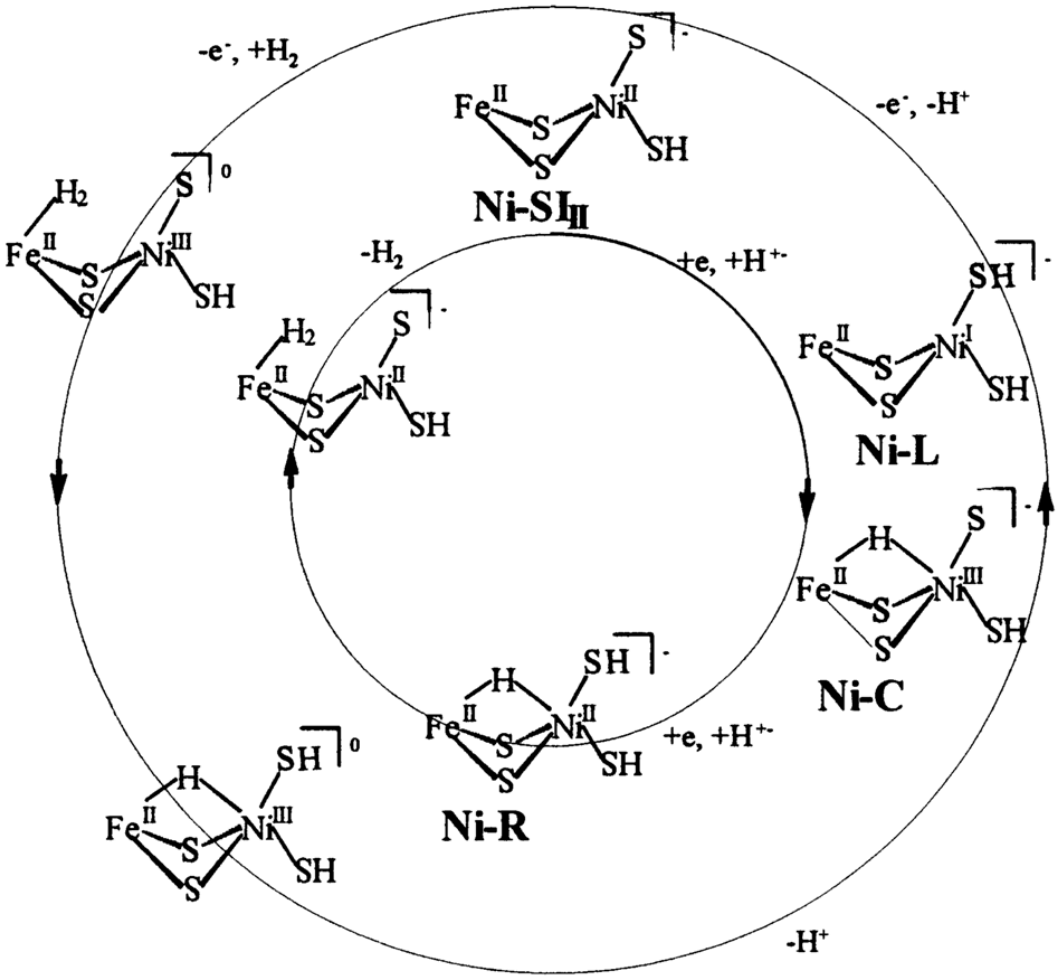

Figure I- 3. Catalytic cycle mechanism proposed for [NiFe]-hydrogenase[28]

The counterclockwise direction pathway, H_2-oxidation, is represented in the outer cycle. The first step involves binding of H_2 to the Fe atom of the Ni-SI_{II} state. There is a debate in the various DFT calculations whether or not the kinetic barrier for the

subsequent heterolytic cleavage step would be lower if the Ni atom was pre-oxidized to Ni(III) . Pardo's work supported pre-oxidized to Ni(III), while Siegbahn's work concluded that Ni(II)-Fe(II) oxidation level is more favored, if the net charge of the model of the active site used is different.[18] Siegbahn's work also concluded that, in the DFT calculations, the bulky environment, including atoms of amino acid residues surrounding the active site, did not impede H_2-binding to the Fe atom.[30] The Ni-C state is formed as a result of transferring of one proton after the heterolytic cleavage. The Ni-C state then forms the transient intermediate which is similar to Ni-L and that is quickly oxidized back to the Ni-SI_{II} state (Figure 3).

2.2. Structure and mechanisms [FeFe]-hydrogenases

[FeFe]-hydrogenases are named due to its lack of nickel atom. They are phylogenetically unrelated to [NiFe]-hydrogenases, and usually catalyze hydrogen evolution.[4,37] They are usually about two orders of magnitude more active with artificial electron donors and acceptors than the [NiFe]-hydrogenases, and bind hydrogen more strongly.[1]

The H-cluster X-ray crystallographic structure for [FeFe]-hydrogenases has been reported by two independent groups in 1998 from two different organisms, *Clostridium pasteurianum* (CpI) and *Desulfovibrio desulfuricans* (DdH).[38-39] Both structures present a similar iron coordination environment yet a small different overall active site composition. The X-ray structure of [FeFe]-hydrogenases (**Figure I-4**) reveal that, besides the Fe diatomic center, there commonly present an accessory iron-sulfur clusters,

which are predicted functioning as shuttle electrons to or from the external physiological electron donors and /or acceptors.

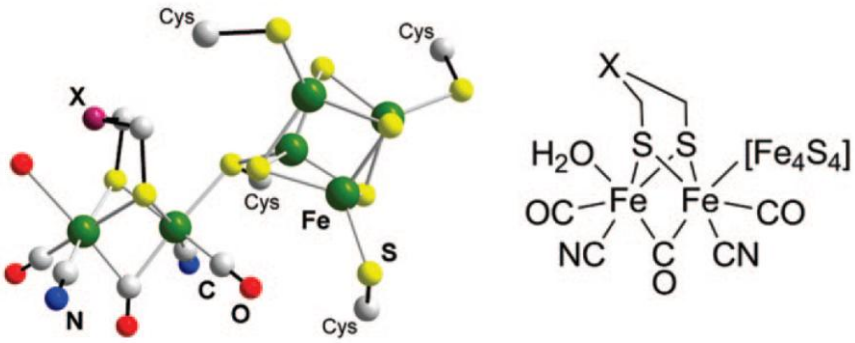

Figure I- 4. X-ray structure and schematic representation of the active site of the [FeFe]-hydrogenases.[9]

The H-cluster consists an [4Fe-4S] cubane core bridged by one cysteine sulfur to a [2Fe-2S] subsite, in which the two iron atoms in the pair are bridged by a "X" dithiol ligand. The X appears from the crystal structure to be either 2-azapropane-1,3-dithiol or propane-1,2-dithiol, which have never been isolated and its biosynthetic pathway is unknown.[38-39] The Fe atoms in the [2Fe-2S] subsite in [FeFe]-hydrogenases, holding a slightly distorted square pyramid geometry, remains low spin Fe(II) with CO and CN^- coordinated as shown in the active site [NiFe]-hydrogenases, which states these elements to be essential to their biological catalytic activity. Low spin ferrous iron is uncommon in non-heme environment, but the presence of strong field ligands such as carbon monoxide and cyanide is consistent with this spin state.

The Scheme of the different redox states of active site of [FeFe]-hydrogenases is shown in **Figure I-5**. Popescu and Munck's work led to the conclusion that in all states of

[FeFe]-hydrogenases, the [4Fe-4S] cubane center remains at the EPR-silent 2+ level: $[4Fe\text{-}4S]^{2+}$.[40] The aerobic inactive state, H_{inact}, is diamagnetic, and could form a paramagnetic state, H_{trans}, via a one-electron reduction. The Fe ions in [2Fe-2S] subsite of H_{trans} are low spin, and the oxidation configuration are favored to be Fe(II)-Fe(II) system by DFT calculations.[41-42] In the H_{OX} form of the enzyme, which is obtained from an irreversible redox-dependent process from $H_{trans,}$ the H-cluster is paramagnetic, and one CO isa bridging the two Fe atoms in the [2Fe-2S] subsite. The experimental data has shown that the [4Fe-4S] cluster is diamagnetic and the unpaired spin in centered at one of the Fe site of the [2Fe-2S] subsite. The continued work with ^{13}CO labeling infrared spectroscopy done by De Lacey, the magnetic study done by Popescu and Munck, as well as DFT calculation done by Hall and De Gioia[41] concluded that both the H_{OX} form and the H_{OX}-CO form were Fe(II)-Fe(I) systems with spin-density located on the iron atom distal to the cubane cluster.[40,43-46] The H_{red} form is diamagnetic,[47] and Mössbauer studies have shown that the Fe irons in the [2Fe-2S] subsite are indistinguishable,[40,47] therefore the Fe(I)-Fe(I) system is favored with supportive results from DFT studies.[48-49] The H_{sred} form was detected by infrared spectroelectrochemistry at every low redox potential, but no further data are available at this point due to its high instability.

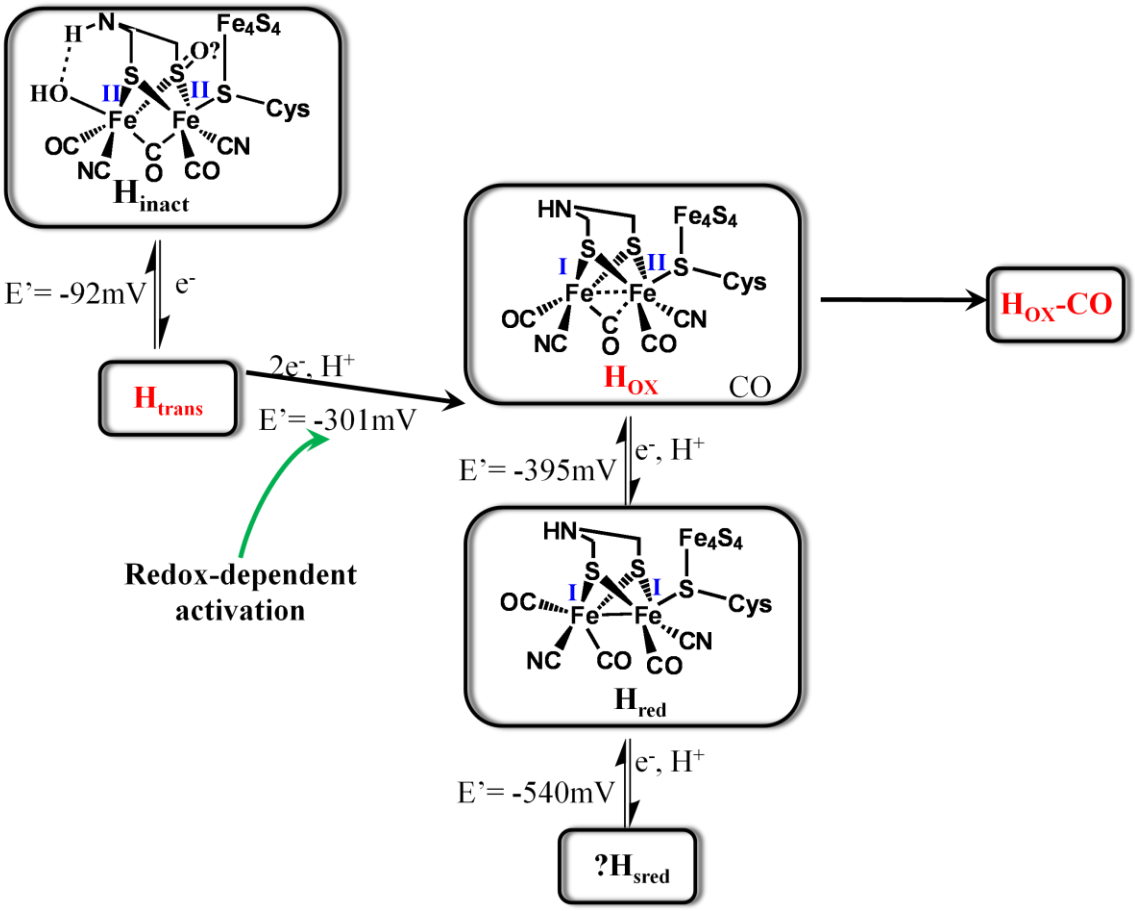

Figure I- 5. Scheme of the different redox states of the active site of [FeFe]-hydrogenases and some of their proposed structure. The paramagnetic EPR-active states are marked with red (the EPR spectra of H_{sred} have not been reported). The formal redox potentials (at pH 8.0) correspond to those measured by FTIR-spectroelectrochemistry of *D. desulfuricans* [FeFe]-hydrogenases.(scheme is modified from refs[18] and the structure is inspired by ref[50])

Similar to the [NiFe]-hydrogenases, all the states of [FeFe]-hydrogenases are within a relatively narrow range of redox potentials, which might result from the combination of different ligand field ligands. The ligands combination: thiolate (good π-donor), carbonyls (good π-acceptor) and cyanides (good σ-donors) provide an electronic buffer that facilitates the entry and exit of electrons in the active site. [18] The formal redox

potentials (at pH 8.0) corresponding to those measured by FTIR-spectroelectrochemistry of *D. desulfuricans* [FeFe]-hydrogenases is shown also in Fig 5.[51]

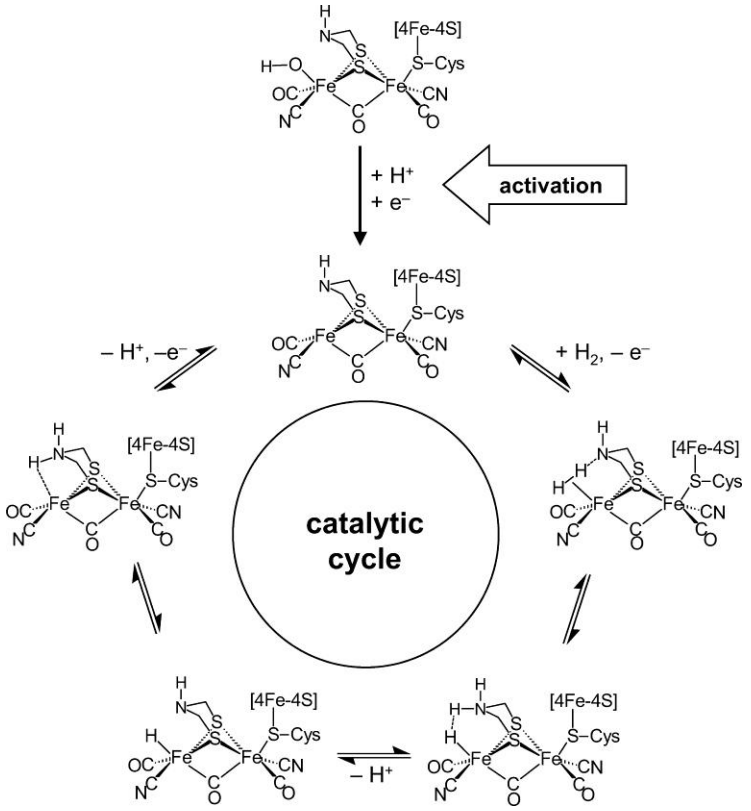

Figure I- 6. Proposed catalytic cycle for [FeFe]-hydrogenase using the central nitrogen of the μ-SCH_2NHCH_2S linker for H^+ transfer. The oxidation states have been left purposely ambiguous.(adopted form ref[43])

Both the proposed catalytic cycles feature therearrangement of the enzyme active site and the use of the central nitrogen of the μ-SCH_2NHCH_2S linker for H^+ transfer,[43]and both are supported by some of the DFT and modelling system results. The latter catalytic cycle is shown in **Figure I-6**. The catalytic cycle should not be understood as if that the order of proton- and electron-transfer events is known or that discrete proton- and electron-transfer events are observed to occur. In fact, the [FeFe]-

hydrogenases mechanism may involve simultaneous proton−electron transfers rather than discrete proton-transfer and electron-transfer steps.[43] The binding of H_2 to the $Fe^{I}Fe^{II}$ H_{ox} may trigger simultaneous proton−electron transfer to yield an $H-Fe^{II}Fe^{II}$ H_{red} form, while the $H-Fe^{II}Fe^{II}$ form H_{red} may then undergo a simultaneous proton−electron transfer to regenerate the $Fe^{I}Fe^{II}$ H_{ox} form. This type of interconversion is in agreement with the experimental results of Albracht et al. that show that the H_{red} form is in equilibrium with $H_{ox} + H_2$.[51-52]

2. 3. Structure and mechanisms [Fe]-hydrogenase

[Fe]-hydrogenase, previous known as Fe-S-cluster-free hydrogenase or H_2-forming methylenetetrahydromethanopterin (Hmd), does not contain nickel or Fe-S clusters. The crystal structure of native enzyme has not been obtained.

[Fe]-hydrogenases were first shown to process Fe ligated by CO in 2004[53] by Lyon and co-workers; and very recently, the structural description of [Fe]-hydrogenase apoenzyme from *Methanothermobacter jannaschii* with an iron cofactor from *Methanothermobacter marburgensis* was revealed with bound Fe site allowing for the first time side by side comparison of these unique active sites.[7]

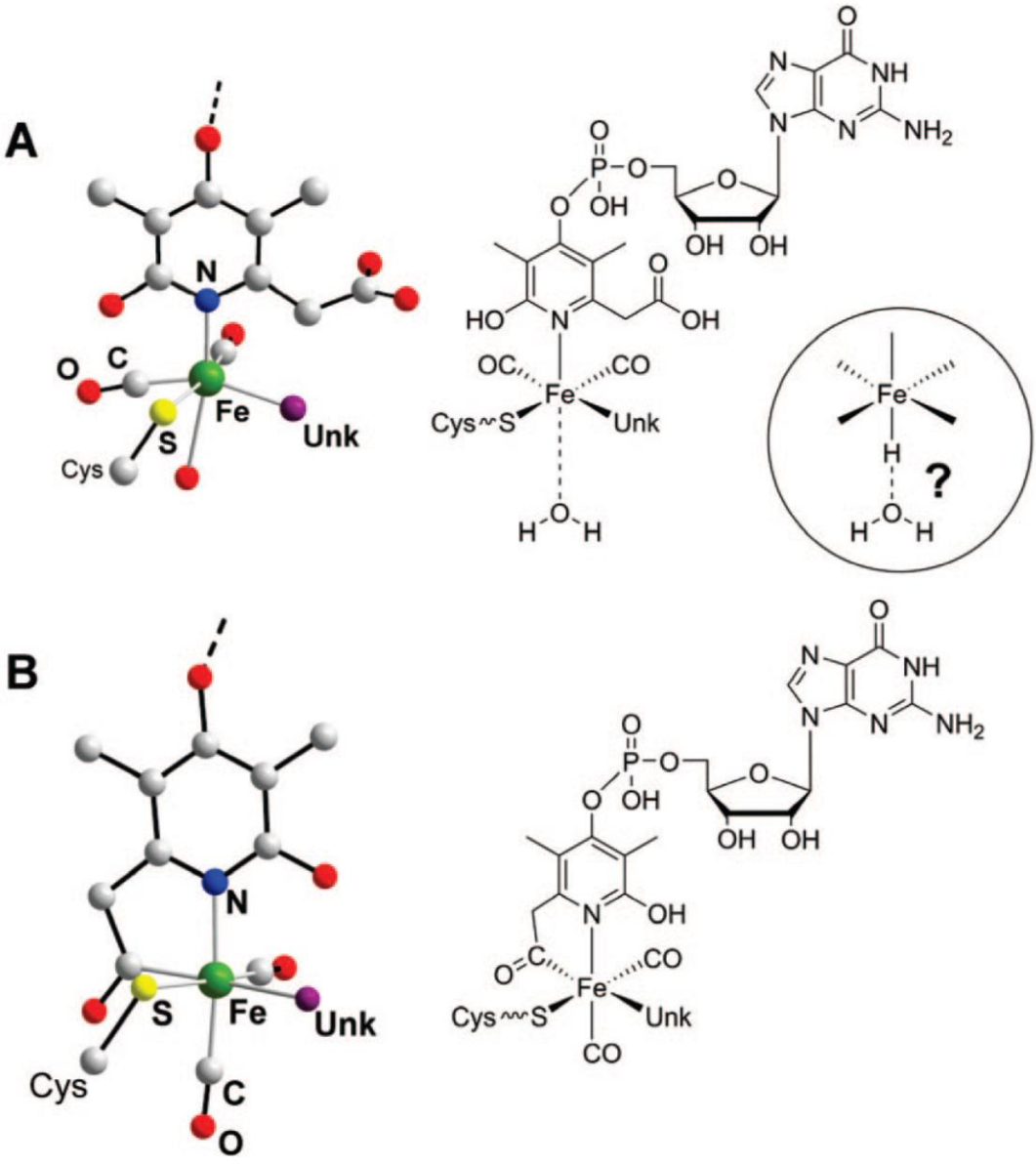

Figure I- 7. Structures of the active site of the [Fe]-hydrogenase. Unk, unknown ligands; this site appears to bind cyanide. A: structure from ref[7]. B: Structure from ref[54]. (adopted from ref [9])

In the structure (**Figure I-7**A), the [Fe]-hydrogenases active site consists of a square pyramidal iron coordinated by two *cis*- CO ligands, a cysteine thiolate, the

nitrogen of 2-pyridinol compound, and a ligand of unknown composition occupying one of the basal positions. The Fe center is not redox active and under all conditions tested remains EPR-silent. Spectroscopic data obtained by FTIR, Mössbauer, and XAS indicate that the Fe is in a low-spin state, although it is yet unknown if it is Fe(0) or Fe(II). In the crystal structure of [Fe]-hydrogenase, the pyridinol, which might have ligand back-bonding properties, is partly disordered, and the possibility of pyridone tautomeric form coordinated in this position was excluded due to the planarity of the heterocyclic ring.[7] On the contrary, the very recent development studies[55] on a mutant protein (Cys176→Ala) have provided a new interpretation of the structure with pyridine and a coordinated acyl group(**Figure I-7**B). Nevertheless, both structure agreed on two *cis*- CO, which was supported by the infrared data, a cysteine thiolate and an unknown "fifth" ligand bonded to Fe.

In contrast to the [NiFe]-hydrogenases and [FeFe]-hydrogenases, [Fe]-hydrogenase does not catalyze the reduction of dyes such as methylviologen with dihydrogen. It facilitates the stereo-selective transfer of a hydride from the H_2 to pterin substrate. In [Fe]-hydrogenase, electrons are not released; rather, the carbocation substrate methenyl-H_4MPT^+ is thought to directly accept hydride from H_2. Shima and Thauer's crystal structure supports this mechanism, which might take two different pathways, shown in **Scheme I-2**. In pathway 1, the scenario involving an center Fe(II) is that dihydrogen coordinated and then a neighboring base heterolytically splits dihydrogen by removing a proton; which would leave a hydride on the metal center for concerted or sequential transfer to the carbocation substrate. In alternative pathway 3, dihydrogen

activation is considered as oxidative addition of dihydrogen to the Fe(0) center which to give a dihydride followed by abstraction of one hydride by the carbocation substrate. The regeneration of dihydride intermediated could occur by proton removal proceeding or concerted with dihydrogen ligation to the mono-hydride.

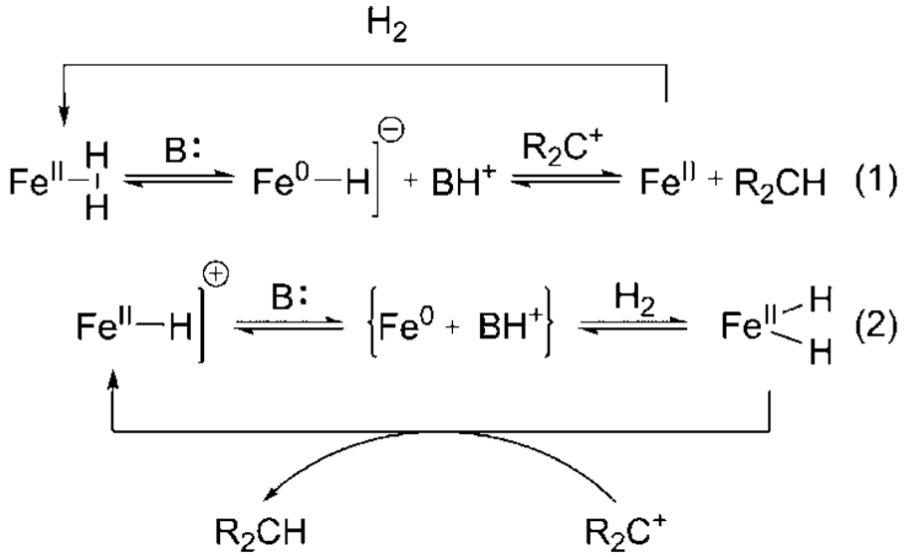

Scheme I- 2. [Fe]-hydrogenase H_2 cleavage mechanism.(adopted from ref[9])

3. Model studies

3.1. [NiFe]-hydrogenase models

Work in this area predates the report on the active site structure, and are mainly divided into three branches: (1) focusing on preparation, structure and reactivity of Ni complexes with sulfur ligation; (2) focusing on preparation, structure of Fe complexes with CO and CN ligands; (3) focusing on preparation, structure of the hetero-dinuclear

Ni/Fe complexes with comparative Ni-Fe distance as the crystal structure (4) focusing on the functional complexes that can actually catalyze H_2 oxidation or proton reduction to H_2.

Attempts to mimick the Ni center of [NiFe]-hydrogenases, predated the report on the active site structure.[56] The work started with interests in achieving a tetragonal Ni(II) center with the capability to reversibly generate the corresponding Ni(III) species. Two general complexes of mononuclear $[Ni(SR)_4]^{2-}$ are known: complexes containing mono-dentate thiolates (R = Ph, p-Tol, m-Tol, p-C1-C_6H_4, m-Cl-C_6H_4, p-NO_2-C_6H_4, Bu^t) together with $[Ni(NMTP)_4]^{2+}$ (NMTP = N-methyl-2-thio~opyrrolidine). These complexes adopt flattened tetrahedral geometries in the solid state, typically with Ni-S bonds of 2.26-2.33 Å and S-Ni-S angles in the range 88-125 °.[56] Square planar Ni-complexes were synthesized later with chelated ligands, such as ethane-1,2-dithiol, quinoxaliedithiol, norborane-2,3,-dithiol. A large number of Ni-complexes S-, N-, and/or O- polydentate chelate ligands have been characterized, and most afford a square planar Ni center. It is notable quite some of these modeling complexes process a redox property as the Ni center of [NiFe]-hydrogenases. For example, the groups of Holm and Yamamura have studied structure and redox chemistry of Ni-complexes of several N_2S_2 chelate type ligands. These form square planar Ni(II) complexes which exhibit chemically reversible oxidations at $E_{1/2}$ = -0.04 to -0.42V vs SCE.[57 58-59]

The first structurally characterized thiolate-bridged Ni–Fe carbonyl complex, **1A** (**Figure I-8**), was reported by M. Y. Darensbourg in 1996[60] with the Ni-Fe distance being 3.76Å, which is much larger than the 2.6-2.9Å that observed in the biological site. The

first example of Ni-Fe complexes with two thiolate bridges, **1B**, was reported by Pohl in 1997[61], with a much more shorter Ni-Fe distance, 2.8Å, as the consequence of double bridge. Compound **1C** is the first reported mimicking complex with a double thiolate bridge and a carbonyl ligand coordinated to Fe, however with a long Ni-Fe distance (3.5Å).[62-63] Due to the soft donor of phosphine, they are better models for cysteinate sulfurs of enzyme than the N-donors that are employed in a large number of models. Compound **1D**, reported in 2005,[64] is one of the better model complexes with phosphine ligand, with a Ni-Fe distance of 2.5Å reproducing the distance in reduced active form of [NiFe]-hydrogenases. In compound **1D,** the Fe ion is Fe(0) with a square-based pyramidal geometry, while the Ni ion is a distorted tetrahedral environment. DFT calculations reveal the bent Ni(dz_2)-Fe(dz_2)σ-bond in the singlet state for compound **1D**, which opens the fascinating possibility that at least some of the forms of [NiFe]-hydrogenases may involve significant metal-metal bonding interactions.[65]

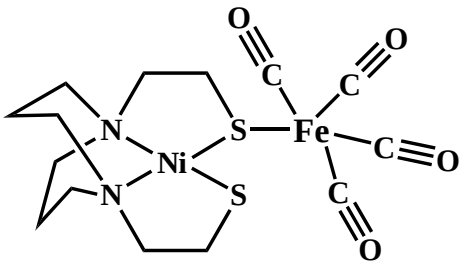

1A

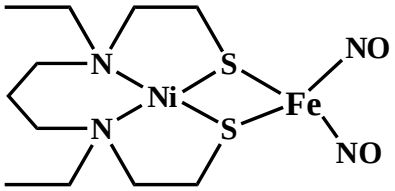

1B

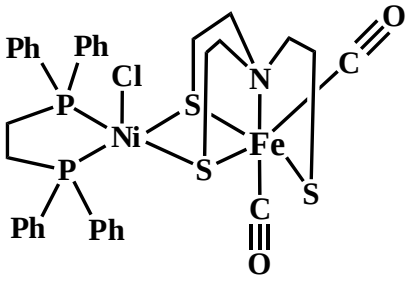

1C

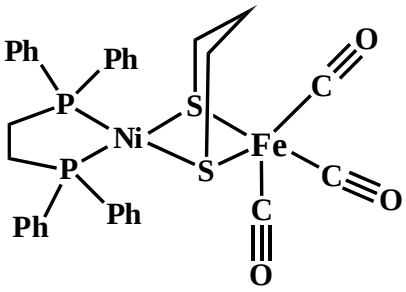

1D

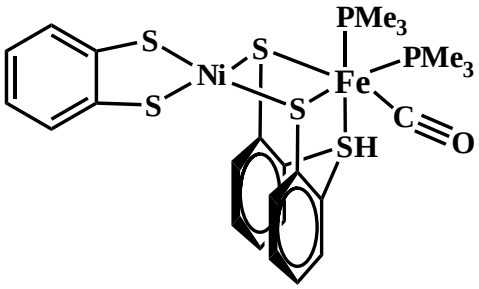

1E

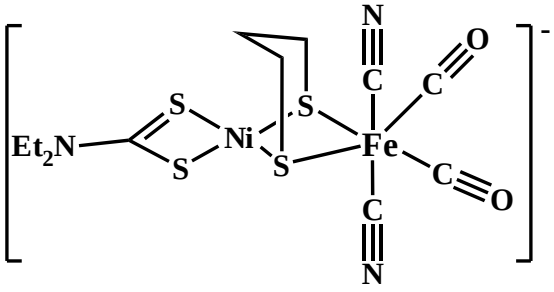

1F

Figure I- 8. Selected structural models for [NiFe]-hydrogenase active site (for refs, see text).

In 2002, D. Sellmann and coworker reported compound **1E**, in which a low-spin Ni^{II} center exclusively coordinated by S atoms connected via two thiolated bridges to a low-spin Fe^{II}-CO moiety and a disappointing Ni-Fe distance of 3.3Å.[66] 10 years after the

initial enzyme structure determination, in 2005, Tatsumi's group reported the closest mimic so far of the enzyme active state with the crucial CO/CN- ligand set on Fe, diamagnetic compound **1F**.[67] The success is result of continuously systematic effort undertaken by several research groups and devoted to the synthesis of new Fe^{II} carbonyl/ cyanide/ thiolate complexes.[68-77] The Ni-Fe distance (3.05Å) and the hinge angle of 85 °in compound **1F** are in the range reported for the oxidized form of [NiFe]-hydrogenases.

Unfortunately none of the complexes described above have been reported as catalysts .. The trinuclear complex, **1G**, shown in **Figure I-9**, is so far the only reported Ni-Fe compound with catalytic activity for proton electro reduction.[78]

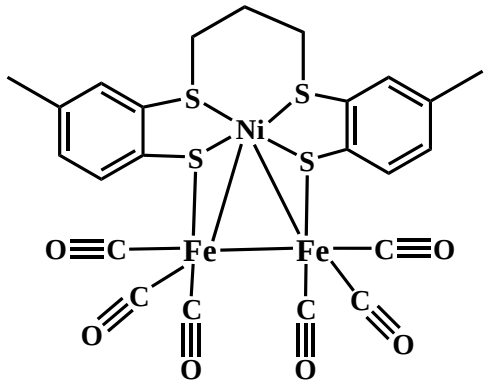

1G

Figure I- 9. Trinuclear Ni-Fe functional models for [NiFe]-hydrogenases active site.[78]

In diamagnetic compound 1**G**, the Fe-Fe distance (2.66Å) and Ni-Fe distance (2.50Å) suggest that there might be bonding interaction between Fe-Fe and Ni-Fe. The electrochemistry shows that compound 1**G** had a reversible one-electron reduction at -1.03V *vs* $Fc^{+/0}$ and generate a paramagnetic reduced specie (S=1/2). Complex 1**G**

catalyzes the reduction of trifluoroacetic acid to H_2 with an activity of 6 TON h^{-1}, and remains stable for 1 hour before decomposition.

3.2. [FeFe]-hydrogenase models

It is clear that the active site of [FeFe]-hydrogenases, which was elucidated by the groups of Peters and Fonticella-Camps, resembles molecular species long known to inorganic chemists

Modeling complexes toward [FeFe]-hydrogenases starts with focusing on mimicking the $(\mu\text{-}S^{-})_2$ [2Fe2S] subsite. The long history of the synthesis and characterization of diiron carbonyl complexes dating back to 1928 and the sequential study in 1980's, provides a good starting point for the H-cluster mimics.

The crystal structure indicate the two Fe centers in the [2Fe2S] subsite are linked by a dithiolate of the type CCH_2YCH_2S, where, Y is only identified as a light atom in the crystallographic studies, and thus may be CH_2 NH or O. None of these dithiolates were previously known in nature. Darensbourg and coworkers first pointed out that complex **2A** (**Figure I-10**) process a similar Fe-Fe distance (2.510Å) to the reported data of the enzyme active site, and also reported the dianionic dicyanide derivative from **2A**.[79] Rauchfuss and coworkers'[80] and Pickett and coworks'[81] independent research utilized ligand substitution on **2A** with cyanide to generate the dianionic dicyano derivatives in different isomer forms. The isomer of **2B** depicted here is the one identified by Rauchfuss and coworkers using X-ray crystallography. Complex **2B** closely resembles

the [2Fe2S] subsite of [FeFe]-hydrogenases with a Fe-Fe distance of 2.6Å, and reaction with acid to generate substoichiometric quantities of H_2.

The [FeFe]-hydrogenase characteristically convert protons to dihydrogen, thus great attentions have been brought into the protonation of model [2Fe2S] subsite and their hydride derivatives. Heineky and coworkers have reported the replacement of carbonyl ligand with isonitrile ligand of **2B** which leads to neutral disubstituted species, **2C**, which can subsequently be protonated and generates the corresponding hydride, **2D**.[82] This result is a successful continuance study of previous effort of cyanide and phosphine derivatives done by Rauchfuss's group[83] and Darensbourg's group.[84] Complex **2C** also undergoes isotope exchange with D_2 upon photolysis, which demonstrates its functional similarity to the actual enzyme subsite. Several reports have described the reduction chemistry of **2A**, with somewhat conflicting results, which indicate that the identity of actual active catalyst is not always well defined. It seems that when the [2Fe2S] center is both electron-rich and has bulky ligands that hinder the turnstile rotation of the hydride iron site, the terminal hydrides are stabled. Complex **2E**, reported by Rauchfuss's group is one of these examples.[85] Protonation of $Fe_2(pdt)(CO)_2(dppv)_2$, **2E**, at -40 ℃ with HBF_4 gives the terminal hydride $[HFe_2(pdt)(CO)_2(dppv)_2]^+$(δ-4.2ppm, t, J_{PH}=73Hz), **[2EH]$^+$**. Complex **[2EH]$^+$** at 0 ℃ undergoes a unimolecular isomerization to a isomeric μ-hydride, **[2EμH]$^+$**, during which course no exchange with CD_3OD is observed. Second protonation from **[2EH]$^+$** or double protonation directly from **2E** with $H(Et_2O)_2BAr^F{}_4$ give the terminal hydride bearing an adjacent ammonium center, **$[2EH_2]^{2+}$** , in which the ammonium center is highly acidic and would even been

deprotonated by MeOD. Complex $\mathbf{[2EH_2]^{2+}}$ is stable in CH_2Cl_2 solution and would release H_2 when the protonation was conducted in a MeCN solution. It is also has recently been reported in their followed up work that in the similar modeling system, other isomers of hydrides, such as terminal-apical hydride, terminal-basal hydride, cis-μ-hydride, trans-μ-hydride, and isomers with different orientation of the dithiolate strap, were observed.[86-87]

Hydrogen redox is theoretically a 2e- process, both for the reductive coupling of two protons or the oxidative cleavage of dihydrogen. Redox by one electron would yields hydrogen radicals, which are high energy species rarely observed near ambient temperatures. In the [FeFe]-hydrogenases, the [2Fe2S] subsite provides one redox equivalent, while the [4Fe4S] subsite supplies the second equivalent. Thus model for the entire H-cluster would be very beneficial. The most complete structural model for the [FeFe]-hydrogenases active site reported to date is complex **2F**, with similar Mössbauer spectroscopy to those reported for the reduced form of the hydrogenase from *Clostridia pasteurianium*.[88] Complex **2F** facilitates efficient electrocatalysis of proton reduction, confirming the functional relevance of this model compound.

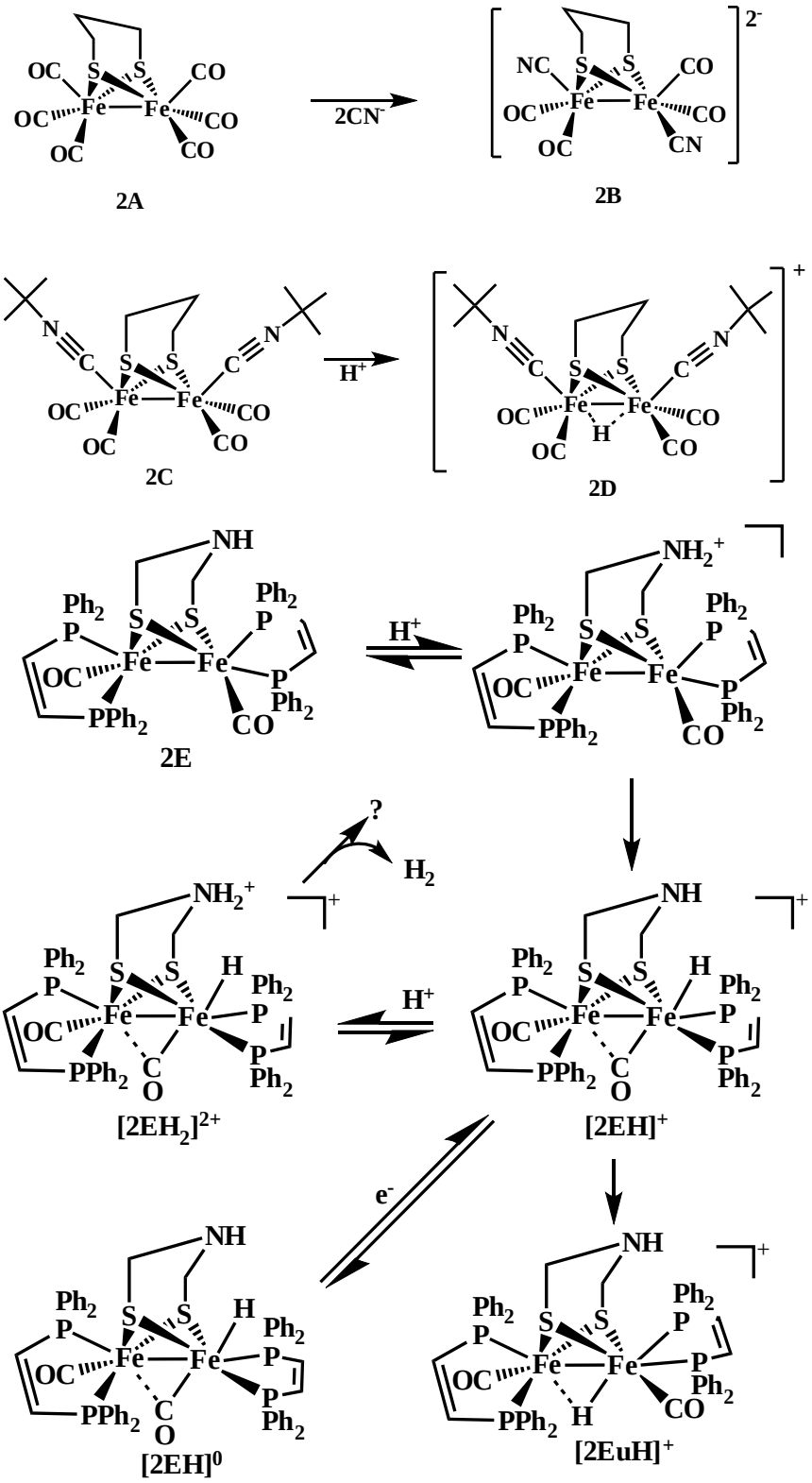
2A
2CN-
2B
2C
H+
2D
2E
H+
?
H2
[2EH2]2+
H+
[2EH]+
e-
[2EH]0
[2EuH]+

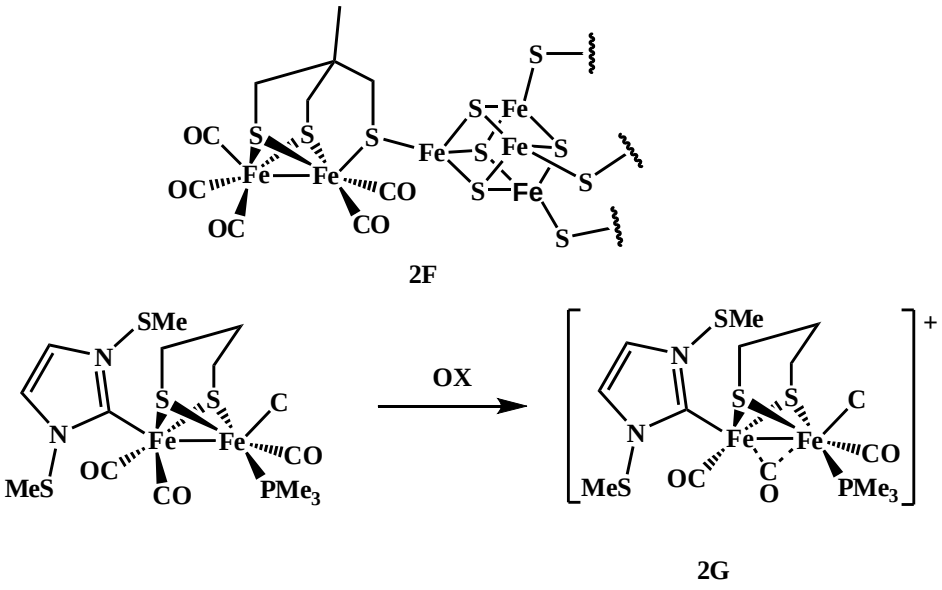

Figure I- 10. Selected structural models for [FeFe]-hydrogenase active site (for refs, see text).

Mixed valency is a defining feature of the oxidized state H_{ox} (S=1/2) of the enzyme supported by protein crystallography and DFT results. There is also great amount of research work directed to modeling the $Fe^{II}Fe^{I}$ redox level in [FeFe]-hydrogenases, but isolated model complexes are rare. Most complexes are amenable to EPR, IR or even crystallographic analyses, but are unfortunately thermally sensitive and typically decompose within minutes near room temperature. Complex **2G**, reported by Darensbourg and coworks,[89] is the only isolated and "stable" example of this mixed-valent $Fe^{II}Fe^{I}$ type of modeling compound, which still shows a good match with the infrared and EPR spectra of the [FeFe]-hydrogenase from *D. desulfuricans*. The Fe-Fe distance is 2.566Å in comlex **2G**, a lightly longer than in the precursor complex. The

same group also reported in 2008 that the mixed valence structure with a semibridging CO ligand is stabilized by adding steric bulk to the propanedithiolated bridge.[90]

3.3. [Fe]-hydrogenase models

Model studies of [Fe]-hydrogenase system are necessarily at an early stage, as knowledge from the crystal structure of active site and the EXAFS studies of the enzyme have only been recently published. But there is some early background chemistry available, which includes the synthesis of Fe centers with *cis*-CO. thiolate and pyridine ligands, similar to those in early stages of [FeFe]-hydrogenases.

4. Choice of ligand

Sulfur is an excellent ligand donor atom for wide range of metals, and the low ionization energy of sulfur as well as the existence of several lone pairs of electrons offers the possibility of a rich sulfur-based chemistry of the complexes.[91] All of these provide thiolate ligand a good starting point for the functional modeling of hydrogenases. A wider range of metals, including second and third row transition metal, seen to be quite promising in catalytic properties. The crystal structure reveals the existence of cysteine thiolate in all three kinds of hydrogenases, which makes thiolate ligand become essential to the structure modeling of hydrogenases. Two of major complications in coordination chemistry of thiolate ligands are C-S bond cleavage and the formation of thiolate-bridged oligomers. Both can be circumvented by the use of aromatic thiolate ligand with ortho-

substituents. The steric hindrance that the aromatic ring provides prevents polymerization and the aromatic C-S bond is generally strong enough to resist cleavage.

Similar to sulfur, phosphorus is also an electron rich ligand donor atom for wide range of metals. Even though phosphines are not found in the natural enzyme systems, the additional electron rich ligand provide extra stabilization to the metal center toward redox reactivity, which is one of the major tasks in functional modeling of hydrogenases.

Chelate complexes are known to be particularly stable, and the reactivity of the metal center may be studied without competing ligand substitution reactions. Compare to monodentate thiolate ligands, the polydentate thiolate ligands have the advantages of more control of the coordination number, stoichiometry and stereochemistry of the resulting metal complexes.[92] Polydentate ligands incorporating both thiolate and tertiary phosphine donor atoms form stable complexes with a wide range of metals including lanthanides and transition and post transition metals. To date, most studies have been focused on bidentate $Ph_2PCH_2CH_2SH$ or $Ph_2P(C_6H_4SH\text{-}2)$ ligands, while the potential tridentate ligand $PhP(C_6H_4SH\text{-}2)_2$ has received less attention. [93]

In this research, tridentate ligand $PhP(C_6H_4SH\text{-}2)_2$ and its derivative have been used with transition metals (Ni, Pd, Pt and Fe) and form modeling complexes whose chemical reactivity was studied.

5. General procedures

Synthetic Techniques

All reactions were carried out under a N_2 atmosphere using standard Schlenk techniques unless otherwise stated. Transfer of air sensitive solid was carried out in a dry box under N_2. All chemicals used are either commercially available or synthesized according to the published preparative methods. All solvents are commercially available and distilled under nitrogen with dying agents prior to use.

^{1}H NMR and ^{31}PNMR spectroscopy

^{1}H NMR and ^{31}P NMR spectra were recorded using a Varian-300 operating at 300MHz or a Varian-400 operating at 400MHz. All proton chemical shifts are referenced to the deuterated solvent and reported as parts per million (ppm) versus the references. All phosphorus spectra used 85% H_3PO_4 as an external reference with phosphorus shift set to 0 ppm. All phosphorus chemical shifts are reported as parts per million (ppm) versus the references.

Electrochemistry (CV)

Cyclic voltammetry (CV) studies were carried out by a BAS 100 potentiostat. The CV spectra were measured in a 2 ml-microelectrochemical cell with an Ag/AgCl electrode as the reference. A platinum electrode or a glassy carbon electrode was used as the working electrode and platinum wire as the counter electrode. The supporting electrolyte was potassium chloride (KCl) in aqueous solvent and tetrabutylammonium tetrafluoroborate in non-aqueous solvents. Typical concentration for the metal

complexes was 1 mM and the supporting electrolyte was one hundred times or more concentrated than the metal complex.

Infrared Spectroscopy (IR)

The infrared spectra were recorded with Thermo Scientific Nicolet iS10 FTIR spectrometer to a resolution of 4 cm^{-1}. Solid samples were prepared in njuol mull or potassium bromide (KBr) pellet. Solution samples were injected into a solution IR cell made of NaCl or CaF_2 with path length of 0.1mm.

Electronic Spectroscopy (UV-vis)

The electronic spectra were recorded with an HP-8453 UV-Visible spectrophotometer. A tungsten lamp was used for the visible region and a deuterium lamp for the ultraviolet region. All samples were prepared a 10-15mM concentration in quartz UV-VIS cells. Each solution was conducted with two pathlengths: 0.1mm and 1.0mm under nitrogen.

X-ray Diffraction

All X-ray crystallography data were obtained on an Oxford single crystal X-ray diffractometer operating at 50kV and 40mA, MoKα (λ = 0.71073 Å) radiation. The structure refinement was done with SHELXL-97 (Sheldrich). All oft the crystal structures were solved by direct methods, and anisotropic refinement for all non-hydrogen atoms was done by a full-matrix least-squares method.

References

(1) Heinekey, D. M. *J. Organomet. Chem.* **2009**, *694*, 2671.

(2) Zhang, Y. H. P. *Energy Environ. Sci.* **2009**, *2*, 272.

(3) Frey, M. *Chembiochem* **2002**, *3*, 153.

(4) Adams, M. W. W. *Biochim. Biophys. Acta* **1990**, *1020*, 115.

(5) Adams, M. W. W.; Stiefel, E. I. *Science* **1998**, *282*, 1842.

(6) Stephenson, M.; Stickland, L. H. *Biochem. J.* **1931**, *25*, 205.

(7) Shima, S.; Pilak, O.; Vogt, S.; Schick, M.; Stagni, M. S.; Meyer-Klaucke, W.; Warkentin, E.; Thauer, R. K.; Ermler, U. *Science* **2008**, *321*, 572.

(8) Volbeda, A.; Charon, M. H.; Piras, C.; Hatchikian, E. C.; Frey, M.; Fontecillacamps, J. C. *Nature* **1995**, *373*, 580.

(9) Tard, C.; Pickett, C. J. *Chem. Rev.* **2009**, *109*, 2245.

(10) Ogata, H.; Hirota, S.; Nakahara, A.; Komori, H.; Shibata, N.; Kato, T.; Kano, K.; Higuchi, Y. *Structure* **2005**, *13*, 1635.

(11) Volbeda, A.; Martin, L.; Cavazza, C.; Matho, M.; Faber, B. W.; Roseboom, W.; Albracht, S. P. J.; Garcin, E.; Rousset, M.; Fontecilla-Camps, J. C. *J. Biol. Inorg. Chem.* **2005**, *10*, 239.

(12) Lamle, S. E.; Albracht, S. P. J.; Armstrong, F. A. *J. Am. Chem. Soc* **2004**, *126*, 14899.

(13) Ogata, H.; Mizoguchi, Y.; Mizuno, N.; Miki, K.; Adachi, S.; Yasuoka, N.; Yagi, T.; Yamauchi, O.; Hirota, S.; Higuchi, Y. *J. Am. Chem. Soc* **2002**, *124*, 11628.

(14) Higuchi, Y.; Ogata, H.; Miki, K.; Yasuoka, N.; Yagi, T. *Structure* **1999**, *7*, 549.

(15) Leroux, F.; Dementin, S.; Burlatt, B.; Cournac, L.; Volbeda, A.; Champ, S.; Martin, L.; Guigliarelli, B.; Bertrand, P.; Fontecilla-Camps, J.; Rousset, M.; Leger, C. *Proc. Natl. Acad. Sci. U. S. A.* **2008**, *105*, 11188.

(16) Garcin, E.; Vernede, X.; Hatchikian, E. C.; Volbeda, A.; Frey, M.; Fontecilla-Camps, J. C. *Structure* **1999**, *7*, 557.

(17) Volbeda, A.; Garcin, E.; Piras, C.; deLacey, A. L.; Fernandez, V. M.; Hatchikian, E. C.; Frey, M.; FontecillaCamps, J. C. *J. Am. Chem. Soc* **1996**, *118*, 12989.

(18) De Lacey, A. L.; Fernandez, V. M.; Rousset, M.; Cammack, R. *Chem. Rev.* **2007**, *107*, 4304.

(19) Vanderzwaan, J. W.; Coremans, J.; Bouwens, E. C. M.; Albracht, S. P. J. *Biochim. Biophys. Acta* **1990**, *1041*, 101.

(20) Trofanchuk, O.; Stein, M.; Gessner, C.; Lendzian, F.; Higuchi, Y.; Lubitz, W. *J. Biol. Inorg. Chem.* **2000**, *5*, 36.

(21) Gessner, C.; Trofanchuk, O.; Kawagoe, K.; Higuchi, Y.; Yasuoka, N.; Lubitz, W. *Chem. Phys. Lett.* **1996**, *256*, 518.

(22) Carepo, M.; Tierney, D. L.; Brondino, C. D.; Yang, T. C.; Pamplona, A.; Telser, J.; Moura, I.; Moura, J. J. G.; Hoffman, B. M. *J. Am. Chem. Soc* **2002**, *124*, 281.

(23) Osz, J.; Bagyinka, C. *Biophys. J.* **2005**, *89*, 1984.

(24) De Lacey, A. L.; Moiroux, J.; Bourdillon, C. *Eur. J. Biochem.* **2000**, *267*, 6560.

(25) Leger, C.; Jones, A. K.; Roseboom, W.; Albracht, S. P. J.; Armstrong, F. A. *Biochemistry* **2002**, *41*, 15736.

(26) Niu, S. Q.; Thomson, L. M.; Hall, M. B. *J. Am. Chem. Soc* **1999**, *121*, 4000.

(27) Foerster, S.; Stein, M.; Brecht, M.; Ogata, H.; Higuchi, Y.; Lubitz, W. *J. Am. Chem. Soc* **2003**, *125*, 83.

(28) Pardo, A.; De Lacey, A. L.; Fernandez, V. M.; Fan, H. J.; Fan, Y. B.; Hall, M. B. *J. Biol. Inorg. Chem.* **2006**, *11*, 286.

(29) Brecht, M.; van Gastel, M.; Buhrke, T.; Friedrich, B.; Lubitz, W. *J. Am. Chem. Soc* **2003**, *125*, 13075.

(30) Siegbahn, P. E. M. In *Advances in Inorganic Chemistry - Including Bioinorganic Studies, Vol 56*; Elsevier Academic Press Inc: San Diego, 2004; Vol. 56, p 101.

(31) Foerster, S.; van Gastel, M.; Brecht, M.; Lubitz, W. *J. Biol. Inorg. Chem.* **2005**, *10*, 51.

(32) De Gioia, L.; Fantucci, P.; Guigliarelli, B.; Bertrand, P. *Int. J. Quantum Chem.* **1999**, *73*, 187.

(33) Volbeda, A.; Fontecilla-Camps, J. C. *Coord. Chem. Rev.* **2005**, *249*, 1609.

(34) Leger, C.; Jones, A. K.; Albracht, S. P. J.; Armstrong, F. A. *J. Phys. Chem. B* **2002**, *106*, 13058.

(35) Fichtner, C.; van Gastel, M.; Lubitz, W. *Phys. Chem. Chem. Phys.* **2003**, *5*, 5507.

(36) Vignais, P. M. *Coord. Chem. Rev.* **2005**, *249*, 1677.

(37) Vignais, P. M.; Billoud, B.; Meyer, J. *Fems Microbiol. Rev.* **2001**, *25*, 455.

(38) Peters, J. W.; Lanzilotta, W. N.; Lemon, B. J.; Seefeldt, L. C. *Science* **1998**, *282*, 1853.

(39) Nicolet, Y.; Piras, C.; Legrand, P.; Hatchikian, C. E.; Fontecilla-Camps, J. C. *Struct. Fold. Des.* **1999**, *7*, 13.

(40) Popescu, C. V.; Munck, E. *J. Am. Chem. Soc* **1999**, *121*, 7877.

(41) Cao, Z. X.; Hall, M. B. *J. Am. Chem. Soc* **2001**, *123*, 3734.

(42) Liu, Z. P.; Hu, P. *J. Am. Chem. Soc* **2002**, *124*, 5175.

(43) Siegbahn, P. E. M.; Tye, J. W.; Hall, M. B. *Chem. Rev.* **2007**, *107*, 4414.

(44) De Lacey, A. L.; Stadler, C.; Cavazza, C.; Hatchikian, E. C.; Fernandez, V. M. *J. Am. Chem. Soc* **2000**, *122*, 11232.

(45) Razavet, M.; Borg, S. J.; George, S. J.; Best, S. P.; Fairhurst, S. A.; Pickett, C. J. *Chem. Commun.* **2002**, 700.

(46) George, S. J.; Cui, Z.; Razavet, M.; Pickett, C. J. *Chem. Eur. J.* **2002**, *8*, 4037.

(47) Fritz, G.; Griesshaber, D.; Seth, O.; Kroneck, P. M. H. *Biochemistry* **2001**, *40*, 1317.

(48) Bruschi, M.; Fantucci, P.; De Gioia, L. *Inorg. Chem.* **2003**, *42*, 4773.

(49) Zhou, T. J.; Mo, Y. R.; Liu, A. M.; Zhou, Z. H.; Tsai, K. R. *Inorg. Chem.* **2004**, *43*, 923.

(50) Ryde, U.; Greco, C.; De Gioia, L. *J. Am. Chem. Soc* **2010**, *132*, 4512.

(51) Roseboom, W.; De Lacey, A. L.; Fernandez, V. M.; Hatchikian, E. C.; Albracht, S. P. J. *J. Biol. Inorg. Chem.* **2006**, *11*, 102.

(52) Albracht, S. P. J.; Roseboom, W.; Hatchikian, E. C. *J. Biol. Inorg. Chem.* **2006**, *11*, 88.

(53) Lyon, E. J.; Shima, S.; Boecher, R.; Thauer, R. K.; Grevels, F. W.; Bill, E.; Roseboom, W.; Albracht, S. P. J. *J. Am. Chem. Soc* **2004**, *126*, 14239.

(54) Yang, X. Z.; Hall, M. B. *J. Am. Chem. Soc* **2008**, *130*, 14036.

(55) Hiromoto, T.; Ataka, K.; Pilak, O.; Vogt, S.; Stagni, M. S.; Meyer-Klaucke, W.; Warkentin, E.; Thauer, R. K.; Shima, S.; Ermler, U. *FEBS Lett.* **2009**, *583*, 585.

(56) Halcrow, M. A.; Christou, G. *Chem. Rev.* **1994**, *94*, 2421.
(57) Kruger, H. J.; Peng, G.; Holm, R. H. *Inorg. Chem.* **1991**, *30*, 734.
(58) Yamamura, T.; Tadokoro, M.; Nakamura, N.; Tanaka, K.; Asakura, K. *Bull. Chem. Soc. Jpn.* **1990**, *63*, 999.
(59) Kruger, H. J.; Holm, R. H. *Inorg. Chem.* **1987**, *26*, 3645.
(60) Lai, C. H.; Reibenspies, J. H.; Darensbourg, M. Y. *Angew. Chem. Int. Edit.* **1996**, *35*, 2390.
(61) Osterloh, F.; Saak, W.; Haase, D.; Pohl, S. *Chem. Commun.* **1997**, 979.
(62) Davies, S. C.; Evans, D. J.; Hughes, D. L.; Longhurst, S.; Sanders, J. R. *Chem. Commun.* **1999**, 1935.
(63) Smith, M. C.; Barclay, J. E.; Cramer, S. P.; Davies, S. C.; Gu, W. W.; Hughes, D. L.; Longhurst, S.; Evans, D. J. *J. Chem. Soc.-Dalton Trans.* **2002**, 3410.
(64) Zhu, W. F.; Marr, A. C.; Wang, Q.; Neese, F.; Spencer, D. J. E.; Blake, A. J.; Cooke, P. A.; Wilson, C.; Schroder, M. *Proc. Natl. Acad. Sci. U. S. A.* **2005**, *102*, 18280.
(65) Canaguier, S.; Artero, V.; Fontecave, M. *Dalton Trans.* **2008**, 315.
(66) Sellmann, D.; Geipel, F.; Lauderbach, F.; Heinemann, F. W. *Angew. Chem. Int. Edit.* **2002**, *41*, 632.
(67) Li, Z. L.; Ohki, Y.; Tatsumi, K. *J. Am. Chem. Soc* **2005**, *127*, 8950.
(68) Chen, C. H.; Chang, Y. S.; Yang, C. Y.; Chen, T. N.; Lee, C. M.; Liaw, W. F. *Dalton Trans.* **2004**, 137.
(69) Contakes, S. M.; Hsu, S. C. N.; Rauchfuss, T. B.; Wilson, S. R. *Inorg. Chem.* **2002**, *41*, 4610.
(70) Chiarella, G. M.; Melgarejo, D. Y.; Koch, S. A. *J. Am. Chem. Soc* **2006**, *128*, 1416.
(71) Jiang, J. F.; Koch, S. A. *Angew. Chem. Int. Edit.* **2001**, *40*, 2629.
(72) Jiang, J. F.; Koch, S. A. *Inorg. Chem.* **2002**, *41*, 158.
(73) Jiang, J. F.; Acunzo, A.; Koch, S. A. *J. Am. Chem. Soc* **2001**, *123*, 12109.
(74) Liaw, W. F.; Lee, J. H.; Gau, H. B.; Chen, C. H.; Jung, S. J.; Hung, C. H.; Chen, W. Y.; Hu, C. H.; Lee, G. H. *J. Am. Chem. Soc* **2002**, *124*, 1680.
(75) Liaw, W. F.; Lee, N. H.; Chen, C. H.; Lee, C. M.; Lee, G. H.; Peng, S. M. *J. Am. Chem. Soc* **2000**, *122*, 488.
(76) Kayal, A.; Rauchfuss, T. B. *Inorg. Chem.* **2003**, *42*, 5046.
(77) Sellmann, D.; Geipel, F.; Heinemann, F. W. *Chem. Eur. J.* **2002**, *8*, 958.
(78) Perra, A.; Davies, E. S.; Hyde, J. R.; Wang, Q.; McMaster, J.; Schroder, M. *Chem. Commun.* **2006**, 1103.
(79) Lyon, E. J.; Georgakaki, I. P.; Reibenspies, J. H.; Darensbourg, M. Y. *Angew. Chem. Int. Edit.* **1999**, *38*, 3178.
(80) Schmidt, M.; Contakes, S. M.; Rauchfuss, T. B. *Journal of the American Chemical Society* **1999**, *121*, 9736.
(81) Le Cloirec, A.; Best, S. P.; Borg, S.; Davies, S. C.; Evans, D. J.; Hughes, D. L.; Pickett, C. J. *Chem. Commun.* **1999**, 2285.
(82) Nehring, J. L.; Heinekey, D. M. *Inorg. Chem.* **2003**, *42*, 4288.
(83) Gloaguen, F.; Lawrence, J. D.; Rauchfuss, T. B. *Journal of the American Chemical Society* **2001**, *123*, 9476.
(84) Zhao, X.; Georgakaki, I. P.; Miller, M. L.; Mejia-Rodriguez, R.; Chiang, C. Y.; Darensbourg, M. Y. *Inorg. Chem.* **2002**, *41*, 3917.

(85) Barton, B. E.; Rauchfuss, T. B. *Inorg. Chem.* **2008**, *47*, 2261.
(86) Barton, B. E.; Zampella, G.; Justice, A. K.; De Gioia, L.; Rauchfuss, T. B.; Wilson, S. R. *Dalton Trans.* **2010**, *39*, 3011.
(87) Olsen, M. T.; Barton, B. E.; Rauchfuss, T. B. *Inorg. Chem.* **2009**, *48*, 7507.
(88) Popescu, C. V.; Munck, E. *Journal of the American Chemical Society* **1999**, *121*, 7877.
(89) Liu, T. B.; Darensbourg, M. Y. *J. Am. Chem. Soc* **2007**, *129*, 7008.
(90) Singleton, M. L.; Bhuvanesh, N.; Reibenspies, J. H.; Darensbourg, M. Y. *Angew. Chem. Int. Edit.* **2008**, *47*, 9492.
(91) Dilworth, J. R.; Wheatley, N. *Coord. Chem. Rev.* **2000**, *199*, 89.
(92) Cotton, F. A.; Eglin, J. L.; Hong, B.; James, C. A. *J. Am. Chem. Soc* **1992**, *114*, 4915.
(93) Fernandez, P.; Sousa-Pedrares, A.; Romero, J.; Garcia-Vazquez, J. A.; Sousa, A.; Perez-Lourido, P. *Inorg. Chem.* **2008**, *47*, 2121.

Chapter 2

Synthesis of Metal-thiolate Complexes

(M=Ni, Pd, Pt)

1. INTRODUCTION

Metal–thiolate bonds are present in many classes of metalloenzyme active sites and make major contributions to their function.[1] The enzyme centers involved in electron transfer include the metal-sulfur sites, which have thiolate–metal bonds of cysteine residues coupling them into the protein matrix.

In order to explore the possibilities of metal thiolate chemistry, we have synthesized polydentate phosphine-thiolate ligands with substituents on the phenyl group to which the thiol group is bound. The work presented in this chapter is focused on the preparation, isomer isolation and characterization of the metal thiolate complexes: $[M^{II}(PS2'H)_2]$ and $[M^{IV}(PS2')_2]$ (M=Ni, Pd and Pt).

The isolation of Ni-thiolate species in different oxidation states, of which some are rare such as Ni(III) and Ni(IV), are important in the catalytic cycle of hydrogenase enzymes. It is notable that for the Ni-thiolate complexes, the redox series shows: $[Ni^{II}(PS2')_2]^{2-}$= $[Ni^{III}(PS2')_2]^{1-}$ = $[Ni^{IV}(PS2')_2]$ two single electron redox steps. The assignments of the oxidation states of metal centers were confirmed by Ni K-edge XAS.

Only the *trans-anti* isomer of $[Ni^{II}(PS2'H)_2]$, was characterized by X-ray crystallography. The opportunity to isolate isomers of $[Pt^{II}(PS2'H)_2]$ is exciting. For the $[M^{II}(PS2'H)_2]$ complexes, there are four possible isomers: the *trans-anti*-$[Pt^{II}(PS2'H)_2]$, *trans-syn*-$[Pt^{II}(PS2'H)_2]$, *cis-anti*-$[Pt^{II}(PS2'H)_2]$, and *cis-syn*-$[Pt^{II}(PS2'H)_2]$ as shown in **Scheme II-1**. All four possible isomers of $[Pt^{II}(PS2'H)_2]$ have been detected in the ^1H and ^{31}P NMR spectra, and the structures of three of the isomers have been characterized

by X-ray crystallography. The ability to identify the isomers using NMR spectroscopy and X-ray crystallography provide us with more insight of the nature of this modeling system.

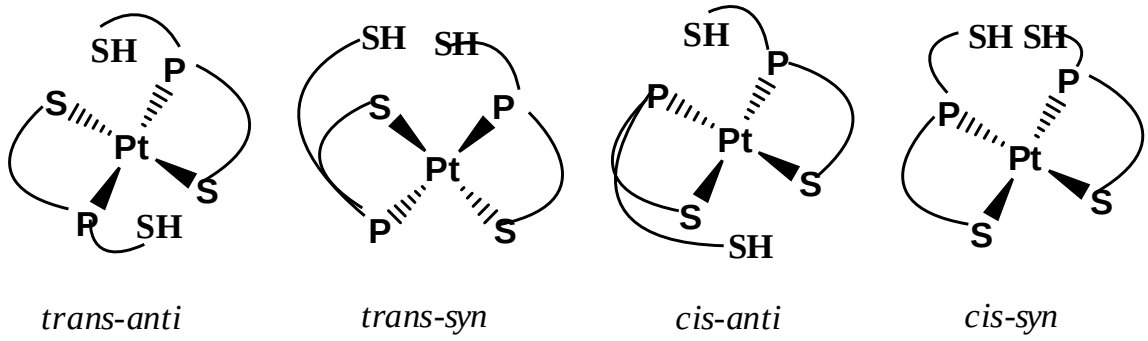

trans-anti *trans-syn* *cis-anti* *cis-syn*

Scheme II- 1. All four possible isomers of $[Pt^{II}(PS2'H)_2]$.

Theoretically, there are three possible isomers of $[Ni^{IV}(PS2')_2]$: *cis*-$[Ni^{IV}(PS2')_2]$, *trans-fac*-$[Ni^{IV}(PS2')_2]$ and *trans-mer*-$[Ni^{IV}(PS2')_2]$, as shown in **Scheme II-2**. We are able to isolate *cis*-$[Ni^{IV}(PS2')_2]$ and *trans-fac*-$[Ni^{IV}(PS2')_2]$ and characterize them by ^{1}H and ^{31}P NMR spectroscopy.

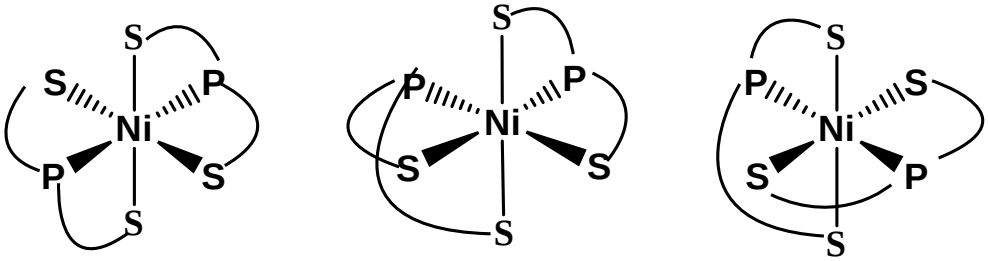

trans-fac *cis* *trans-mer*

Scheme II- 2. The three possible isomers of $[Ni^{IV}(PS2')_2]$.

2. RESULTS AND DISCUSSION

The ligand that we used for this series of complexes are: [bis-phenyl-(5-methyl-2-thio-phenyl)phosphine] (abbreviated H(PS1')), [bis(5-methyl-2-thio-phenyl)phenyl-phosphine] (abbreviated H_2(PS2')), and [bis(*ortho*-thio-phenyl)phenylphosphine] (abbreviated H_2(PS2). **Scheme II-3** shows the structure of these ligands:

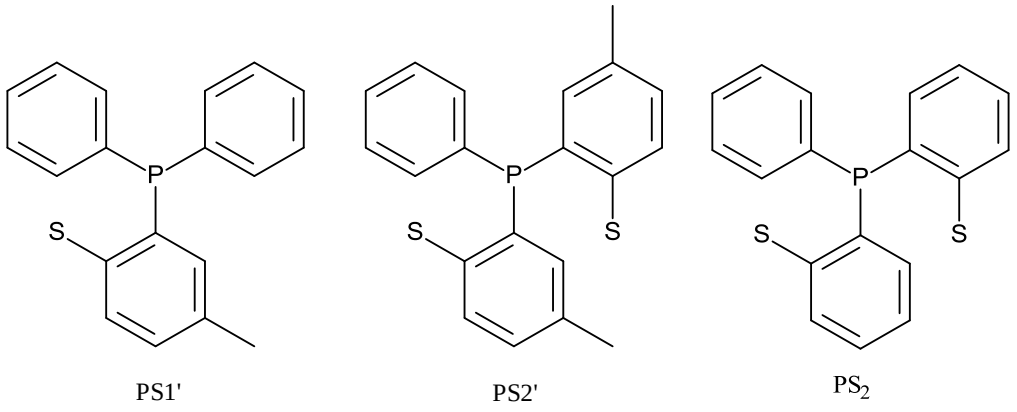

PS1' PS2' PS_2

Scheme II- 3. Structure of ligands

The preparation of ligands have been reported previously,[2] and previous members from Millar and Koch groups, successfully optimized the synthetic routes with better yields. The ligands used in this chapter were prepared by following the optimized route, or were graciously donated by Daniel Amarante.

Synthesis of $[M^{II}(PS2'H)_2]$ (M=Ni, Pd, Pt)

The $[M^{II}(PS2'H)_2]$ complexes comprise a series in which a thiol group of the ligand is not covalently bound to the metal but is able to interact through an -SH···M hydrogen bond with the metal center. The thiol -SH group orients itself toward the metal center. There are four possible isomers for the $[M^{II}(PS2'H)_2]$ complexes, as shown in **Scheme II-4**. For each of the metals Ni, Pd and Pt, the major product from the synthetic route is the *trans-anti*-isomer.

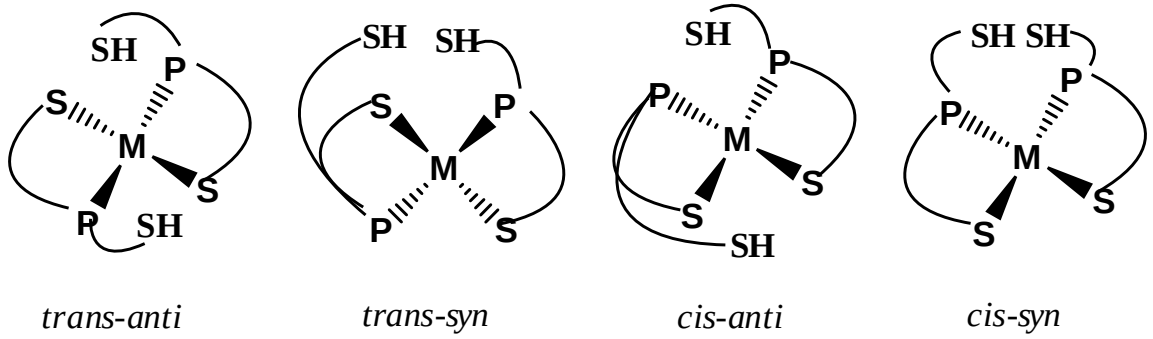

trans-anti *trans-syn* *cis-anti* *cis-syn*

Scheme II- 4. All four possible isomers of $[M^{II}(PS2'H)_2]$.

Previously, Beatty and Voorhies in the Millar group, prepared the *trans-anti*-$[Ni^{II}(PS2'H)_2]$ complex, from nickel (II) chloride hexahydrate and the mono-deprotonated lithium thiolate salt Li(HPS2'). The *trans-anti*-$[Ni^{II}(PS2'H)_2]$ rapidly isomerizes into mixture of and *trans-syn*-isomers on NMR time scale. We are reporting a higher yield synthetic route from the reaction of nickel acetylacetonate with the fully protonated ligand.

Previously, Voorhies prepared $[Pd^{II}(PS2'H)_2]$ and $[Pt^{II}(PS2'H)_2]$ from $PdCl_2(benzonitrile)_2$/ $PtCl_2(benzonitrile)_2$ and the mono-deprotonated lithium thiolate salt, Li(HPS2'). We report new synthetic routes: with palladium acetylacetonate and the fully

protonated ligand, or with K_2PdCl_4/ K_2PtCl_4 with the mono-deprotonated lithium thiolate salt Li(HPS2'). The metal reactants for the new routes are commercially available, and the products are easier to isolate with higher yields. The X-ray crystal structures were repeated using our new Oxford Gemini X-ray diffractometer, which is equipped with a low temperature attachment. Data with much higher resolution was collected at 100K which enabled the location and the refinement of the SH protons of the pendant thiol groups.

X-ray Crystallography Structures of *trans-anti*-[M^{II}(PS2'H)$_2$] (M=Ni, Pd, Pt)

The crystals of *trans-anti*-[M^{II}(PS2'H)$_2$] (M=Ni, Pd, Pt) were obtained by recrystallization of the isolated synthetic reaction products. The crystals for the three-[M^{II}(PS2'H)$_2$] (M=Ni, Pd, Pt) compounds, which were obtained by recrystallization from methylene chloride and hexane, are isomorphous and isostructural. The structures show a *trans* arrangement of the P and S donors and with the two pendant non coordinated thiols on opposite sides of the [MS_2P_2] square plane; we designate these structures as the *trans-anti* isomer. In these structures (**Figure II-1, Figure II-2 and Figure II-3**), the thiophenol rings occupy the position equatorial to the [MS_2P_2] plane. The equatorial thiophenol ring are neatly perpendicular to the axial phenyl rings. The P1-M-S1 angle of all the trans-*anti*-[M^{II}(PS2'H)$_2$] (M=Ni, Pd, Pt) complexes are about 90 º, which with the 180 º angle of P1-M-P1 reinforces the expected square planar geometry.

Bond length*(Å)*	***trans-anti*-[$Ni^{II}(PS2'H)_2$] 2CH_2Cl_2**	***trans-anti*-[$Pd^{II}(PS2'H)_2$] 2CH_2Cl_2**	***trans-anti*-[$Pt^{II}(PS2'H)_2$] 2CH_2Cl_2**
M-P1	2.1709(3)	2.2819(3)	2.2796(5)
M-S1(bonded)	2.1881(3)	2.3221(3)	2.3209(5)
M-S2(non bonded)	3.4717(4)	3.5199(4)	3.5683(5)
M-H1	2.561(18)	2.521 (22)	2.369 (26)
H1-S2	1.21 (2)	1.19(2)	1.24(3)
S2-C8	1.7800(14)	1.7787(14)	1.7705(19)
Angle(°)			
P1-M-P1	180.000(17)	180.000(16)	180.00(2)
P1-M-S1	87.619(11)	85.410(11)	85.819(16)
P1-M-H1	79.6(3)	77.3(4)	71.7(5)
S1-M-H1	108.2(4)	103.7(4)	97.2(4)
Unit Cell			
Space group	Pbca	Pbca	Pbca
Volume($Å^3$)	4072.90(9)	4109.43(8)	4106.76(10)

Table II- 1. Selected distances, angles and unit cell parameter for *trans-anti*-[$M^{II}(PS2'H)_2$] (M=Ni, Pd, Pt)

Although the structures of the *trans-anti*-[$M^{II}(PS2'H)_2$] (M=Ni, Pd, Pt) complexes are essentially the same, the difference in atomic radius of the metal does impose some

changes in the bond angles and distances. Both ionic (+2) and covalent radii of palladium and platinum are similar, and are significantly larger than for nickel. The M-P1 distance in *trans-anti*-[$Ni^{II}(PS2'H)_2$] is much shorter than in the Pd and Pt complexes(**Table II-1**). In all three compounds the SH protons of the pendant thiols were clear in the difference Fourier maps and were successfully refined. Therefore, reliable M-H1 distances are reported. Unlike the M-S1 bond and M-P1 bond, the M-H1 distance is shorter as you move down the periodical table. The Ni-H1 distance is 2.561(18), whereas Pd-H1 is 2.521(22) and Pt-H1 is 2.369(26). The M-H1 distances reveal a strong hydrogen bonding between metal center and thiol proton. The –SH thiols are not coordinated, but are in the second order coordination sphere. The angle of P1-M-H1 and S1-M-H1 enforce the location of the thiol proton in a location from which it can advantageously interact with the d_Z^2 orbital.

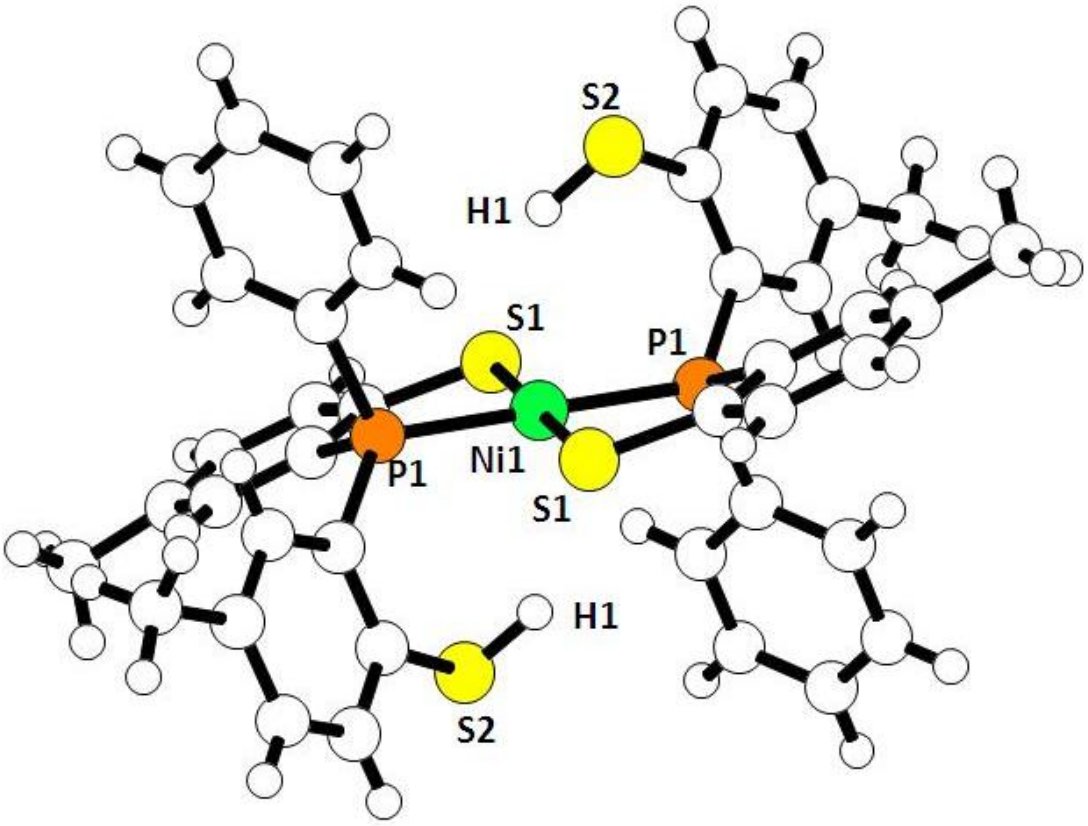

Figure II- 1. X-ray crystal structure of *trans-anti*-[$Ni^{II}(PS2'H)_2$] $2CH_2Cl_2$, Chem-Ray structure. The solvent molecules are omitted for clarity.

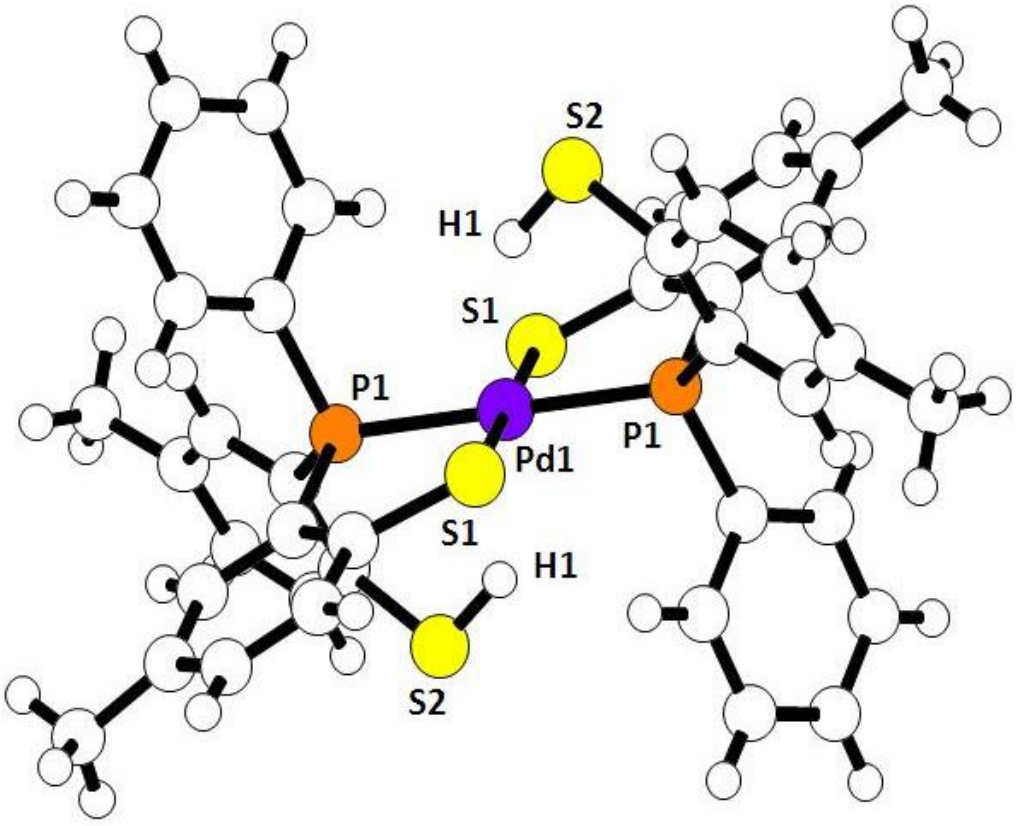

Figure II- 2. X-ray crystal structure of *trans-anti*-[$Pd^{II}(PS2'H)_2$] $2CH_2Cl_2$, Chem-Ray structure. The solvent molecules are omitted for clarity.

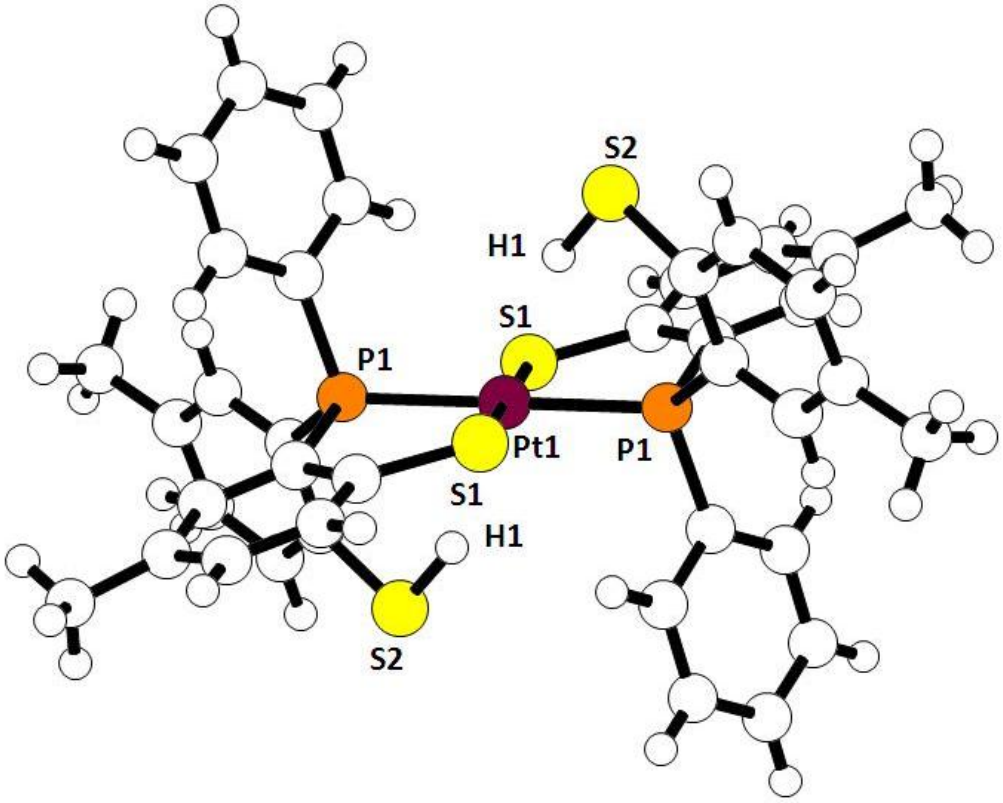

Figure II- 3. X-ray crystal structure of *trans-anti*-[$Pt^{II}(PS2'H)_2$] $2CH_2Cl_2$, Chem-Ray structure. The solvent molecules are omitted for clarity.

NMR of [$M^{II}(PS2'H)_2$] (M=Ni, Pd, Pt) and phosphorus decoupling

Even though we only observe crystals of the *trans-anti-* isomer as the synthetic products throughout the whole series of [$M^{II}(PS2'H)_2$] compounds, two phosphorus resonances are observed in the ^{31}P NMR spectrum of [$Ni^{II}(PS2'H)_2$] in $CDCl_3$ and other solvents(**Figure II-5**). We assign the two resonances to the *trans-syn-* and *trans-anti-*

isomers, which are almost in a 1:1 ratio. This assignment is supported by the ^{1}H NMR of the same sample (**Figure II-4**), where two sets of –SH, methyl and aromatic peaks are observed at 1:1 ratio. The methyl peaks are the most structurally informative; the methyl groups are chemically equivalent in one isomer and are chemically inequivalent in the other.

Similar results are observed for $[Pd^{II}(PS2'H)_2]$, with a *trans-syn-* and *trans-anti-* ratio of 1:2 ratio(**Figure II-6**). By contrast, in the case of the $[Pt^{II}(PS2'H)_2]$ compound, only pure *trans-anti-* isomer is observed in the ^{1}H and ^{31}P NMR spectrum. Interestingly, the only thiol peak observed in $[Pt^{II}(PS2'H)_2]$ is exceptionally complicated, with two side bands on addition to a triplet(**Figure II-8**). The triplet is a virtual triplet that is resulted from thiol proton coupled with both its own and the *trans* phosphorus nucleus; while the side bands are resulted from proton-platinum coupling (J_{Pt-H}=15Hz) (^{195}Pt, I=1/2, natural abundance 33.8%). The area difference between the broad band and "virtual triplet" agreed with the difference in natural abundance between ^{31}P and ^{195}Pt

Support for the existence of hydrogen-bonding interactions in the $[M^{II}(PS2'H)_2]$ complexes is observed in their ^{1}H NMR spectra. Hydrogen-bonding interactions tend to shift peaks downfield of their counterpart nonbonded positions.[3] The thiol proton of free $[PS2'H_2]$ is reported at 4.02 ppm in its ^{1}H NMR spectrum.[4] As shown in **Table II-2**, all three of the $[M^{II}(PS2'H)_2]$ complexes have thiol resonances which are shifted downfield, which is an indication of pendant thiols being in the secondary coordination sphere.

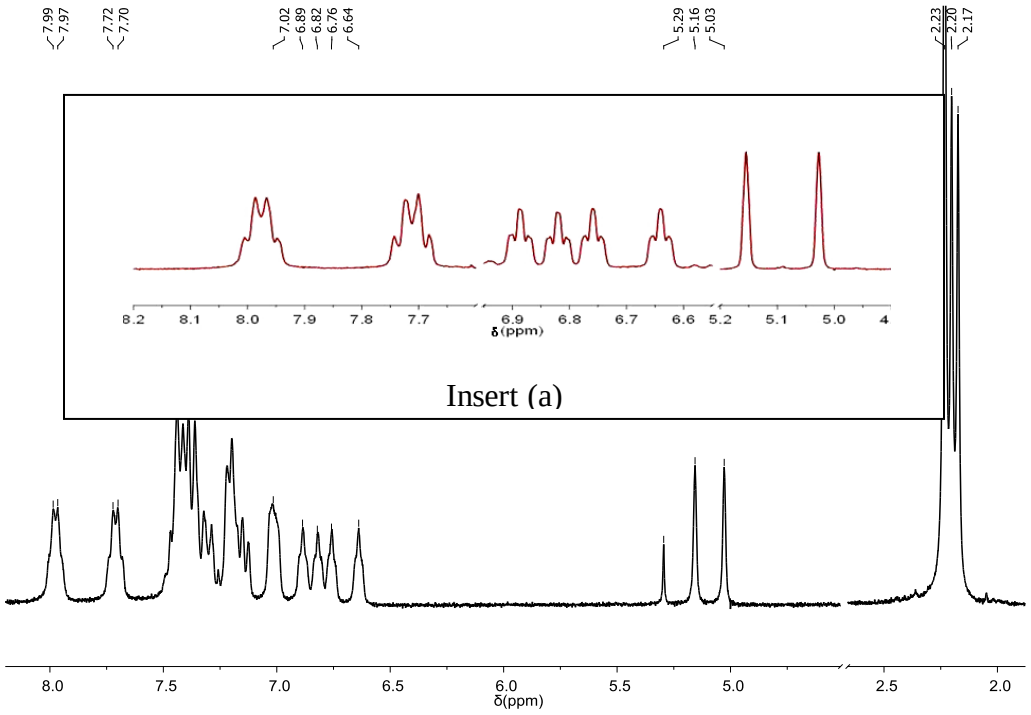

Figure II- 4. ^{1}H NMR spectrum of $[Ni^{II}(PS2'H)_2]$ in $CDCl_3$, 300MHz; insert(a) the zoom in of coupling proton-phosphorus peaks

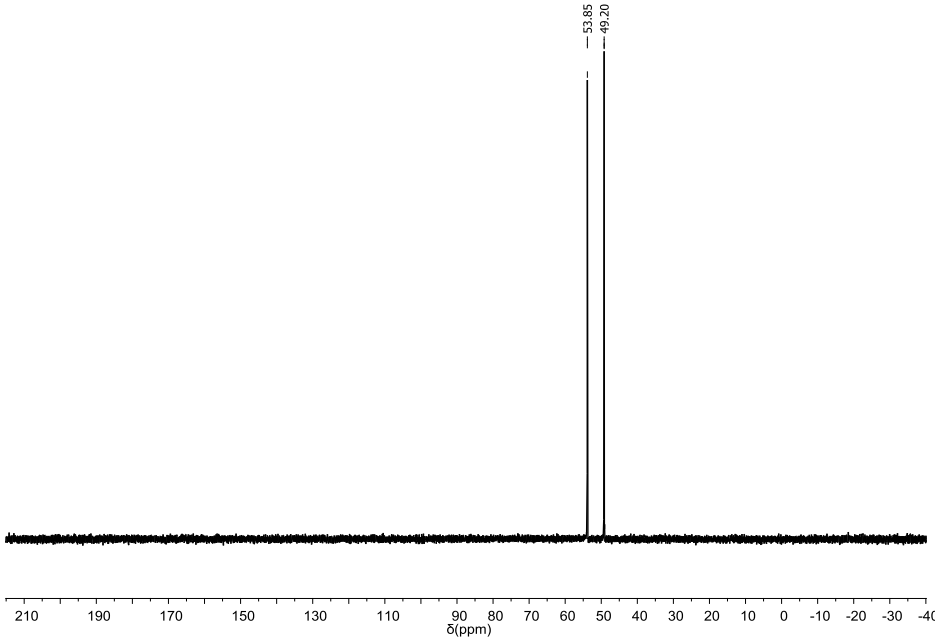

Figure II- 5. ^{31}P NMR spectrum of $[Ni^{II}(PS2'H)_2]$ in $CDCl_3$, 300MHz

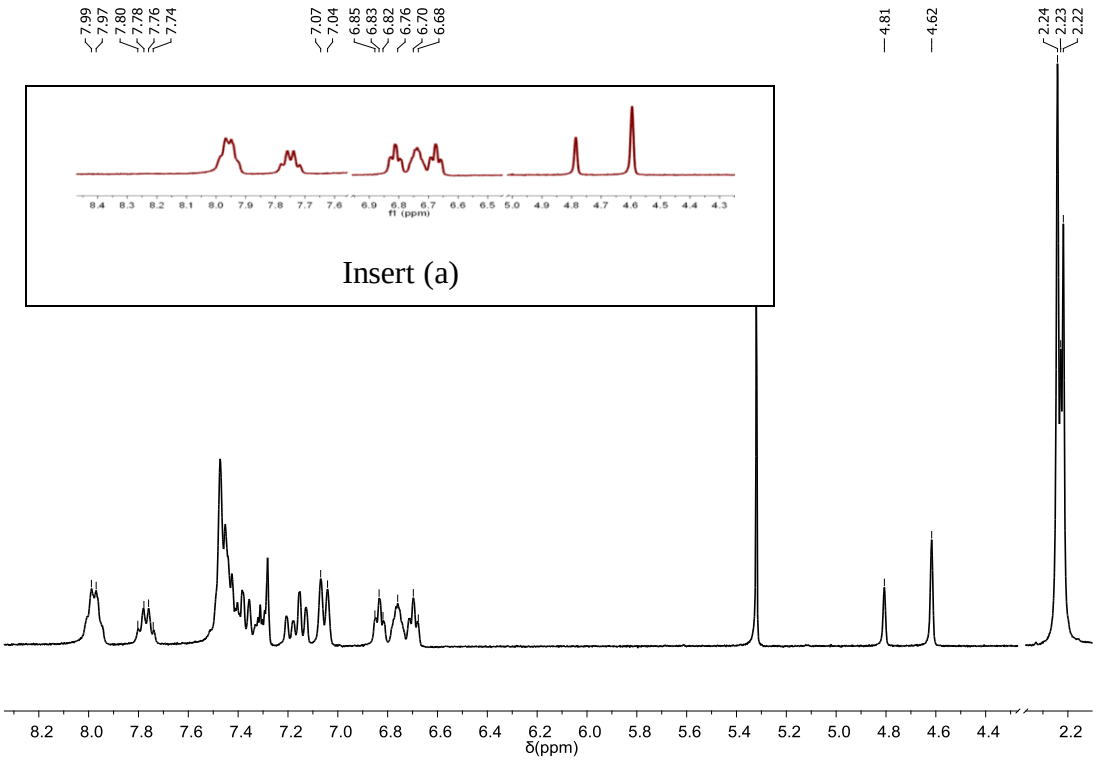

Figure II- 6. ^{1}H NMR spectrum of $[Pd^{II}(PS2'H)_2]$ in $CDCl_3$, 300MHz; insert(a) the zoom in of coupling proton-phosphorus peaks

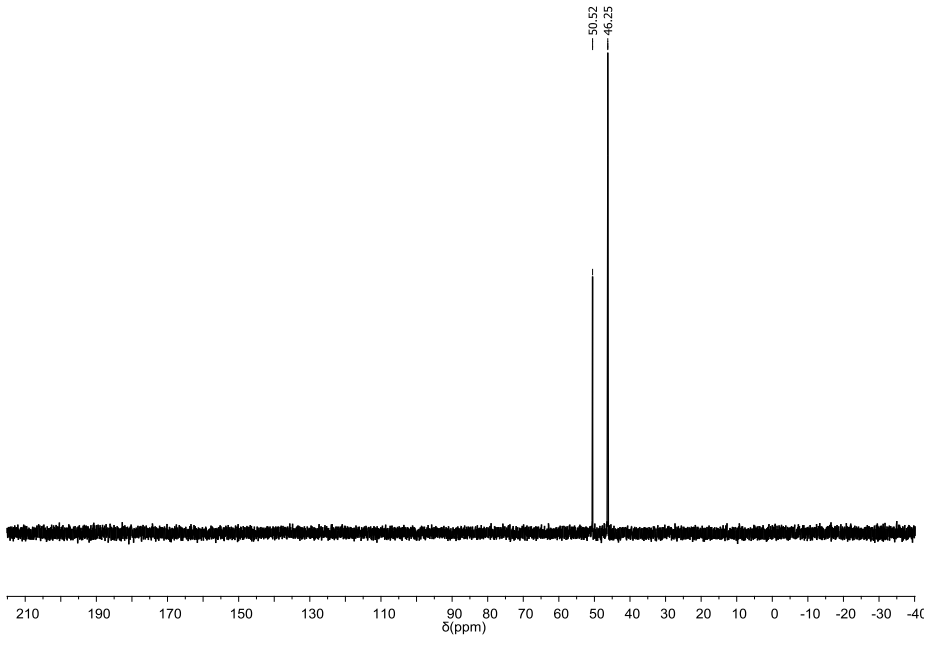

Figure II- 7. ^{31}P NMR spectrum of $[Pd^{II}(PS2'H)_2]$ in $CDCl_3$, 300MHz

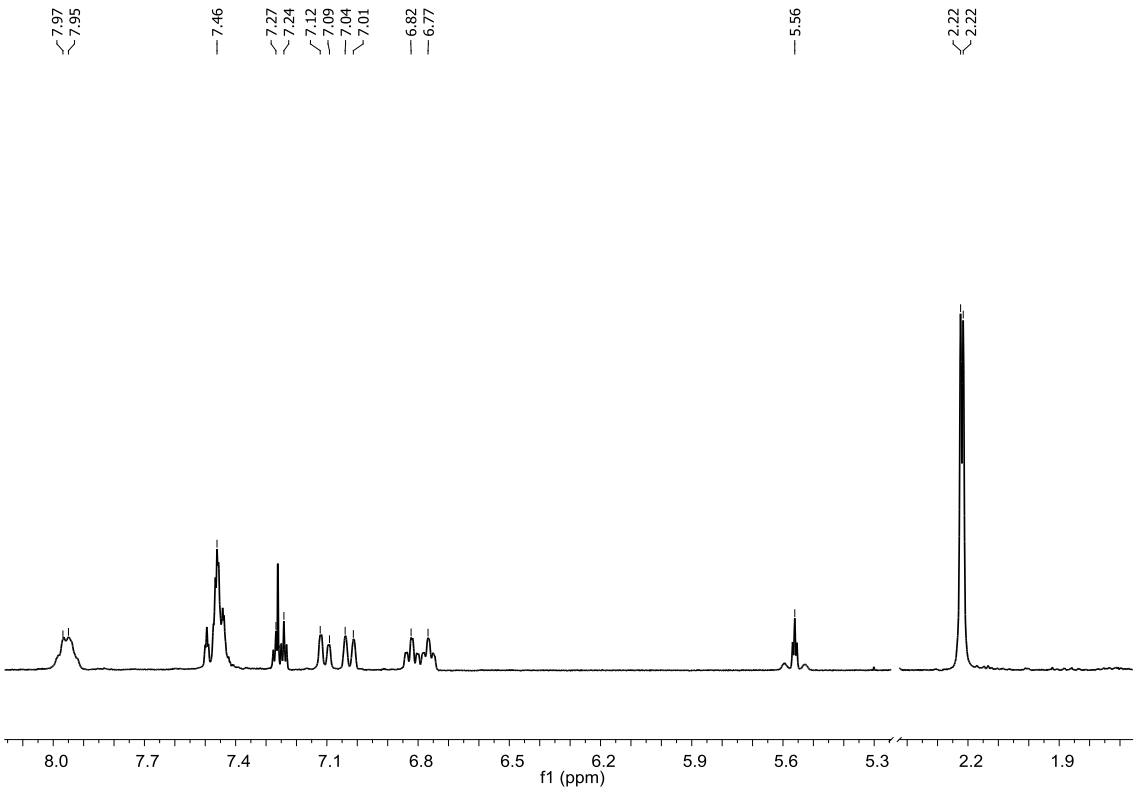

Figure II- 8. ^{1}H NMR spectrum of $[Pt^{II}(PS2'H)_2]$ in $CDCl_3$, 400MHz

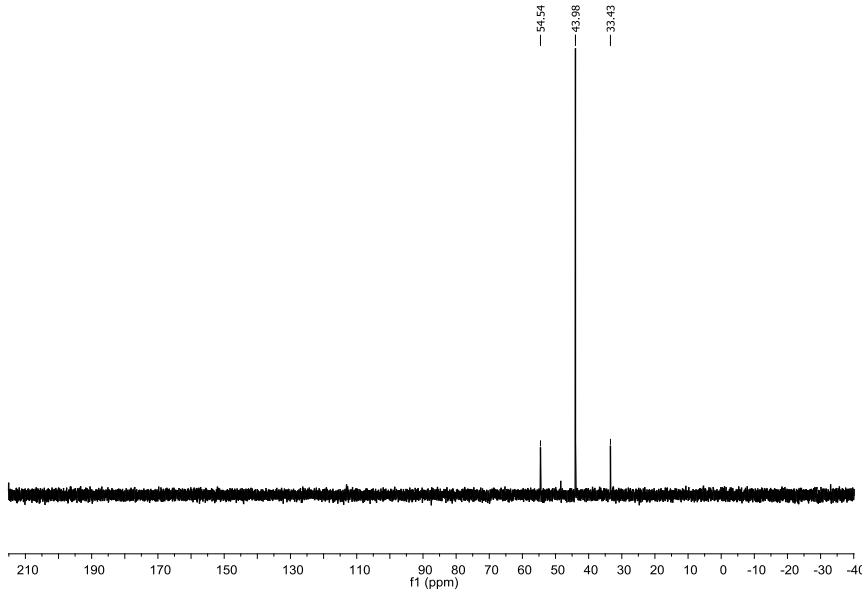

Figure II- 9. ^{31}P NMR spectrum of $[Pt^{II}(PS2'H)_2]$ in $CDCl_3$, 300MHz

Table II-2 also reveals that the ^{31}P shift for the *trans-anti-* isomers shifted upfield along the group, which confirmed the back bonding nature of phosphine coordinated transition metal and the Pt-phosphine back bonding being strongest due to the hydrogen bonding with pendant thiol proton.

	^{31}P resonances(ppm) *trans-syn*; *trans-anti*	-SH peaks(ppm) *trans-syn*; *trans-anti*	$-CH_3$ peaks(ppm) *trans-syn*; *trans-anti*
$[Ni^{II}(PS2'H)_2]$	53.85; 49.20	5.16; 5.03	2.23; 2.17/2.20
$[Pd^{II}(PS2'H)_2]$	50.52; 46.25	4.81;4.62	2.24; 2.23/2.22
$[Pt^{II}(PS2'H)_2]$	43.98	5.56	2.22/2.22;-

Table II- 2. NMR spectra of $[M^{II}(PS2'H)_2]$ (M=Ni, Pd, Pt)

It is notable that the peaks at around 6.8ppm and 7.9ppm in ^1H NMR spectra of $[M^{II}(PS2'H)_2]$ appear as triplets (**Figure II-4**, insert (a); **Figure II-6**, insert (a); **Figure II-8**). Instead of resulting from coupling to two equivalent nuclei, these triplets are "virtual triplet" as is the thiol resonance in $[Pt^{II}(PS2'H)_2]$. The virtual coupling nature is confirmed by ^{31}P-decoupled ^1H NMR spectra. The spectra of the ^{31}P-decoupled ^1H NMR study are shown in **Figure II-10** and **Figure II-11** for $[Ni^{II}(PS2'H)_2]$ and $[Pd^{II}(PS2'H)_2]$ respectively. When the phosphorus of *trans-anti-* isomer (49.199ppm) is decoupled, the triplet at 6.64, 6.89 and 7.98ppm sharpened into singlets, which confirmed the P-H coupling. A first order interpretation of the splitting pattern would be that the protons are coupled to two equivalent P atoms. Such an interpretation is obviously inconsistent with the geometric relationship between the protons and the two P atoms. Such so called

"virtual triplet" have been observed in the reported literature, where the coupling of the proton to two equivalent phosphorus nuclei with large $^{2}J_{(P,P)}$ coupling.[5] In particular, this has been frequently seen in square complexes with two *trans* phosphorous donors. Thus the 6.64, 6.89 and 7.98 ppm peaks belong to protons on the *trans-anti-* isomer which are assigned to be 6-proton on bonded thiophenyl ring, the 6-proton on pendant thiophenyl ring and the *ortho*-proton on phenyl ring, respectively (b, c and d in **Figure II-10**). In the same manner, the 6.76, 6.82 and 7.71 resonances are virtual triplet belonging to protons on the *trans-syn-* isomer which are assigned to be the 6-proton on bonded thiophenyl ring, the 6-proton on pendant thiophenyl ring and *ortho*-proton on phenyl ring, respectively (b', c' and d' in **Figure II-10**). Even though no virtual triplet is observed for –SH peaks, the effect of decoupling is observed in the sharpening of resonances. The magnitude of the coupling is too small to be resolved in the spectra.

Almost identical spectrum are seen in case of $[Pd^{II}(PS2'H)_2]$ complex(**Figure II-11**). The resonces are assigned in a similar manner as for the $[Ni^{II}(PS2'H)_2]$ complex. The 4.62ppm, 6.69ppm, 6.84ppm and 7.98ppm peaks are assigned to the *trans-anti* isomer, while peaks at 4.81ppm, 6.76ppm and 7.77ppm belong to the *trans-syn* isomer.

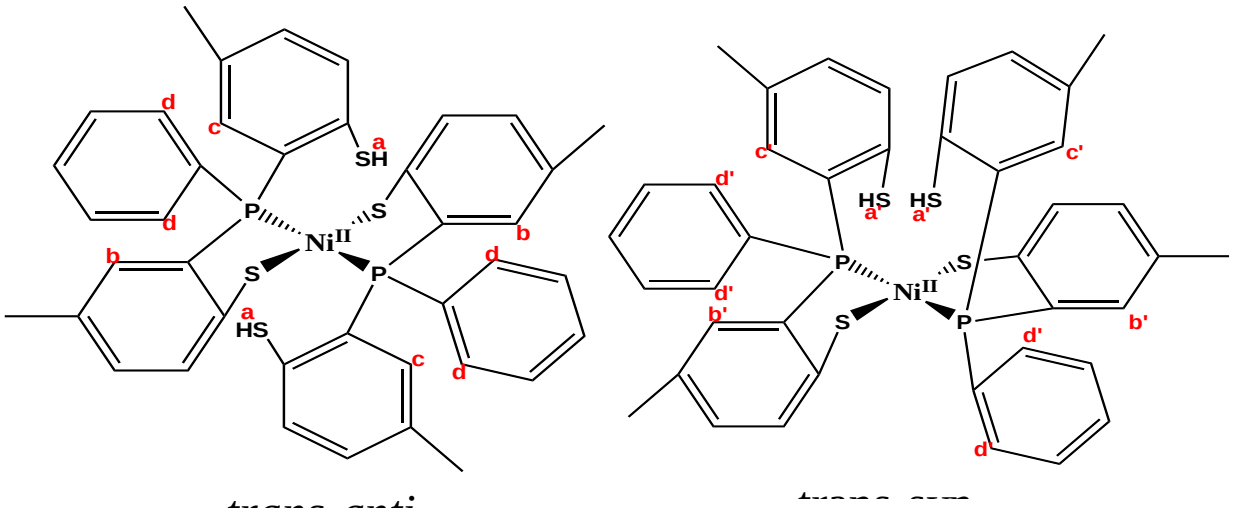

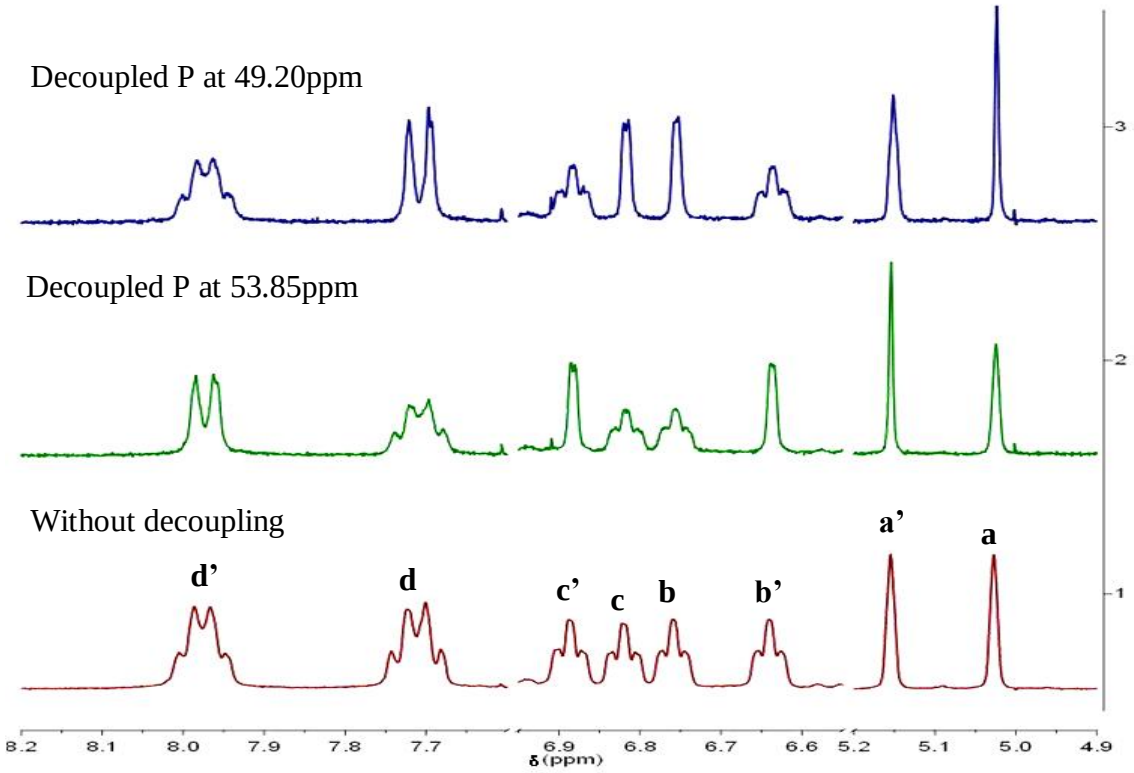

Figure II- 10. Selective ^{31}P Decoupling of the ^{1}H NMR spectra of $[Ni^{II}(PS2'H)_2]$ in $CDCl_3$, 300 MHz

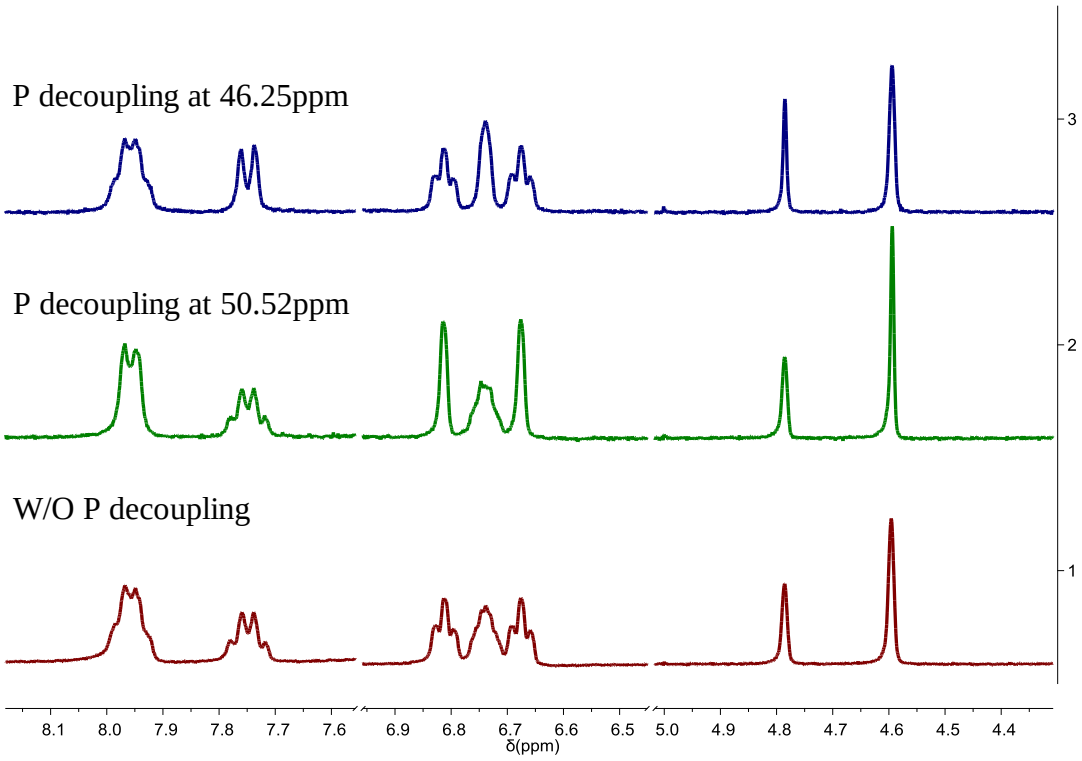

Figure II- 11. Decoupling of $[Pd^{II}(PS2'H)_2]$ at in $CDCl_3$, 300 MHz

NMR identification of $[Pt^{II}(PS2'H)_2]$ isomers

The NMR spectra of the isolated $[Pt^{II}(PS2'H)_2]$ indicated only a single isomer. However, as will be discussed in more detail in a subsequent chapter, when a solution is exposed to room light, all four isomers of $[Pt^{II}(PS2'H)_2]$ are formed.

With the comparison of ^{31}P NMR of pure *trans-anti*-$[Pt^{II}(PS2'H)_2]$ and the mixture of all four isomers (**Figure II-12**), we are able to assign all the four isomers and their splitting peaks in the ^{31}P NMR spectra. Platinum has ^{195}Pt (I = 1/2) with natural abundance of 33.7%, while the other isotopes have I = 0. Therefore, 66.3% of platinum

does not couple with phosphorus while 33.7% of platinum coupled with phosphorus. The proton decoupled ^{31}P NMR spectrum of pure *trans-anti*-[$Pt^{II}(PS2'H)_2$] shows a singlet (phosphorus bonded with Pt other than ^{195}Pt) as well as a doublet (phosphorus bonded with ^{195}Pt) with a large phosphorus-platinum coupling constant: (43.98ppm, s and d, $^1J_{P\text{-}Pt}$: 2566.5Hz). Even though phosphorus integrations are not as reliable as that of the proton, it helped in the peak assignments.

As expected, all the other isomers present the same feature in ^{31}P NMR as *trans-anti*-[$Pt^{II}(PS2'H)_2$], a large singlet plus a satellite doublet. Peaks at 48.43, 43.98, 40.66 and 38.66ppm are assigned to be the singlets (**Table II-3**). Due to *trans* influence of phosphorus ligand, the platinum-phosphorus σ bond are weakened in *trans* isomers, therefore a decrease in $^1J_{P\text{-}Pt}$ spin-spin coupling constant are observed (2625.6 and 2566.5 Hz for *trans*- isomers compare to 2841.9 and 2877.1 Hz for *cis*-isomers). Smaller ^1J coupling constant suggested weaker bond strength between platinum and phosphorus, which has been confirmed by the crystal structure. Previous research on Pt PR3 complexes has found that *cis*-isomers are present at higher field than the counterpart *trans*- isomers in ^{31}P NMR.[6] Our results are consistent, with the assignment of the resonances at 40.66 and 38.66 ppm for *cis*- isomers and with 48.43 and 43.98 ppm for the *trans*- isomers.

The of the four isomers helped us define the *trans*- and *cis*- isomers of [$Pt^{II}(PS2'H)_2$] without any doubt. With the additional help of the pure *trans-anti*- isomer

spectrum, the *trans-syn-* peak was also assigned, but cis-*syn-* and *cis-anti-* isomers could not be differentiated in the ^{31}P NMR spectra. The ^{1}H NMR spectra came into the picture.

$[Pt^{II}(PS2'H)_2]$ in $CDCl_3$ in glass tube under room light for 42hours:

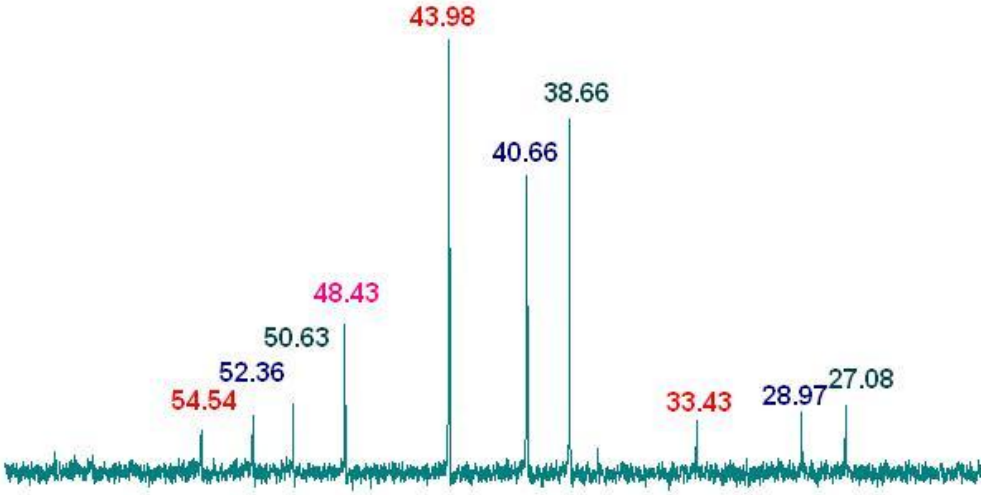

$[Pt^{II}(PS2'H)_2]$ in $CDCl_3$ in the dark:

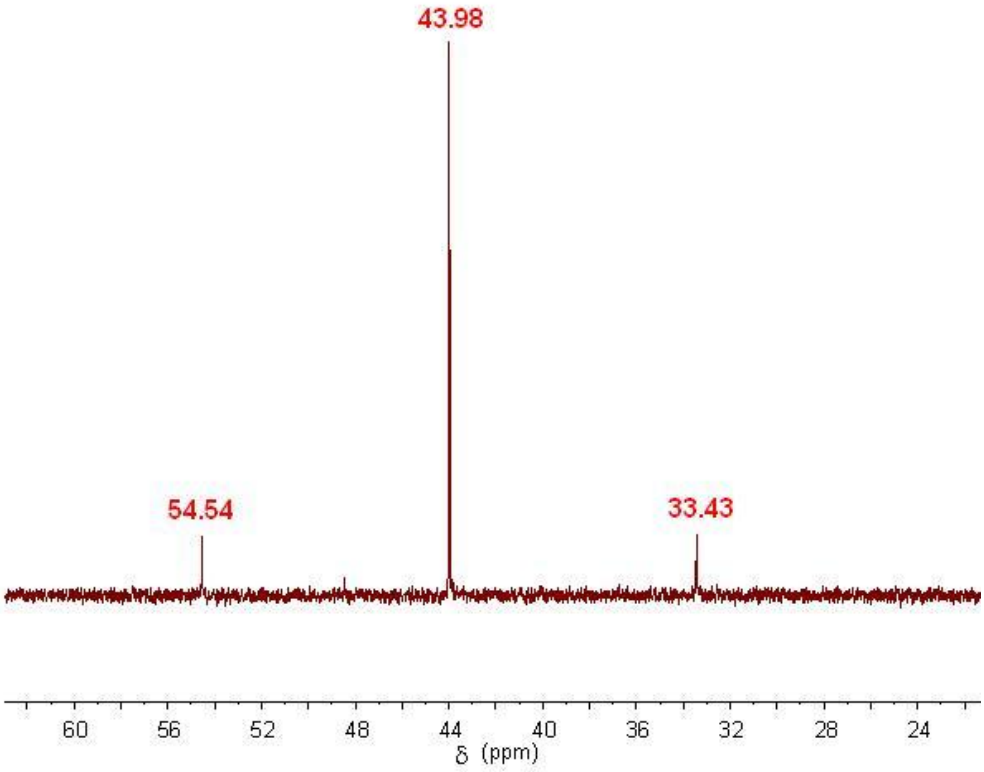

Figure II- 12. Comparison of ^{31}P NMR of *trans-anti*-[Pt^{II}(PS2'H)$_2$] and mixture of all four isomers in $CDCl_3$,300MHz

Configuration	Singlet peak(ppm)	Doublet peaks(ppm)	$^1J_{P\text{-}Pt}$(Hz)
trans-syn-	48.43	59.26/37.65	2625.6Hz
trans-anti-	43.98	54.54/33.43	2566.5Hz
cis-syn-	40.66	52.36/28.97	2841.9Hz
cis-anti-	38.66	50.76/27.08	2877.1Hz

Table II- 3. Comparison of and $^1J_{P\text{-}Pt}$ coupling constant of all four isomers of [Pt^{II}(PS2'H)$_2$] in $CDCl_3$.

The ^{1}H NMR of [Pt^{II}(PS2'H)$_2$] presents a unique virtual triplet peak of SH at around 5.55ppm, which is resulted from ^{1}H ^{31}P spin-spin coupling, we would expected that virtual coupling would be observed in all the other isomers. If we compare the ^{1}H NMR spectra of pure *trans-syn*-[Pt^{II}(PS2'H)$_2$] and the mixture of all four isomers (**Figure II-13**), we would notice a small peak with similar splitting at ~5.23ppm. Taken both the configuration and ^{31}P NMR into consideration, it is assigned to be the -SH peak of *trans-anti*-[Pt^{II}(PS2'H)$_2$]. The remaining two peaks are assigned to the *cis*- isomers.

As we've reported in next chapter, -SH proton of the *syn*- isomers would be affected by the π-π interactions of the thiophenol ring and therefore result shifting high field in NMR proton spectrum. The *trans-syn*-[Pt^{II}(PS2'H)$_2$] peak confirms the assumption. Thus we assign the peak at around 4.74 ppm to be the –SH of *cis-anti*-[Pt^{II}(PS2'H)$_2$] while the peak at around 4.90 ppm to be the –SH of *cis-syn*-[Pt^{II}(PS2'H)$_2$].

$[Pt^{II}(PS2'H)_2]$ in $CDCl_3$ in glass tube under room light for 42 hours:

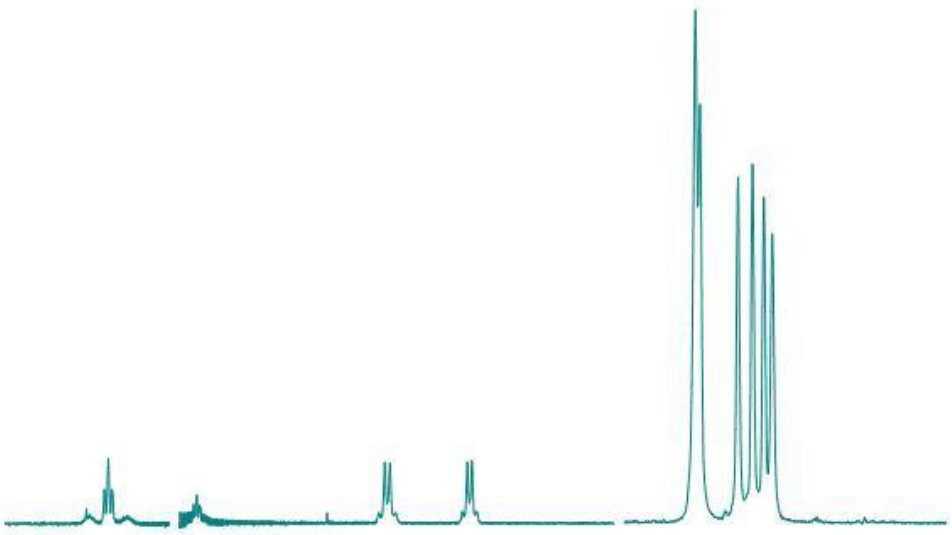

Trans-anti-$[Pt^{II}(PS2'H)_2]$ in $CDCl_3$ in the dark:

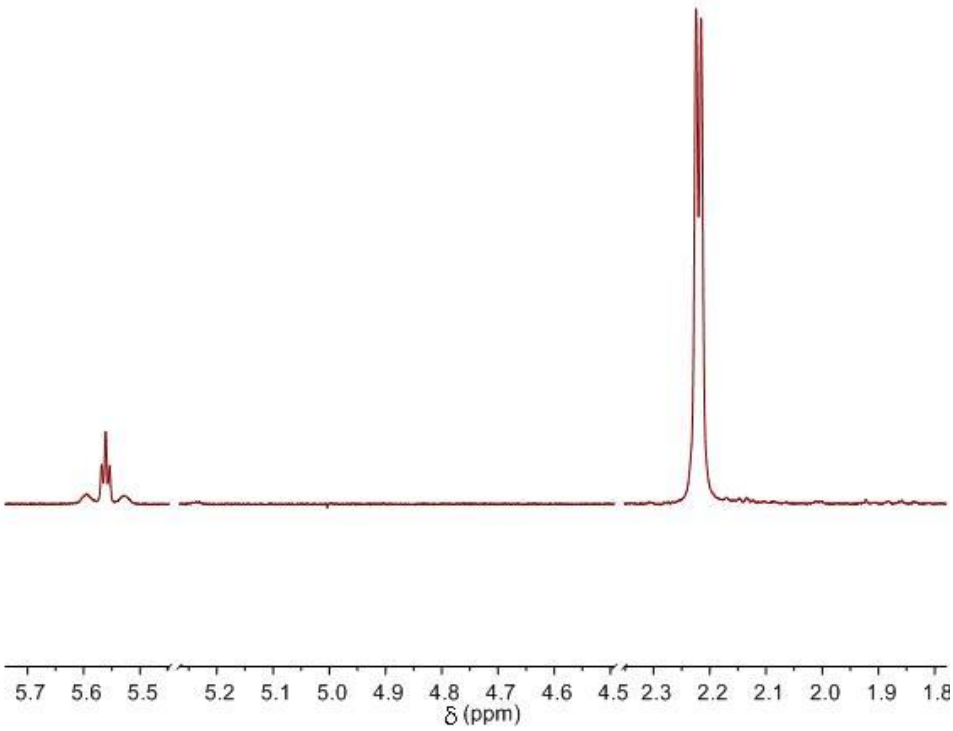

Figure II- 13. Comparison of ^1H NMR of *trans-anti*- $[Pt^{II}(PS2'H)_2]$ and mixture of all four isomers in $CDCl_3$, 300MHz

It is notable that two *cis*- -SH peaks have different coupling pattern than the *trans*- ones. The –SH and $–CH_3$ peaks region of ^1H NMR spectrum of mixture of all four isomers was shown in **Figure II-14**. The –SH protons have long range coupling with P. The insert shows the relationship between the configuration and the coupling pattern. The -SH resonances of both *trans*-isomers are virtual triplets owning to the strong P-trans-P coupling, whereas the resonances of *cis*-isomers are just a simple doublet. The side bands for each of these –SH resonance resulted from proton-platinum coupling. The integration of these –SH peaks agreed with the ^{31}P NMR assignment, where both *trans*- isomers are about the same concentration with *trans-anti*-$[Pt^{II}(PS2'H)_2]$, while *trans-syn*-$[Pt^{II}(PS2'H)_2]$ is significantly less.

The $–CH_3$ peaks (**Figure II-14**) are used to distinguish the isomers as well. There are four sets of $–CH_3$ peaks in spectrum of the mixture of all four isomers, two sets of two singlets (2.10 and 2.08ppm, total 5.31H, *cis-syn*-; 2.15 and 2.12ppm, total 5.79H, *cis-anti*-) and two pseudo-"singlets" (2.22ppm, 5.97H, *trans-anti*-; 2.21ppm, 1.32H, *trans-syn*-). All the integrations supported the proton NMR assignment, and helped the assignment of two *cis*- isomers in the phosphorus-31 NMR. It is notable that the two methyl groups are related by a mirror plane and an inversion center in the *cis-syn*- and the *trans-anti*-$[Pt^{II}(PS2'H)_2]$ isomers respectively in their configuration, and theoretically should show only one singlet for the methyl groups. In the actual spectrum, both the *trans-syn*-$[Pt^{II}(PS2'H)_2]$ and *trans-anti*-$[Pt^{II}(PS2'H)_2]$ isomers appear to be singlet, while both *cis-anti*-$[Pt^{II}(PS2'H)_2]$ and *cis-syn*-$[Pt^{II}(PS2'H)_2]$ show two singlets peaks for the methyl groups. Meanwhile, the ^1H NMR of pure *trans-anti*-$[Pt^{II}(PS2'H)_2]$ shows two

resolved singlets for the methyl groups. This reveals that no matter whether the two methyl groups are symmetry related or not, they are magnetically in-equivalent in all four isomers. The shift of two methyl groups of the *trans-anti-* and *trans-syn-* isomers cannot be resolved at 300 MHz, and appear as singlets.

The peak positions and integration of –SH and -CH_3 are summarized in **Table II-4**, where all the assignment agree with each other perfectly. For each isomers, the integration of the –SH protons agrees with the integration of the methyl groups.

configuration	-SH peak(ppm, H)	-CH_3 peak(ppm, H)
trans-syn-	~5.23, 0.39H	"2.21", 1.32H
trans-anti-	~5.55, 1.00H	"2.22", 5.97H
cis-syn-	~4.90, 0.96H	2.15/2.12, 5.79H
cis-anti-	~4.74, 0.86H	2.10/2.08, 5.31H

Table II- 4. The peak positions and integration of –SH and -CH_3 in $CDCl_3$, 300MHz

Synthetically, we exposed the reaction mixture to light for days at room temperature, so that both the *cis-anti* and *cis-syn* isomers are populated. Therefore the crystals of both *cis-* isomers are achieved. By exposing the methylene dichloride solution of [Pt^{II}(PS2'H)$_2$] to room light under N_2 for a week, we are able to populate both the *cis-* isomers. Recrystallized from chloroform and hexane in the dark, we are able to get X-ray quality crystals for both the *cis-syn-*[Pt^{II}(PS2'H)$_2$] and *cis-anti-*[Pt^{II}(PS2'H)$_2$] isomers.

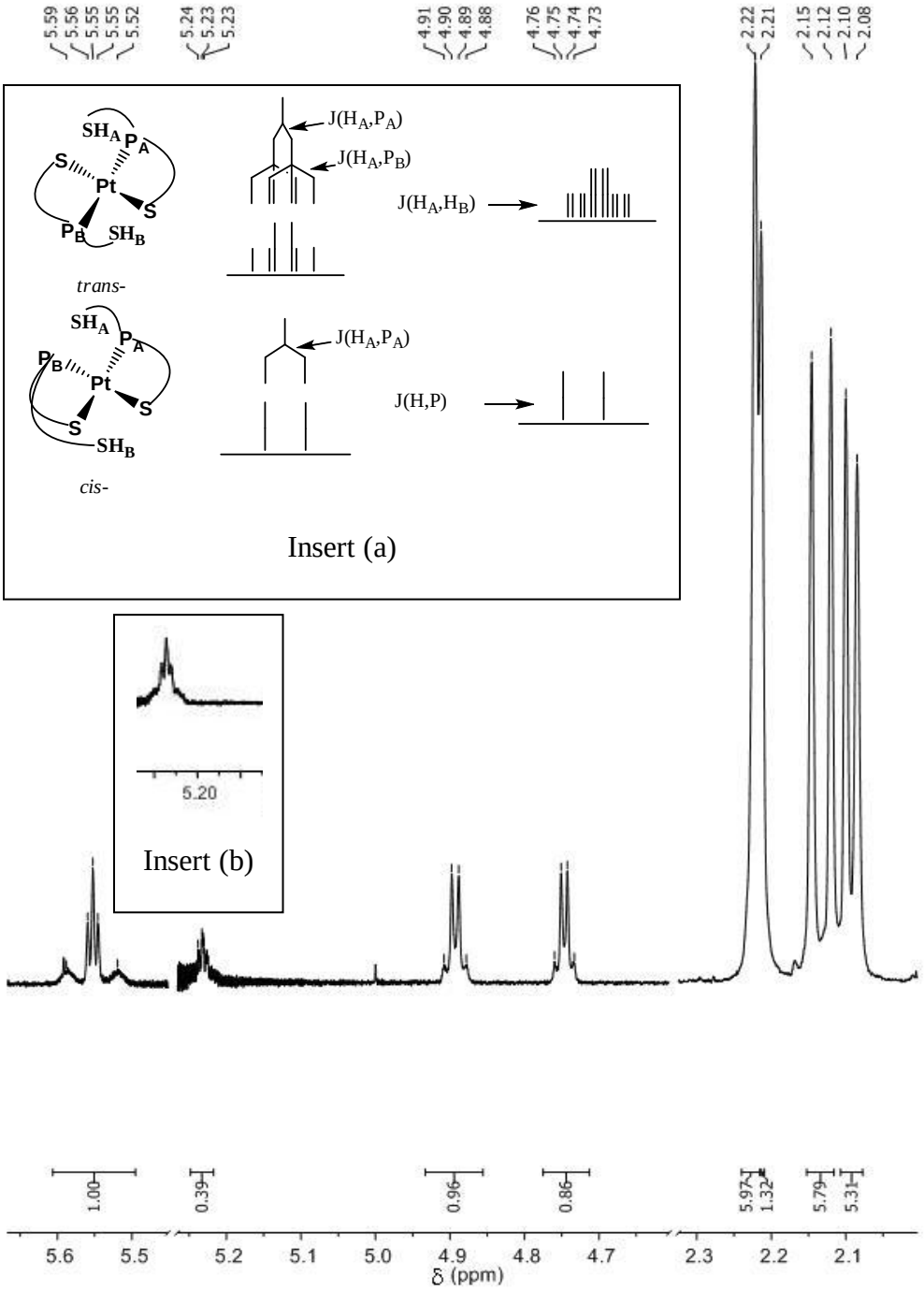

Figure II- 14. ^{1}HNMR of [Pt^{II}(PS2'H)$_2$] (mixture of all four isomers) in $CDCl_3$, 300MHz (Insert (a): coupling pattern of *trans*- and *cis*- isomers; Insert (b): Zoom in of *tran-syn*- isomer)

The X-ray crystal structures of three out of the fours possible isomers are shown below (**Figure II-15**, **Figure II-16** and **Figure II-17**). As shown the comparison in **Table II-5**, the unit cells of the crystals are solvent dependent. In the case of *trans-anti*-$[Pt^{II}(PS2'H)_2]$, despite the identical structure of Pt compound, the space group changed from Pbca to P1(bar) as the co-crystallized solvent changing from CH_2Cl_2 to $CHCl_3$.

Crystal structure of $[Pt^{II}(PS2'H)_2]$ isomers.

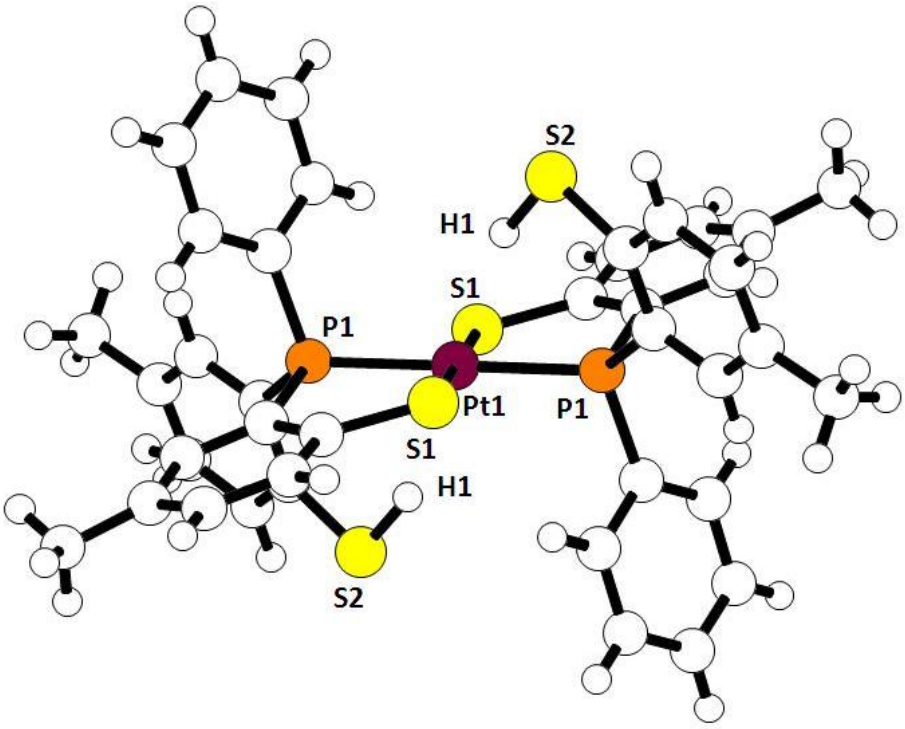

Figure II- 15. X-ray crystal structure of *trans-anti*-$[Pt^{II}(PS2'H)_2]$ $2CH_2Cl_2$, Chem-Ray structure. The solvent molecules are omitted for clarity.

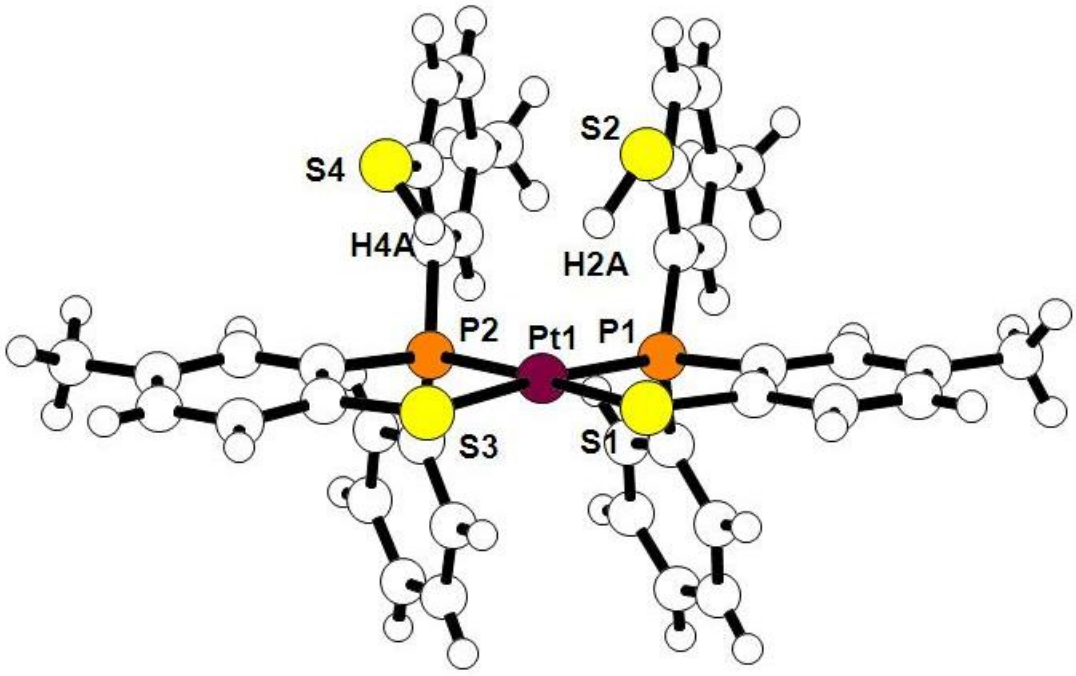

Figure II- 16. X-ray crystal structure of *cis-syn*-[Pt^{II}(PS2'H)$_2$] $CHCl_3$, Chem-Ray structure. The solvent molecules are omitted for clarity.

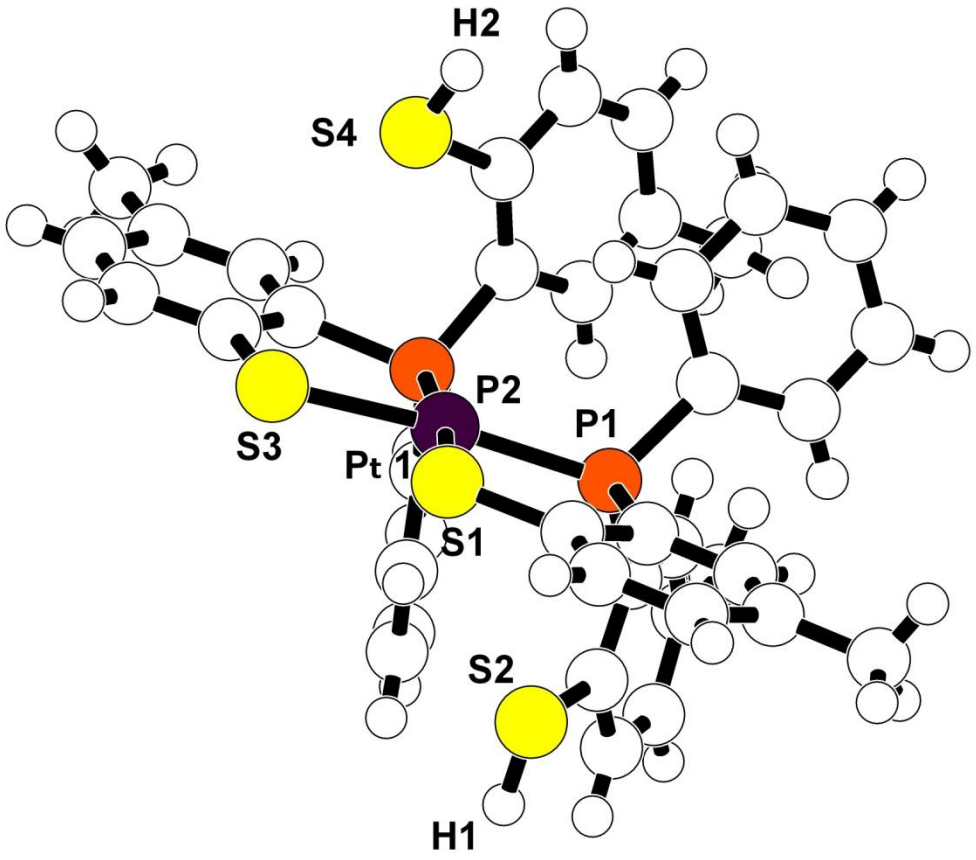

Figure II- 17. X-ray crystal structure of *cis-anti*-[Pt^{II}(PS2'H)$_2$] $CDCl_3$, Chem-Ray structure. The solvent molecules are omitted for clarity.

Bond length(Å)	***trans-anti*-[Pt^{II}(PS2'H)$_2$] 2CH_2Cl_2**	***trans-anti*-[Pt^{II}(PS2'H)$_2$] 4$CHCl_3$**	***cis-syn*-[Pt^{II}(PS2'H)$_2$] $CDCl_3$**	***cis-anti*-[Pt^{II}(PS2'H)$_2$] $CHCl_3$**
M-P1(P2)	2.2796(5)	2.2880(5)	2.2742(18)	2.2561(6)
			2.2629(18)	2.2601(6)
M-S1(bonded)	2.3209(5)	2.3138(5)	2.3885(17)	2.3193(5)
			2.3266(18)	2.3252(6)
M-S2(non bonded)	3.5683(5)		3.64733(18)	3.9930(6)
			3.8819(17)	3.9388(7)
M-H1	2.369(26)		2.44(7)	4.97(3)
			2.81(4)	4.64(6)
H1-S2	1.24(3)	1.23(3)	1.24(7)	1.22(3)
			1.18(2)	1.10(6)
S2-C8	1.7705(19)	1.769(2)	1.782(7)	1.770(2)
			1.776(6)	1.771(3)
Angle( )				
P1-M-P1(P2)	180	180	98.78(6)	99.12(2)
P1-M-S1	85.819(16)	86.991(19)	87.52(6)	87.61(2)
P1-M-H1	71.7(5)		70.1(17)	62.9(4)
S1-M-H1	97.2(4)		112.2(17)	75.5(4)
Unit Cell				
Space group	Pbca	P1(bar)	P1(bar)	P1(bar)
Volume(Å3)	4106.76(10)	1307.38(11)	1954.45(11)	2024.34(7)

Table II- 5. Selected distances angles and unit cell parameter for *trans-anti-*, *cis-syn-*, and *cis-anti*-[Pt^{II}(PS2'H)$_2$].

Formed from similar solvent combination, the crystal structures of *trans-anti-*, *cis-syn-*, and *cis-anti*-[$Pt^{II}(PS2'H)_2$] are isomorphous, having the same space group (P1(bar)) and comparative unit cell parameters. It is notable that the M-P distance is significantly shorter in both the cis-*syn-*, and *cis-anti*-[$Pt^{II}(PS2'H)_2$] than in the *trans-anti*-[$Pt^{II}(PS2'H)_2$] isomer. The average M-P bond distances are 2.2687 and 2.2581Å for cis-*syn-*, and *cis-anti*-[$Pt^{II}(PS2'H)_2$], respectively; whereas the M-P bond distance is 2.2880(5) for *trans-anti*-[$Pt^{II}(PS2'H)_2$]. This is a typical "trans influence", which is the tendency of a ligand to influence the rate of the ligand substitution of a ligand *trans* to itself and therefore weaken the bond *trans* to itself.[7]

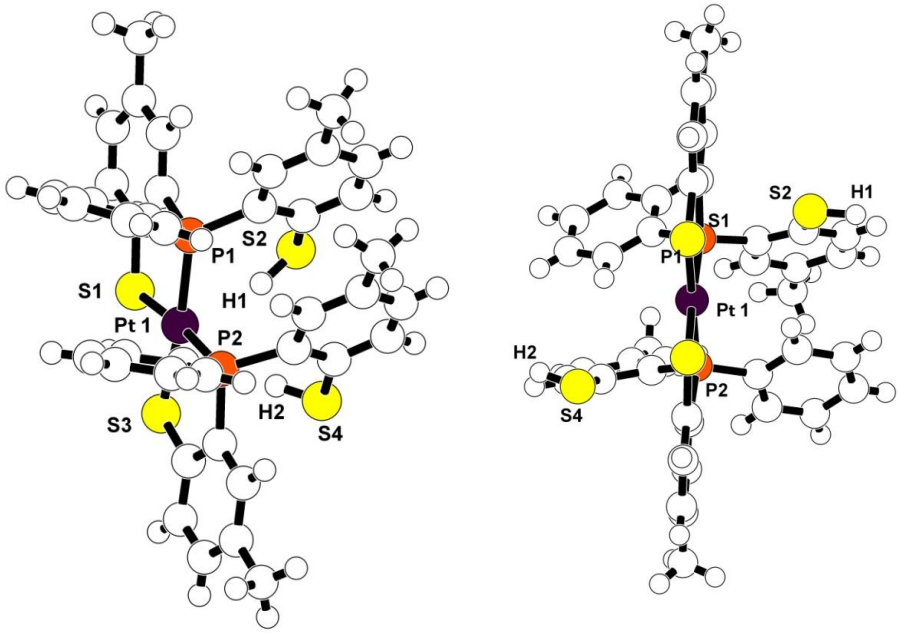

(a) *cis-syn*-[$Pt^{II}(PS2'H)_2$] (b) *cis-anti*-[$Pt^{II}(PS2'H)_2$]

Figure II- 18. Selected distances structure of *cis-syn*-[$Pt^{II}(PS2'H)_2$] $CHCl_3$(a) and *cis-anti*-[$Pt^{II}(PS2'H)_2$] $CDCl_3$(b), Chem-Ray structure. The solvent molecules are omitted for clarity.

The most interesting observation is that in the structure of *cis-anti*-[Pt^{II}(PS2'H)$_2$], the pendant thiol protons are pointing away from the platinum metal, opposite to the observation with *trans-anti*-[Pt^{II}(PS2'H)$_2$] and *cis-syn*-[Pt^{II}(PS2'H)$_2$]. The pendant thiol protons are 4.97 and 4.64 Å away from platinum What we've noticed at the same time is that distance between platinum and the non-coordinated thiol sulfur is much shorter in *cis-anti*-[Pt^{II}(PS2'H)$_2$] than in others. As shown in the comparison view (**Figure II-18**), in *cis-syn*-[Pt^{II}(PS2'H)$_2$], the pendant thiophenol rings are almost parallel (dihedral angle 6.43 º) to each other, separated by 3.479Å; whereas in *cis-anti*-[Pt^{II}(PS2'H)$_2$], the pendant thiophenol rings are π-π interacted with the phenyl ring from the other ligand (dihedral angle 19.93 º), minimum separation only 2.660Å. It is probably this relatively strong π-π interaction that helps to compensate the absence of Pt···HS hydrogen bonding and stabilize the compound. The distortion results in shorter Pt-S(non-coordinated) distance, and therefore push the pendant thiol protons away from the platinum center.

Synthesis and Characterization of [M^{IV}(PS2')$_2$] (M = Ni, Pd, Pt)

The [M^{II}(PS2'H)$_2$] (M=Ni, Pd and Pt) complexes are oxidized by O_2 to form [M^{IV}(PS2')$_2$] (M=Ni, Pd and Pt). The Ni complex had been previously characterized by Susan Beatty. All the octahedral structures have the *cis* arrangement of the P atom. Thus the *trans* P atoms in the [M^{II}(PS2'H)$_2$] compounds have become *cis* in the [M^{IV}(PS2')$_2$] products.

The geometries of the *cis*-[$M^{IV}(PS2')_2$] (M = Ni, Pd, Pt) complexes are essentially the same. The crystal structures of *cis*-[$M^{IV}(PS2')_2$] (M = Ni, Pd, Pt) complexes are shown in **Figure II-19**, **Figure II-20** and **Figure II-21**. The M-P bond distances have the same trend as in the trans-*anti*-[$M^{II}(PS2'H)_2$] series which is resulted from the difference in atomic radius of the metal. The case of distance of metal-sulfur bond, the ones which are *trans*- to each other, are on average shorter than the ones, which are *cis*- to each other. Again, this is due to the *trans* influence of the phosphorus ligand.

The unique thing about Ni(IV) complexes is that, by controlling the reaction time, we are able to populate one of the other Ni(IV) isomers: the *trans-fac*-isomer. With different UV-vis spectrum, the synthetic isolation route is discovered. Despite the lack of X-ray crystal structure, we are able to assign the structure of it by NMR spectra.

There are three possible isomers for [$Ni^{IV}(PS2')_2$] (**Scheme II-2**). In *trans-fac*-isomer the thiolate sulfurs are all *trans*- to each other, whereas one of the pairs of S donors are *trans* to P in the *cis*-isomer. It is expected that this would have influence on the metal sulfur bond distances. And so the metal phosphorus bond distances would be affected by the different configuration.

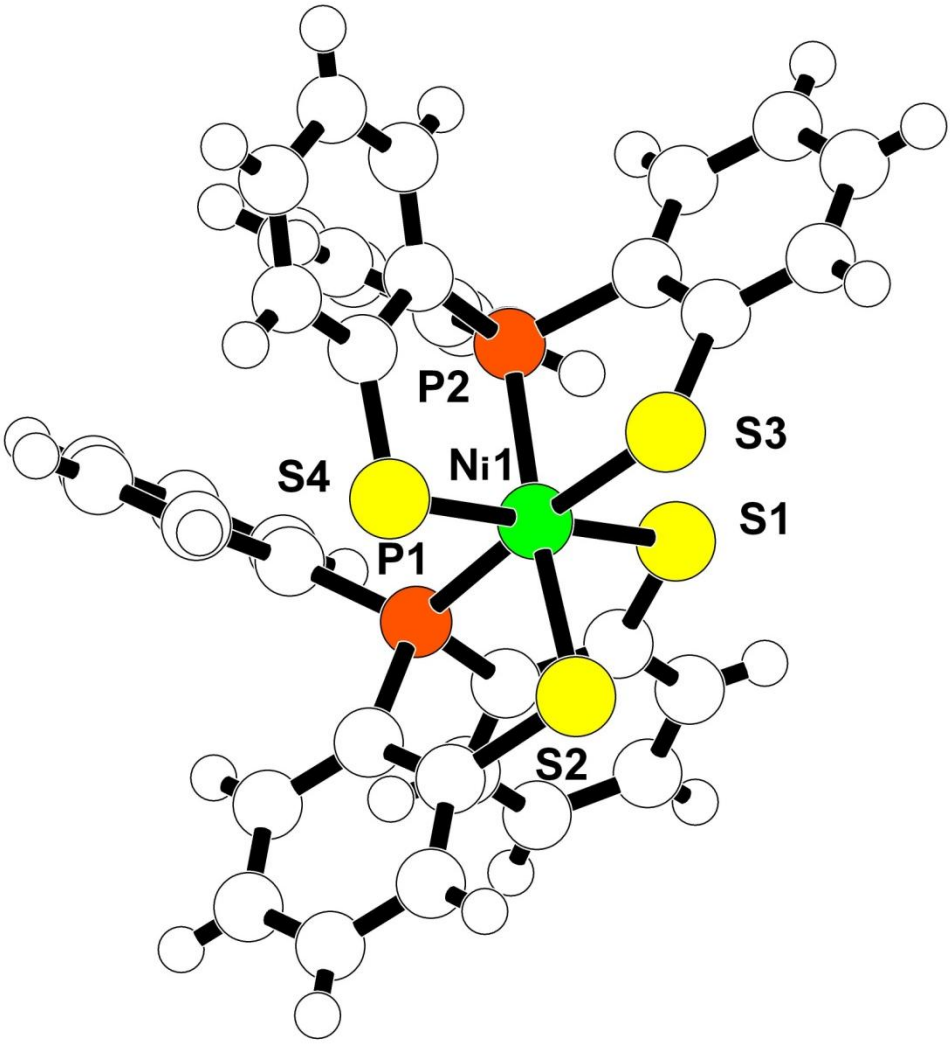

Figure II- 19. X-ray crystal structure of *cis*-[$Ni^{IV}(PS2')_2$] $2CH_2Cl_2$, Chem-Ray structure. The solvent molecules are omitted for clarity.

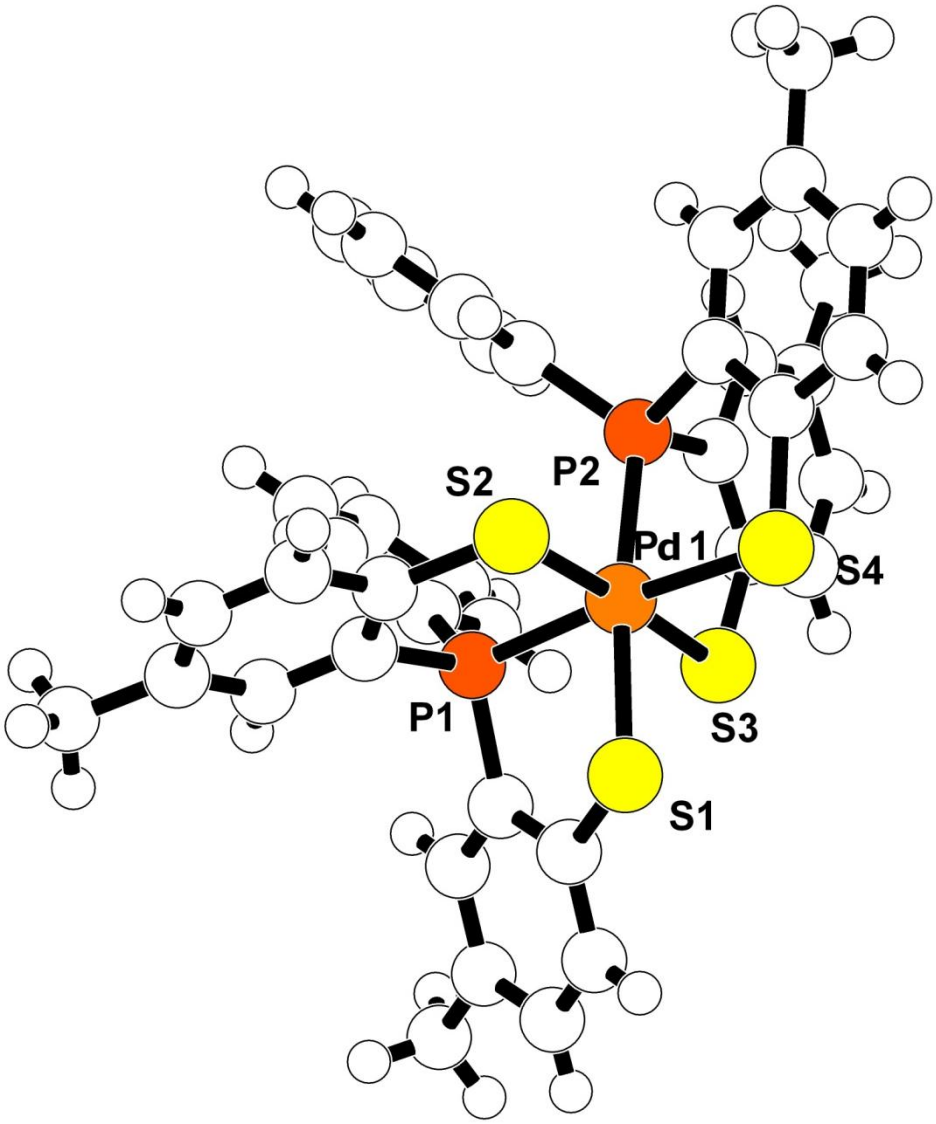

Figure II- 20. X-ray crystal structure of *cis*-[$Pd^{IV}(PS2')_2$] $2CH_2Cl_2$, Chem-Ray structure. The solvent molecules are omitted for clarity.

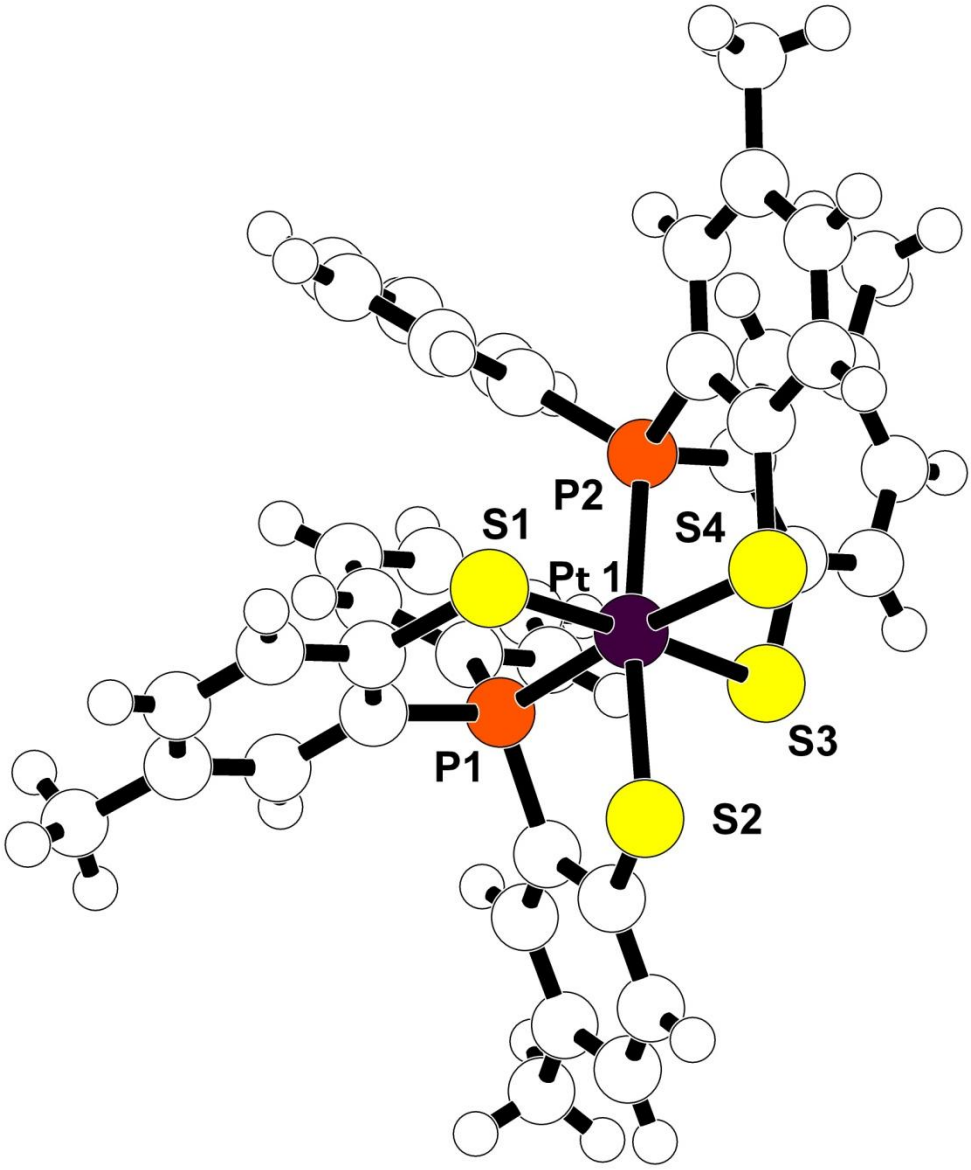

Figure II- 21. X-ray crystal structure of *cis*-[Pt^{IV}(PS2')$_2$] $2CH_2Cl_2$, Chem-Ray structure. The solvent molecules are omitted for clarity.

Bond length*(Å)*	***cis*-[Ni^{IV}(PS2')$_2$] 2CH_2Cl_2**	***cis*-[Pd^{IV}(PS2')$_2$] 2CH_2Cl_2**	***cis*-[Pt^{IV}(PS2')$_2$] 2CH_2Cl_2**
M-P	2.1969(3)	2.2816(11)	2.2800(4)
	2.1860(5)	2.2912(11)	2.2871(4)
M-S (trans)	2.2595(5)	2.3449(11)	2.3542(4)
	2.2599(5)	2.3467(11)	2.3557(4)
M-S (cis)	2.2762(5)	2.3954(11)	2.4013(4)
	2.2945(5)	2.3999(11)	2.4043(4)
Unit Cell			
Space group	$P2_1/n$	$P2_1/c$	$P2_1/c$
Volume($Å^3$)	6580.9(7)	3924(2)	3947.28(4)

Table II-6. Selected distances and unit cell parameter for *cis*-[M^{IV}(PS2')$_2$] (M=Ni, Pd, Pt)

The ^{1}H NMR and ^{31}P NMR spectra of the *cis* and *trans* isomers of [Ni^{IV}(PS2')$_2$] are shown in **Figure II-22**, **Figure II-23**, **Figure II-24** and Figure **II-25**. The ^{31}P resonances of the *cis*- isomer are shifted downfield compared to the *trans-fac* isomer.

The ^{1}H NMR spectrum of the C_{2h} symmetric *trans-fac* isomer is simpler than the spectrum of C_2 symmetric *cis*- isomer. In the *cis*-isomer spectrum, there are two singlets for methyl group resonance, since that two methyl groups in the same ligand are inequivalent. The doublet at 6.57 ppm and 6.46 ppm (b) belong to the protons *ortho*-to the phosphorus on the thiophenolate ring, which are resulted from the ^{31}P-^{1}H coupling (J_{P-H} = 9Hz). The peak at 7.36 ppm (e) belongs to the *para*- and *meta*- protons on the

phenol rings. It is a triplet of doublet, the doublet resulted from the proton-phosphorus coupling (J_{P-H} = 3Hz) and the triplet is due to the protons on the same ring. The region of c and d is not very well resolved, but the "virtual triplets" from proton- phosphorus coupling of *ortho*- protons on the phenol rings in region c are observed.

The resolution of the ^{1}HNMR spectrum of *trans-fac* is limited, but the proton-phosphorus coupled doublet (J_{P-H} = 9Hz), that belongs to the *ortho*-phosphorus proton on thiophenol ring, is observed.

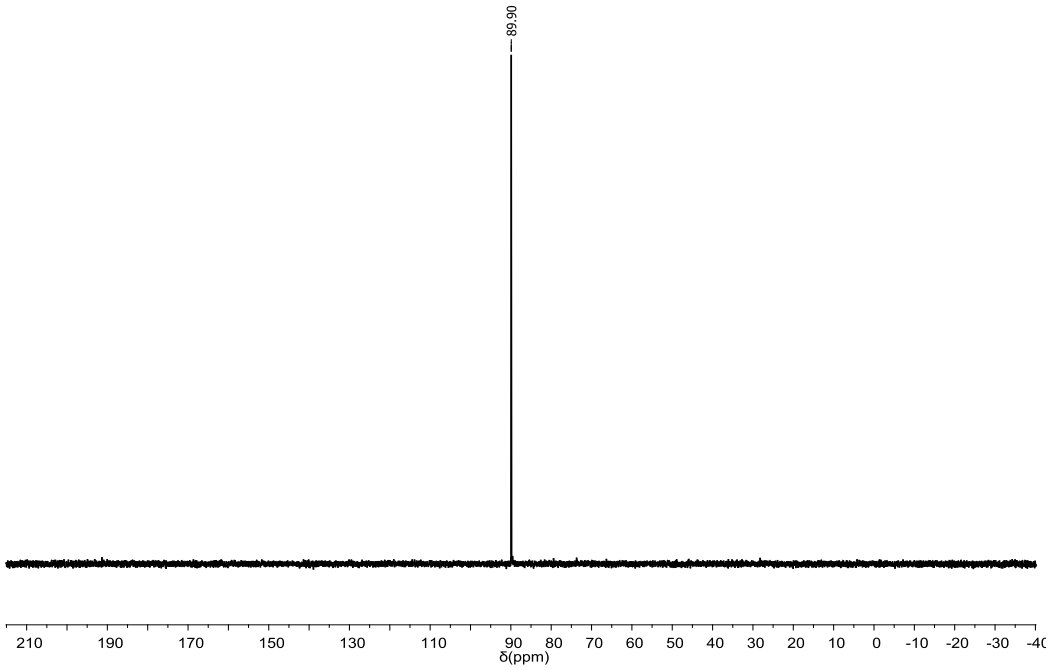

Figure II- 22. ^{31}P NMR spectrum of *cis*-[Ni^{IV}(PS2')$_2$] in $CDCl_3$, 300MHz

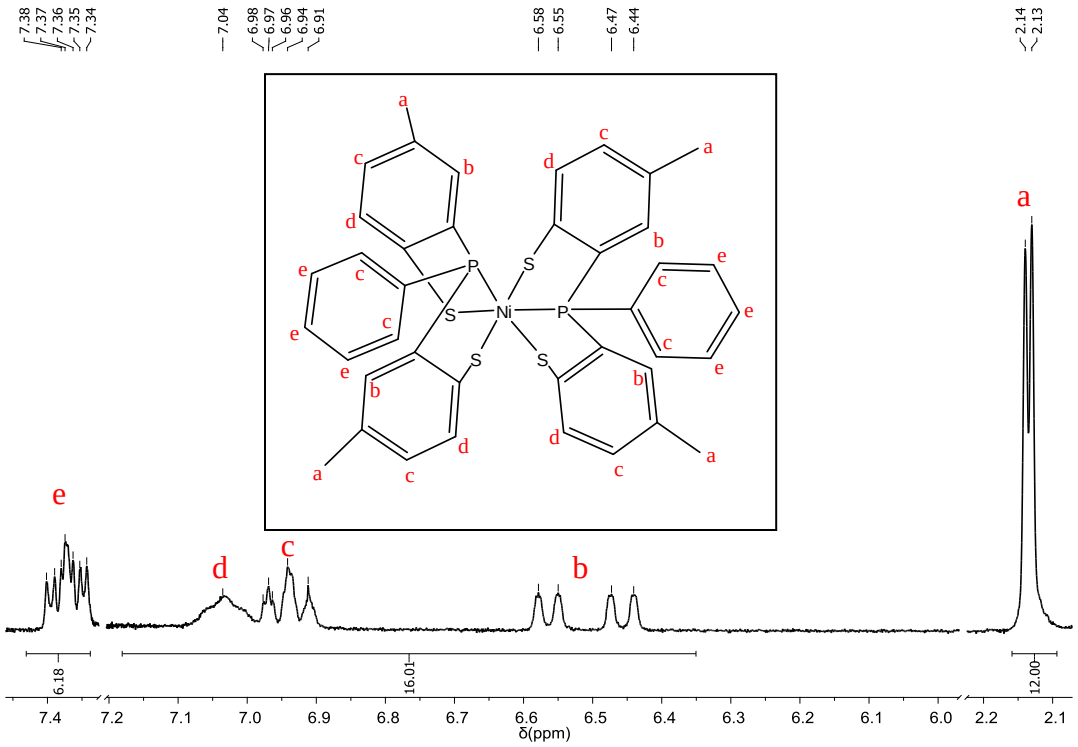

Figure II- 23. ^{1}H NMR spectrum of *cis*-[Ni^{IV}(PS2')$_2$] in $CDCl_3$, 300MHz

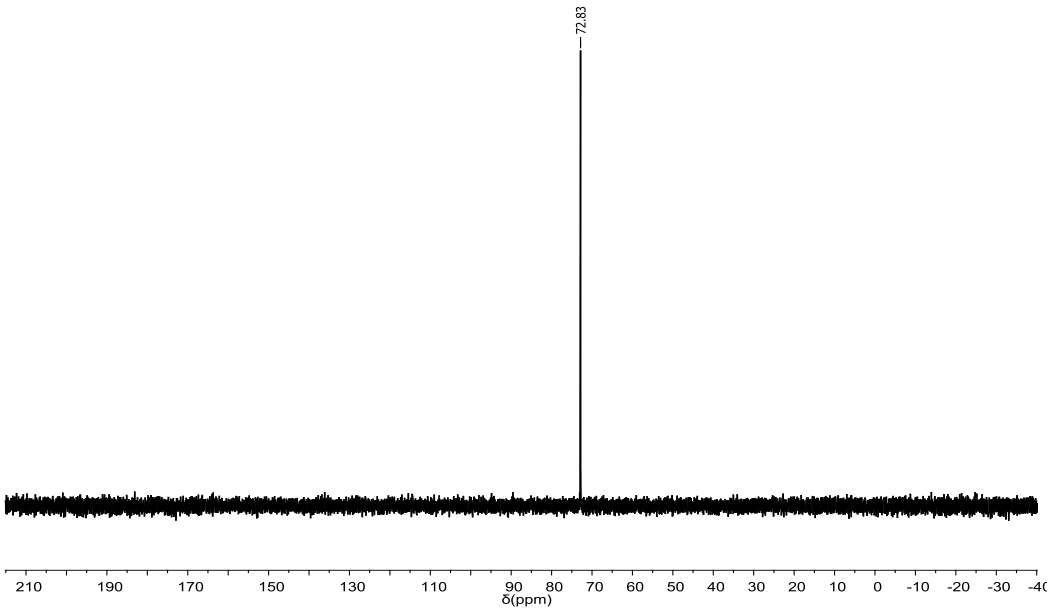

Figure II- 24. ^{31}P NMR spectrum of *trans-fac*-[Ni^{IV}(PS2')$_2$] in $CDCl_3$, 300MHz

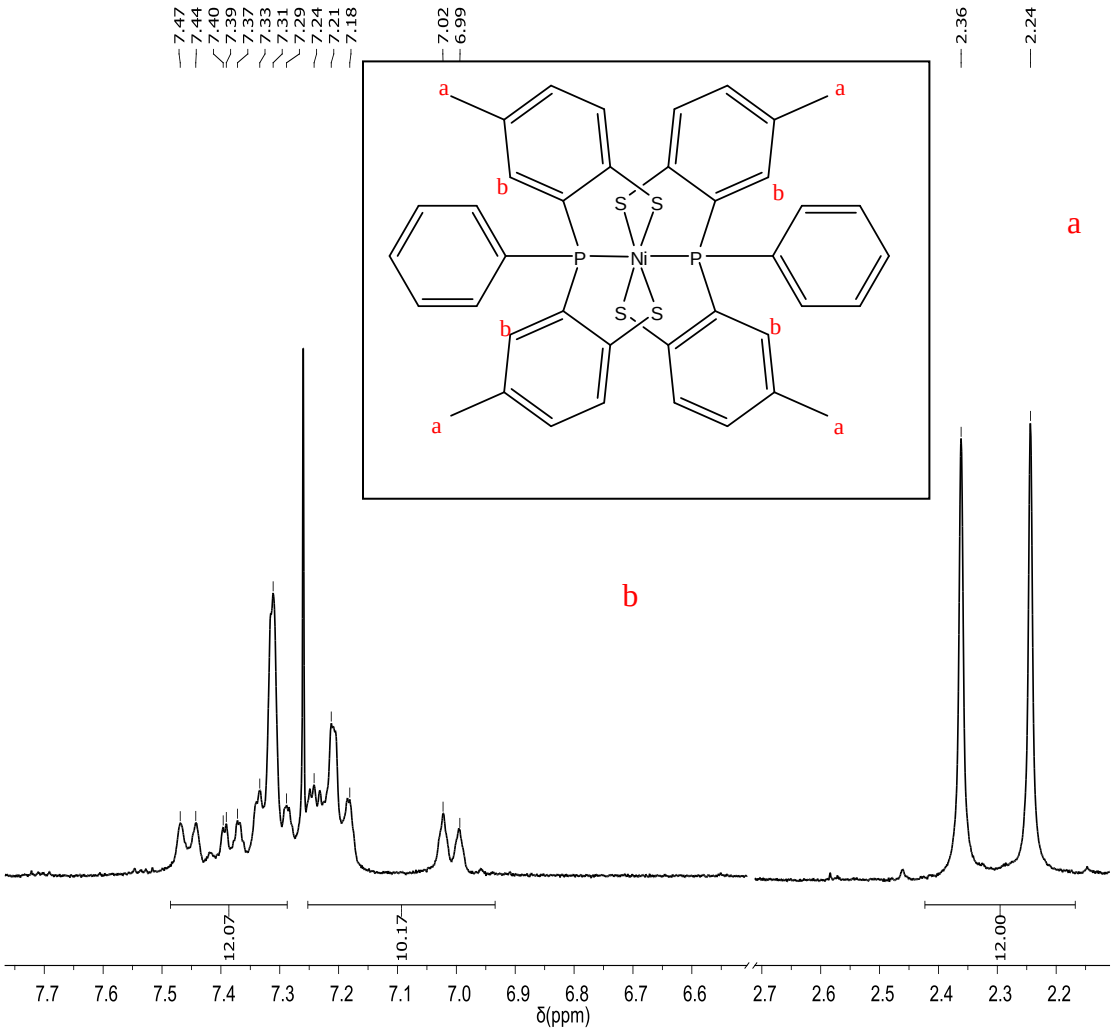

Figure II- 25. ^{1}H NMR spectrum of *trans-fac*-[Ni^{IV}(PS2')$_2$] in $CDCl_3$, 300MHz

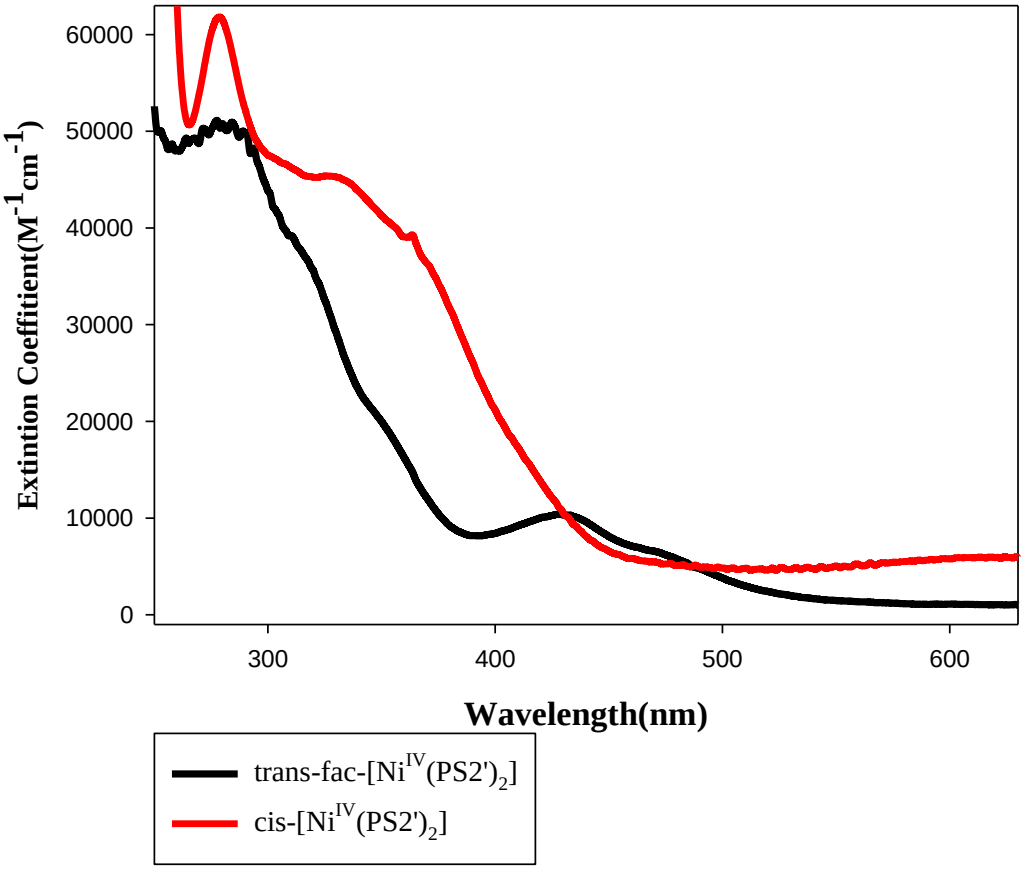

Figure II- 26. UV-vis spectra of $[Ni^{IV}(PS2')_2]$ in CH_2Cl_2, 10mM

UV-*vis* spectra also demonstrate the energy difference between two isomers (**Figure II-26**). A decrease in the absorbance of the intra-ligand ^{1}IL [dπ→dπ*] transition of the phenol group of the PS2' ligand[8-9] at ~278nm, is observed from *cis-* to *trans-fac-* isomer. The *trans-fac-* isomer has a red shifted absorption of metal-to-ligand charge transfer ^{1}MLCT [dπ(Pt)→dπ(P)] band at 325nm (ε = $4.53\times10^5 M^{-1}cm^{-1}$) 427nm (ε = $1.04\times10^5 M^{-1}cm^{-1}$) compared to the *cis-* spectrum. The red shift of metal-to-ligand charge

transfer demonstrates the less pi-back-bonding in the *trans-fac-* isomer due to the *trans* effect.

Oxidation state study of nickel center for series of Ni(II) ↔ Ni(III) ↔ Ni(IV)

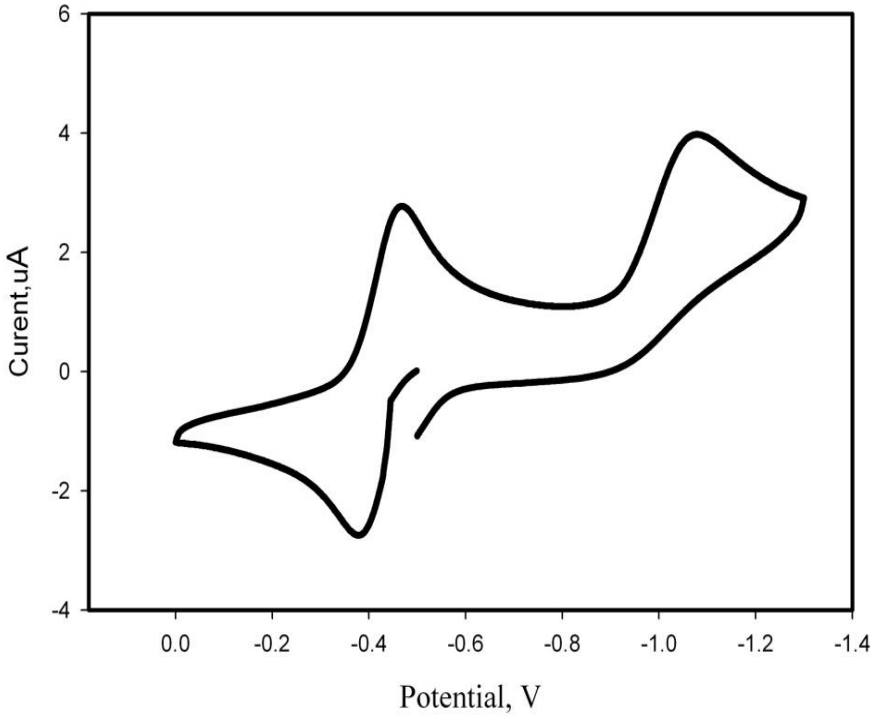

Figure II- 27.Cyclic voltammogram of $[Et_4N][Ni^{III}(PS2')_2]$ in DMF vs Ag/AgCl

Ni-PS2' complexes are the only one in the whole group with a full series of M(II), M(III) and M(IV) complexes. The cyclic voltammetry of $[Et_4N][Ni^{III}(PS2')_2]$ (**Figure II-27)** show a reversible one electron oxidation to a Ni(IV) species at -0.420V(vs Ag/AgCl) and an irreversible reduction to a Ni(II) species at -1.079V (vs Ag/AgCl). The cyclic voltammetry of $[Ni^{IV}(PS2')_2]$ in DMF (**Figure II-28**) matches that of its Ni(III) counterpart: a reversible one electron reduction to Ni(III).

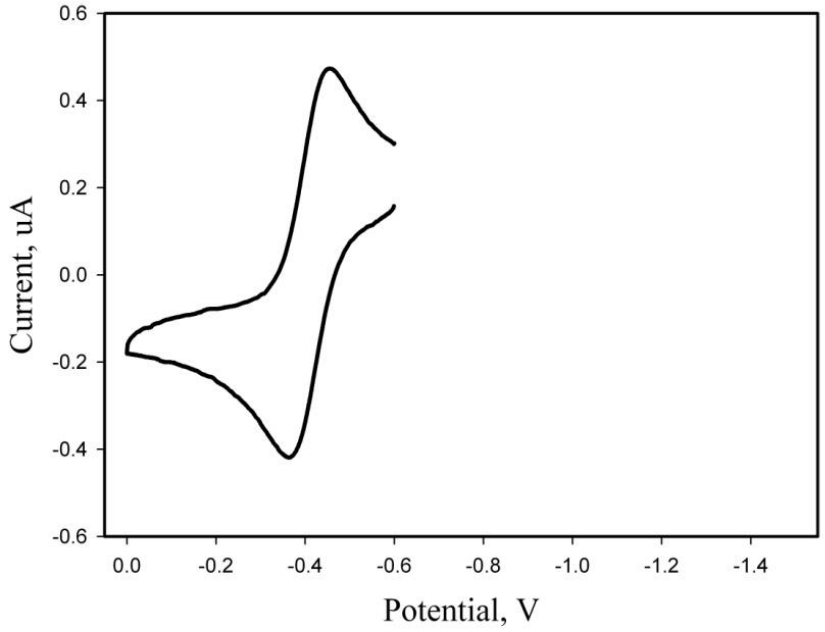

Figure II- 28.Cycle voltammogram of $[Ni^{IV}(PS2')_2]$ in DMF vs Ag/AgCl

The absorption of X-ray can excite the 1s (K edge) or 2s, 2p (L edge) electrons of an element to empty localized orbitals or, for higher-energy X-ray photons, the continuum.[10] By examining the energy of X-ray absorption edge, where the onset of absorptions occurs, one can often determine the oxidation state of the metal ion of interest. Transitions from an inner shell of electrons to the valence level allow one also to get electronic structural information in favorable cases.

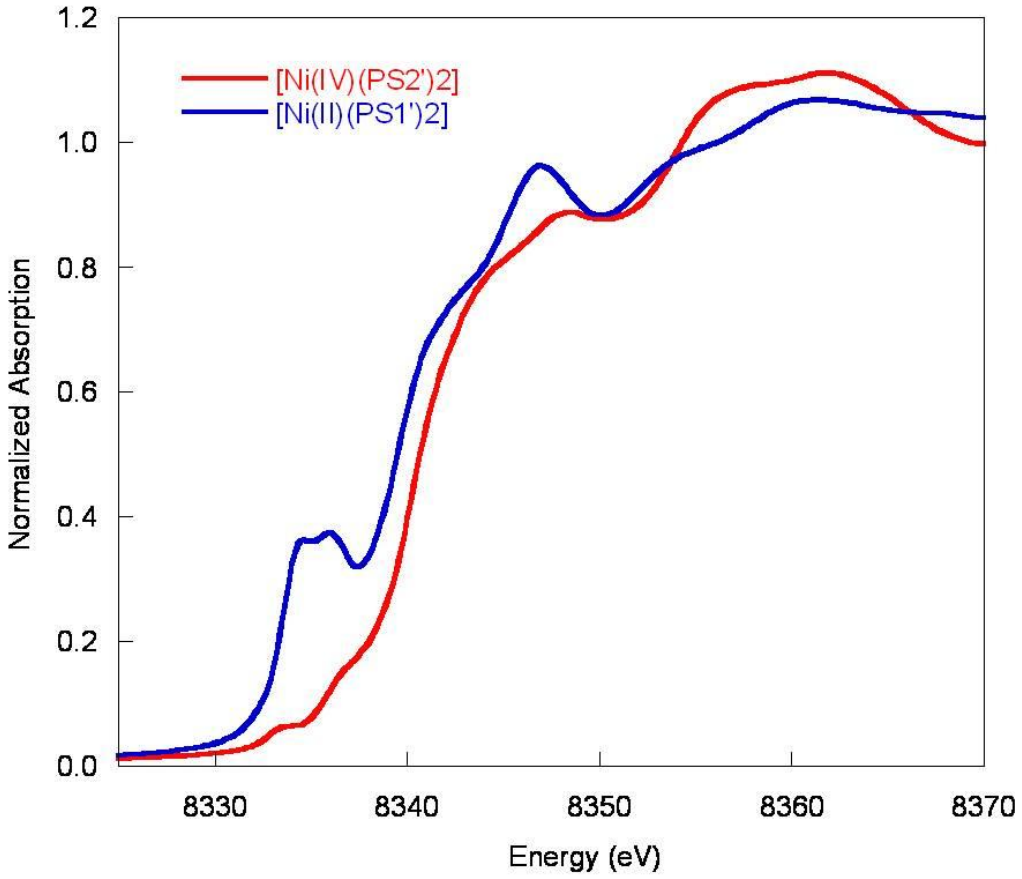

Figure II- 29.Comparison of the normalized Ni K-edge XAS spectra for the $[Ni^{IV}(PS2')_2]$ and $[Ni^{II}(PS1')_2]$ complexes.

Comparison of the normalized Ni K-edge XAS spectra for $[Ni^{IV}(PS2')_2]$ and $[Ni^{II}(PS1')_2]$ complexes (**Figure II-29**) shows that the Ni(IV) is clearly to higher energy than the Ni(II) complex, consistent with an increase in oxidation state. Comparison of the Ni K-edges of the $[Ni^{III}(PS2')_2]^{1-}$ to the $[Ni^{IV}(PS2')_2]$ (**Figure II-30**) demonstrate that the Ni(IV) data is clearly shifted to higher energy by ~1 eV (from 8340.0 to 8340.9eV) from Ni(III) complex. The whole series of Ni(II), Ni(III) and Ni(IV) is complete with the

trend of shifting higher energy from Ni(IV) to Ni(III) and to Ni(II), which indicates a metal-based oxidation has occurred.

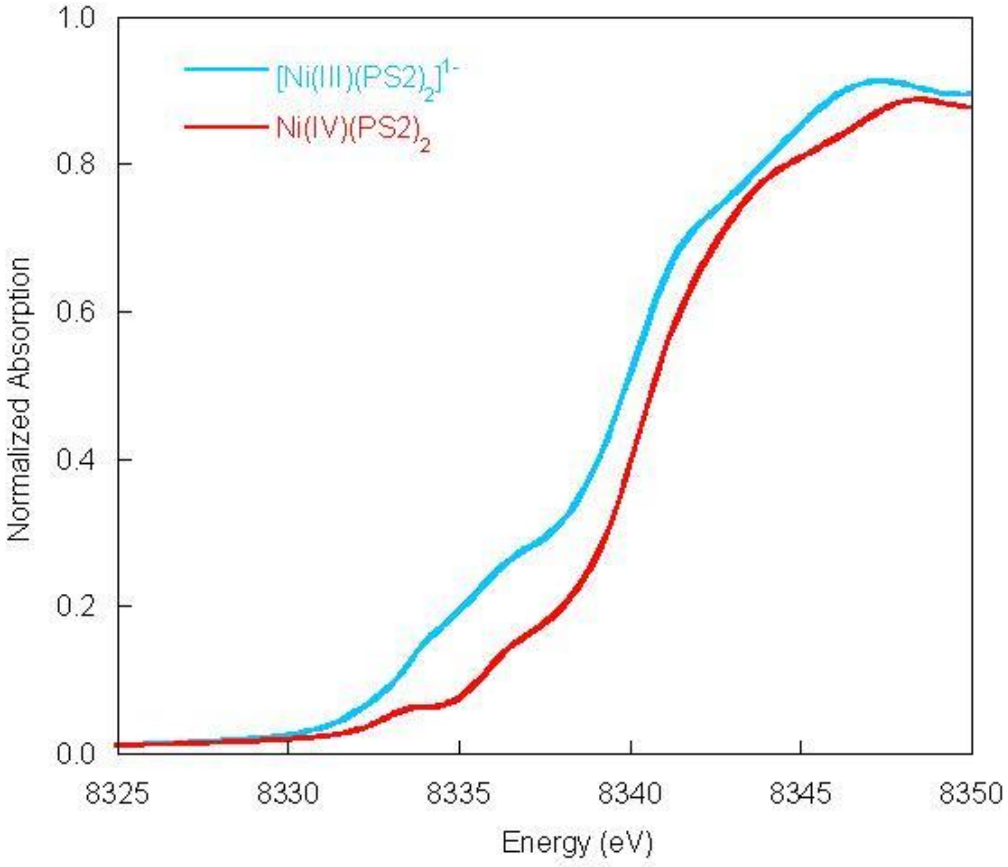

Figure II- 30. Comparison of the Ni K-edges of the $[Ni(III)(PS2)_2]^{1-}$ to the [Ni(IV)(PS2)].

Comparison of the S K-edges of the $[Ni^{III}(PS2')_2]^{1-}$ to the $[Ni^{IV}(PS2')_2]$ is shown in **Figure II-31**. The sulfur oxidation state appears unchanged (based on the feature marked 1). However, a new feature (marked 2) occurs at lower energy, which reflects the in-equivalent sulfurs in the Ni(III) structure. The pre-edge has increased in intensity, but no additional feature appears at lower energy (as we would expect for a ligand-based

radical) – so again, support for a Ni(IV) assignment. The oxidation states of the metal in these model complexes are then not ambiguous.

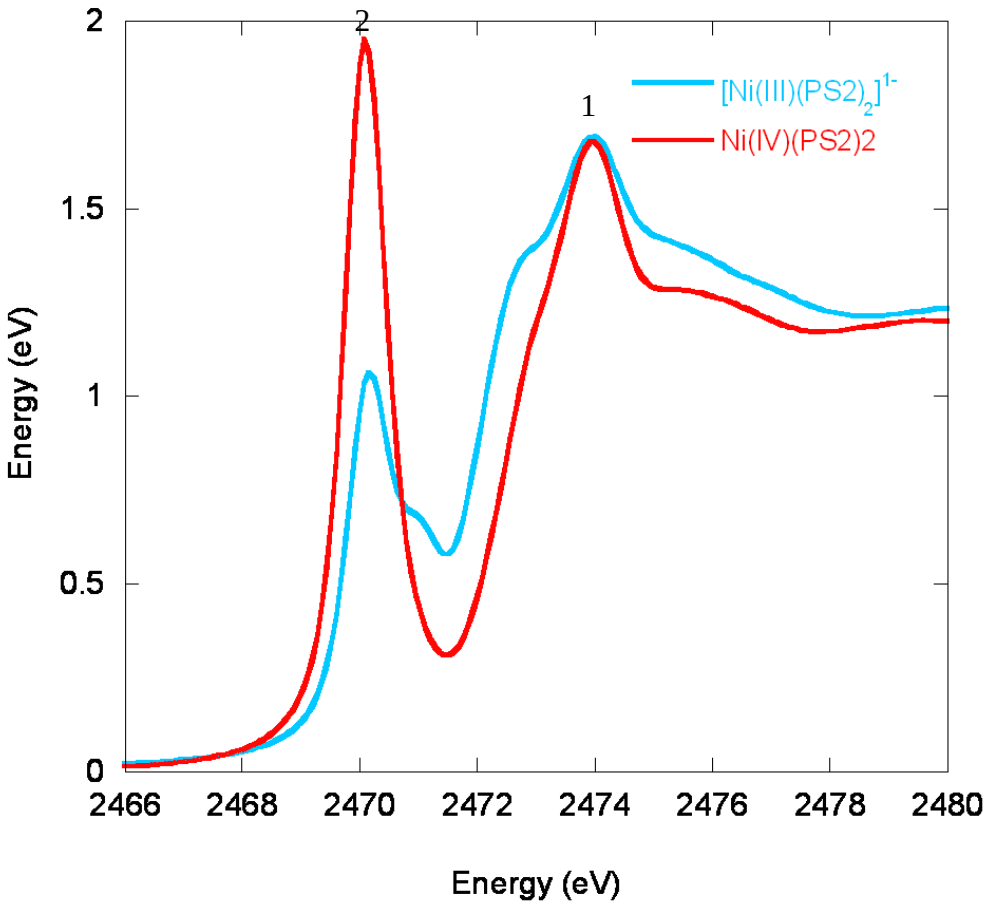

Figure II- 31. Comparison of the S K-edges of the $[Ni(III)(PS2)_2]^{1-}$ to the [Ni(IV)(PS2)].

3. CONCLUSION

$[M^{II}(PS2'H)_2]$ and $[M^{II}(PS2')_2]^{2-}$ (M = Ni, Pd and Pt) are square planar complexes with $[MS_2P_2]$ coordination with two coordinated thiolates and two non-coordinated pendant thiols. These M(II) complexes can be oxidized to form octahedral M(IV) complexes, $[M^{IV}(PS2')_2]$, in which the pendant thiolates have coordinated to the metal.

The pendant thiol SH's in the $[M^{II}(PS2'H)_2]$ complexes are engaged in hydrogen bonding interactions with the metal. This interaction has been demonstrated by X-ray crystallography and by NMR studies that indicates coupling between the thiol SH and ^{195}Pt.

All the four possible isomers of $[Pt^{II}(PS2'H)_2]$ have been detected in the ^{1}H and ^{31}P NMR spectra, and the structures of three of the isomers have been characterized by X-ray crystallography. Two isomers of Ni(IV) complexes are synthetically isolated, and have been characterized by ^{1}H NMR, ^{31}P NMR and X-Ray absorption spectroscopy.

Significantly, a biologically relevant three membered redox series of Ni(II) ↔ Ni(III) ↔ Ni(IV) have been synthesized and the oxidation state of metal center was confirmed by Ni K-edge XAS.

In metalloproteins, the reactivity of the metal center is determined by the residues in the second coordination sphere as well as the groups that bind directly to the metal. Therefore, this work, which is focused on the second coordination sphere –SH, is significant.

4. EXPERIMENTAL

Syntheses

$[Ni^{II}(PS2'H)_2]$ or $][Ni^{II}(C_6H_5P(CH_3\text{-}C_6H_3S)(CH_3\text{-}C_6H_3SH))_2]$:

The $[Ni^{II}(PS2'H)_2]$ complex was prepared by two method.

A) The nickel acetylacetonate ($Ni(acac)_2 \cdot 2H_2O$, 0.1490g, 0.502mmol) was dissolved in 15ml of methanol and was added dropwise to a methanol slurry of the $PS2'H_2$ ligand (0.3683g, 1.04mmol) . After 30mins stirring, a light green yellowish precipitate was formed and filtered. The product was recrystallized from dichloromethane (0.2870g, 75.0%).

B) The mono-deprotonated lithium thiolate salt solution was obtained by combining $PS2'H_2$ ligand (0.3541g, 1.00mmol) with lithium wire (0.0072mg, 1.02mmol) in 15ml methanol and stirring. Once the lithium wire had been consumed, a methanol solution of nickel(II) chloride hexahydrate (0.1184g, 0.498mmol) was added. A light green yellowish precipitate was formed immediately, and was filtered after 30mins stirring. The product was recrystallized from dichloromethane (0.2675g, 70.4%).

Green X-ray quality crystals were grown via vapor diffusion with dichloromethane into hexane under nitrogen.

^{1}HNMR ($CDCl_3$): δ 8.02-6.62ppm (22h, m, aromatic); 5.16 and5.03 ppm (2H, 3s, SH); and 2.23 and 2.19ppm (12H, 1s and 1d, CH_3)

^{31}P NMR ($CDCl_3$): 53.85ppm (*trans-syn*); 49.20ppm (*trans-anti*)

UV-Vis (in CH_2Cl_2, 10mM),), λ_{max} (ε_m): 375(4500)

Unit cell: Orthorhombic; Pbca, a = 14.5328(2)Å , b = 15.0982(2) Å , c = 18.5622(2) Å ,α= 90°, β=90°, γ = 90°, 4072.90(9) Å^3.

[Pd^{II}(PS2'H)$_2$] or][Pd^{II} ($C_6H_5P(CH_3$-$C_6H_3S)$ (CH_3-$C_6H_3SH)$)$_2$]:

The [Pd^{II}(PS2'H)$_2$] complex was prepared by two method.

A) The palladium acetylacetonate ($Pd(acac)_2$, 0.1526g, 0.501mmol) was dissolved in 15ml of methanol and was added dropwise to a methanol slurry of PS2'H_2 l (0.3683g, 1.04mmol). After 2 hours stirring, a light bright orange precipitate was formed and filtered. The product was recrystallized from dichloromethane (0.3040g, 74.7%).

B) The mono-deprotonated lithium thiolate salt solution was obtained by combining PS2'H_2 ligand (0.3541g, 1.00mmol) with lithium wire (0.0072mg, 1.02mmol) in 15ml methanol and stirring. Once the lithium wire had been onsumed, the reaction mixture was vacuum dried. Potassium tetrachloropalladate (K_2PdCl_4, 0.1633g, 0.500mmol) solid was added under N_2 before the freshly dried methanol

was added into the flask. The reaction suspension was heated to reflux. A bright orange precipitate started to form about 20 mins after reflux, and was filtered after one hour of reflux. The product was recrystallized from dichloromethane in the dark (0.2610g, 64.3%).

Orange X-ray quality crystals were grown via vapor diffusion with dichloromethane into hexane under nitrogen.

^{1}H NMR ($CDCl_3$): δ 7.99-6.68ppm (22H, m, aromatic); 4.81 and 4.62ppm (2H, 2s, SH); and 2.24 and 2.22(12H, 1d and 1s, CH_3)

^{31}P NMR ($CDCl_3$): 46.25ppm (*trans-anti*); 50.52 (*trans-syn*)

UV-Vis (5mM in DMF), λ_{max} (ε_m):305(57120); 380(4550) $M^{-1}cm^{-1}$

Unit cell: Orthorhombic, Pbca, a = 14.3965(2) Å , b = 15.17420(10) Å , c = 18.8113(2) Å ,α= 90°, β=90°, γ = 90°, 4109.43(8) $Å^3$.

[Pt^{II}(PS2'H)$_2$] or][Pt^{II} ($C_6H_5P(CH_3$-$C_6H_3S)$ (CH_3-$C_6H_3SH)$)$_2$]:

The mono-deprotonated lithium thiolate salt solution was obtained by combining PS2'H_2 ligand (0.3541g, 1.00mmol) with lithium wire (0.0072mg, 1.02mmol) in 15ml methanol. Once the lithium wire had been consumed, the reaction mixture was vacuum dried. Potassium tetrachloropalladate (K_2PdCl_4, 0.1633g, 0.500mmol) solid was added under N_2 before the freshly dried methanol was added into the flask. The reaction suspension was heated to reflux. A light yellow precipitate started to form after 45min,

and was filtered after two hours of reflux. The product was recrystallized from dichloromethane in the dark (0.2521g, 56.0%).

Light yellow X-ray quality crystals were grown via vapor diffusion with dichloromethane into hexane under nitrogen.

Trans-anti-:

^{1}H NMR($CDCl_3$): δ 7.97-6.77 (22H, m, aromatic); 5.56ppm (2H, t, SH), $J_{H\text{-}Pt}$ = 15Hz, and $J_{H\text{-}P}$ = 1.5Hz; 2.2ppm (12H, 2s, CH_3)

^{31}P NMR ($CDCl_3$): 43.98ppm (*trans-anti*)

UV-Vis (5mM in DMF), λ_{max} (ε_m):297(21870); 410(2100) $M^{-1}cm^{-1}$

Unit cell: (from $CHCl_3$) Triclinic, $P\bar{1}$, a = 9.2352(4) Å , b = 11.9200(5) Å , c = 13.1912(7) Å ,α= 101.774(4) °, β=101.062(4) °, γ = 107.236(4) °, 1307.38(11) $Å^3$.

(from CH_2Cl_2) Orthorhombic, P, a = 14.3769(2) Å , b = 15.1969(2) Å , c = 18.7966(3) Å ,α= 90°, β=90°, γ = 90°, 4106.76(10) $Å^3$.

Cis-anti:

Unit cell: (from $CHCl_3$): Triclinic, $P\bar{1}$, a = 11.4230(3) Å , b = 13.4334(2) Å , c = 14.7934(2) Å , α= 76.8410(10) °, β=75.245(2) °, γ = 68.878(2) °, 2014.34(7) $Å^3$

Cis-syn:

Unit cell: (from $CDCl_3$): Triclinic, $P\bar{1}$, a = 9.6006(3) Å , b = 12.9302(4) Å , c = 17.6838(6) Å , α= 100,997(3) °, β=101.740(3) °, γ = 108.856(3) °, 1954.45(11) $Å^3$

$[Amyl_4N]_2[Ni^{II}(PS2')_2]$ or $[(CH_3(CH_2)_4)_4N]_2[Ni^{II}(C_6H_5P(CH_3\text{-}C_6H_3S)_2)_2]$:

The di-deprotonated lithium thiolate salt solution was obtained by combining $PS2'H_2$ ligand (0.3540g, 1.00mmol) with lithium wire (0.0141mg, 2.01mmol) in 15ml methanol and stirring until all the lithium wire was consumed. Nickel (II) chloride hexahydrate (0.1184g, 0.498mmol) was degassed *in vacuo* for hours and the resultant pale yellow powder was dissolved in 10ml of methanol. Addition of the nickel solution slowly into the lithium thiolate salt solution yielded a brown solution immediately. Upon adding of *n*-tetrapentylammonium bromide ($Amyl_4NBr$, 0.5100g, 1.35mmol) methanol solution, brown precipitate was formed and filtered (0.5961g, 88.0%).

$[Ni^{IV}(PS2')_2]$ or $[Ni^{IV}(C_6H_5P(CH_3\text{-}C_6H_3S)_2)_2]$:

The di-deprotonated lithium thiolate salt solution was obtained by combining $PS2'H_2$ ligand (0.3540g, 1.00mmol) with lithium wire (0.0141mg, 2.01mmol) in 15ml methanol and stirring until the lithium wire was consumed. Nickel (II) chloride hexahydrate (0.1184g, 0.498mmol) was degassed *in vacuo* for hours and the resultant pale yellow powder was dissolved in 10ml of methanol. Addition of the nickel solution

slowly into the lithium thiolate salt solution yielded a brown solution immediately. After 30min of stirring, the reaction mixture was exposed to air, a precipitate was formed and filtered after standing overnight (0.2881g, *cis*-[Ni^{IV} $(PS2')_2$], 75.8%).

Purification of *cis*- and *trans-fac*-[$Ni^{IV}(PS2')_2$] or [$Ni^{IV}(C_6H_5P(CH_3\text{-}C_6H_3S)_2)_2$]:

When the reaction mixture of [$Ni^{IV}(PS2')_2$] reaction was only exposed to air for 10 hours, the resulting complexes were a mixture of *cis*- and *trans-fac* isomers. Gravity column chromatography was carried out to separate the two isomers. Chloroform solution of isomer mixtures (0.1450g) was subjected to chromatography over an alumina column (2.5cm, i.d. $\times 25\text{cm}$) with $CHCl_3/C_6H_{14}$ (3:1, 250ml) as eluent to give ten subfractions (I-X). Fraction III-VII were dried and yielded the yellow *trans-fac*-[$Ni^{IV}(PS2')_2$] (0.403g, about 95% pure). The same column was eluted again with 100% CH_3CN (200ml) and give eight more subfractions (XI-XVIII). Fraction XIII-XVII were dried and yielded the dark green cis-[$Ni^{IV}(PS2')_2$] (0.0870g, 100% pure).

Dark Green X-ray quality crystals of cis-[$Ni^{IV}(PS2')_2$] were grown via vapor diffusion with dichloromethane into hexane in air.

^{1}H NMR of *cis*-[$Ni^{IV}(PS2')_2$] ($CDCl_3$): δ7.45-6.44ppm (22H,m, aromatic); 2.14 and 2.13ppm (12H, 2s, CH_3)

^{1}H NMR of *trans-fac*-[$Ni^{IV}(PS2')_2$] ($CDCl_3$): δ7.47-6.99ppm (22H, m, aromatic); 2.36 and 2.24ppm (12H, 2s, CH_3)

^{31}P NMR of *trans-fac*-[$Ni^{IV}(PS2')_2$] ($CDCl_3$): 87.590ppm

^{31}P NMR of *trans-mer*-[Ni^{IV} $(PS2')_2$] ($CDCl_3$):72.840ppm

UV-Vis of *trans-fac*-[Ni^{IV} $(PS2')_2$], (10mM in CH_2Cl_2), λ_{max} (ε_m): 325nm (453000) 427nm (104000) $M^{-1}cm^{-1}$

UV-Vis of *cis*-[$Ni^{IV}(PS2')_2$], (10mM in CH_2Cl_2), λ_{max} (ε_m): 278nm (615200); 330nm (445700) $M^{-1}cm^{-1}$

Unit cell of *cis*-[$Ni^{IV}(PS2')_2$]: a = 9.8947(6) Å, b = 19.0213(8) Å, c = 35.033(3) Å, α= 90°, β=93.547(8)°, γ = 90°, 6580.9(7) $Å^3$

[$Pd^{IV}(PS2')_2$] or [$Pd^{IV}(C_6H_5P(CH_3\text{-}C_6H_3S)_2)_2$]:

The di-deprotonated lithium thiolate salt solution was obtained by combining $PS2'H_2$ ligand (0.3540g, 1.00mmol) with lithium wire (0.0141mg, 2.01mmol) in 15ml methanol. After the lithium wire had been consumed, the reaction mixture was vacuum dried. Potassium tetrachloropalladate (K_2PdCl_4, 0.1633g, 0.500mmol) solid was added under N_2 before the freshly dried methanol was added into the flask. The reaction suspension was refluxed for 30 minutes before the reaction mixture was exposed to air. The dark red precipitate was filtered after stirring overnight in air. (0.2395g, 0.300mmol *cis*-[Pd^{IV} $(PS2')_2$], 59.9% yield).

^{1}H NMR ($CDCl_3$): δ7.99-6.51ppm (22H, m, aromatic); 2.15 and 2.13ppm (12H, 2s, CH_3)

^{31}P NMR ($CDCl_3$): 81.21ppm

Unit cell: (from CH_2Cl_2) Monoclinic, $P2_1/c$, a = 14.681(5) Å , b = 15.094(4) Å , c = 17.723(5) Å ,α= 90 °, β=92.270(5) °, γ = 90 °, 3924(2) $Å^3$.

***Cis*-[Pt^{IV}(PS2')$_2$] or [Pt^{IV}($C_6H_5P(CH_3$-$C_6H_3S)_2)_2$]:**

The di-deprotonated lithium thiolate salt solution was obtained by combining PS2'H_2 ligand (0.3540g, 1.00mmol) with lithium wire (0.0141mg, 2.01mmol) in 15ml methanol. Once the lithium wire had been consumed, the reaction mixture was vacuum dried. Potassium tetrachloropalladate (K_2PdCl_4, 0.1633g, 0.500mmol) solid was added under N_2 before the freshly dried methanol was added into the flask. The reaction suspension was refluxed for 75 minutes before the reaction mixture was exposed to air. The dark red precipitate was filtered after overnight stirring in air. (0.2300g, 0.256mmol *cis*-[Pd^{IV} (PS2')$_2$], 51.2% yield).

^{1}H NMR ($CDCl_3$): δ 6.56-7.20ppm (22H, m, aromatic); 2.14ppm (12H, 1s, CH_3)

^{31}P NMR ($CDCl_3$): 57.00ppm

Unit cell: (from CH_2Cl_2) Monoclinic, $P2_1/c$, a = 14.76440(10) Å , b = 15.09140(10) Å , c = 17.73020(10) Å ,α= 90 °, β=92.3350(10) °, γ = 90 °, 3947.28(4) $Å^3$.

Unit cell: (from Et_2O) Monoclinic, $P2_1/c$, a = 15.000(5) Å , b = 14.915(2) Å , c = 18.036(4) Å ,α= 90°, β=90.900(5)°, γ = 90°, 4035 (2) $Å^3$.

X-ray Crystallography

***Trans-anti*-[$Ni^{II}(PS2'H)_2$] 2CH_2Cl_2:**

A yellowish green crystal measuring 0.20 x 0.20 x 0.15 mm^3 was mounted on a nylon loop and centered on the X-ray beam at 100K. The accurate unit cell was obtained using reflection with 2θ= 2.91- 32.90 °: a = 14.5328(2)Å , b = 15.0982(2) Å , c = 18.5622(2) Å ,α = β = γ = 90°, V= 4072.90(9) $Å^3$. The structure was solved under the primitive orthorhombic crystal system (space group Pbca) using 6842 reflections. The asymmetric unit consist one molecule of the nickel complex with inversion center and two methylene dichloride solvent molecules. The data reduction was done with CrysAlis Pro and the structure refinement was done with SHELXL-97 (Sheldrick). All the non-hydrogen atoms were located by Direct Methods and were refined anisotropically by a full-matrix least-squares method. The position of the hydrogen atom of each thiol group was located using Fourier difference maps. The positions of the remaining hydrogen atoms were calculated. The crystallographic parameters and atomic coordinates for this complex are located in **Table A-2**.

***Cis*-[$Ni^{IV}(PS2')_2$] MeCN:**

A dark green crystal measuring 0.30 x 0.30 x 0.50 mm^3 was mounted on a nylon loop and centered on the X-ray beam at 100K. The accurate unit cell was obtained using reflection with 2θ= 2.97- 32.96 °: a = 9.8947(6) Å, b = 19.0213(8) Å, c = 35.033(3) Å, α= 90 °, β=93.547(8) °, γ = 90°, V= 6580.9(7) $Å^3$. The structure was solved under the

primitive monoclinic crystal system (space group $P2_1/n$) using 22114 reflections. The asymmetric unit consist two molecules of the nickel complex with a mirror plane and one acetonitrile solvent molecules. The data reduction was done with CrysAlis Pro and the structure refinement was done with SHELXL-97 (Sheldrick). All the non-hydrogen atoms were located by Direct Methods and were refined anisotropically by a full-matrix least-squares method. T he position of the hydrogen atom of each methyl group was located using Fourier difference maps. The positions of the remaining hydrogen atoms were calculated. The crystallographic parameters and atomic coordinates for this complex are located in **Table A-3**.

$[Pd^{II}(PS2'H)_2]$ 2CH_2Cl_2:

A bright orange crystal measuring 0.50 x 0.30 x 0.15 mm^3 was mounted on a nylon loop and centered on the X-ray beam at 100K. The accurate unit cell was obtained using reflection with 2θ= 3.22- 32.92°. a = 14.3965(2) Å, b = 15.17420(10) Å, c = 18.8113(2) Å, $\alpha = \beta = \gamma = 90°$, V= 4109.43(8) $Å^3$. The structure was solved under the primitive orthorhombic crystal system (space group Pbca) using 7344 reflections. The asymmetric unit consist one molecule of the palladium complex with inversion center and two methylene dichloride solvent molecules. The data reduction was done with CrysAlis Pro and the structure refinement was done with SHELXL-97 (Sheldrick). All the non-hydrogen atoms were located by Direct Methods and were refined anisotropically by a full-matrix least-squares method. The position of the hydrogen atom of each thiol group was located using Fourier difference maps. The positions of the remaining hydrogen

atoms were calculated. The crystallographic parameters and atomic coordinates for this complex are located in **Table A-4**.

$[Pd^{IV}(PS2')_2]$ CH_2Cl_2:

A dark red crystal measuring 0.25 x 0.35 x 0.04 mm^3 was mounted on the nylon loop and centered on the X-ray beam at 100K. The accurate unit cell was obtained using reflection with 2θ= 3.23- 32.89°: a = 14.681(5) Å , b = 15.094(4) Å , c = 17.723(5) Å, α = 90°, β = 92.270(5)°, γ = 90°, V = 3924(2) $Å^3$. The structure was solved under the primitive monoclinic crystal system (space group $P2_1/c$) using 13160 reflections. The asymmetric unit consist one molecule of the palladium complex with inversion center and one methylene dichloride solvent molecules. The data reduction was done with CrysAlis Pro and the structure refinement was done with SHELXL-97 (Sheldrick). All the non-hydrogen atoms were located by Direct Methods and were refined anisotropically by a full-matrix least-squares method. The position of the hydrogen atom of each methyl group was located using Fourier difference maps. The positions of the remaining hydrogen atoms were calculated. The crystallographic parameters and atomic coordinates for this complex are located in **Table A-7**.

***trans-anti*-$[Pt^{II}(PS2'H)_2]$ $2CH_2Cl_2$:**

A light yellow crystal measuring 0.25 x 0.20 x 0.05 mm^3 was mounted on a nylon loop and centered on the X-ray beam at 100K. The accurate unit cell was obtained using reflection with 2θ= 3.22- 32.96°: a = 14.3769(2) Å , b = 15.1969(2) Å, c = 18.7966(3) Å,

$\alpha = \beta = \gamma = 90°$, V = 4106.76(10) $Å^3$. The structure was solved under the primitive orthorhombic crystal system (space group Pbca) using 7245 reflections. The asymmetric unit consist one molecule of the platinum complex with inversion center and one methylene dichloride solvent molecules. The data reduction was done with CrysAlis Pro and the structure refinement was done with SHELXL-97 (Sheldrick). All the non-hydrogen atoms were located by Direct Methods and were refined anisotropically by a full-matrix least-squares method. The position of the hydrogen atom of each thiol group was located using Fourier difference maps. The positions of the remaining hydrogen atoms were calculated. The crystallographic parameters and atomic coordinates for this complex are located in Table A-8.

***trans-anti*-$[Pt^{II}(PS2'H)_2]$ $4CHCl_3$:**

A light yellow crystal measuring 0.40 x 0.20 x 0.15 mm^3 was mounted on the nylon loop and centered on the X-ray beam at 100K. The accurate unit cell was obtained using reflection with 2θ= 3.25- 29.60°. a = 9.2352(4) Å, b = 11.9200(5) Å, c = 13.1912(7) Å, α = 101.774(4)°, β = 101.062(4)°, γ = 107.236(4)°, V = 1307.38(11) $Å^3$. The structure was solved under the primitive triclinic crystal system (space group $P\bar{1}$) using 6211 reflections. The asymmetric unit consist half molecule of the platinum complex with inversion center and two chloroform solvent molecules. The data reduction was done with CrysAlis Pro and the structure refinement was done with SHELXL-97 (Sheldrick). All the non-hydrogen atoms were located by Direct Methods and were

refined anisotropically by a full-matrix least-squares method. The position of the hydrogen atom of each thiol group was located using Fourier difference maps. The positions of the remaining hydrogen atoms were calculated. The crystallographic parameters and atomic coordinates for this complex are located in **Table A-9**.

***cis-anti*-[Pt^{II}(PS2'H)$_2$] $CHCl_3$:**

A light yellow crystal measuring 0.30 x 0.15 x 0.06 mm^3 was mounted on the nylon loop and centered on the X-ray beam at 100K. The accurate unit cell was obtained using reflection with 2θ= 3.16- 30.49 °. a = 11.4230(3) Å, b = 13.4334(2) Å, c = 14.7934(2) Å, α = 76.8410(10) °, β = 75.245(2) °, γ = 68.878(2)°, V = 2014.34(7) $Å^3$. The structure was solved under the primitive triclinic crystal system (space group P_1) using 10865 reflections. The asymmetric unit consist one molecule of the platinum complex and one chloroform solvent molecule. The data reduction was done with CrysAlis Pro and the structure refinement was done with SHELXL-97 (Sheldrick). All the non-hydrogen atoms were located by Direct Methods and were refined anisotropically by a full-matrix least-squares method. The position of the hydrogen atom of each thiol group was located using Fourier difference maps. T he positions of the remaining hydrogen atoms were calculated. The crystallographic parameters and atomic coordinates for this complex are located in **Table A-10**.

***cis-syn*-[Pt^{II}(PS2'H)$_2$] $CDCl_3$:**

A light yellow crystal measuring 0.10 x 0.10 x 0.05 mm^3 was mounted on the nylon loop and centered on the X-ray beam at 100K. The accurate unit cell was obtained using reflection with 2θ= 3.20- 29.48 °: a = 9.6006(3) Å, b = 12.9302(4) Å, c = 17.6838(6) Å, α = 100,997(3) °, β = 101.740(3) °, γ = 108.856(3)°, V = 1954.45(11) $Å^3$. The structure was solved under the primitive triclinic crystal system (space group P_1) using 9092 reflections. The asymmetric unit consist one molecule of the platinum complex and one deuterated chloroform solvent molecule. The data reduction was done with CrysAlis Pro and the structure refinement was done with SHELXL-97 (Sheldrick). All the non-hydrogen atoms were located by Direct Methods and were refined anisotropically by a full-matrix least-squares method. The position of the hydrogen atom of each methyl group was located using Fourier difference maps. The positions of the remaining hydrogen atoms were calculated. The crystallographic parameters and atomic coordinates for this complex are located in **Table A-11**.

***cis* -[Pt^{IV}(PS2')$_2$] CH_2Cl_2:**

A yellow crystal measuring 0.40 x 0.20 x 0.05 mm^3 was mounted on the nylon loop and centered on the X-ray beam at 100K. The accurate unit cell was obtained using reflection with 2θ= 3.22- 32.93 °: a = 14.76440(10) Å, b = 15.09140(10) Å, c = 17.73020(10) Å, α= 90°, β = 92.3350(10) °, γ = 90°, V= 3947.28(4) $Å^3$. The structure was solved under

the primitive monoclinic crystal system (space group $P2_1/c$) using 13876 reflections. The asymmetric unit consist one molecule of the platinum complex and one methylene dichloride solvent molecule. The data reduction was done with CrysAlis Pro and the structure refinement was done with SHELXL-97 (Sheldrick). All the non-hydrogen atoms were located by Direct Methods and were refined anisotropically by a full-matrix least-squares method. The position of the hydrogen atom of each methyl group was located using Fourier difference maps. The positions of the remaining hydrogen atoms were calculated. The crystallographic parameters and atomic coordinates for this complex are located in **Table A-13**.

***Cis*-[Pt^{IV}(PS2')$_2$] ·Et_2O:**

A yellow crystal measuring 0.20 x 0.10 x 0.10 mm^3 was mounted on the nylon loop and centered on the X-ray beam at 100K. The accurate unit cell was obtained using reflection with 2θ= 3.25- 33.26°: a = 15.000(5) Å, b = 14.915(2) Å, c = 18.036(4) Å, α= 90°, β=90.900(5)°, γ = 90°, V = 4035 (2) $Å^3$. The structure was solved under the primitive monoclinic crystal system (space group $P2_1/c$) using 10949 reflections. The asymmetric unit consist one molecule of the platinum complex and one ether solvent molecule. The data reduction was done with CrysAlis Pro and the structure refinement was done with SHELXL-97 (Sheldrick). All the non-hydrogen atoms were located by Direct Methods and were refined anisotropically by a full-matrix least-squares method. The position of the hydrogen atom of each methyl group was located using Fourier

difference maps. The positions of the remaining hydrogen atoms were calculated. The crystallographic parameters and atomic coordinates for this complex are located in **Table A-14.**

REFERENCES

(1) Venkateswara Rao, P.; Holm, R. H. *Chem. Rev.* **2004**, *104*, 527.

(2) Block, E.; Oforiokai, G.; Zubieta, J. *J. Am. Chem. Soc* **1989**, *111*, 2327.

(3) Silverstein, R. M.; Bassler, G. C.; Morrill, T. C. *Spectrometric Indentification of Organic Compounds*; 5th ed.; John Wiley & Sons, Inc.: New York, 1991.

(4) Chiarella, G. M. *Ph. D Dissertation*; State University of New York at Stony Brook, 2006.

(5) Crabtree, R. H. *The organometallic chemistry of the transition metals*; Wiley-Interscience, 2005.

(6) Nixcon, J. F.; Pidcock, A. *Annual Review of NMR Spectroscopy* **1969**, *2*, 345.

(7) Lyne, P. D.; Mingos, D. M. P. *Journal of the Chemical Society, Dalton Transactions* **1995**, 1635.

(8) Chan, K. H.-Y.; Chow, H.-S.; Wong, K. M.-C.; Yeung, M. C.-L.; Yam, V. W.-W. *Chemical Science* **2010**, *1*, 477.

(9) Drew, M. G. B.; Wilkins, J. D. *Journal of the Chemical Society, Dalton Transactions* **1974**, 1973.

(10) Lippard, S. J. *Principles of bioinorganic chemistry*; University Science Books: Mill Valley, Calif, 1994.

Chapter 3

Alkylation reactivity study of $[M^{II}(PS2')_2]^{2-}$

(M=Pd, Pt)

1. INTRODUCTION

It has been recognized that thiolate groups bound to a certain transition-metal center possess relatively high nucleophilicity.[1] In the past two decades, ligand-based reactivity of thiolates coordinated to late transition metals, *via* alkylation, metallation, oxygenation, and adduct formation is well documented.[2] For example, oxidation reactions afford coordinated sulfenato and sulfinato species.[3-6] while alkylation reactions produce various coordinated thioether species.[7-10]

Sulfur containing species such as thiolate (RS^-) have been found to possess the ability to activate the C-X (X=halogen) bonds in organic electrophiles[11]. Alkylation of ruthenium-bound thiolates has been reported by Sellmann *et al.*[12] and Grapperhaus *et al.*[2], Jones and co-workers[13] have reported the alkylation of nickel bound sulfides by 1,2-dichloroethane, and Chikamoto *et al.*[14] recently reported alkylation of an S-bridged $Co^{III}Pd^{II}Co^{III}$ trinuclear complex containing two non-bridging thiolato groups with 1,2-Bis(bromomethyl)benzene in water.

The alkylation of the thiolates is attracting some interests since it is relevant to metal-containing alkyl transfer enzymes, such as DNA repair protein Ada.[15] *Escherichia coli* Ada protein possesses a $[Zn(S\text{-}Cys)_4]$ zinc center in the N-terminal side, and among the four cysteines of its zinc core, Cys38 is specifically alkylated.[16-17] The methyl group transferred from the phosphotriester DNA backbone is irreversible and therefore, Ada is considered as a sacrificial agent for DNA repair.[18-19] To date, these investigations have been extensively made with mononuclear complex systems, such as Co^{III}, Ru^{II} and Ni^{II},

and it has been shown that the modification at thiolato donors affects the spectroscopic and stereochemical properties of complexes.[1] On the other hand, alkylations of the Pd^{II} and Pt^{II} coordinated thiolates have not been reported to our best knowledge.

Previously, Voorhies and Millar prepared and crystallographically characterized *trans-syn*-$[Ni^{II}(PS2')_2][Li][PPh_4]$ and *trans-anti*-$[Ni^{II}(PS2')_2][Et_4N]_2$ complexes. These complexes, for the first time, successfully demonstrated that $[Ni^{II}(PS2')]^{2-}$ form could be stabilized and isolated. It also confirmed the conjecture that both *syn-* and *anti-* configurations are possible for the non-coordinated pendant thiolates in these square planar complexes.

We have investigated the chemistry of Pd and Pt with the $(PS2)^{2-}$ ligand. A Pd analog, $[Pd^{II}(PS2')_2]^{2-}$, was successfully prepared, isolated and crystallographically characterized. Reacting the deprotonated pendant metal thiolate complexes, $[M^{II}(PS2')_2]^{2-}$, with methylene dichloride, gave neutral alkylated complexes with a CH_2 group linking the non-coordinated thiolates . $[M^{II}(PS2'(CH_2)S2'P)]$ (M= Pd, Pt), were successfully synthesized and fully characterized. The corresponding nickel complex reaction was not observed under similar reaction conditions. The general Scheme is shown in **Scheme III-1**.

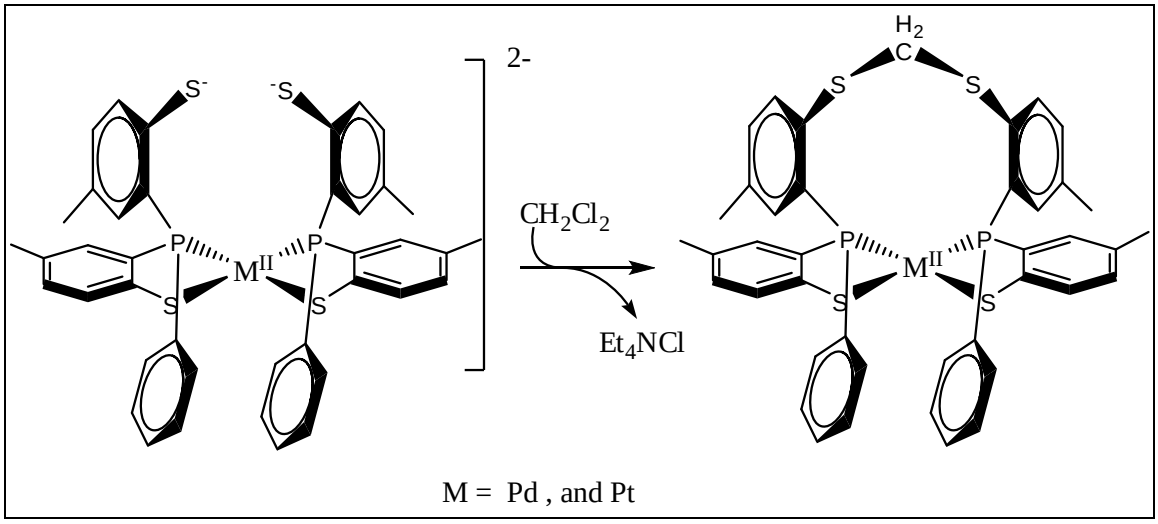

Scheme III- 1. General scheme for alkylation of $[M^{II}(PS2')_2]^{2-}$.

These results revealed that the nucleophilicity of non-coordinated pendant thiolate of $[M^{II}(PS2')_2]^{2-}$ (M= Pd, Pt) is quite strong such that it was able to activate both C-Cl bonds and form two C-S bonds with the same methylene dichloride molecule. The result of having one pure isomer as product also revealed that in solution, the *cis-syn*-$[M^{II}(PS2')_2]^{2-}$ isomer is favored in alkylation. The mild reaction condition, room temperature with or without light, also suggests that the activation energy of isomerization of the $[M^{II}(PS2')_2]^{2-}$ is low. The ability to accomplish the same metal group, Pd and Pt, for the same reaction provides us an opportunity to compare the product and gain more insight for thiolate alkylation reactions.

An often-encountered scenario with the attempted reactivity study of alkylation of thiolates is the tendency of aggregation and the formation of a multi-metal polymeric species. The steric hindrance provided by the combination of square planar metal center

and the large chelating ligands made it possible for the alkylated monomers to be the only product.

2. RESULT AND DISCUSSION

$[(Et_4N)_2][M^{II}(PS2')_2]$ and alkylated products (palladium and platinum) complexes were synthesized under mild condition and crystallographically characterized.

A dried sample of $(Et_4N)_2[Pt^{II}(PS2')_2]$ was dissolved in dichloromethane and layered with hexanes. After 1-2 days, colorless needle shaped crystals were observed in the Schlenk tube; X-ray diffraction studies identified these crystals as Et_4NCl on the basis of its unit cell dimensions(a = 8.429Å, b= 8.109Å, c=14.499Å, α= 90, β = 91.38, γ = 90, V = 990.73 Å; space group: $P2_1/c$). Over the next 2-3 days, yellow, columnar crystals were also observed. Refinement of X-ray crystal structure of this crystal revealed that the pendant thiolates have been alkylated yielding the methylene bridged thioether complex $[Pt^{II}(PS2'(CH_2)S2'P)]$. The platinum maintains the square planar geometry as in the pendant complex, but the complex with cis-phosphorus atoms was the only product.

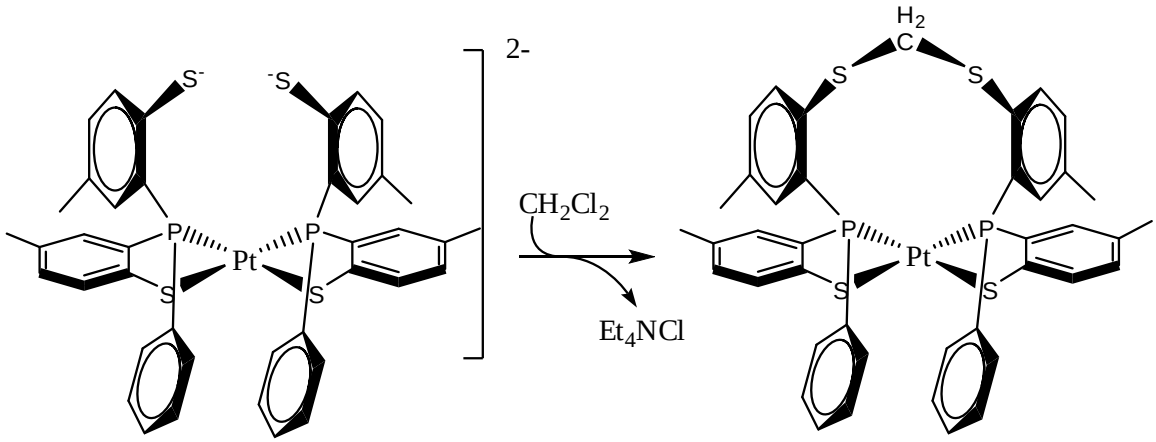

Scheme III- 2. Scheme for alkylation of $[Pt^{II}(PS2')_2]^{2-}$.

The diagram of the crystal structure of $[Pt^{II}(PS2'(CH_2)S2'P)]$ is shown in **Figure III-1**. The bonded sulfurs, S(1) and S(3), have similar shorter metal-sulfur bond distances, 2.3177(11) Å for S(1) and 2.3289(8) Å for S(3), than the pendant sulfurs, 3.6696(13) Å for S(3) and 3.6428(17) Å for S(4). The bonded metal-sulfur distance is similar to the ones of protonated pendant complex, $[Pt^{II}(PS2'H)_2]$. The long distance between alkylated sulfur and platinum atom confirmed that S(2) and S(4) are not bonded to the platinum, so that the square planar coordination geometry remained. The Pt(1)-P(1) and Pt(1)-P(2) bond distances slightly decrease from 2.2561(6) Å and 2.2601(6) Å in the pendant $[Pt(PS2'H)_2]$ complex to 2.2480(6) Å and 2.2539(6) Å in the alkylated $[Pt(PS2'(CH_2)S2'P)]$.

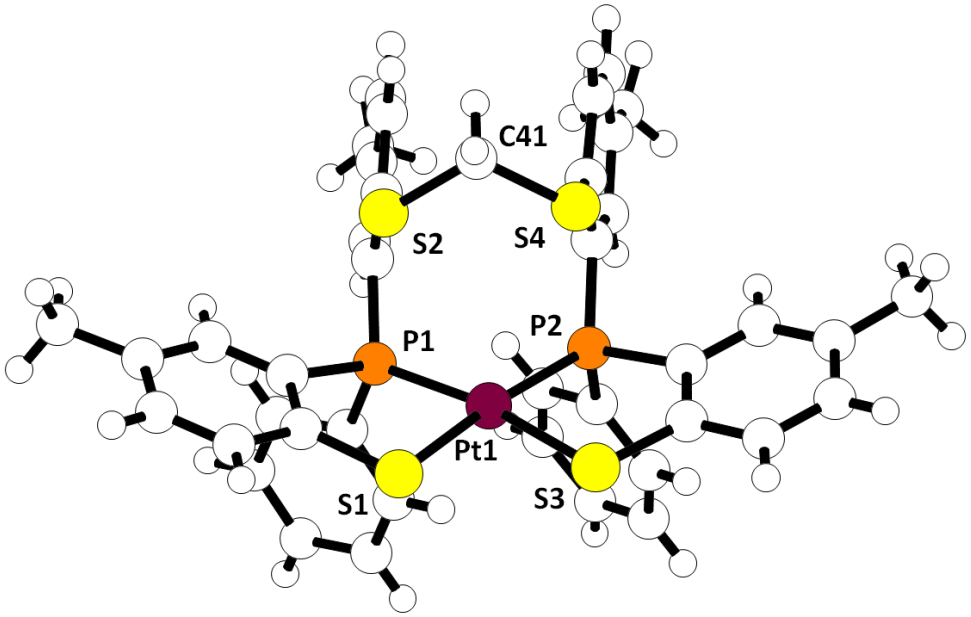

Figure III- 1. Molecular structure of [Pt^{II}(PS2'(CH_2)S2'P)], Chem-Ray structure. The solvent molecules are omitted for clarity.

The ten membered ring, Pt(1)-P(2)-C(29)-C(28)-S(4)-C(41)-S(2)-C(8)-C(9)-P(1), resulted from the formation of the methylene bridge, has a chair confirmation. Among all the bond angles, P(2)-Pt(1)-P(1), C(41)-S(2)-C(8), and C(41)-S(4)-C(28) angles are 101.59(3) °, 101.8(3) °, and 101.5(4) °respectively, while the rest are around 120 °, ranging from 117.0(3) °to 124.15(14) °.

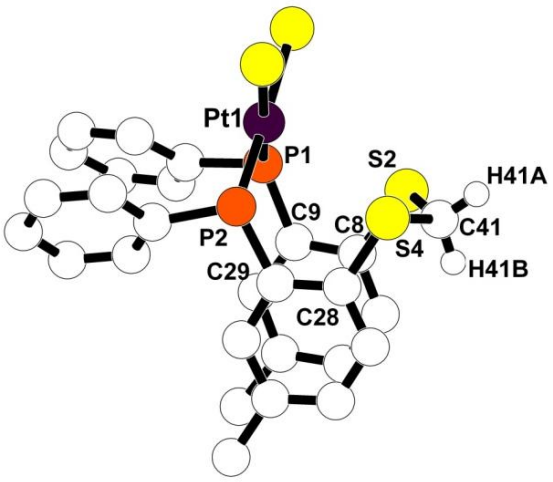

Figure III- 2. Chair confirmation of chelated ten-membered ring of $[Pt^{II}(PS2'(CH_2)S2'P)]$. Parts of the structure and the hydrogen atoms are omitted for clarity.

The chair conformation of the ten-membered ring is different from the stable crown conformation of cyclodecane (**FigureIII-2**), which is as expected with existence of the π-bond from the alkylated thiophenol ring and the lone pair electrons on the pendant sulfur atom.

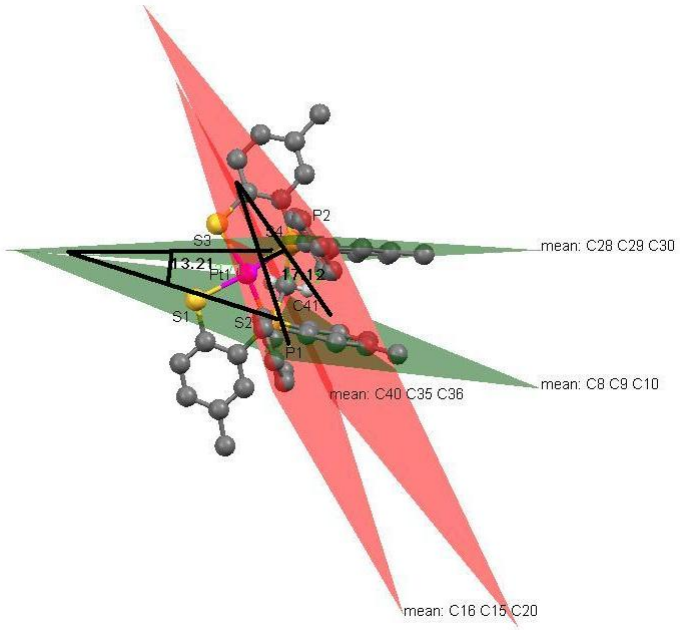

Intramolecular π-π interactions in [Pt^{II}(PS2'(CH_2)S2'P)], their dihedral angles

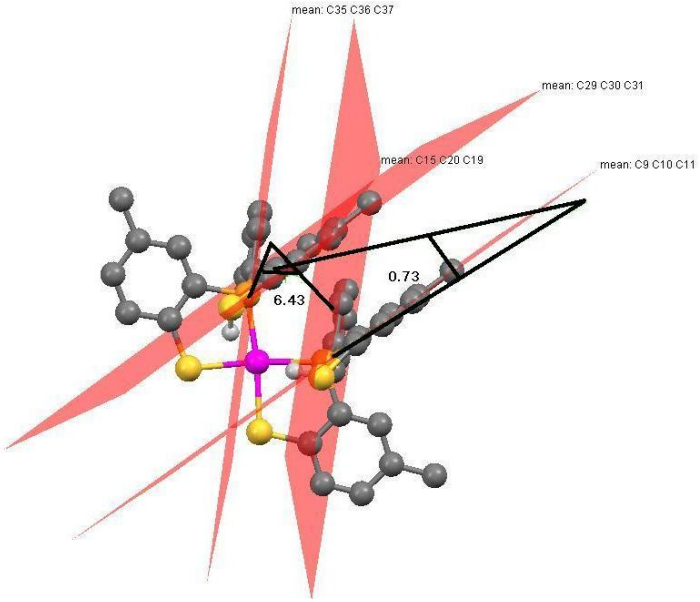

Intramolecular π-π interactions in *cis-syn*-[Pt^{II}(PS2'H)$_2$], their dihedral angles

Figure III- 3. Intramolecular π-π interactions in Pt(II) complexes and their dihedral angles.(a) [Pt^{II}(PS2'(CH_2)S2'P)] (b) *cis-syn*-[Pt^{II}(PS2'H)$_2$]. Mercury figure, the solvent molecules and hydrogen atoms are omitted for clarity.

With the crystal structure of *cis-syn*-[Pt^{II}(PS2'H)$_2$], we are able to compare the structure before and after alkylation, and therefore have a better understanding of the alkylation reaction. It was notable that, two pairs of intramolecular π-π interactions were found in both the protonated pendant complex and alkylated complex (**Figure III-3**), two phenyl rings on phosphorus and the two non-coordinated thiophenol rings. All intramolecular π-π interactions are face-to-face π-overlap stacking, but compared to the pendant protonated complex, *cis-syn*-[Pt^{II}(PS2'H)$_2$], the dihedral angles of both pairs of π-π interactions in the alkylated complexes, [Pt^{II}(PS2'(CH_2)S2'P)], are larger. It is 13.21 ° for two thiophenol ring planes and is 17.12 ° for the two phenyl ring planes on phosphorus, compared to the 6.43 ° and 0.73 ° respectively in *cis-syn*-[Pt^{II}(PS2'H)$_2$]. The electrons in the methylene group in the alkylated complex increase the electron richness in the aromatic ring, hence increase the repulsion of face-to-face stacking[20] (**Figure III-4**); while the spatial restraint provided by the bridging methylene forces one end of the aromatic plane stay closer to each other.

In the protonated pendant complex, [Pt^{II}(PS2'H)$_2$], the two non-bonded thiophenol ring planes are separated by 3.479Å and the two phenyl ring planes on phosphorus are separated by 3.111Å. In contrast, in the alkylated complex [Pt^{II}(PS2'(CH_2)S2'P)] , the two non-bonded thiophenol ring planes are 3.269Å apart at the minimum and 3.837Å apart at the maximum; the two phenyl ring planes on phosphorus are 2.568Å apart at the minimum and 3.341Å apart at the maximum. All these distance confirmed the existence of the intramolecular π-π interactions.

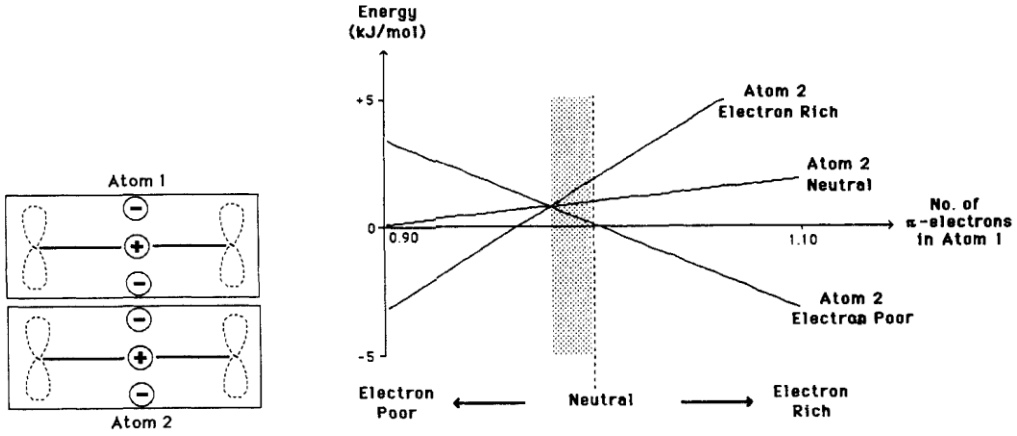

(b)

Figure III- 4. Calculated model for π-π interaction (adopted from ref[20]) (a) face-to-face π-stacked geometry (b) effect of π-electron polarization on the interaction between two idealized π-atoms in a face-to–face π-stacked geometry. Electron deficient and electron rich refer to net charges of ±0.10

Intermolecular π-π interactions are also found in the crystal structure of both the protonated pendant complex and alkylated complex (**Figure III-5**). One of the most significant intermolecular π-π interactions in the alkylated complex, $[Pt^{II}(PS2'(CH_2)S2'P)]$, is the offset stacking between the two phenyl rings from two independent molecules. The two planes are perfectly parallel to each other. In contrast, in *cis-syn*-$[Pt^{II}(PS2'H)_2]$, the protonated pedant complex, the two bonded thiophenolate rings from independent molecules engage in weak intermolecular π-π interaction. They are at 4.37 ° tilt from being parallel and separated by 3.687Å with an offset stacking orientation. The two non-bonded thiophenol ring planes from independent molecules are

parallel to each other, but they are too staggered that the crystal packing is more regulated by the hydrogen bonding between two protons on the non-bonded thiophenol.

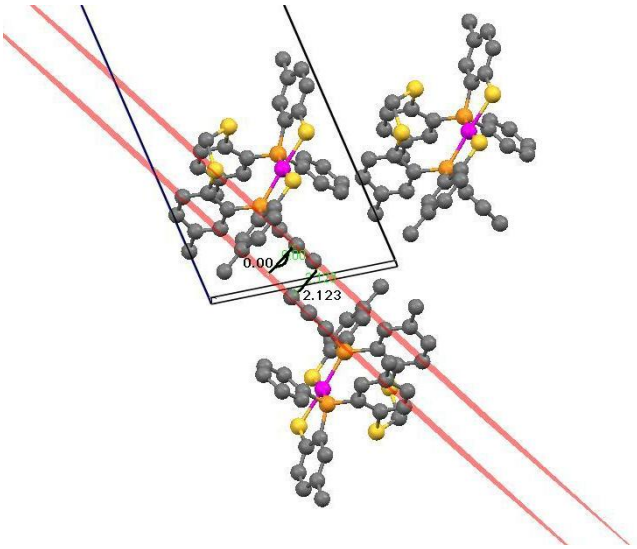

Intermolecular π-π interactions in [Pt^{II}(PS2'(CH_2)S2'P)].

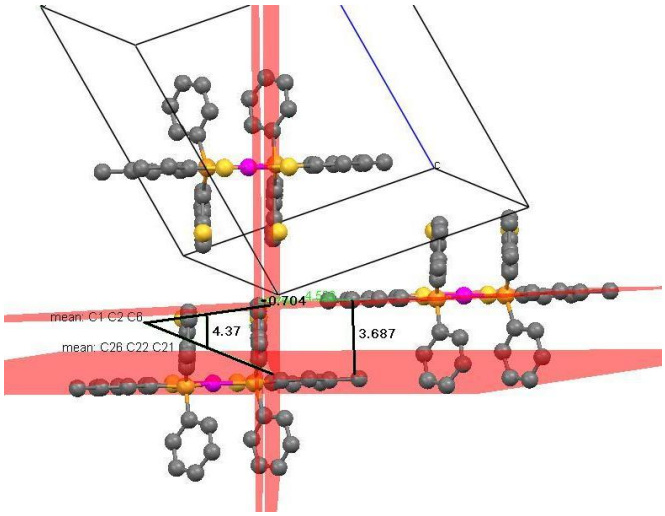

Intermolecular π-π interactions in *cis-syn*-[Pt^{II}(PS2'H)$_2$]

Figure III- 5. Intermolecular π-π interactions in Pt(II) complexes and their dihedral angles. (a) [Pt^{II}(PS2'(CH_2)S2'P)] (b) cis-syn-[PtII(PS2'H)$_2$]. Mercury figure, the solvent molecules and hydrogen atoms are omitted for clarity.

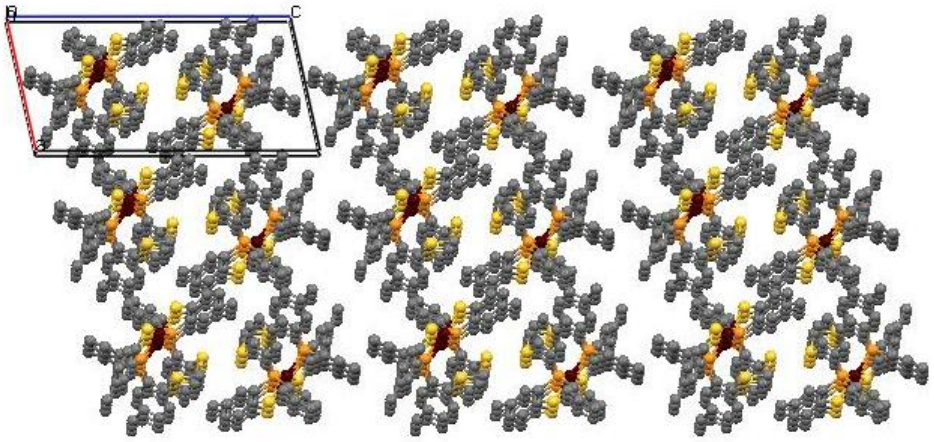

Figure III- 6. Crystal packing diagram of [Pt^{II}(PS2'(CH_2)S2'P)], (view slightly off the C* axis, Mercury figure, the solvent molecules and hydrogen atoms are omitted for clarity.)

The crystal packing diagram of [Pt^{II}(PS2'(CH_2)S2'P)] (**Figure III-6**) reveals the bilayer packed structure, with the alkylated thiophenol ring and phenyl ring on phosphorus are acting like the hydrophobic tail and hydrophilic head in a phospholipid.

[Pd^{II}(PS2')$_2$]$^{2-}$ was prepared and successfully isolated for the first time from double deprotonated PS2' ligand and Pd(II) starting materials. Even though four isomers are possible, only the *trans-anti*-[Pd^{II}(PS2')$_2$]$^{2-}$ was crystallographically observed (**Figure III-7**). The two pendant thiolates are *anti*- to each other while phosphorus on two different ligands are *trans*- to each other, hence it is named as *trans-anti*-[Pd^{II}(PS2')$_2$]$^{2-}$. The average distance between Pd and pendant thiolates is about 3.988Å, which confirms

the nonbonding interactions. The palladium has the same square planar center as in the protonated pendant counterpart. There is an inversion center in the structure of *trans-anti*-$[Pd^{II}(PS2')_2]^{2-}$. The bonding situation and the number of counter cations confirmed that the palladium remains in the +2 oxidation state. The oxidation state would be unreasonable if the pendant thiolates were, in fact, protonated but these protons were not observed in the X-ray structure.

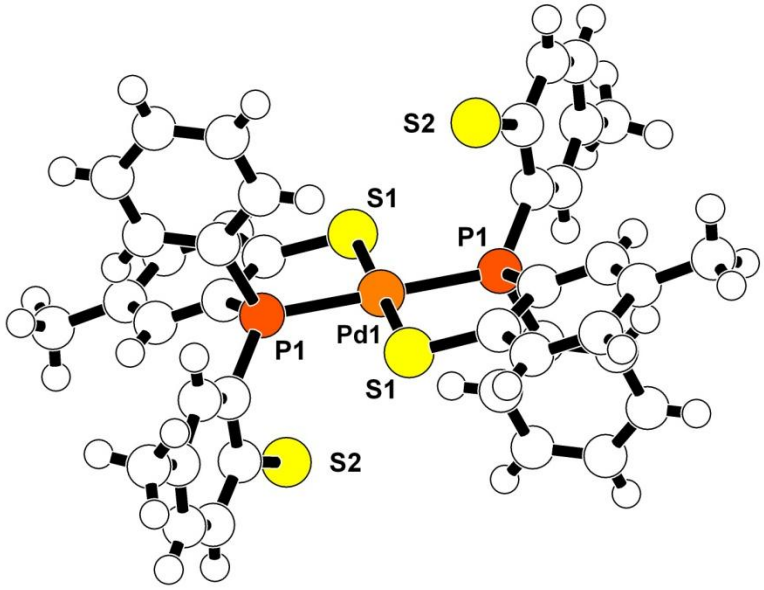

Figure III- 7. Molecular structure of $[(Et_4N)_2][Pd^{II}(PS2')_2]$, ChemRay structure. The solvent molecules and cations are omitted for clarity.

In the unit cell, the asymmetric unit contains a half $[Pd^{II}(PS2')_2]^{2-}$ anion, one $[Et_4N]^+$ cation and two methanol solvent molecules. The packed views along the c axis (**Figure III-8** (a) and (b)) of the $[Pd^{II}(PS2')_2]^{2-}$ reveal that the complex is forming a ordered structure 3D channel structure with methanol solvent molecules "absorbed" in this channel. One of two different methanol molecules in the unit cell is hydrogen bonded to the thiolate with the S^-•••H-O-CH_3 being 2.274Å, while the other methanol molecule has hydrogen bonding between methanol molecules with O•••H being 1.936Å. The S^-•••H-O-CH_3 hydrogen bonding is very strong, with ion involved and the length shorter than the sum of van der Waals radii.

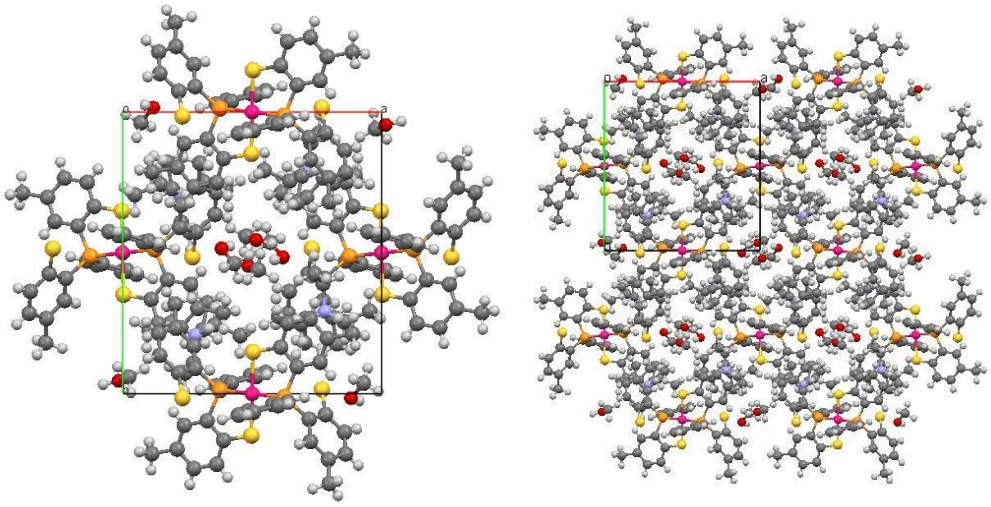

(a) "Single channel" (b) "multi channel"

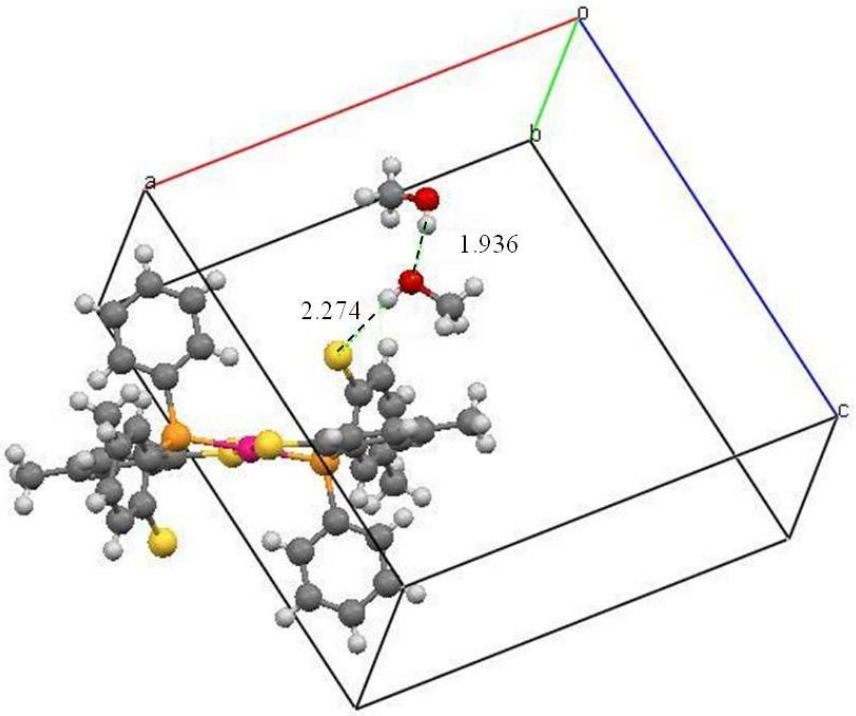

(c) Hydrogen bonding in the structure of $(Et_4N)_2[Pd^{II}(PS2')_2]$

Figure III- 8. Crystal packing structure and hydrogen bonding for $[(Et_4N)_2][Pd^{II}(PS2')_2]$•2MeOH (Mercury figures) (a) "single channel" of $[Pd^{II}(PS2')_2]^{2-}$ (c axis view) (b) aggregated "multi channel" of $[Pd^{II}(PS2')_2]^{2-}$ (c axis view) (c) Hydrogen bonding in the structure of $(Et_4N)_2[Pd^{II}(PS2')_2]$

A dried sample of $[(Et_4N)_2][Pd^{II}(PS2')_2]$ were dissolved in dichloromethane and layered with hexanes. After 1-2 days, colorless needle shaped crystals were observed in the Schlenk tube; subsequent X-ray diffraction studies identified these crystals as Et_4NCl on the basis of the unit cell dimensions from pre-experiment: (a = 8.429Å b = 8.109Å, c = 14.499Å; α = 90.00, β = 91.38, γ = 90.00; V = 990.7; space group = $P2_1/c$). Over the next 2-3 days, orange, rectangular plate crystals were also observed. Refinement of X-

ray crystal structure of this crystal reveals that the pendant thiolates have been alkylated yielding the methylene bridged thioether complex [Pd^{II}(PS2'(CH_2)S2'P)]. The square planar geometry of the Pd complex is maintained but the alkylation of the pendant thiolates, forces the two phosphorus ligand to adopt a cis arrangement.

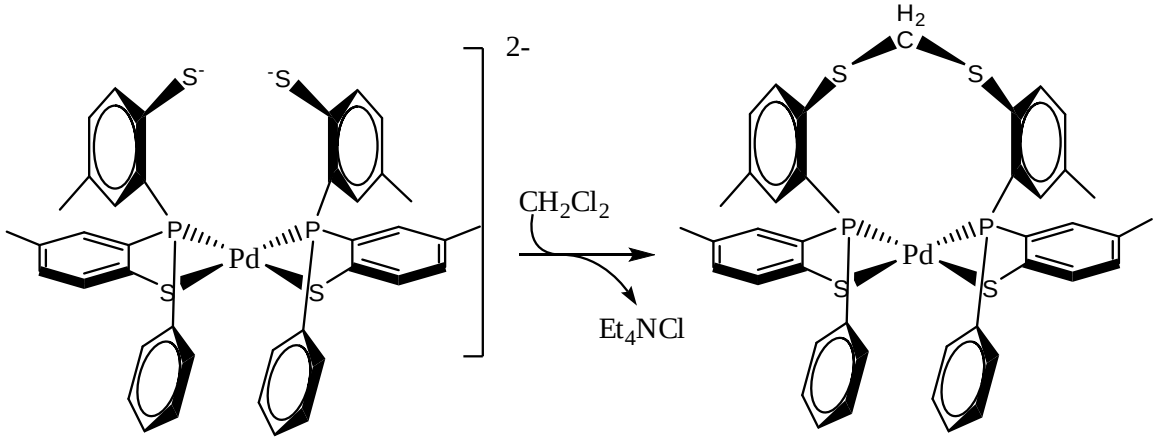

Scheme III- 3. Scheme for alkylation of $[Pt^{II}(PS2')_2]^{2-}$.

The diagram of the crystal structure of [Pd^{II}(PS2'(CH_2)S2'P)] is shown in **Figure III-9**. It is interesting that we noticed that Pd-P bond are slightly longer than the Pt-P bond, being 2.2598(6) Å for Pd1-P1 and 2.2788(5) Å for Pd1-P2, so as the Pd-S bond length compare to the corresponding Pt-S bond. As we all know, even though the ionic radius of Pd^{2+} and Pt^{2+} are similar, the atomic radius of platinum (135pm) is smaller than palladium (140pm)[21] as well as the covalent radius (128pm for platinum and 131pm for

palladium).[22] These result in the longer metal-ligand bond distance. The ten membered ring, Pd(1)-P(2)-C(29)-C(28)-S(4)-C(41)-S(2)-C(8)-C(9)-P(1), resulted from the formation of the methylene bridge, has a similar chair confirmation as observed in its platinum counterpart.

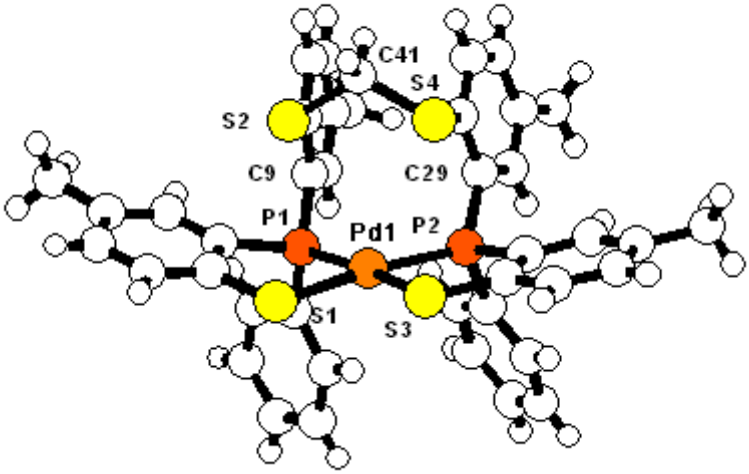

Figure III- 9. Molecular structure of [Pd^{II}(PS2'(CH_2)S2'P)], Chem-Ray structure. The solvent molecules are omitted for clarity.

Similar to [Pt^{II}(PS2'(CH_2)S2'P)], the alkylation reaction results in the only isomer, *cis-syn*-[Pd^{II}(PS2'(CH_2)S2'P)] with two alkylated thiophenol planes, as well as, the two phenyl planes, slightly deviate from being parallel. The alkylated thiophenol planes have a dihedral angle of 16.6 ° and are 3.209Å separated at the minimum and 3.980 Å separated at the maximum. The phenyl planes on phosphorus have a dihedral angle of 18.96 ° and are 2.739Å separated at the minimum and 3.649Å at the maximum. All the

separations are larger than the ones in the corresponding platinum complex, consistent with longer metal-ligand bond lengths. As concluded in the case of [Pt^{II}(PS2'(CH_2)S2'P)], the two alkylated thiophenol rings of [Pd^{II}(PS2'(CH_2)S2'P)] have quite strong intramolecular π-π interactions while the two phenyl rings on phosphorus have a weaker π-π interactions.

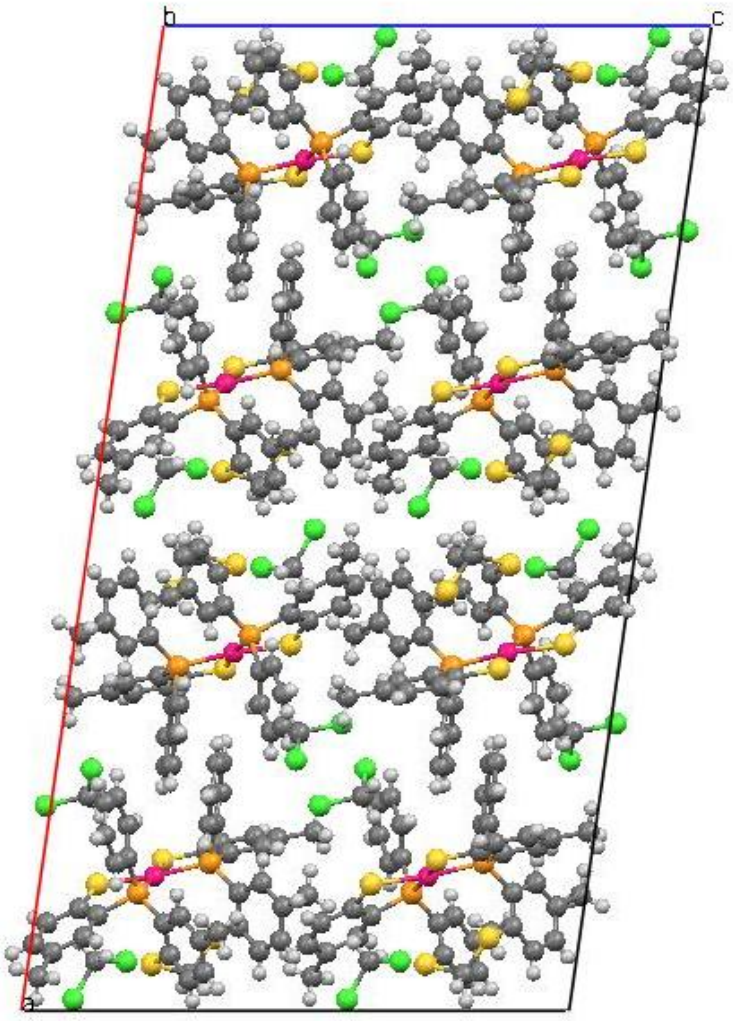

Figure III- 10. Crystal packing view of [Pd^{II}(PS2'(CH_2)S2'P)] (b* axis, mercury figure).

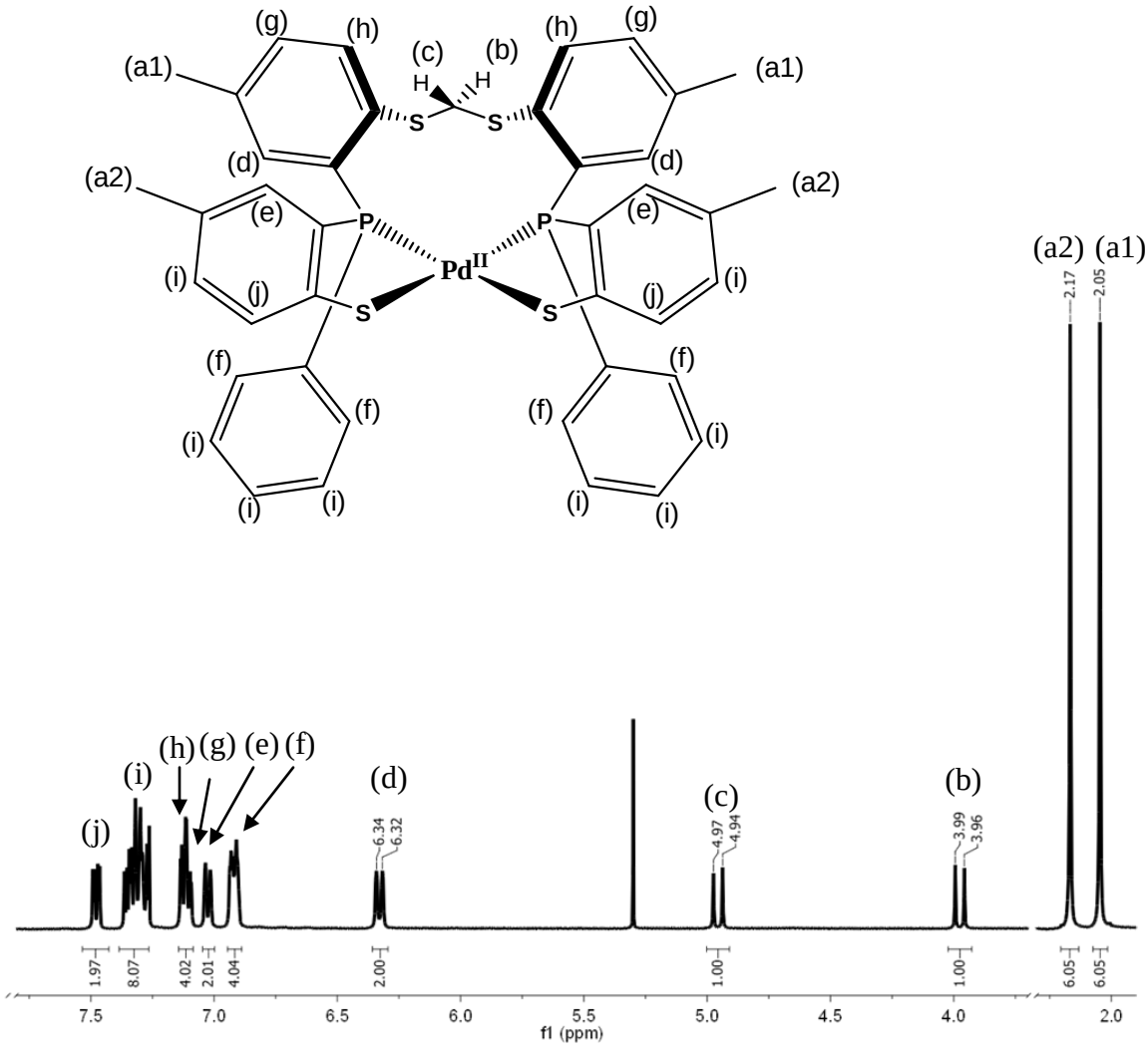

Figure III- 11. ^{1}HNMR spectrum of [Pd^{II}(PS2'(CH_2)S2'P)] in DMSO-d_6

The packing diagram of [Pd^{II}(PS2'(CH_2)S2'P)] **(Figure III-10**), unlike the packed view of [Pt^{II}(PS2'(CH_2)S2'P)], does not display the bilayer packed structure. Instead, the packed structure reveals a single layer structure with methylene dichloride solvent molecules interacting with both the phenyl rings on phosphorus and bridged thiophenol rings. The single layer structure was regulated mainly by the face-to-edge π-π interaction between the metal-bonded thiophenol ring and the bridged thiophenol ring.

The ^{1}H NMR spectrum of [Pd^{II}(PS2'(CH_2)S2'P)] in DMSO-d_6, is shown in **Figure III-11**. It confirmed that with simple and mild reaction condition, the alkylation reaction is done and the product can be purified. There are two methyl peaks at 2.17 and 2.05ppm, both with integration of 6H. Since the methylene bridging group is electron donating and is *para*- to the methyl substitution on alkylated thiophenol, the peak at 2.05ppm is tentatively assigned to be the methyl group on alkylated thiophenol (a1) and the peak at 2.17ppm is assigned to be the methyl group on the coordinated thiophenolate ring (a2). The two doublet peaks at 3.98 and 4.96ppm are assigned to be the two protons on bridging methylene group (both 1H, J = 9 Hz). These two peaks are almost 1ppm apart due to the extreme electron shielding difference; as we observed in crystal structure, one proton is reaching out between the two interacted π-eletron systems (b) and the other is kept outside of π-π interaction (c). This NMR shifts supports the conclusion that was previously discussed, the intramolecular π-π interactions of the alkylated thiophenols are relatively strong. Two sets of singlet at 6.34/6.32 and 7.06/7.04ppm are assigned to be aromatic proton that *ortho*- to phosphorus (both 2H), with the former one being one the alkylated thiophenol ring (d) and the latter one being one the thiophenol bonded to the

palladium (e). The doublet peak at 6.85ppm is assigned to the aromatic proton on phenyl ring that *ortho*- to phosphorus (f) (4H, J = 6 Hz). The two doublet peaks at around 7.1ppm are assigned to two aromatic protons on the thiophenol ring (g, h) (total 4H, J = 3Hz). The doublet peak at 7.48ppm is assigned to the aromatic proton on the metal-bonded thiophenol that *ortho*- to sulfur (j) (2H, J = 6Hz). The rest peaks at around 7.3ppm belong to the rest aromatic protons (i) in the structure (8H). In theory, they are predicted to be a doublet (predicted 2H) and a doublet of doublet (predicted 6H), while in the experimental spectrum they are on top of each other and indiscernible.

The preparation of $[Ni^{II}(PS2')_2][Li][PPh_4]$ by Voorhies suggested the feasibility of the counterpart Nickel alkylation. However, the attempted alkylation reaction under the same mild condition was not successful.

Similar alkylation reactions have been studied in depth both experimentally and theoretically[1,7-13] and S_N2 reaction mechanism is widely taken. Here we propose the multi-steps isomerization-S_N2-S_N2 mechanism for the alkylation reaction of $[M^{II}(PS2')_2]^{2-}$ (M= Pd, Pt). The detail is shown in **Scheme III-4**.

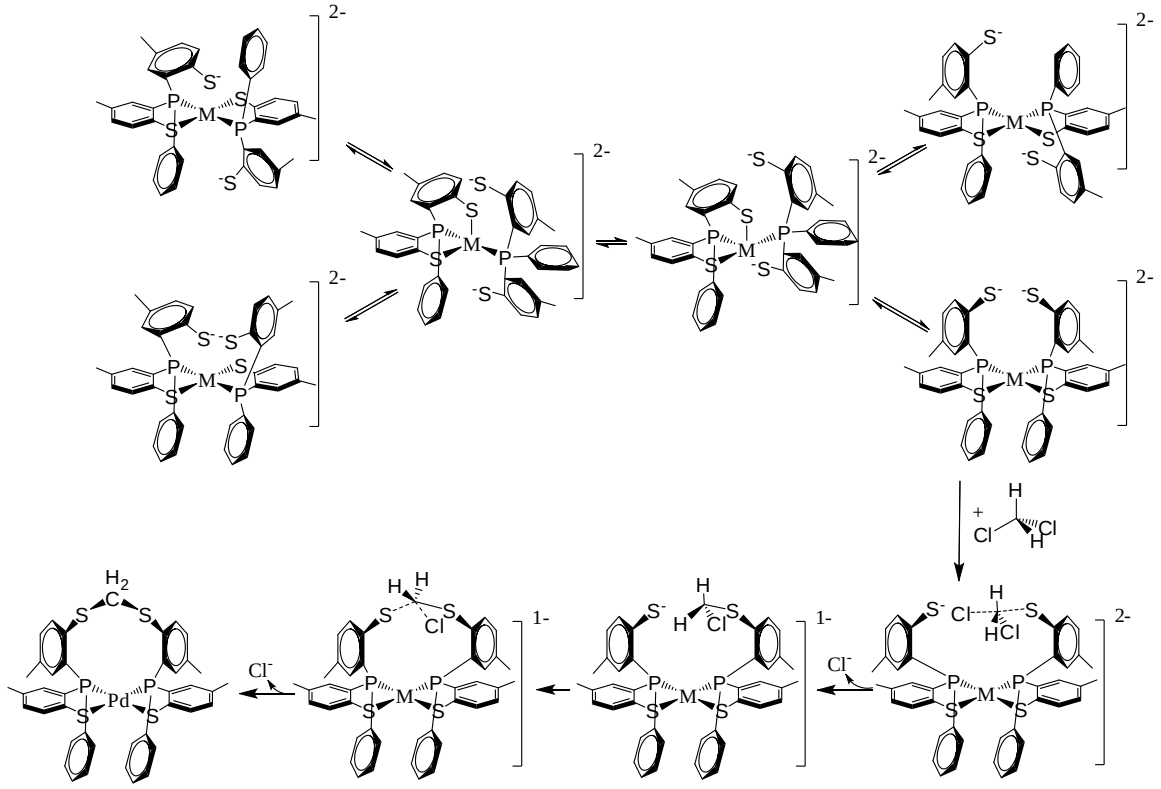

Scheme III- 4. Proposed isomerization-S_N2-S_N2 mechanism for the alkylation reaction of $[M(PS2')_2]^{2+}$.

Since we observed only the *trans-anti-* isomer of $[Pd^{II}(PS2')_2]^{2-}$ in crystal structure, while only the *cis-syn-* isomer is observed after alkylation both crystallographically and NMR. To fully finish the alkylation reaction and yield the neutral methylene bridged complex, the isomerization that forms the *cis-syn-* isomer with the configuration suitable for the alkylation reaction is the most crucial step. The interconversion of isomers must involve a mechanism that involves a metal ligand bond-breaking step. Mechanisms that involve square planar-tetrahedral rearrangements will not result in the interconversion. The rational mechanism for the isomerization involves

the intermediate, in which both sets of the coordinated thiolates and the pendant thiols are equivalent. Thiolate (RS^-) have been found to possess the ability to activate the C-X (X=halogen) bonds in organic electrophiles[11]. The non-bonded thiolate activates the C-Cl bond in methylene dichloride and go through the S_N2 mechanism to form the S-C bond. Two consecutive S_N2 reactions are fast steps compared to the isomerization. The nature of the methylene bridged complexes made it insoluble in the methylene dichloride and precipitate out, therefore push the reaction to the completeness. The failure of synthesizing the corresponding nickel complex under the same reaction condition supports the proposed mechanism, since the isomerization of nickel complex to form *cis* - isomers has not been observed.

3. CONCLUSIONS

In conclusion, this chapter presents the synthesis and study of several Metal-PS2' ligand complexes in the series: $[(Et_4N)_2][Pd^{II}(PS2')_2]$, $[Pd^{II}(PS2'(CH_2)S2'P)]$ and $[Pt^{II}(PS2'(CH_2)S2'P)]$. Thus, the alkylation reaction of the thiolates in the $[M^{II}(PS2')_2]$ is integrally studied. The alkylated complexes show configurationally selectively being the *cis-syn-* isomer, which is confirmed by NMR and X-ray crystal structure. By comparing the $[Pt^{II}(PS2'(CH_2)S2'P)]$ with $[Pt^{II}(PS2'(CH_2)S2'P)]$, the π-π interactions of the aromatic rings are discovered. The strength of these interactions is reflected in their crystal structures and in ^1H NMR spectra. The selectivity offers us insight into the mechanism of the alkylation reaction. By comparing the $[(Et_4N)_2][Pd^{II}(PS2')_2]$ and $[Pd^{II}(PS2'(CH_2)S2'P)]$, we were able to conclude that isomerization is involved and crucial. The proposed multi-steps isomerization-S_N2-S_N2 mechanism starts with isomerization equilibrium and the *cis-syn-* isomer activate the C-Cl bond of methylene dichloride and the undergo two consecutive S_N2 steps which completes the reaction.

4. EXPERIMENTAL

Syntheses:

$[Et_4N]_2[Pd^{II}(PS2')_2]$ or $[Et_4N]_2[Pd^{II}(C_6H_5P(CH_3\text{-}C_6H_3S)(CH_3\text{-}C_6H_3SH))_2]$:

The di-deprotonated lithium thiolate salt was obtained by combining $PS2'H_2$ ligand (0.3540 g, 1.00 mmol) with lithium wire (0.0141 mg, 2.01 mmol) in 15mL methanol, stirring until all the lithium wire been consumed and remove all the solvent under vacuum. Potassium tetrachloropalladate (K_2PdCl_4, 0.1633 g, 0.500 mmol) was added as solid under N_2. After the addition of 15mL of methanol to the solid mixture, the suspension was stirred under room temperature for 90mins until an almost clear deep orange solution was observed. The reaction mixture was filtered and a 10mL methanol solution of tetraethylammonium bromide (Et_4NBr, 0.2507 g, 1.19 mmol) was added. The resultant orange precipitate was filtered and dried under vacuum (0.374 g, 70%).

Orange X-ray diffraction quality crystals were prepared by layering the methanol reaction mixture resulting from $[PS2']^{2-}$ and K_2PdCl_4 with the methanol solution of Et_4NBr, and allowed to stand in the freezer at -20 ℃ for 4-5 days.

Unit Cell: Monoclinic; $P2_1/n$ (# 15); a = 14.1703(2) Å; b = 15.1766(2) Å; c = 14.3726(2) Å; α= 90 °; β= 99.7320(10)°; γ = 90°; V= 3046.45(7) $Å^3$

$[Pd^{II}(PS2'(CH_2)S2'P)]$ or $[Pd^{II}(C_6H_5P(CH_3\text{-}C_6H_3S)\text{-}CH_2\text{-}(SC_6H_3\text{-}CH_3)C_6H_5P)]$:

The alkylated palladium complexes could be made in both one-pot and stepwise syntheses.

(a): One-pot synthesis: The di-deprotonated lithium thiolate salt, Li_2[PS2'], was obtained by combining PS2'H_2 ligand (0.3540 g, 1.00 mmol) with lithium wire (0.0141 mg, 2.01 mmol) in 15mL methanol, and stirring until all the lithium wire had been consumed and the solvent was removed under vacuum. Potassium tetrachloropalladate (K_2PdCl_4, 0.1633 g, 0.500 mmol) was added as solid under N_2. After the addition of 15mL of methanol, the suspension was stirred under room temperature for 90mins until an almost clear deep orange solution was observed. The solvent was removed under vacuum and the solid was dissolved in methylene dichloride. After being stirred two days, the reaction mixture was filtered and hexanes was added. Orange precipitate was filtered and dried under vacuum. (0.2204 g, 48.1% yield from K_2PdCl_4).

(b): Stepwise synthesis: The di-deprotonated lithium thiolate salt, Li_2[PS2'], was obtained by combining PS2'H_2 ligand (0.3540 g, 1.00 mmol) with lithium wire (0.0141 mg, 2.01 mmol) in 15mL methanol, and stirring until all the lithium wire had been consumed and the solvent was removed under vacuum. Potassium tetrachloropalladate (K_2PdCl_4, 0.1633 g, 0.500 mmol) was added as solid under N_2. After the addition of 15mL of methanol to the solid mixture, the suspension was stirred under room temperature for 90mins until an almost clear deep orange solution was observed. Filter and add 10mL of a methanol solution of tetraethylammonium bromide (Et_4NBr, 0.2507 g, 1.19 mmol) to

the filtrate. Stir the mixture for 15mins, and orange precipitate was filtered and dried under vacuum (0.374g, 70%).

The 10mL methylene dichloride solution of $(Et_4N)_2[Pd^{II}(PS2')_2]$ (0.2001 g, 0.187 mmol) was treated with 30mL of hexanes, stirred for two day. The resulting orange solid was filtered, washed with methanol and dried under vacuum (0.126 g, 81.7% yield from $(Et_4N)_2[Pd^{II}(PS2')_2]$).

Dark orange X-ray diffraction quality crystals were prepared by layering the methylene dichloride solution of $(Et_4N)_2[Pd^{II}(PS2')_2]$ with hexanes and allowed to stand at room temperature for 4-5 days.

^{1}H NMR (DMSO-d_6): δ7.48-6.33ppm (22H, m, aromatic); 4.96ppm (1H, d, one of S-CH_2-S, J=9 Hz); 3.98ppm (one of S-CH_2-S, d, 1H, J=9 Hz); 2.17ppm (6H, s, CH_3); and 2.05ppm (6H, s, CH_3).[details, see **Figure III-11**]

Unit Cell: Monoclinic; C_2/c(# 15); a = 39.0154(9) Å; b = 10.2450(2) Å; c = 21.4834(4) Å; α= 90 °; β= 98.231(2)°; γ = 90°; V=8493(3) Å^3

[Pt^{II}(PS2'(CH_2)S2'P)] or [Pt^{II}(C_6H_5P(*p*-CH_3-C_6H_3S)-CH_2-(SC_6H_3-*p*-CH_3)C_6H_5P)]:

The alkylated platinum complexes were made in both a one-pot and a stepwise synthesis.

(a): One-pot synthesis: The di-deprotonated lithium thiolate salt was generated by combining PS2'H_2 ligand (0.354 g, 1.00 mmol) with lithium wire (0.0141 mg, 2.01 mmol) in 15mL methanol; upon stirring the lithium wire was consumed and the solvent was removed under **v**acuum. Potassium tetrachloroplatinate (K_2PtCl_4, 0.2077 g, 0.500 mmol) was added as a solid under N_2. After the addition of 15 mL of methanol to the solid mixture, the suspension was stirred under reflux for 90 min until an almost clear yellow solution was observed. The reaction mixture was filtered and the solvent removed under vacuum. The methylene dichloride solution of the solid was stirred for two days, and filtered. The orange precipitate, which was obtained by the addition of hexanes, was collected and dried under vacuum. (0.180 g, 39% yield from K_2PtCl_4).

(b): Stepwise synthesis: The di-deprotonated lithium thiolate salt, $[PS2']^{2-}$, was obtained by combining PS2'H_2 ligand (0.354 g, 1.00 mmol) with lithium wire (0.0141 mg, 2.01 mmol) in 15mL methanol, stirring until all the lithium wire been consumed and remove all the solvent under vacuum. Potassium tetrachloroplatinate (K_2PtCl_4, 0.2077 g, 0.500 mmol) was added as solid under N_2. After the addition of 15mL of methanol to the solid mixture, the suspension was refluxed for 90mins until an almost clear yellow solution was observed. The cooled solution was filtered and a 10mL methanol solution of tetraethylammonium bromide (Et_4NBr, 0.251 g, 1.19 mmol) was added to the filtrate. The light precipitate was collected and dried under vacuum (0.310 g, 53%).

The 10mL methylene dichloride solution of $(Et_4N)_2[Pt^{II}(PS2')_2]$ (0.201 g, 0.173 mmol) was treated with 30mL of hexanes, stirred for two day, filtered under N_2. The resulting

orange yellow solid was filtered and washed with methanol and dried under vacuum (0.116 g, 73% yield from $(Et_4N)_2[Pt^{II}(PS2')_2]$).

Yellow/light orange X-ray diffraction quality crystals were prepared by layering the methylene dichloride solution of $(Et_4N)_2[Pt^{II}(PS2')_2]$ with hexanes and allowed to stand at room temperature for 4-5days. (0.4 x 0.4 x 0.2 mm^3).

^1H NMR (DMSO-d_6): δ7.40-6.25ppm (22H, m, aromatic); 4.74ppm (1H, d, one of S-CH_2-S, J=9 Hz); 3.86ppm (one of S-CH_2-S, d, 1H, J=9 Hz); 2.15ppm (6H, s, CH_3); and 2.07ppm (6H, s, CH_3).

Unit Cell: Triclinic; $P\bar{1}$; a = 10.2541(3) Å ; b = b = 10.6811(3) Å ; c = 20.6573(4) Å ;α= 87.306(2)°; β= 77.159(2)°; γ = 74.299(2)°; V = 2123.39(10) $Å^3$.

X-ray Crystallography

$[Et_4N]_2[Pd^{II}(PS2')_2]$:

A crystal measuring 0.4 x 0.3 x 0.25 mm^3 was mounted on the nylon loop and centered on the X-ray beam at 100K. The accurate unit cell was obtained using reflection with 2θ = 3.17- 35.07 º: a = 14.1703(2) Å; b = 15.1766(2) Å; c = 14.3726(2) Å; α = 90 º; β = 99.7320(10)°; γ = 90°; V = 3046.45(7) $Å^3$. The structure was solved under the primitive monoclinic crystal system (space group $P2_1/n$) using 12811 reflections. The asymmetric unit consists of a half molecules of the palladium complex ions with inversion center, one Et_4N^+ counter cation and two methanol solvent molecules. The data

reduction was done with CrysAlis Pro and the structure refinement was done with SHELXL-97 (Sheldrick). All the non-hydrogen atoms were located by Direct Methods and were refined anisotropically by a full-matrix least-squares method. The positions of the hydrogen atoms were calculated.

The crystallographic parameters and atomic coordinates are located in Table A-5.

$[Pd^{II}(PS2\text{-}CH_2\text{-}S2P)]\ 2CH_2Cl_2$:

A crystal measuring 0.5 x 0.15 x 0.05 mm^3 was mounted on the nylon loop and centered on the X-ray beam at 100K. The accurate unit cell was obtained using reflection with 2θ = 3.17-31.42 °: a = 39.0154(9) Å; b = 10.2450(2) Å; c = 21.4834(4) Å; α= 90 °; β = 98.231(2)°; γ = 90°; V=8493(3) $Å^3$. The structure was solved under the C-base centered monoclinic crystal system (space group C2/c) using 12623 reflections. The asymmetric unit contained one molecules of the palladium complex and two methylene dichloride solvent molecules. The data reduction was done with CrysAlis Pro and the structure refinement was done with SHELXL-97 (Sheldrick). All the non-hydrogen atoms were located by Direct Methods and were refined anisotropically by a full-matrix least-squares method. The position of the hydrogen atom of each methyl group was located using Fourier difference maps. The positions of the remaining hydrogen atoms were calculated.

The crystallographic parameters and atomic coordinates are located in Table A-6.

$[Pt^{II}(PS2\text{-}CH_2\text{-}S2P)]\ 2CH_2Cl_2$:

A crystal measuring 0.4 x 0.4 x 0.2 mm^3 was mounted on the nylon loop and centered on the X-ray beam at 100K. The accurate unit cell was obtained using reflection with 2θ = 3.26-32.98°: a = 10.2541(3) Å ; b = 10.6811(3) Å ; c = 20.6573(4) Å ;α = 87.306(2)°; β = 77.159(2)°; γ = 74.299(2)°; V = 2123.39(10) $Å^3$. The structure was solved under the primitive triclinic crystal system (space group $P\bar{1}$) using 14423 reflections. The asymmetric unit contains one full molecules of the platinum complex and two methylene dichloride solvent molecules.

The data reduction was done with CrysAlis Pro and the structure refinement was done with SHELXL-97 (Sheldrick). All the non-hydrogen atoms were located by Direct Methods and were refined anisotropically by a full-matrix least-squares method. The position of the hydrogen atom of each methyl group was located using Fourier difference maps. The positions of the remaining hydrogen atoms were calculated.

The crystallographic parameters and atomic coordinates are located in Table A-12.

REFERENCES

(1) Chikamoto, Y.; Hirotsu, M.; Kawamoto, T.; Konno, T. *Chem. Lett.* **2005**, *34*, 362.

(2) Grapperhaus, C. A.; Poturovic, S.; Mashuta, M. S. *Inorg. Chem.* **2002**, *41*, 4309.

(3) Buonomo, R. M.; Font, I.; Maguire, M. J.; Reibenspies, J. H.; Tuntulani, T.; Darensbourg, M. Y. *J. Am. Chem. Soc* **1995**, *117*, 963.

(4) Grapperhaus, C. A.; Maguire, M. J.; Tuntulani, T.; Darensbourg, M. Y. *Inorg. Chem.* **1997**, *36*, 1860.

(5) Murata, M.; Kojima, M.; Hioki, A.; Miyagawa, M.; Hirotsu, M.; Nakajima, K.; Kita, M.; Kashino, S.; Yoshikawa, Y. *Coord. Chem. Rev.* **1998**, *174*, 109.

(6) Galvez, C.; Ho, D. G.; Azod, A.; Selke, M. *J. Am. Chem. Soc* **2001**, *123*, 3381.

(7) Okamoto, K.; Sasaki, C.; Yamada, Y.; Konno, T. *Bull. Chem. Soc. Jpn.* **1999**, *72*, 1685.

(8) Musie, G.; Reibenspies, J. H.; Darensbourg, M. Y. *Inorg. Chem.* **1998**, *37*, 302.

(9) Smee, J. J.; Miller, M. L.; Grapperhaus, C. A.; Reibenspies, J. H.; Darensbourg, M. Y. *Inorg. Chem.* **2001**, *40*, 3601.

(10) Hirotsu, M.; Kobayashi, A.; Yoshimura, T.; Konno, T. *J. Chem. Soc.-Dalton Trans.* **2002**, 878.

(11) Nova, A.; Gonzalez-Duarte, P.; Lledos, A.; Mas-Balleste, R.; Ujaque, G. *Inorg. Chim. Acta* **2006**, *359*, 3736.

(12) Sellmann, D.; Waeber, M.; Binder, H.; Boese, R. *Z.Naturforsch.(B)* **1986**, *41*, 1541.

(13) Oster, S. S.; Lachicotte, R. J.; Jones, W. D. *Inorg. Chim. Acta* **2002**, *330*, 118.

(14) Chikamoto, Y.; Yoshinari, N.; Kawamoto, T.; Konno, T. *J. Organomet. Chem.* **2007**, *692*, 156.

(15) Picot, D.; Ohanessian, G.; Frison, G. *Inorg. Chem.* **2008**, *47*, 8167.

(16) He, C.; Hus, J. C.; Sun, L. J.; Zhou, P.; Norman, D. P. G.; Dotsch, V.; Wei, H.; Gross, J. D.; Lane, W. S.; Wagner, G.; Verdine, G. L. *Mol. Cell* **2005**, *20*, 117.

(17) Takinowaki, H.; Matsuda, Y.; Yoshida, T.; Kobayashi, Y.; Ohkubo, T. *Protein Sci.* **2006**, *15*, 487.

(18) Myers, L. C.; Terranova, M. P.; Ferentz, A. E.; Wagner, G.; Verdine, G. L. *Science* **1993**, *261*, 1164.

(19) Ohkubo, T.; Sakashita, H.; Sakuma, T.; Kainosho, M.; Sekiguchi, M.; Morikawa, K. *J. Am. Chem. Soc* **1994**, *116*, 6035.

(20) Hunter, C. A.; Sanders, J. K. M. *J. Am. Chem. Soc* **1990**, *112*, 5525.

(21) Slater, J. C. *J. Chem. Phys.* **1964**, *41*, 3199.

(22) Sanderson, R. T. *Chemical Periodicity*; Reinhold: New York, USA, 1960.

Chapter 4.

Nuclear Magnetic Resonance Study of Metal-Thiolate complexes

1. INTRODUCTION

The observation that the *trans-anti*-[M^{II}(PS2'H)$_2$] complex can be thermally converted quantitatively into the *cis*-[M^{IV}(PS2')$_2$] complex (**Scheme IV-1**) raised several important questions.

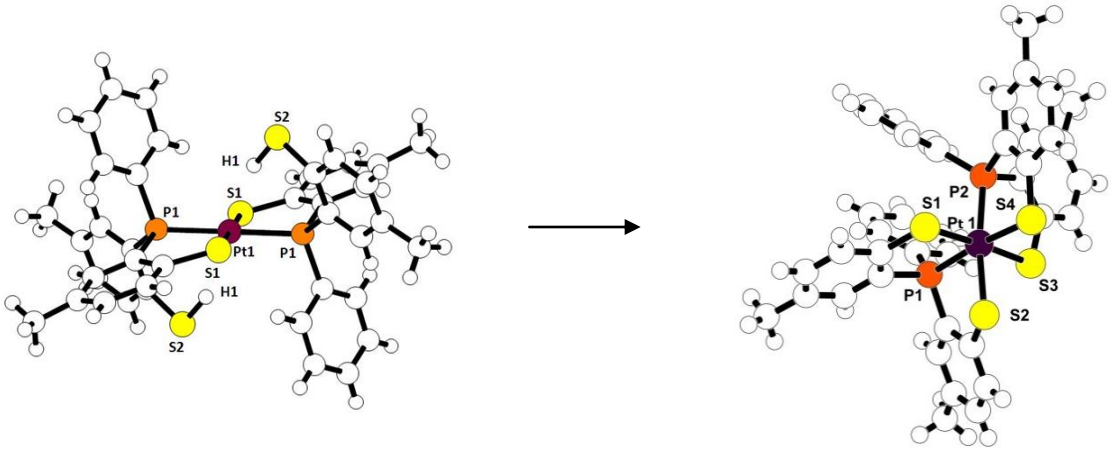

Scheme IV- 1. From Pt(II) to Pt(IV)

First, the most obvious reaction, which would involve the direct coordination of the pendant groups, generates the *trans* rather than the *cis* isomer. The *trans* P atoms in the starting material have a *cis* arrangement in the product. The reaction must take place with a significant rearrangement of the reactant and/or the product. Second, the oxidation takes place without the addition of an external oxidizing agent. The fate of the SH protons of the pendant thiols, which are the prime candidate for the oxidizing agent, needed to be determined. The simplest possibility would be that the SH protons are reduced and form H_2. To attempt to answer these questions, we undertook a series of *in-*

situ ^{1}H and ^{31}P NMR experiments to study the reaction. During these studies, we discovered that there was a photochemical reaction pathway, as well as, a thermal process. Also during these studies, we structurally characterized two isomers of the *trans-anti*-[$M^{II}(PS2'H)_2$]; the characterization of these isomers was presented in chapter 2.

^{1}H NMR spectroscopy has been used to determine the structure of many coordination compounds. In addition, ^{31}P NMR spectroscopy has been oftern involved in structure determination. For example, the coupling constant between *trans*- phosphorus atoms is very large (> 500 Hz) in platinum and palladium complexes.[1] With ^{195}Pt having nuclear spin I=1/2 (natural abundance of 33.7%), spin multiplets arising from $^{1}J_{P\text{-}Pt}$ have been observed since the late 1950's.[2-3]

According to the original definition[2,4], the *trans* influence of a ligand is related to the extent to which such ligand weakens the bond *trans* to itself in the ground state of the complex. The *cis* influence can be defined, similarly, as the weakening of a metal-ligand bond induced by a cis ligand.[3] Several techniques have been employed to investigate these influences,[5] the most popular being X-ray crystallography ("structural" trans or cis influence) and NMR spectroscopy. The latter has been used extensively[6-8] when both the metal and the donor atoms are NMR active (such as, in the present case, ^{195}Pt and ^{31}P). The ^{195}Pt-^{31}P ^{1}J values can be considered as an estimate of the bond strength between these atoms.

The fact that H_2 binding is accompanied by the oxidation of the nickel ion from Ni^{2+} to Ni^{3+} in hydrogenase enzymes[9] brings importance to the series of $[M^{II}(PS2'H)_2]$ and $[M^{IV}(PS2')_2]$ complexes. Our synthetic study presented in the previous chapter described the preparation of stable complexes in two different oxidation states with same ligand system, a M(II) and a striking M(IV). A reactivity study of this transformation could possibly provide insight into possible intermediates in the reaction of hydrogenase enzymes.

The paradigm in inorganic photochemistry consists of a transition metal complex that absorbs light, usually in the visible and UV, undergoes internal conversion and/or intersystem crossing, and reaches an excited state that can undergo chemical reaction and has a lifetime long enough to do so.[10] The excited stated complex may be able to make use of its additional electronic energy to undergo reactions, such as oxidation, reduction, ligand substitution or decomposition, which may not be available to the ground state molecule. Photooxidation has important applications in catalysis, oxidation of biomolecules and organic synthesis.[11] With a wealth of accessible d-d and charge transfer electronic states, and often several available oxidation states, transition metal complexes are particularly well suited for this role.

Metal halogen complexes,[12-15] as well as metal complexes bonded with pyridine-type ligand,[16-17] have been extensively investigated for their photooxidation. The known photo-redox behavior of platinum (II) and platinum (IV) complexes may be summarized by the statement that excitation to ligand to metal charge transfer (LMCT) states of

Pt(IV) frequently leads to reduction to Pt(II), while metal to ligand charge transfer (MLCT) excitation of Pt(II) complexes frequently yields Pt(IV).[18] Some thiolate ligand complexes have been reported with photooxidation study.[19-20] It is concluded that, one, the photoreaction could be solvent-initiated photoreactions other than metal-centered photoreactions; and two, the oxidation would be ligand-based rather than at the metal. Relative to the tremendous amount of photooxidation research that has been done with metal complexes, the photochemistry of Pt/Pd-thiolate complexes has received little attention.

The successful preparation and full characterization of both the $[M^{II}(PS2'H)_2]$ and $[M^{IV}(PS2')_2]$ series makes it possible to study the oxidation reaction of $[M^{II}(PS2'H)_2]$. The fact that they exhibit absorption with charge transfer character in the UV/Vis spectrum and their structures are very similar in the different oxidation states raises the feasibility of photooxidation reactions. Plus their structure are very similar in the M(II) and M(IV) oxidation states, which should favor rapid electron transfer reactionss with minimal inner-sphere reorganization barriers.

Typical photooxidation reactions were conducted with monitoring by UV/Vis spectroscopy, where increase absorbance was observed. As we mentioned in previous chapter, the $[M^{II}(PS2'H)_2]$ and $[M^{IV}(PS2')_2]$ series of complexes have distinctive and characteristic peaks in their NMR spectra, especially in ^{31}P NMR spectra. *In-situ* UV irradiation reaction studies were done in a NMR tube and followed by ^{1}H NMR and ^{31}P

NMR spectroscopy. The resultant spectra are fully analyzed and the reaction scheme and possible mechanism are presented.

2. RESULT AND DISCUSSION

From the regular synthetic route of $[Pt^{II}(PS2'H)_2]$, we discovered that we always produce only *trans-anti*-$[Pt^{II}(PS2'H)_2]$ which is one of the four possible isomers (**Scheme IV-2**). As we also presented in a previous chapter, room light irradiation produced a mixture of all four isomers. From these reaction mixures, two other isomer, *cis-syn*-$[Pt^{II}(PS2'H)_2]$ and *cis-anti*-$[Pt^{II}(PS2'H)_2]$, were isolated and crystallographically characterized. The last *trans-syn i*somers was identified by ^{1}H and ^{31}P NMR spectroscopy.

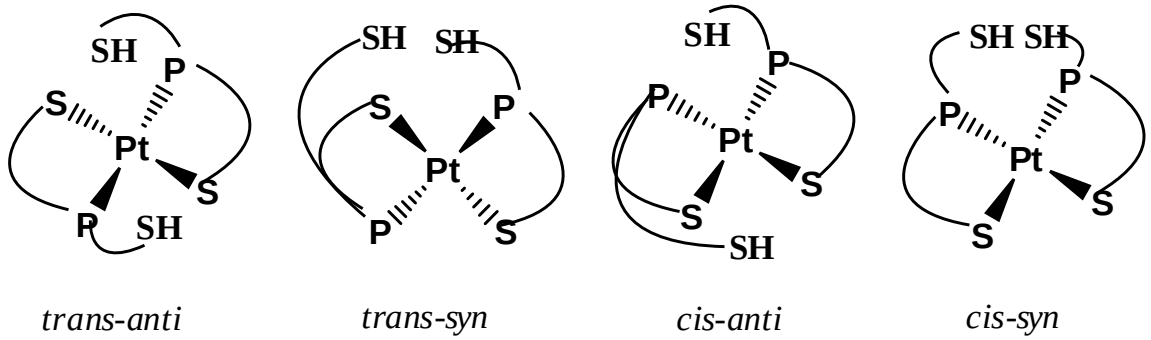

trans-anti *trans-syn* *cis-anti* *cis-syn*

Scheme IV- 2. All four possible isomers of $[Pt^{II}(PS2'H)_2]$

Reactivity study with regular light in glass NMR tube

The reactivity study of pure *trans-anti*-$[Pt^{II}(PS2'H)_2]$ in $CDCl_3$ was first conducted under a N_2 atmosphere in a regular glass NMR tube under the regular fluoro

scent lamp (room light). The reaction was monitored by both ^{31}P NMR and ^{1}H NMR. Both the ^{31}P and ^{1}H NMR spectra revealed that the isomerization takes place without oxidation to Pt(IV) complexes.

Figure IV-1 shows selected regions of the ^{31}P NMR and ^{1}H NMR spectra of the *in-situ* reaction of *trans-anti*-[$Pt^{II}(PS2'H)_2$] in $CDCl_3$ in a glass NMR tube under regular light. Over time, all four isomers are populated in the solution; with both *cis-* isomers having higher concentration than *trans-* isomers. There is no evidence of the thermal product [$Pt^{IV}(PS2')_2$].

The region of the ^{31}P NMR spectra only shows the central ^{31}P resonance for each of the [$Pt^{II}(PS2'H)_2$] isomers, the doublet due to the large coupling with ^{195}Pt lie outside this region. It can be seen that the *cis-syn-* and *cis-anti-* [$Pt^{II}(PS2'H)_2$] isomers are growing together and remain in a 1:1 ratio; while the *trans-syn-* isomer did not seem to increase after its initial appearance. The –SH and $–CH_3$ regions of the ^{1}H NMR spectra at the same temperature are also shown in **Figure IV-1**, the relative intensities of the –SH and $–CH_3$ peaks among the four isomers supports our isomer peak assignments.

The complete spectrum of *in-situ* ^{31}P NMR study of [$Pt^{II}(PS2'H)_2$] in $CDCl_3$ solution in glass NMR tube under regular light is shown in **Figure IV-2**. Starting from pure *trans-anti*-[$Pt^{II}(PS2'H)_2$], the isomerization reaction progressed very slowly under irradiation by regular fluorescent light. After 3 hours, both *cis-* isomers appeared with low concentration in about a 1:1 ratio, while the *trans-syn*-[$Pt^{II}(PS2'H)_2$] isomer remained absent. Starting from 18 hours, all four isomers are observed in the reaction

mixture. And starting from 66 hours, the equilibrium within two *cis*- and two *trans*-isomers was reached: the ratio of *trans-anti*-[$Pt^{II}(PS2'H)_2$] and *trans-syn*-[$Pt^{II}(PS2'H)_2$] remained static about 2:1 and the ratio of *cis-anti*-[$Pt^{II}(PS2'H)_2$] and *cis-syn*-[$Pt^{II}(PS2'H)_2$] remained static at about 1:1. After 66 hours, the concentration of *cis*-isomers continued to increase while the concentration of *trans*- isomers kept decreassiing. At 163 hours, the *cis*- isomers surpassed the *trans*- isomers, and became the major isomers. Spectra of the reaction mixture did not change after 163 hours, which suggests that the reaction mixture had reached equilibrium.

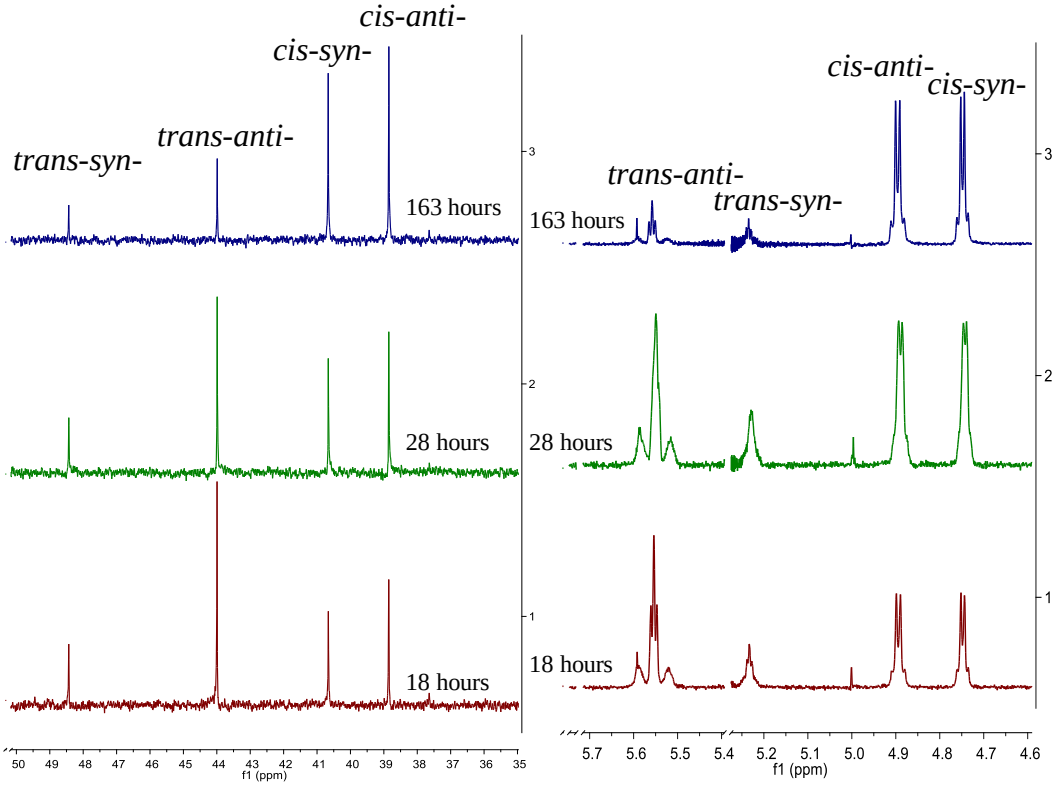

(a) Fragment of selective ^{31}P NMR (b) –SH Fragment of selective ^{1}H NMR

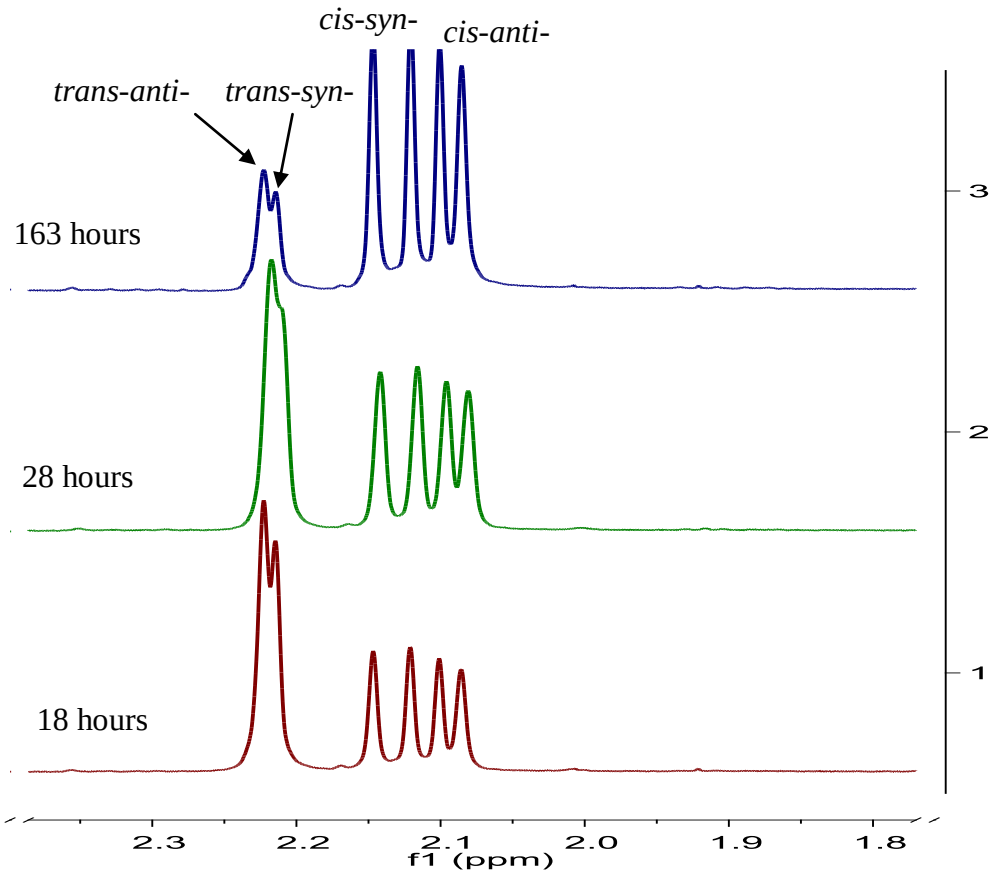

(c) the methyl region of selective ^{1}H NMR spectra

Figure IV- 1. All four possible isomers of ^{31}P NMR and ^{1}H NMR, *In-situ* NMR study of *trans-anti*-[$Pt^{II}(PS2'H)_2$] in $CDCl_3$ in glass tube under regular light, 300MHz

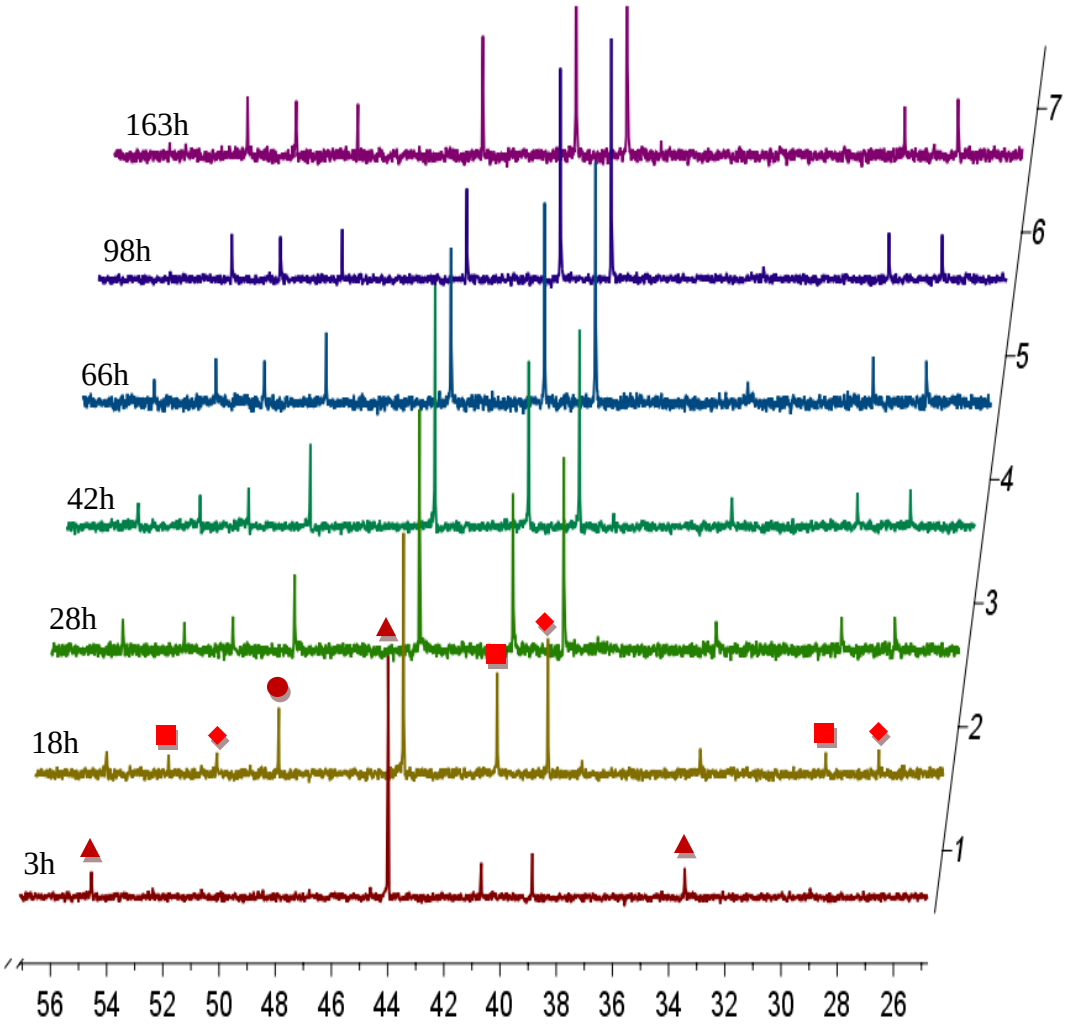

Figure IV- 2. Complete spectra of *in-situ* ^{31}P NMR study of [Pt^{II}(PS2'H)$_2$] in $CDCl_3$ in glass tube under regular light, 300MHz

▲ : *trans-anti*-[Pt^{II}(PS2'H)$_2$] 43.98ppm (s and d, $^1J_{P\text{-}Pt}$: 2566.5Hz)

● : *trans-syn*-[Pt^{II}(PS2'H)$_2$] 48.43ppm(s and d, $^1J_{P\text{-}Pt}$: 2625.6Hz)

■ : *cis-syn*-[Pt^{II}(PS2'H)$_2$] 40.66ppm(s and d, $^1J_{P\text{-}Pt}$: 2841.9Hz)

◆ : *cis-anti*-[Pt^{II}(PS2'H)$_2$] 38.66ppm(s and d, $^1J_{P\text{-}Pt}$: 2877.1Hz)

It is notable that even after 163 hours, there are no observed resonances in the ^{31}P NMR spectra for the *cis* or *trans*-[$Pt^{IV}(PS2')_2$] compounds. Thus, under fluorescent light irradiation, complete isomerization of [$Pt^{II}(PS2'H)_2$] occurred but no redox chemistry was observed.

Peaks that belonged to different isomers are labeled with different symbols in **Figure IV-2**. With ^{195}Pt having nuclear spin I=1/2 (natural abundance of 33.7%), satellite doublet arising from $^{1}J_{P\text{-}Pt}$ is an important feature of [$Pt^{II}(PS2'H)_2$] in the ^{31}P NMR spectra. It is demonstrated in **Figure IV-2**, that the concentration is essential for this satellite doublet to be observed. Theoretically, all isomers of [$Pt^{II}(PS2'H)_2$] should have a set of three peaks for the –SH protons: a satellite doublet and a singlet. When the concentration of both *trans*- isomer are still quite low after 3 hours of reaction, only the phosphorus peak that was not coupled with the ^{195}Pt can be observed. The same situation as in case of *trans-anti*-[$Pt^{II}(PS2'H)_2$], their satellite doublet peaks are not very visible in 98 hours and 163 hours spectra, when the concentration of *trans-anti*-[$Pt^{II}(PS2'H)_2$] became too low.

Repeated reactions of pure *trans-anti*-[$Pt^{II}(PS2'H)_2$] in $CDCl_3$ under regular light demonstrated that the isomerization reaction was reproducible. Putting the sample in the dark stopped the progress of the isomerization reaction. Is light the only energy source for isomerization reaction? Can heat trigger the same reaction in this system? To gain further insight of isomerization and reactivity of the isomers of [$Pt^{II}(PS2'H)_2$], we did the

in-situ ^{31}P NMR study by heating pure *trans-anti*-[Pt^{II}(PS2'H)$_2$] in $CDCl_3$ solution in the dark.

Reactivity study with heat in glass NMR tube

The glass NMR tube was heated at 50 ℃ with an oil bath in the dark, and the reaction was monitored by both ^{1}H NMR and ^{31}P NMR.

Figure IV-3 is the complete spectra of the *in-situ* ^{31}P NMR study of [Pt^{II}(PS2'H)$_2$] in $CDCl_3$ in a glass tube at 50 ℃ in the dark with all the satellite peaks labeled. The reaction progress is very different from the reaction at room temperature under regular light. The mixture goes through isomerization and then oxidation. After 8 hours of heating, all four isomers appeared in the ^{31}P NMR spectrum, with very small concentration of both *cis-* isomers at about 1:1 ratio and huge proportion of both *trans-syn-* and *trans-anti-* isomers at about 3:4 ratio. At 22 hours of heating, *trans-syn-*, *cis-anti-* and *cis-syn*-[Pt^{II}(PS2'H)$_2$] isomers ebbed away with very small amount being left, while *trans-anti*-[Pt^{II}(PS2'H)$_2$] isomers flowed back. It is also notable that small amount of *cis*-[Pt^{IV}(PS2')$_2$] are observed at 22 hours of heating. At 30 hours of heating, *trans-syn-* and *trans-anti*-[Pt^{II}(PS2'H)$_2$] isomers populated back to 1:2 ratio while *cis*-[Pt^{IV}(PS2')$_2$] grown significantly and become majority. It is necessary to emphasize that both *cis-anti-* and *cis-syn*-[Pt^{II}(PS2'H)$_2$] isomers still exist even though are barely visible in the spectrum of 30 hours. At 46 hours, the spectrum presented almost pure peaks *cis*-[Pt^{IV}(PS2')$_2$] along with a very small peak of *trans*-[Pt^{IV}(PS2')$_2$].

The observation of $[Pt^{IV}(PS2')_2]$ complexes from $[Pt^{II}(PS2'H)_2]$ without air is significant, because redox chemistry of the metal center is proposed to be essential in catalytic cycle of hydrogenase enzymes. Additionally, with the known structure of $[Pt^{IV}(PS2')_2]$ and $[Pt^{II}(PS2'H)_2]$ complexes, there is no doubt that the $[Pt^{II}(PS2'H)_2]$ complexes are acting as proton source when being oxidized into $[Pt^{IV}(PS2')_2]$complexes.

The spectra demonstrated that isomerization is not the only thermal reaction, but it was also followed by an oxidation. The *in-situ* ^1H NMR study of same reaction confirmed our observation with the ^{31}P NMR spectra (**Figure IV-4**). The ^1H NMR spectra of the –SH and methyl regions revealed the isomerization than the deceased of the $[Pt^{II}(PS2'H)_2]$ isomers and the generation of $[Pt^{IV}(PS2')_2]$. It is notable that, along with the appearance of $[Pt^{IV}(PS2')_2]$, a CH_2Cl_2 singlet and $CDHCl_2$ triplet peaks are observed in ^1H NMR. They are not shown in the **Figure IV-4** for clarity, and their integration grows slowly but steadily. One example of these peaks is shown in the insert (a) of **Figure IV-5**, where the signature equal intensity triplet of $CDHCl_2$ (along with the singlet for CH_2Cl_2) is observed at around 5.3 ppm.

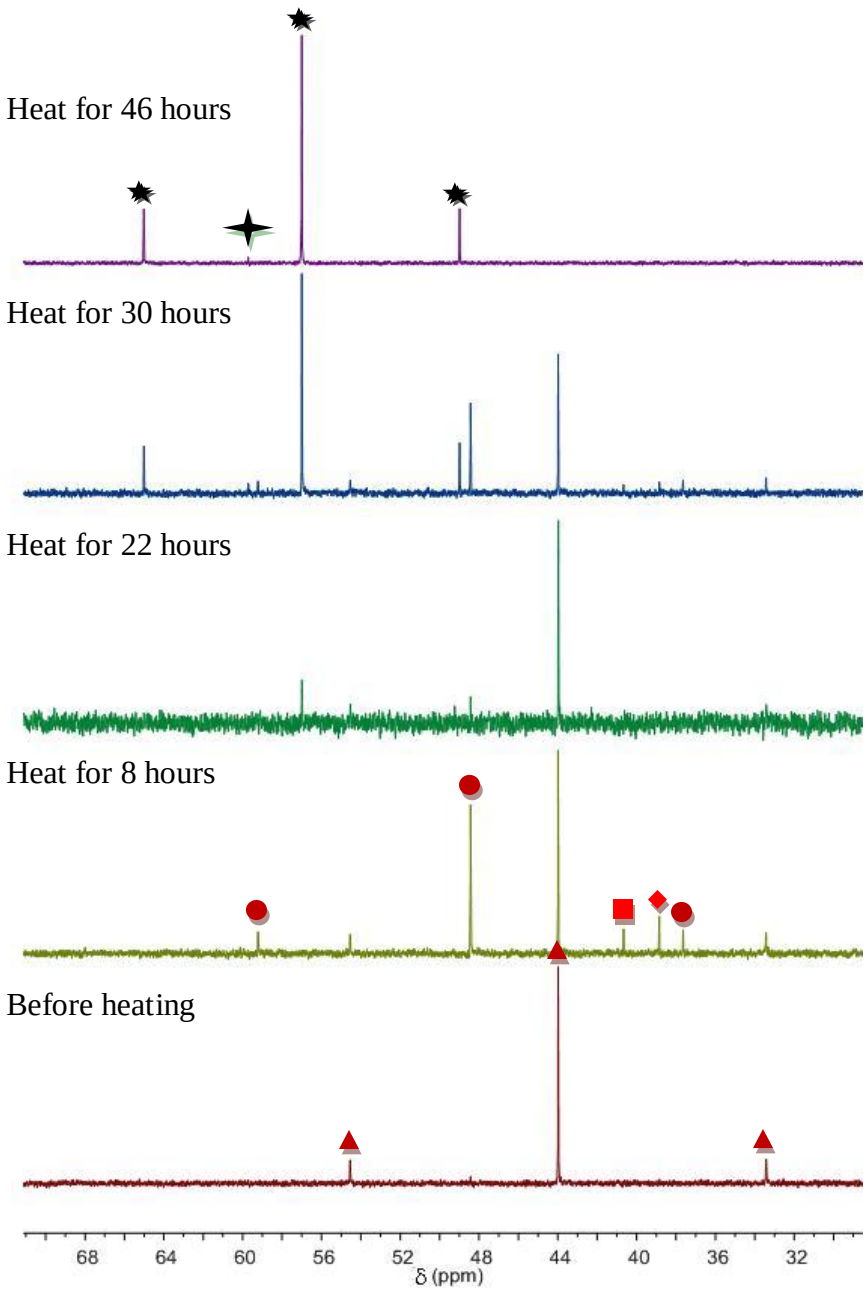

Figure IV- 3. Complete spectra of *in-situ* ^{31}P NMR study of [$Pt^{II}(PS2'H)_2$] in $CDCl_3$ in glass tube at 50 ℃ without light, 300MHz

▲ :*trans-anti*-[$Pt^{II}(PS2'H)_2$] 43.98 ppm

◆ : *cis-anti*-[$Pt^{II}(PS2'H)_2$] 38.85 ppm

● :*trans-syn*-[$Pt^{II}(PS2'H)_2$] 48.43 ppm

★ : *cis*-[$Pt^{IV}(PS2')_2$] 57.00 ppm

■ :*cis-syn*-[$Pt^{II}(PS2'H)_2$] 40.66 ppm

✦ : *trans*-[$Pt^{IV}(PS2')_2$] 59.71 ppm

The full ^{1}H NMR spectrum of reaction mixture after 64 hours of heating is shown in **Figure IV-5** with all the peaks and integration. The singlet peak at 2.13ppm (12H) belongs to the methyl groups. Four singlets from 6.55 to 6.70ppm (1H each) belong to four *ortho*- protons on the thiophenol rings. The rest of the aromatic region has a combined integration of 18H. There is no doubt that almost pure *cis*-[$Pt^{IV}(PS2')_2$] is achieved after 64 hours of heating in the dark.

This isomerization-oxidation reaction was reproducible. The repeat of the thermal reactivity study also revealed that the *cis*-[$Pt^{IV}(PS2')_2$] solution is stable with additional heating after 64 hours.

The thermal isomerization of *trans-anti*-[$Pt^{II}(PS2'H)_2$] in the dark and the isomerization under regular light are totally different. This suggests that *trans*-isomers are thermodynamically stable while the *cis*- isomers are more kinetically stable. And it may suggest that the energy difference between the *trans-anti* and *trans-syn* isomers are quite significant. The fact that oxidation happened under heating and not under room light revealed that the oxidation reaction from *cis*-Pt(II) to Pt(IV) is dynamically driven. Only the *cis* isomer of [$Pt^{IV}(PS2')_2$] was formed; there is no resonance for the trans-[$Pt^{IV}(PS2')_2$]. The observation of CH_2Cl_2 and $CDHCl_2$ peaks indicated that $CDCl_3$ solvent is involved in the reaction mechanism. We also noticed that, after 64 hours heating, the integration of CH_2Cl_2 and $CDHCl_2$ peak adds up to almost 2H. This indicated that the protons from the uncoordinated thiols are transferred to $CDCl_3$ as a result of the oxidation reaction.

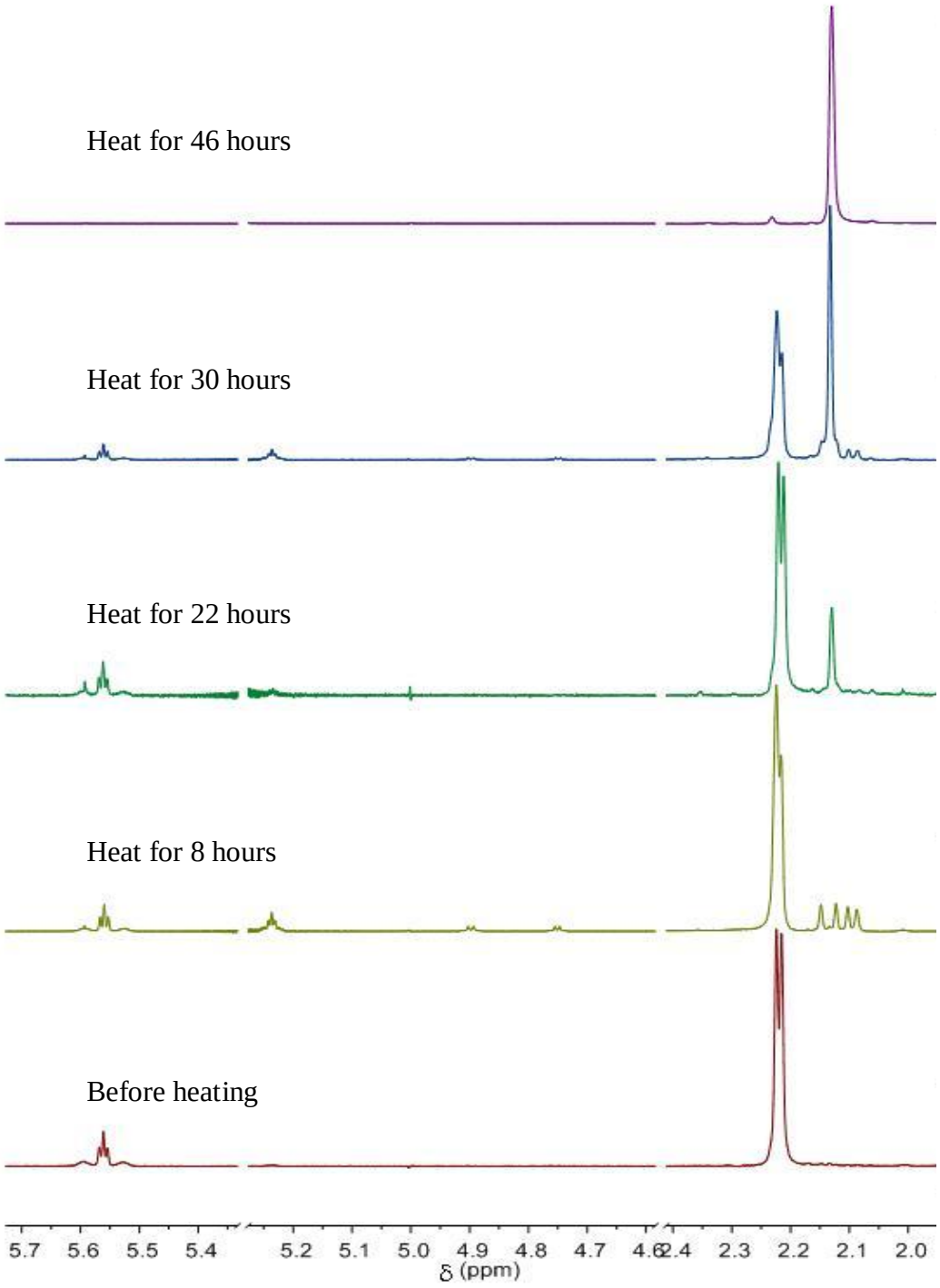

Figure IV- 4. Section of ^{1}H NMR spectra of *in-situ* study of $[Pt^{II}(PS2'H)_2]$ in $CDCl_3$ in glass tube at 50 ℃ in the dark, 300MHz

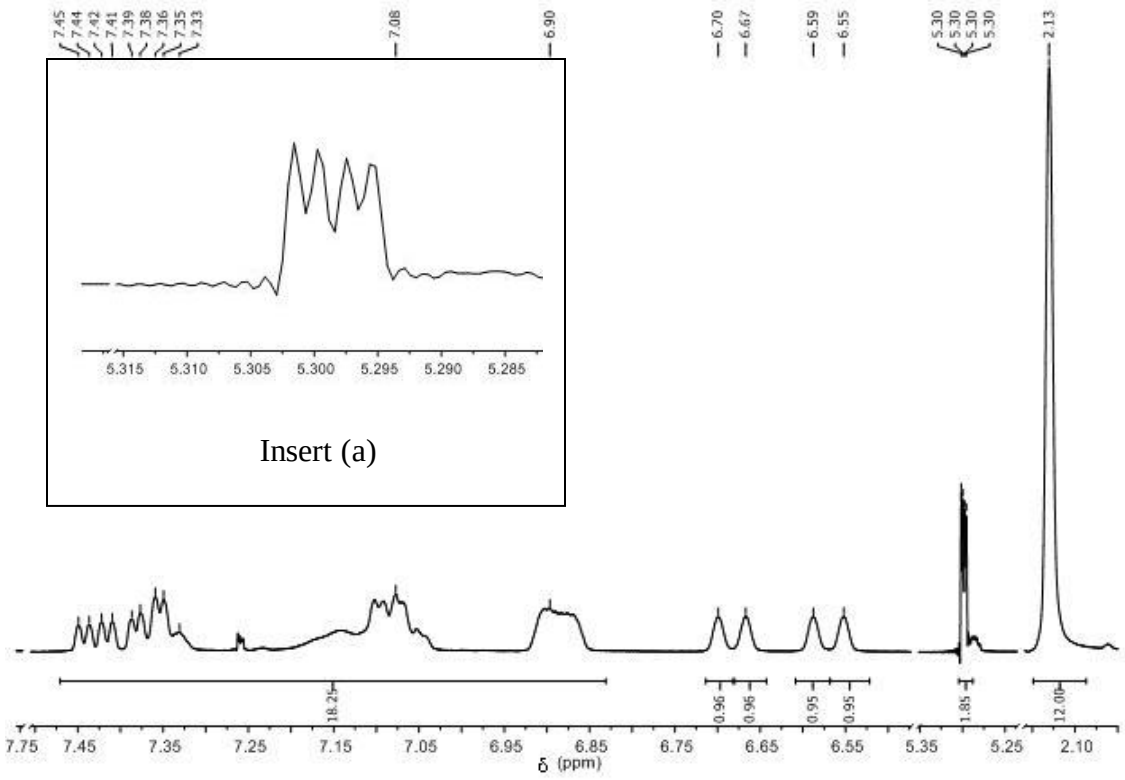

Figure IV- 5. ^{1}H NMR Spectrum of *in-situ* study of [Pt^{II}(PS2'H)$_2$], 300MHz. (In $CDCl_3$, glass tube, at 50 ℃ in the dark for 64 hours) (Insert (a): a blowup of CH_2Cl_2 and $CDHCl_2$)

Reactivity study with UV irradiation in glass NMR tube

UV irradiation is known as a good energy source. By undertaking similar reactivity study with UV irradiation, more insight could be revealed about the mechanism of oxidation of [Pt^{II}(PS2'H)$_2$]. The *in-situ* ^{31}P NMR of pure *trans-anti*-[Pt^{II}(PS2'H)$_2$] was carried out in a glass NMR tube in "100%" $CDCl_3$ with continuous UV-*vis* irradiation. The spectra are shown in **Figure IV-6**. The regular glass NMR tube absorbs the UV light

with wavelength shorter than 300nm. Unlike the reaction under regular fluorescent lamp, the *trans-syn*-[$Pt^{II}(PS2'H)_2$] isomer appeared before the two *cis*- isomers; it was populated and reached a steady state at about 2:1 ratio to the *trans-anti*-[$Pt^{II}(PS2'H)_2$] isomer before oxidation started. The [$Pt^{IV}(PS2')_2$] peaks were observed along with a small amount of both *cis*-[$Pt^{II}(PS2'H)_2$] isomers. The ratio of *cis-anti*-[$Pt^{II}(PS2'H)_2$] and *cis-syn*-[$Pt^{II}(PS2'H)_2$] reached a steady state ratio of 1:1. It was also noticed that the reaction time was significantly reduced, at 41 hours, the [$Pt^{II}(PS2'H)_2$] were fully converted into [$Pt^{IV}(PS2')_2$]. The result mixture had *cis*-[$Pt^{IV}(PS2')_2$] as the major product and a small amount of *trans*-[$Pt^{IV}(PS2')_2$]. There was no change with additional UV irradiation.

Comparing the reaction under a fluorescent lamp, under heat and under UV-vis irradiation lamp, the most significant difference was the appearance of the oxidation reaction. The light from a regular fluorescent lamp is not able to catalyze the oxidation of Pt(II) into Pt(IV), while heat and glass filtered UV irradiation can. The common phenomena of oxidation reaction are: 1) small amount of both *cis*-[$Pt^{II}(PS2'H)_2$] isomers are present before the oxidation products are observed, 2) appearance of CH_2Cl_2 and $CDHCl_2$ peaks and 3) only *cis*-[$Pt^{IV}(PS2')_2$] was produced. This suggests that *cis*-[$Pt^{II}(PS2'H)_2$] isomers act as the intermediate in the oxidation, and $CDCl_3$ is involved in the mechanism. To further study the mechanism, we did the *in-situ* NMR study of pure *trans-anti*-[$Pt^{II}(PS2'H)_2$] in $CDCl_3$ in a quartz NMR tube under UV irradiation.

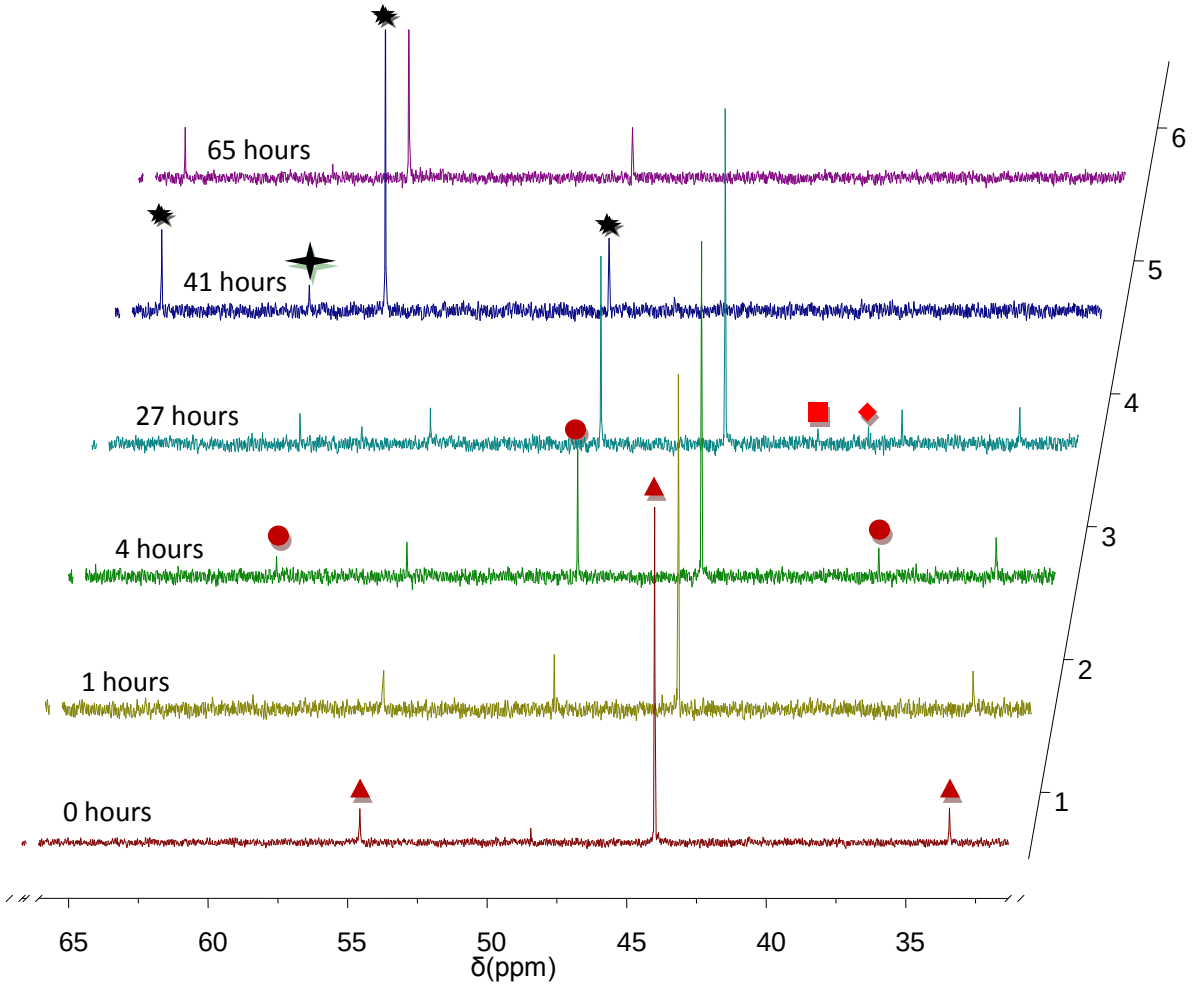

Figure IV- 6. *In-situ* ^{31}P NMR study of $[Pt^{II}(PS2'H)_2]$ in "100%" $CDCl_3$ in glass tube under UV irradiation, 300MHz

▲ : *trans-anti*-$[Pt^{II}(PS2'H)_2]$ 43.99ppm

● : *trans-syn*-$[Pt^{II}(PS2'H)_2]$ 48.43ppm

■ : *cis-anti*-$[Pt^{II}(PS2'H)_2]$ 40.66ppm

◆ : *cis-syn*-$[Pt^{II}(PS2'H)_2]$ 38.85ppm

✸ : *cis*-$[Pt^{IV}(PS2')_2]$ 57.00ppm

✦ : *trans*-$[Pt^{IV}(PS2')_2]$ 59.71ppm

Reactivity study with UV irradiation in quartz NMR tube

The *in situ* ^{31}P NMR of [Pt^{II}(PS2'H)$_2$] was carried out in a sealed quartz NMR tube in "100%" $CDCl_3$ under UV irradiation, the spectra over the time are shown in **Figure IV-7**. The distinguishing feature of this study was the rapid isomerization and oxidation. After 5 mins of irradiation, all four Pt(II) isomers and the two Pt(IV) isomers were present. This is the first time that we observed the *trans*-[Pt^{IV}(PS2')$_2$] isomer in the *in-situ* NMR study. Within the [Pt^{II}(PS2'H)$_2$] isomers, the *trans*-isomers were always the major species, similar to the reaction in the glass NMR tube. The ratio of *trans-anti*-[Pt^{II}(PS2'H)$_2$] and *trans-syn*-[Pt^{II}(PS2'H)$_2$] remained constant at about 2:1; while the ratio of *cis-anti*-[Pt^{II}(PS2'H)$_2$] to *cis-syn*-[Pt^{II}(PS2'H)$_2$] remained constant at about 1:1.

At 75 minutes, the oxidation reaction was complete with no [Pt^{II}(PS2'H)$_2$] isomers remaining. The *trans*-[Pt^{IV}(PS2')$_2$] and *cis*-[Pt^{IV}(PS2')$_2$] were present with a 1:2 ratio. For the first time in our *in-situ* studies, significant amounts of *trans*-[Pt^{IV}(PS2')$_2$] were observed, with its corresponding satellite Pt-P coupling peaks. The Pt-P coupling constants of *trans*-[Pt^{IV}(PS2')$_2$] (1735.0Hz) is smaller than the counterpart of *cis*-[Pt^{IV}(PS2')$_2$] (1947.6Hz), which is consistent with literature observations.[21] The isomerization of *trans*-[Pt^{IV}(PS2')$_2$] into pure *cis*-[Pt^{IV}(PS2')$_2$] was observed with further UV irradiation.

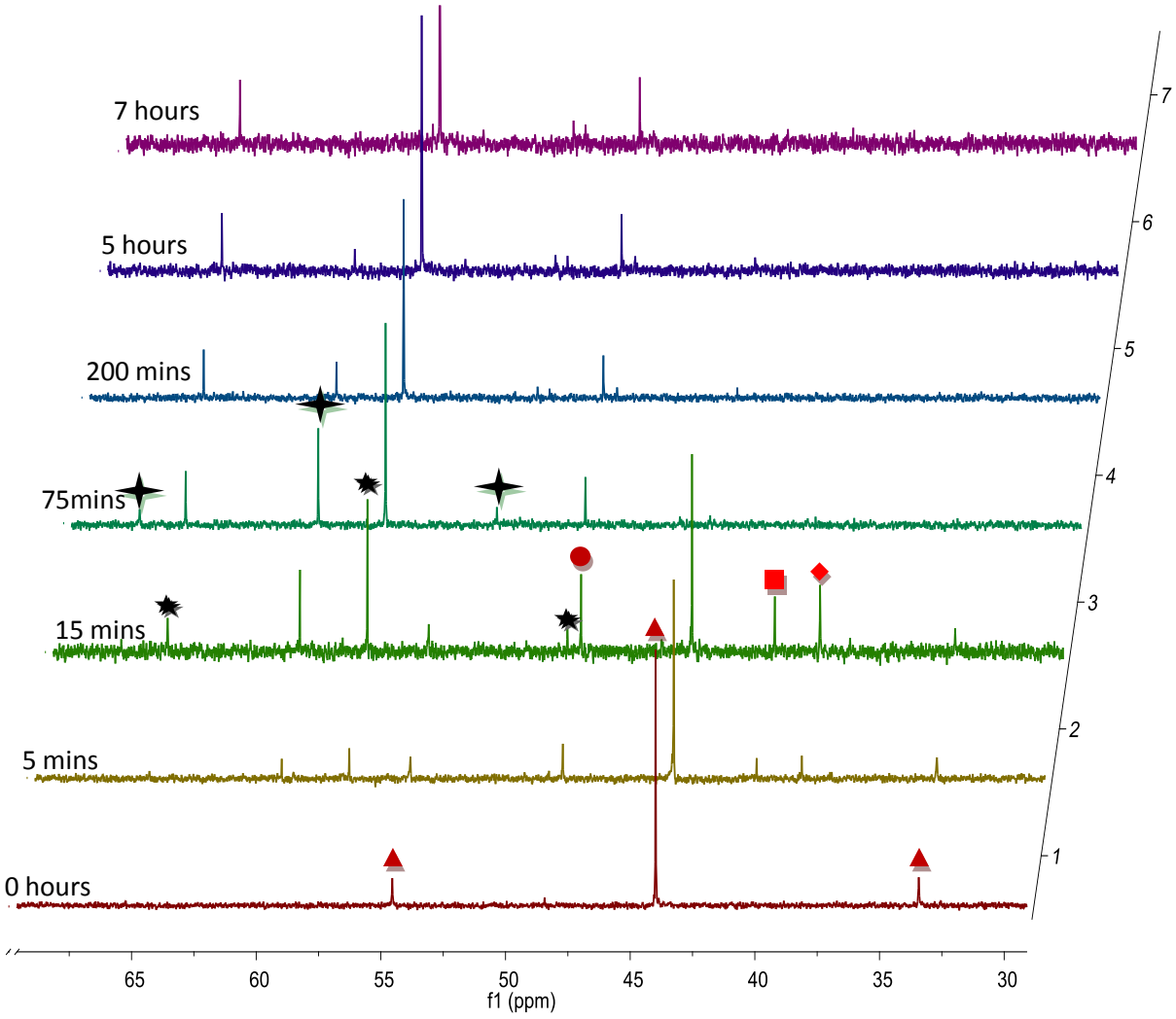

Figure IV- 7. *In-situ* ^{31}P NMR study of *trans-anti*-[Pt^{II}(PS2'H)$_2$] in "100%" $CDCl_3$ in a quartz tube under UV irradiation, 300MHz

▲ : *trans-anti*-[Pt^{II}(PS2'H)$_2$] 43.99 ppm

● : *trans-syn*-[Pt^{II}(PS2'H)$_2$] 48.43 ppm

■ : *cis-anti*-[Pt^{II}(PS2'H)$_2$] 40.66 ppm

◆ : *cis-syn*-[Pt^{II}(PS2'H)$_2$] 38.85 ppm

★ : *cis*-[Pt^{IV}(PS2')$_2$] 57.00 ppm(s and d, $^1J_{P\text{-}Pt}$: 1947.6Hz)

✦ *trans*-[Pt^{IV}(PS2')$_2$] 59.7 1 ppm(s and d, $^1J_{P\text{-}Pt}$: 1735.0 Hz)

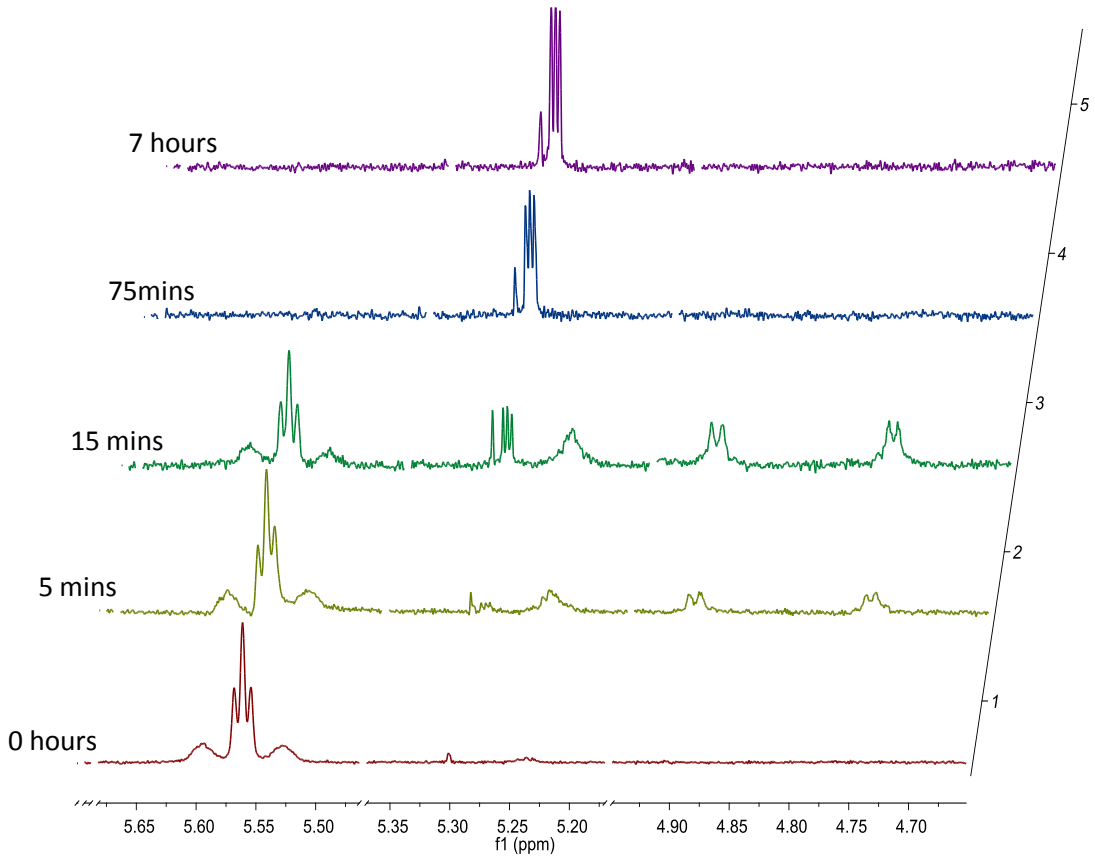

Figure IV- 8. Selective sections of the *in-situ* ^{1}H NMR study of pure *trans-anti*-[Pt^{II}(PS2'H)$_2$] spectra in $CDCl_3$ under UV irradiation (in a sealed quartz NMR tube), 300MHz

The ^{1}H NMR spectra of *in-situ* study of pure *trans-anti*-[Pt^{II}(PS2'H)$_2$] in $CDCl_3$ in quartz tube under UV irradiation are consistent with the ^{31}P NMR spectra. The –SH proton and methyl group protons regions of the ^{1}H NMR spectra are particularly informative. **Figure IV-8** shows selective regions of the *in-situ* ^{1}H NMR study of pure *trans-anti*-[Pt^{II}(PS2'H)$_2$] spectra in $CDCl_3$, where the population of –SH peaks of different isomers reveals that isomerization occurs before the oxidation reaction took place. CH_2Cl_2 and $CDHCl_2$ peaks start to show up in the spectrum after 15 minutes of

UV irradiation. The synchronic appearance of CH_2Cl_2, $CDHCl_2$ peaks and Pt(IV), endorses the critical function of $CDCl_3$ for the oxidation reaction.

The reaction rate is much faster in the quartz NMR tube than in glass tube. The regular glass is partially transparent to UV-A radiation, but is opaque to shorter wavelengths. Ordinary glass blocks over 90% of the light below 300 nm. Only the relatively low energy UV-A radiation are utilized in the study. The quartz NMR tube that we used in this study is transparent in majority of the UV region, therefore, higher energy is provided.

The isomerization of the $[Pt^{IV}(PS2'H)_2]$ isomers is very slow under UV irradiation, compared to the isomerization and oxidation of the $[Pt^{II}(PS2'H)_2]$ complexes, which may lead to the conclusion that Pt(IV) complexes are thermodynamically more stable than any Pt(II) isomers. Continuous UV irradiation seems to be essential for Pt(IV) isomerization, since letting the mixture of *cis* and *trans*-$[Pt^{IV}(PS2')_2]$ isomers stand in dark for overnight does not affect their relative concentrations.

Kinetic analysis of $[Pt^{II}(PS2'H)_2]$ *in-situ* NMR study for reactivity

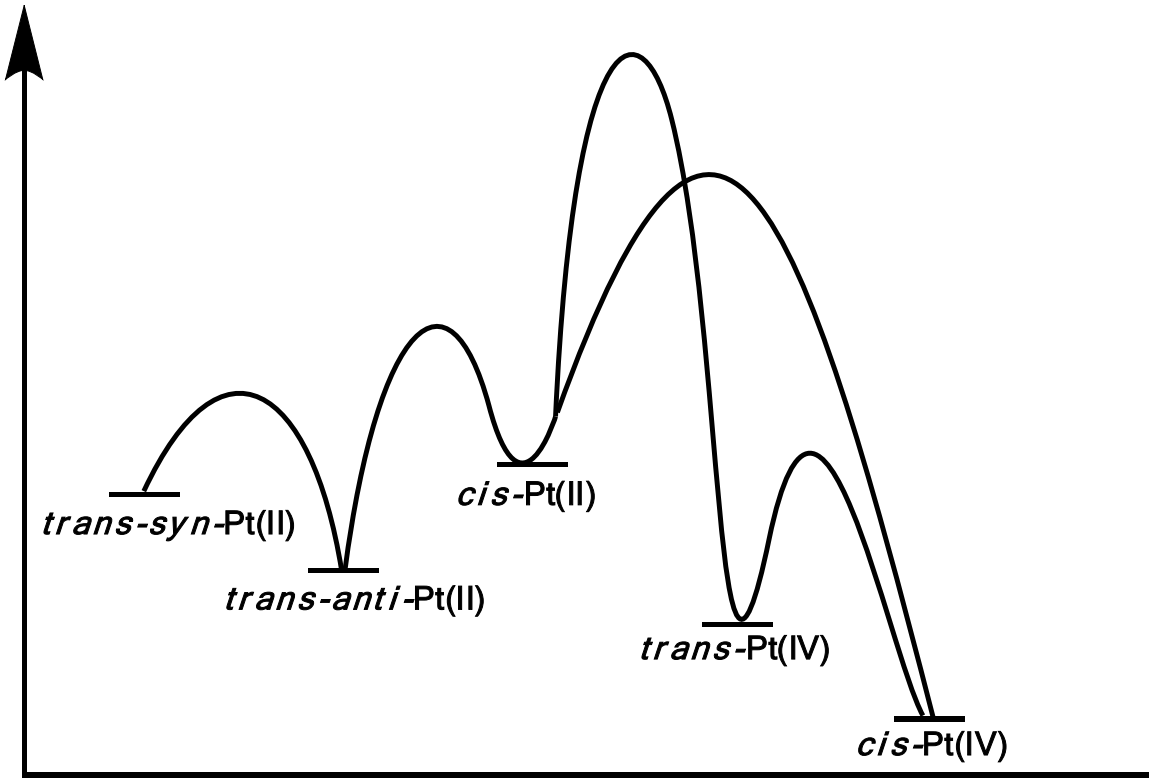

Figure IV- 9. Possible thermodynamic sketch of the $[Pt^{II}(PS2'H)_2]$ isomers and $[Pt^{IV}(PS2')_2]$ isomers.

In-situ NMR study of pure *trans-anti*-$[Pt^{II}(PS2'H)_2]$ have been conducted under 1) regular fluorescent lamp, 2) heating at 50 ℃ in the dark, 3) UV irradiation with a regular glass NMR tube and 4) UV irradiation with a quartz NMR tube. Combining the results under various conditions, the possible thermodynamic sketch of $[Pt^{II}(PS2'H)_2]$ and $[Pt^{IV}(PS2'H)_2]$ isomers are drawn (**Figure IV-9**).

(a) Under a fluorescence lamp, the energy barriers of the reaction *trans-anti*-$[Pt^{II}(PS2'H)_2]$ → *cis*-$[Pt^{II}(PS2'H)_2]$ and the reaction *trans-anti*-$[Pt^{II}(PS2'H)_2]$ → *trans*-

syn-[$Pt^{II}(PS2'H)_2$] are overcame, so that all four isomers are populated over time. The high barriers of the reaction *cis*-[$Pt^{II}(PS2'H)_2$] → *trans*-[$Pt^{IV}(PS2')_2$] and the reaction *cis*-[$Pt^{II}(PS2'H)_2$] → *cis*-[$Pt^{IV}(PS2')_2$] prevent the oxidation reaction under light, so that *cis*-[$Pt^{II}(PS2'H)_2$] is kinetically stable.

(b) Heating at 50 ℃ or UV irradiation in a regular glass tube, the energy barrier of the reaction *cis*-[$Pt^{II}(PS2'H)_2$] → *cis*-[$Pt^{IV}(PS2')_2$] is overcame as well, so the oxidation reaction proceeds and the thermodynamically more stable *cis*-[$Pt^{IV}(PS2')_2$] is formed. But the high barrier of reaction *cis*-[$Pt^{II}(PS2'H)_2$]→ *trans*-[$Pt^{IV}(PS2')_2$] still prevent the formation of *trans*-[$Pt^{IV}(PS2')_2$]. The difference between heating at 50 ℃ and UV irradiation in a regular glass tube is the rate. Since the rate constant *k* depends on the activation energy E_a and the temperature according to the Arrhenius equation,

$$k = k_0 e^{-E_a/RT}$$

A lower *k* results from a large ratio E_a/RT. Heating at 50 ℃ increase the rate constant *k*, so that thermodynamically more stable *trans-anti*-[$Pt^{II}(PS2'H)_2$] isomer predominant before the oxidation starts. The oxidation reaction under heating is significantly slower than that of under UV in regular glass tube, which suggests different reaction pathways.

(c) Under UV irradiation in a quartz tube, all the energy barriers of the reactions in the sketch are overcame, so that both oxidation reactions proceed. As a result, both *trans*-[$Pt^{IV}(PS2')_2$] and *cis*-[$Pt^{IV}(PS2')_2$] are formed initially, but *trans*-[$Pt^{IV}(PS2')_2$] is both thermodynamically and kinetically unstable and is converted to *cis*-[$Pt^{IV}(PS2')_2$].

Mechanism of isomerization and oxidation

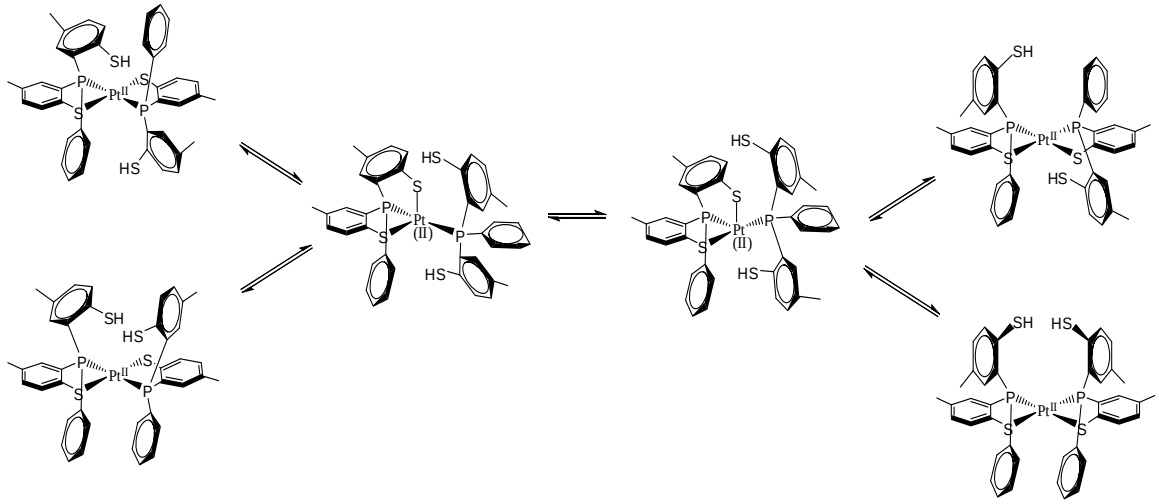

Scheme IV- 3. Proposed isomerization mechanism of $[Pt^{II}(PS2'H)_2]$

The mechanism of isomerization of $[Pt^{II}(PS2'H)_2]$ is proposed as in **Scheme IV-3**. Similar to the isomerization of $[Pt^{II}(PS2')_2]^{2-}$, a metal ligand bond-breaking step is involved. An appealing mechanism for isomerization involves the intermediate, in which both sets of the coordinated thiolates and the pendant thiols are equivalent. It is also notable that, in this proposed mechanism, proton transfer from thiol to thiolate occurs, which is not seen in the isomerization of $[Pt^{II}(PS2')_2]^{2-}$.

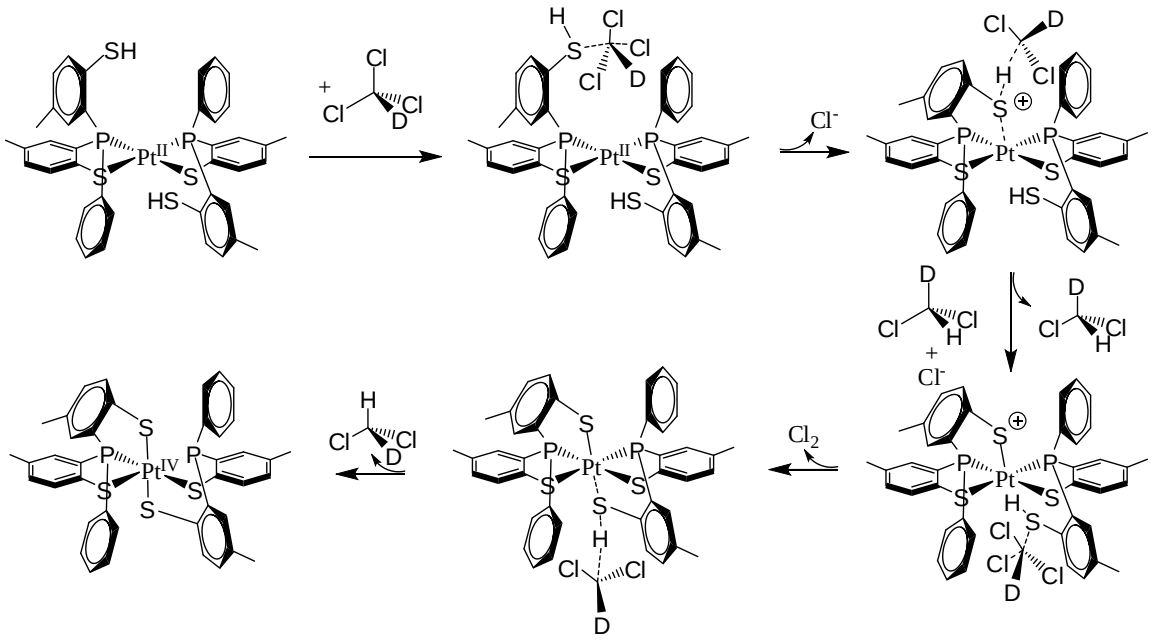

Scheme IV- 4. Proposed oxidation mechanism from $[Pt^{II}(PS2'H)_2]$ to *cis*-$[Pt^{IV}(PS2')_2]$ under heating.

The mechanism of the oxidation reaction was proposed based on the *in-situ* NMR studies. The oxidation reaction is significantly faster under UV irradiation than under heating, therefore different pathways are proposed for each condition. The proposed thermal oxidation mechanism from $[Pt^{II}(PS2'H)_2]$ to *cis*-$[Pt^{IV}(PS2')_2]$ is shown in **Scheme IV-4**, in which the C-Cl bonds in $CDCl_3$ are activated by thiol followed by S-H bond cleavage and S-Pt and H-C bond formation. Repeating this step twice results in the octahedral *cis*-$[Pt^{IV}(PS2')_2]$ complex. Protons from thiols end in the methylene dichloride solvent, and $CHDCl_2$, CH_2Cl_2 and CD_2Cl_2 are expected to form due to the H-D exchange, consistent with our ^{1}H NMR observations.

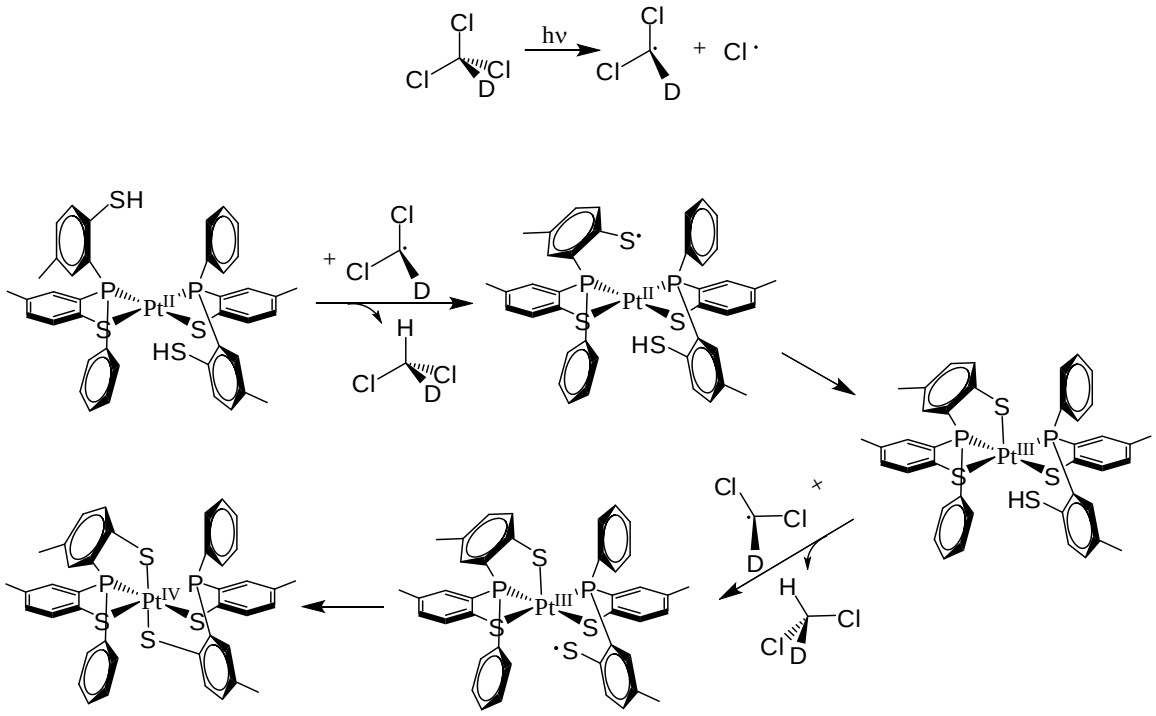

(a) *cis-anti*-[Pt^{II}(PS2'H)$_2$] to *cis*-[Pt^{IV}(PS2')$_2$]

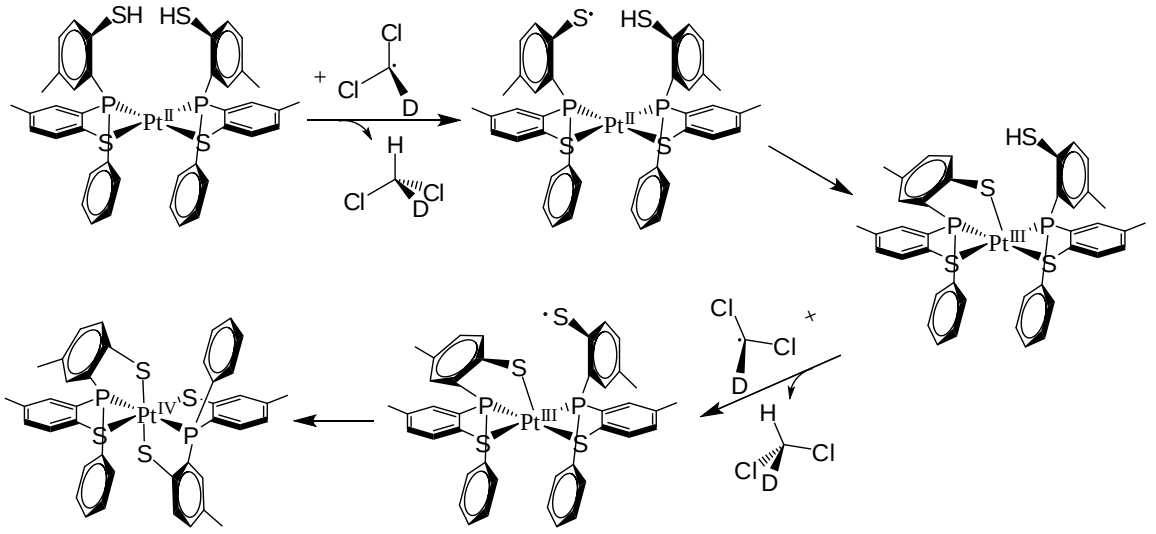

(b)*cis-syn*-[Pt^{II}(PS2'H)$_2$] to *trans*-[Pt^{IV}(PS2')$_2$]

Scheme IV- 5. Proposed oxidation mechanism from [Pt^{II}(PS2'H)$_2$] to *cis*-[Pt^{IV}(PS2'H)$_2$] under UV irradiation: (a) *cis-anti*-[Pt^{II}(PS2'H)$_2$] to cis-[Pt^{IV}(PS2')$_2$] (b) *cis-syn*-[Pt^{II}(PS2'H)$_2$] to *trans*-[Pt^{IV}(PS2')$_2$]

The oxidation mechanism from $[Pt^{II}(PS2'H)_2]$ to *cis*-$[Pt^{IV}(PS2')_2]$ and *trans*-$[Pt^{IV}(PS2')_2]$ under UV irradiation is shown in **Scheme IV-5**, in which a radical mechanism is proposed. As mentioned several time before, the rate of oxidation reaction under UV irradiation (both in regular glass tube and in quartz tube) is much faster, the idea of radical mechanisms seems more appealing. The formation of radicals from deuterated chloroform is followed by radical transfer to the pendant thiol to form a thiolate radical, which then bonds to the platinum metal and proceeds with the oxidation of the metal center. Unlike other common radical reactions, the radical in this proposed mechanism does not form a catalytic cycle. The formation of di-chlorine from two chloride radicals quenches the radical cycle. *Cis-anti*-$[Pt^{II}(PS2'H)_2]$ and *cis-syn*-$[Pt^{II}(PS2'H)_2]$ actually goes through the same pathway, but the difference in initial configurations results in the different isomeric products.

Reactivity study of $[Ni^{II}(PS2'H)_2]$ with UV irradiation in quartz NMR tube in $CDCl_3$

Trans-anti-$[Ni^{II}(PS2'H)_2]$ is isostructural with its platinum analog. It is interesting to compare the results of the *in-situ* reactivity study of $[Ni^{II}(PS2'H)_2]$ with those of platinum. As reported in a previous chapter, the ^{1}H NMR and ^{31}P NMR of pure *trans-anti*-$[Ni^{II}(PS2'H)_2]$ demonstrate that it spontaneously isomerized into a mixture of both *trans-anti*-$[Ni^{II}(PS2'H)_2]$ and *trans-syn*-$[Ni^{II}(PS2'H)_2]$ isomers in a variety of

solvents,. This shows that the isomerization of $[Ni^{II}(PS2'H)_2]$ complex is fast in solution, and the barrier for isomerization is considerably lower than that of its platinum analog.

The *in-situ* ^{31}P NMR and ^{1}H NMR of pure $[Ni^{II}(PS2'H)_2]$ was carried out in a sealed quartz NMR tube in "100%" $CDCl_3$ with continual UV irradiation. The ^{31}P NMR spectrum is shown in **Figure IV-10**.

configuration	^{31}P NMR (ppm)	-SH (ppm)	$-CH_3$(ppm)
trans-anti-$[Ni^{II}(PS2'H)_2]$	49.20	5.16	2.23
trans-syn-$[Ni^{II}(PS2'H)_2]$	53.95	5.03	2.20/2.17
cis-$[Ni^{IV}(PS2')_2]$	87.71		
trans-fac-$[Ni^{IV}(PS2')_2]$	76. 89		
trans-mer-$[Ni^{IV}(PS2')_2]$	56.09, 52.59		

Table IV- 1 Selective peak positions of $[Ni^{II}(PS2'H)_2]$ reactivity study in $CDCl_3$, 300MHz

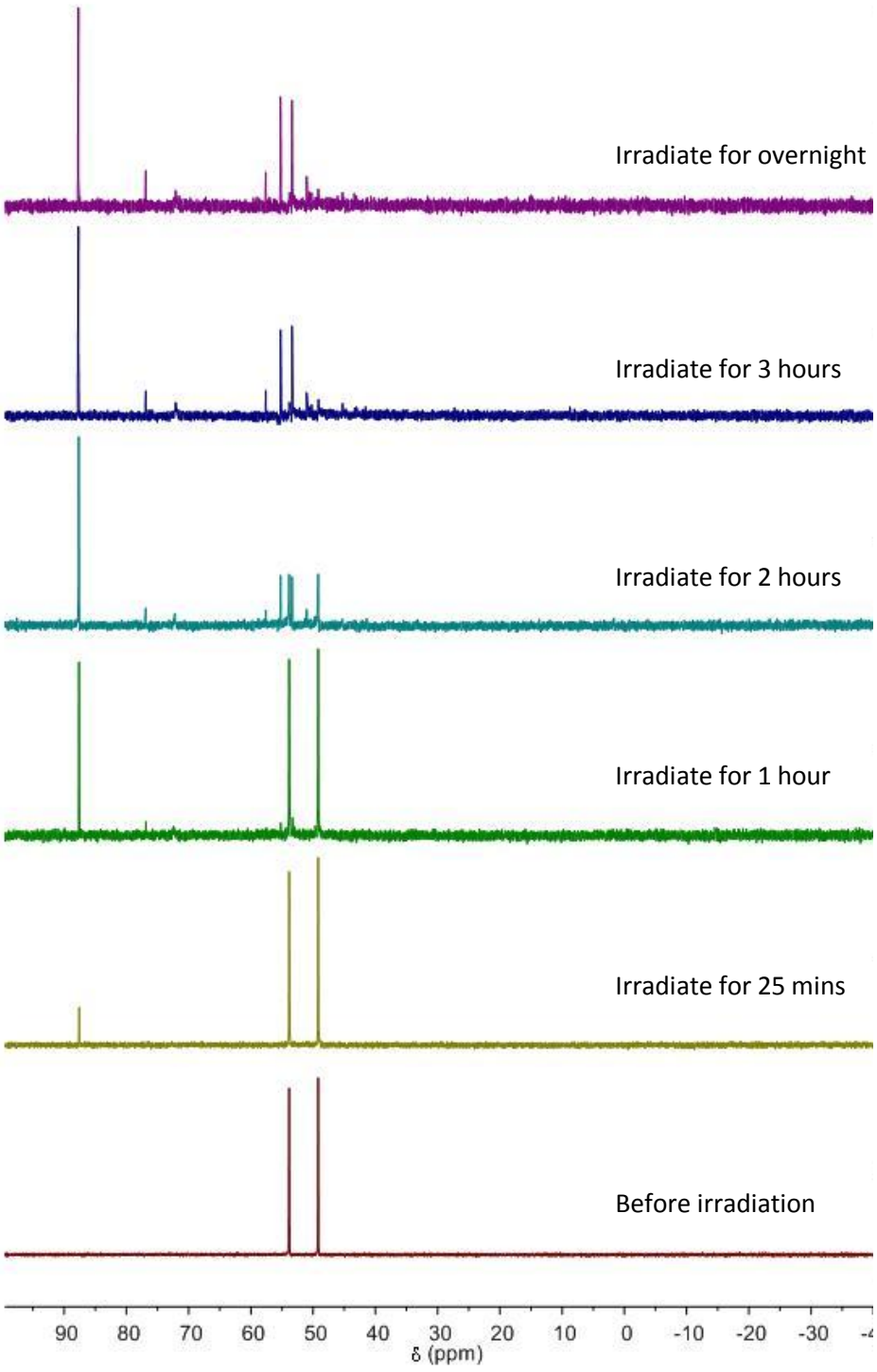

Figure IV- 10 *In-situ* ^{31}P NMR study of $[Ni^{II}(PS2'H)_2]$ in "100%" $CDCl_3$ in quartz tube under UV irradiation, 300MHz

The trend of the phosphorus spectra is totally different from the counterpart platinum study. The spectra are complicated, revealing that a mixture is generated in instead of forming a pure Ni(IV) complex. From the NMR data of pure $[Ni^{II}(PS2'H)_2]$ and cis-$[Ni^{IV}(PS2')_2]$, which we reported in chapter2, we learned that $[Ni^{II}(PS2'H)_2]$ complexes have their ^{31}P chemical shifts in a distinct region, so as the corresponding Ni(IV) complexes. These shift ranges make it possible for us to elucidate the spectra (**Table IV-1**).

In contrast to the platinum case, there is no evidence for the formation of the *cis-anti* or the *cis-syn*-$[Ni^{II}(PS2'H)_2]$ isomers. It is suggested that the *cis*-$[Ni^{II}(PS2'H)_2]$ isomers are destabilized by the steric interaction between the phenyl substituted phosphines. The longer Pt-P vs Ni-P distance would reduce the steric interaction and thus stabilize the *cis*-$[Pt^{II}(PS2'H)_2]$ isomers.

No further isomerization of the Ni(II) complexes is observed before oxidation starts for $[Ni^{II}(PS2'H)_2$. At 25 minutes of irradiation, there are only *trans-anti*-$[Ni^{II}(PS2'H)_2]$ and *trans-syn*-$[Ni^{II}(PS2'H)_2]$ isomers and a small amount of *cis*-$[Ni^{IV}(PS2')_2]$ in the reaction mixture. At one hour of irradiation, along with the growth of the *cis*-$[Ni^{IV}(PS2)_2]$, a small amount of *trans-fac*-$[Ni^{IV}(PS2)_2]$ starts to appear in the spectrum as well as some small undistinguishable but negligible peak in "Ni(II) range". At two hours of irradiation, in addition to the disappearance of both $[Ni^{II}(PS2'H)_2]$ isomers and the rapid growth of *cis*-$[Ni^{IV}(PS2')_2]$ a symmetrical pseudo-quartet ^{31}P resonance appears at 57.61, 55.25, 53.41 and 51.05 ppm. As reaction goes on after two

hours, the amount of *cis*-[$Ni^{IV}(PS2')_2$] decreases while intensity of the pseudo- "quartet " increases, until it reaches equilibrium after overnight UV irradiation. We had not observed this pseudo-quartet peak in our synthetic studies. There are no other resonances showing P-P coupling in the spectrum, which rules out its assignment as a first order quartet. Instead it is suggested that the pseudo-quartet is actually a second order AB quartet of two isolated but mutually spin-coupled spin ½ nuclei: 56.06, 52.59 ppm (ABq, J=286.7Hz). The phenomenon arises when the frequency separation between a chemically inequivalent sets of nuclei is similar in magnitude to the coupling constant between them.[22] The peak determining, quantum mechanical arrangement, the transition energies relative to center of the multiplet and relative intensities for this textbook AB second order system are in **Table IV-2** and **Figure IV-11**.

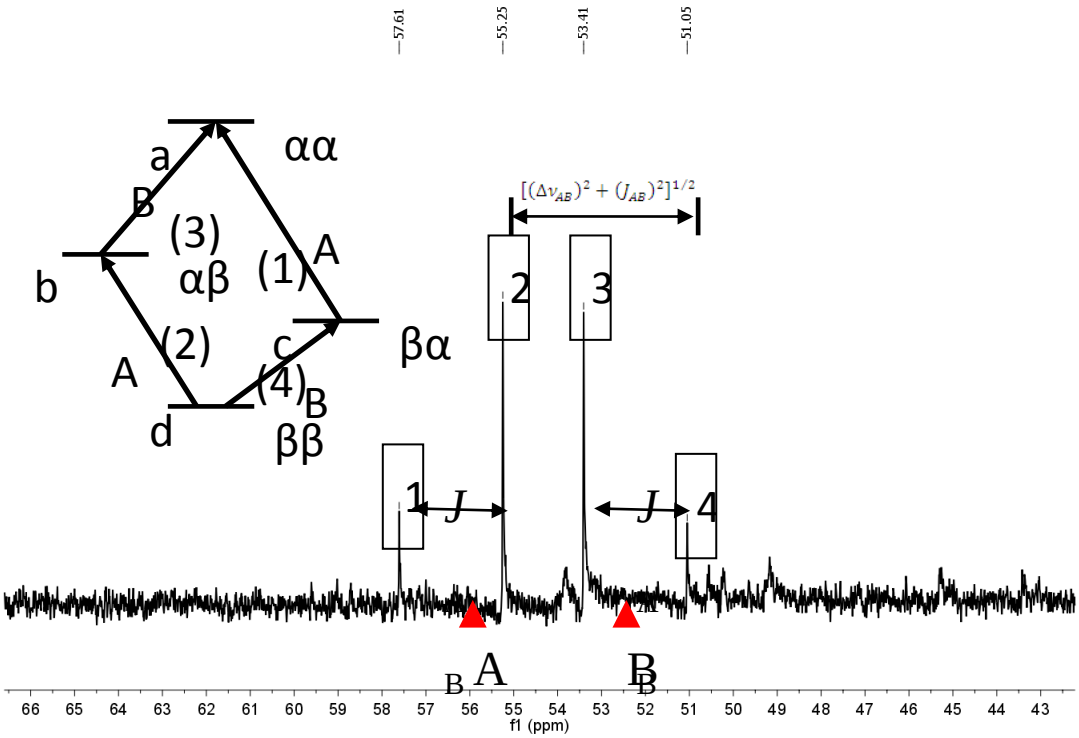

Figure IV- 11 The energy level diagram and spectrum analysis for the AB quartet 31P peaks, 300MHz

Peak calculations are done as below:

$$|J_{AB}| = (\nu_1 - \nu_2) = (\nu_3 - \nu_4) = 286.7Hz$$

$$\nu_{center} = {}^{1}/_{2}\,(\nu_2 + \nu_3) = 6601.1Hz$$

$$\Delta\nu_{AB} = \sqrt{(\nu_1 - \nu_4)(\nu_2 - \nu_3)} = 422.1Hz$$

$$\nu_A = \nu_{center} + {}^{1}/_{2}\,\Delta\nu_{AB} = 6812.15Hz$$

$$\nu_A = \nu_{center} - {}^{1}/_{2}\,\Delta\nu_{AB} = 6390.05Hz$$

$$\delta_A = \nu_A/0.405MHz = 56.06ppm$$

$$\delta_B = \nu_B/0.405MHz = 52.59ppm$$

Transition	Energy (Hz)	Relative intensity
1 c→a	$+\frac{1}{2}J_{AB}+\frac{1}{2}[(\Delta\nu_{AB})^2+(J_{AB})^2]^{1/2}$	$1-J/[(\Delta\nu_{AB})^2+(J_{AB})^2]^{1/2}$
2 d→b	$-\frac{1}{2}J_{AB}+\frac{1}{2}[(\Delta\nu_{AB})^2+(J_{AB})^2]^{1/2}$	$1+J/[(\Delta\nu_{AB})^2+(J_{AB})^2]^{1/2}$
3 b→a	$+\frac{1}{2}J_{AB}-\frac{1}{2}[(\Delta\nu_{AB})^2+(J_{AB})^2]^{1/2}$	$1+J/[(\Delta\nu_{AB})^2+(J_{AB})^2]^{1/2}$
4 d→c	$-\frac{1}{2}J_{AB}-\frac{1}{2}[(\Delta\nu_{AB})^2+(J_{AB})^2]^{1/2}$	$1-J/[(\Delta\nu_{AB})^2+(J_{AB})^2]^{1/2}$

Table IV- 2 Transition energies relative to center of multiplet and relative intensities for AB system

Contemporaneous ^{1}H NMR spectra help elucidate the structure that is responsible for the AB quartet (**Figure IV-12**). The appearance and growth of the four equal intense peaks in the methyl group region, is observed at the same time as the AB quartet phosphorus peak. It is notable that the AB quartet and the corresponding methyl proton peaks appeared only after the completion of the oxidation reaction. We propose that this new compound is *trans-mer*-[$Ni^{IV}(PS2')_2$]. There is no precedent for this isomer in known octahedral $[M(PS2)_2]^{n-}$ complexes but the PS2 ligand is known to coordinate in a tridentate fashion in square planar [Ni^{II}(PS2)L] complexes. Attempts to crystallize the

new compound have not been successful.

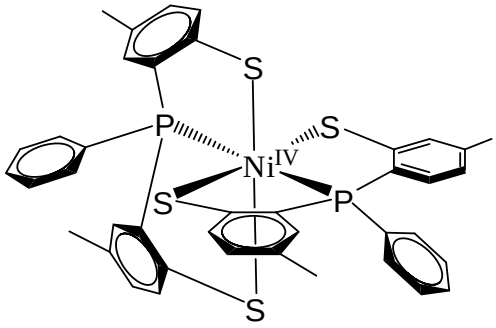

Trans-mer-[Ni^{IV}(PS2')$_2$]

Due to the steric restrain from the chelating ligands, the octahedral structure has to be distorted, and the two phosphorus atoms in the *trans-mer*-[Ni^{II}(PS2')$_2$] structure are magnetically in-equivalent, as are all four methyl groups. Very small frequency separation would be expected for the two phosphorus atoms, therefore arises the AB quartet that we observed. The observation of methyl group peaks also support the proposed structure. Therefore, we conclude that the reaction mixture is going through a isomerization at Ni(IV) level after the oxidation.

A comparison of the overnight spectrum with the spectrum after 3 hours, indicates that the isomerization seems to reach equilibrium with *cis*-[Ni^{IV}(PS2')$_2$] and *trans-fac*-[Ni^{IV}(PS2')$_2$] at ratio of 1:1.

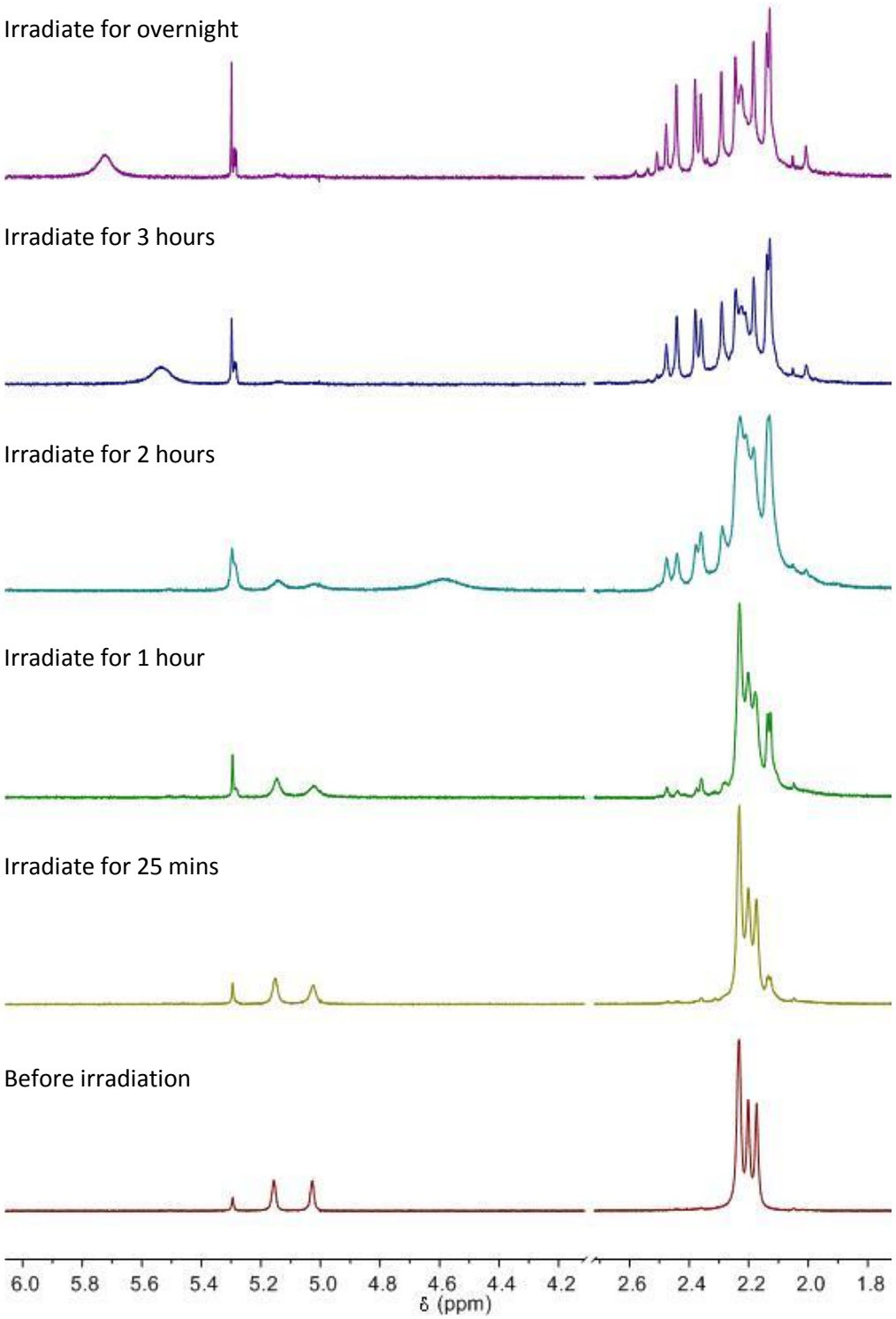

Figure IV- 12. *In-situ* ^{1}H NMR study of [Ni^{II}(PS2'H)$_2$] in "100%" $CDCl_3$ in quartz tube under UV irradiation, 300MHz.

Another distinguished feature of the proton NMR spectra is the appearance and growth of a migrating broad peak simultaneously with the methyl reasonance of *trans-mer*-$[Ni^{IV}(PS2')_2]$. In summary, the *trans*-$[Ni^{II}(PS2'H)_2]$ isomers undergoes photochemical oxidation with the formation of *cis*-$[Ni^{IV}(PS2')_2]$ as the major product and *trans-fac*--$[Ni^{IV}(PS2')_2]$ as a minor product. Continued irradiation changes these products into a compound which has been tentatively assigned as the *trans-mer*-$[Ni^{IV}(PS2')_2]$ isomer.

This observation suggests that the Ni-PS2' complexes in $CDCl_3$ have the same mechanism as the proposed radical mechanism of oxidation from Pt(II) to Pt(IV) under UV irradiation. It is not surprising that the *trans-mer*-Ni(IV) complex, which is not formed in our oxidation mechanism, is not seen at the oxidation stage.

The isomerization of Ni(IV) complex after oxidation is probably going through bond-breaking step as the isomerization of $[Pt^{II}(PS2'H)_2]$. The sketch of the three possible Ni(IV) isomers and the propose isomerization mechanism is shown below (**Figure IV-13**). Repeated reactions of $[Ni^{II}(PS2'H)_2]$ in $CDCl_3$ under UV irradiation demonstrate that the oxidation and isomerization reactions are reproducible. Stopping the UV irradiation after the completion of the oxidation has no effect on the isomerization of Ni(IV), which supports our proposed mechanism of isomerization.

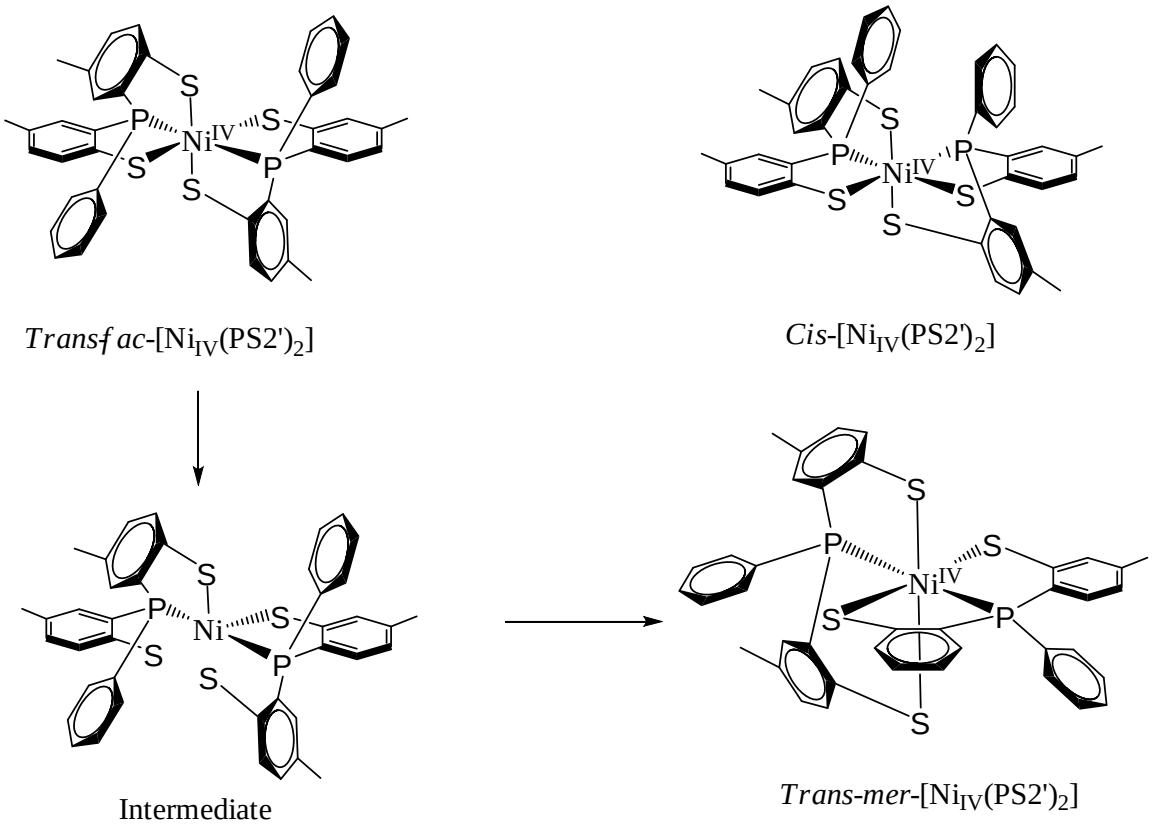

Figure IV- 13. Sketch of three possible Ni(IV) isomers and propose isomerization mechanism of Ni(IV) complexes

Reactivity study of [Ni^{II}(PS2'H)$_2$] with UV irradiation in quartz NMR tube in CD_2Cl_2

According to our proposed mechanism, the oxidation of the [M^{II}(PS2'H)$_2$] system, especially the reaction under UV irradiation, the solvent $CHCl_3$ is closely involved in the oxidation reaction. The *in-situ* ^{31}P NMR and ^{1}H NMR of pure *trans-anti*-[Ni^{II}(PS2'H)$_2$] was carried out in a sealed quartz NMR tube in CD_2Cl_2 with continual UV irradiation. The ^{31}P NMR spectra are shown in **Figure IV-14**.

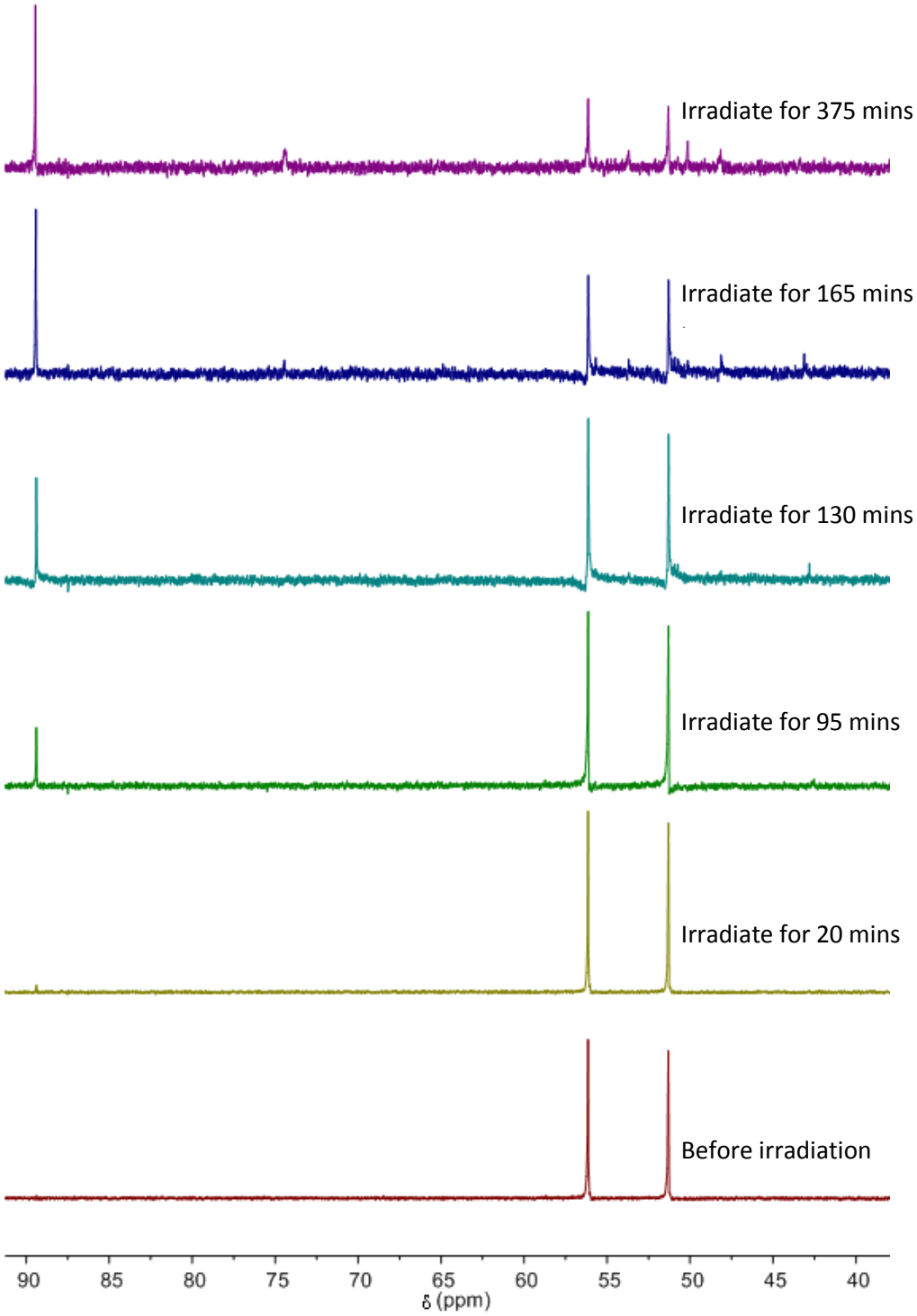

Figure IV- 14 *In-situ* ^{1}H NMR study of [Ni^{II}(PS2'H)$_2$] in CD_2Cl_2 in quartz tube under UV irradiation, 300MHz

We noticed that the initial two phosphorus peaks in the ^{31}P NMR in CD_2Cl_2 are shifted downfield compare to the resonances in $CDCl_3$, so the peak at 89.44ppm is assigned to be *cis*-[$Ni^{IV}(PS2')_2$]. The most significant features of the spectra are: at 375 minutes, the spectrum is almost identical to the one at 165 minutes, where the oxidation into Ni(IV) complex is not complete; and the AB quartet resonance of *trans-mer*-Ni(IV) is not seen in the spectrum. This confirmed that the oxidation reaction is slower due to the lower photo-activity of CD_2Cl_2. Therefore, our proposed photo radical mechanism is supported.

The ^1H NMR of Ni(II) complexes in CD_2Cl_2 before irradiation (**Figure IV-15**) is similar to the spectrum in $CDCl_3$: the compound in solution convert into a 1:1 mixture of *trans*-anti-[$Ni^{II}(PS2'H)_2$] and *trans-syn*-[$Ni^{II}(PS2'H)_2$]. The peak at 5.22 and 5.12ppm belongs to –SH peak of each isomer. The peak at 2.24ppm is the methyl group of *trans*-[$Ni^{II}(PS2'H)_2$] and the 2.20, 2.17ppm peaks belong to the methyl groups of *cis*-[$Ni^{II}(PS2'H)_2$] .

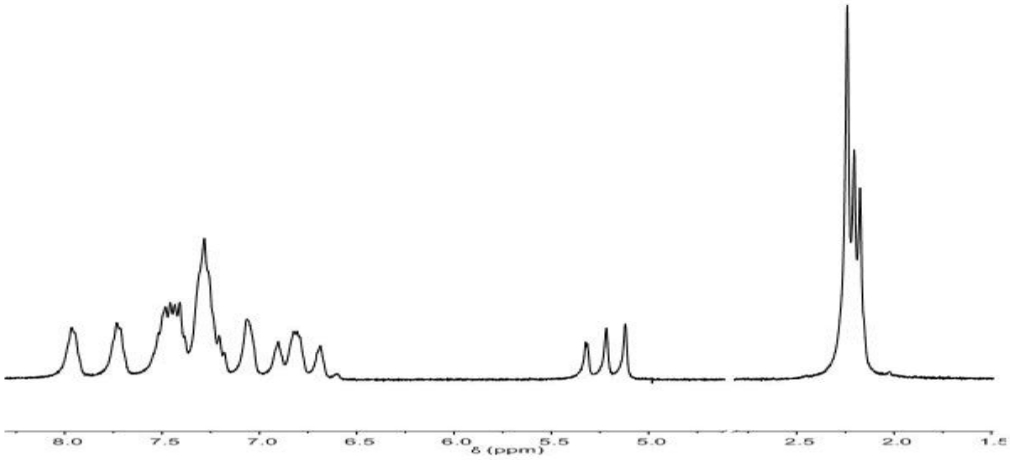

Figure IV- 15. ^1H NMR of [$Ni^{II}(PS2'H)_2$] in CD_2Cl_2, 300MHz

The *in-situ* ^{1}H NMR spectra (**Figure IV-16**) under UV irradiation reveal the CH_3Cl peak (3.00ppm) appears synchronously with the appearance of the Ni(IV) product. It also confirmed that even after more than 6 hours of irradiation, the $[Ni^{II}(PS2'H)_2]$ is not fully oxidized.

Repeat reactions of $[Ni^{II}(PS2'H)_2]$ in CD_2Cl_2 under UV irradiation demonstrate that the oxidation reaction is reproducible and that extended overnight UV irradiation does not push the reaction to completeness.

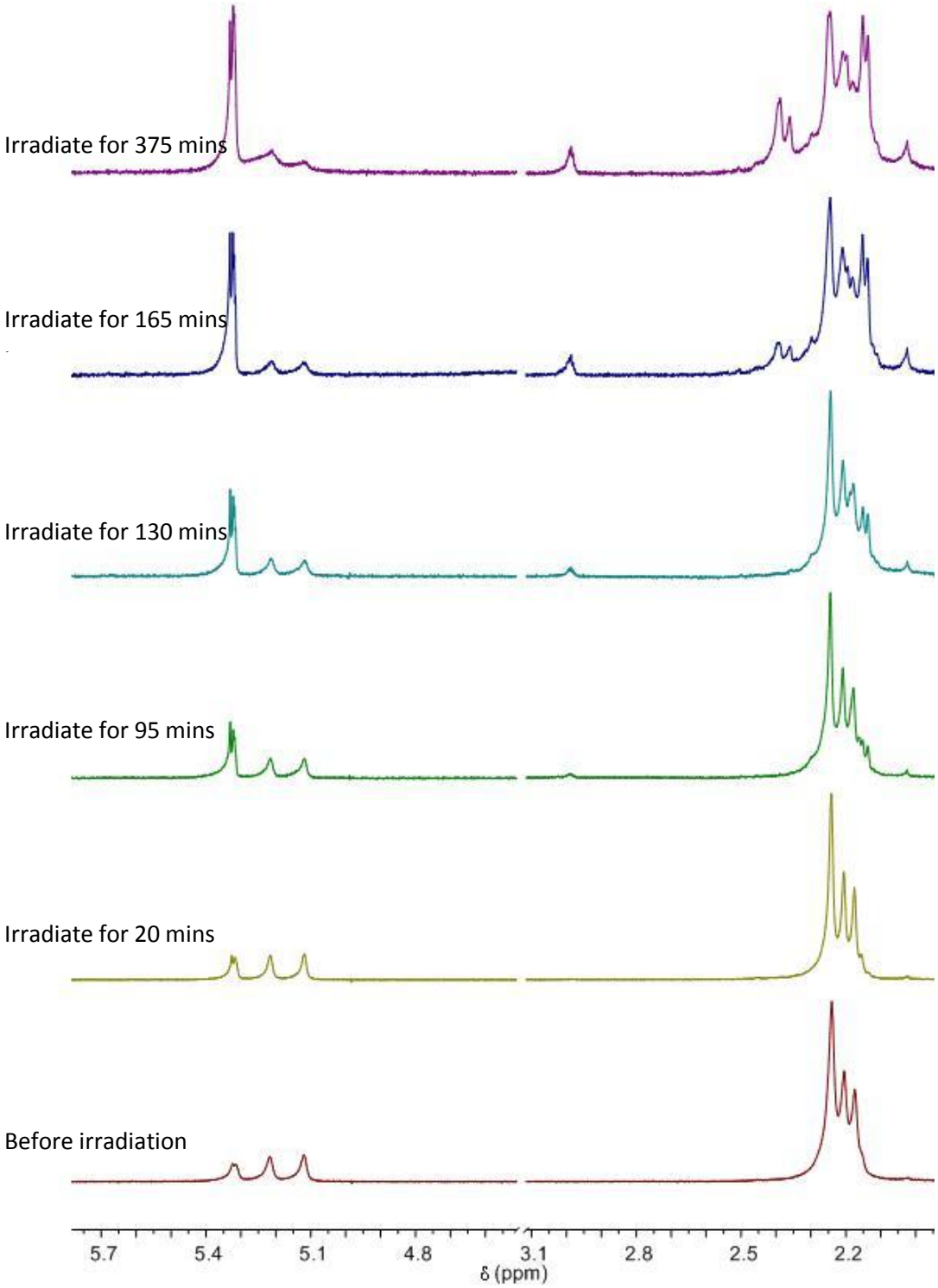

Figure IV- 16. *In-situ* ^{1}H NMR study of $[Ni^{II}(PS2'H)_2]$ in CD_2Cl_2 in quartz tube under UV irradiation, 300MHz.

3. CONCLUSION

A series of *in-situ* ^{1}H NMR and ^{31}P NMR studies of pure *trans-anti*-[$Pt^{II}(PS2'H)_2$] were done in $CDCl_3$ under different conditions. All four isomers of [$Pt^{II}(PS2'H)_2$] were detected and characterized by ^{1}H NMR and ^{31}P NMR and fully characterized with interesting virtual coupling observation. Analysis of the results provides approximate kinetic information: *trans*-[$Pt^{II}(PS2'H)_2$] isomers are thermodynamically more stable compared to *cis*-[$Pt^{II}(PS2'H)_2$] isomers. [$Pt^{II}(PS2'H)_2$] complexes can be oxidized to [$Pt^{IV}(PS2'H)_2$] complexes in the absence of oxygen but with a high activation energy barrier.

The mechanisms of isomerization and oxidation are suggested. The isomerization reaction mechanism appears to be independent of reaction conditions, with an intermediate, in which both sets of the coordinated thiolates and the pendant thiols are equivalent. The oxidation reaction is dependent on reaction conditions. A mechanism involving activation of the C-Cl bonds in chloroform is proposed for the thermal reactions, while a radical mechanism is proposed for reactions under UV irradiation.

The NMR study proved that the [$Pt^{II}(PS2'H)_2$] complexes could be oxidized from Pt(II) to Pt(IV) in certain solutions and act as a proton source, therefore they are both structural and functional analogies of the metal center in hydrogenase enzymes.

4. EXPERIMENTAL

Reactivity study with regular light in glass NMR tube

The NMR sample was prepared with pure *trans-anti*-[Pt^{II}(PS2'H)$_2$] (14mg, 0.016mmol) orange power dissolved in "100%" $CDCl_3$ inside the glove box. J. Young glass NMR tubes were used to carry out the *in-situ* study. The *in-situ* ^{1}H NMR and ^{31}P NMR spectra were measured as needed for a week, while the NMR tube was under persistent irradiation with a fluorescent lamp.

^{1}H NMR and ^{31}P NMR: Isomerization of [Pt^{II}(PS2'H)$_2$]. All four isomers were observed at 163 hours.

Reactivity study with heat in glass NMR tube

NMR samples were prepared with pure *trans-anti*-[Pt^{II}(PS2'H)$_2$] (13mg, 0.014mmol) orange power dissolved in "100%" $CDCl_3$ inside the glove box. J. Young glass NMR tube was used to carry out the *in-situ* study. The *in-situ* ^{1}H NMR and ^{31}P NMR spectra were recorded as needed for two days, while the NMR tube was heated at 50 ℃ in the dark.

^{1}H NMR and ^{31}P NMR: Isomerization of [Pt^{II}(PS2'H)$_2$] followed by oxidation reaction. *Cis*-[Pt^{IV}(PS2')$_2$] was formed along with CH_2Cl_2/$CHDCl_2$ peaks.

Reactivity study with UV irradiation in glass NMR tube

NMR samples were prepared with pure *trans-anti*-[$Pt^{II}(PS2'H)_2$] (13mg, 0.014mmol) orange power dissolved in "100%" $CDCl_3$ inside the glove box. J. Young glass NMR tube was used to carry out the *in-situ* study. The *in-situ* ^1H NMR and ^{31}P NMR spectra were taken as needed for two days, while the NMR tube was under persistent irradiation with a Hanovia UV 450W lamp.

^1H NMR and ^{31}P NMR: Isomerization of [$Pt^{II}(PS2'H)_2$] followed by oxidation reaction. *Cis*-[$Pt^{IV}(PS2')_2$] was formed along with CH_2Cl_2/$CHDCl_2$ peaks.

Reactivity study with UV irradiation in quartz NMR tube

NMR samples were prepared with pure *trans-anti*-[$Pt^{II}(PS2'H)_2$] (13mg, 0.014mmol) orange power dissolved in "100%" $CDCl_3$ inside the glove box. J. Young quartz NMR tube was used to carry out the *in-situ* study. The *in-situ* ^1H NMR and ^{31}P NMR spectra were taken as needed for two days, while the NMR tube was under persistent irradiation with a Hanovia UV 450W lamp.

^1H NMR and ^{31}P NMR: Isomerization of [$Pt^{II}(PS2'H)_2$], oxidation reaction to Pt(IV)-PS2' complexes and isomerization of Pt(IV)-PS2'. *Cis*-[$Pt^{IV}(PS2')_2$] was formed along with CH_2Cl_2/$CHDCl_2$ peaks.

REFERENCES

(1) Nixcon, J. F.; Pidcock, A. *Annual Review of NMR Spectroscopy* **1969**, *2*, 345.

(2) Pidcock, A.; Richards, R. E.; Venanzi, L. M. *Journal of the Chemical Society a - Inorganic Physical Theoretical* **1966**, 1707.

(3) Rigamonti, L.; Forni, A.; Manassero, M.; Manassero, C.; Pasini, A. *Inorg Chem* **2010**, *49*, 123.

(4) Venanzi, L. M. *Chem. Br.* **1968**, *4*, 162.

(5) Appleton, T. G.; Clark, H. C.; Manzer, L. E. *Coord. Chem. Rev.* **1973**, *10*, 335.

(6) Otto, S.; Roodt, A. *Inorg. Chim. Acta* **2004**, *357*, 1.

(7) Roodt, A.; Otto, S.; Steyl, G. *Coord. Chem. Rev.* **2003**, *245*, 121.

(8) Arnold, D. P.; Bennett, M. A. *Inorg. Chem.* **1984**, *23*, 2117.

(9) Loscher, S.; Burgdorf, T.; Zebger, I.; Hildebrandt, P.; Dau, H.; Friedrich, B.; Haumann, M. *Biochemistry* **2006**, *45*, 11658.

(10) Hoggard, P. E. *Coord. Chem. Rev.* **1997**, *159*, 235.

(11) Hu, J.; Xu, H.; Nguyen, M. H.; Yip, J. H. K. *Inorg. Chem.* **2009**, *48*, 9684.

(12) Cohen, J. L.; Hoggard, P. E. *Inorg. React. Mech.* **2008**, *6*, 293.

(13) Hoggard, P. E.; Bridgeman, A. J.; Kunkely, H.; Vogler, A. *Inorg. Chim. Acta* **2004**, *357*, 639.

(14) Hoggard, P. E.; Gruber, M.; Vogler, A. *Inorg. Chim. Acta* **2003**, *346*, 137.

(15) Mann, K. R.; Gray, H. B. *J. Am. Chem. Soc* **1977**, *99*, 306.

(16) Jaryszak, E. M.; Hoggard, P. E. *Inorg. Chim. Acta* **1998**, *282*, 217.

(17) Whang, S.; Estrada, T.; Hoggard, P. E. *Photochem. Photobiol.* **2004**, *79*, 356.

(18) Hoggard, P. E.; Vogler, A. *Inorg. Chim. Acta* **2003**, *348*, 229.

(19) Clemenson, P. I. *Coord. Chem. Rev.* **1990**, *106*, 171.

(20) Knoblauch, S.; Hartl, F.; Stufkens, D. J.; Hennig, H. *Eur. J. Inorg. Chem.* **1999**, 303.

(21) Crabtree, R. H. *The organometallic chemistry of the transition metals*; Wiley-Interscience, 2005.

(22) Akitt, J. W. *NMR and Chemistry: An introduction to modern NMR spectroscopy* Third ed., 1992.

Chapter 5

Fe-Fe Thiolate Dimers and Their Reactivity Study with Carbon Monoxide and Oxygen

1. INTRODUCTION

Iron-sulfur proteins are the most widely known class of electron transfer proteins. It is not surprising that proteins containing Fe–S clusters (referred to as Fe–S proteins) are present in all living organisms and have prominent roles in multiple important cellular processes, including respiration, central metabolism, gene regulation, RNA modification, and DNA repair and replication.[1] Fe–S clusters endow proteins with diverse biochemical abilities, including: 1) electron transfer, due to their access to various redox states; 2) redox catalysis, due to its possible very low redox potentials and thereby reducing redox-resistant substrates; 3) non-redox catalysis, due to its ability to allow small compounds binding to accessible ferric sites with extensive Lewis acid properties; and 4) the ability to regulate gene expression, due to its reversible interconversion that makes it exquisite sensors of several redox- or iron-related stresses.[2-4]

At their active sites, these metalloenzymes have either one iron atom (rubredoxin) or a cluster of iron and inorganic sulfur atoms bound to the protein through cysteine sulfurs. In general, Fe-S cluster arise as rhombic, [2Fe-2S], or cubic, [4Fe-4S] types (**Figure V-1**). Iron can change oxidation states from Fe^{II} to Fe^{III}, whereas sulfur remains at S^{2-} oxidation level.

Nitrogenases, which are used by some organisms to fix atmospheric nitrogen gas (N_2), consist of two proteins, the Fe protein and FeMo protein.[5] The Fe protein is a dimer of two identical subunits bridged by one [4Fe-4S] cluster, and acts as a one-electron donor to the FeMo protein. The FeMo protein is a tetramer containing two P-cluster units

and two FeMo cofactors. The FeMo cofactor is the active center where bonding, activation and reduction of the N_2 molecule occur.[5]

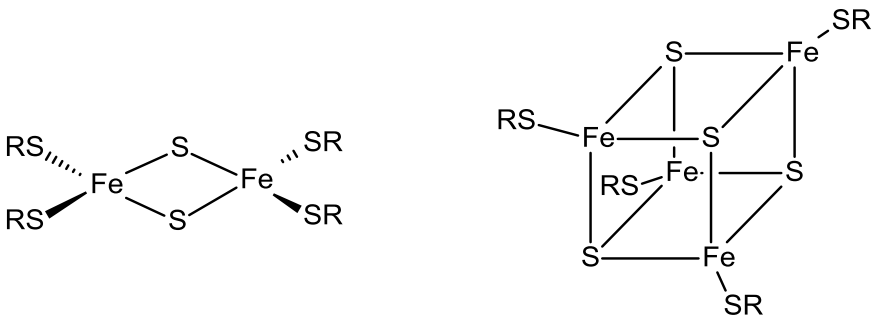

[2Fe-2S] [4Fe-4S]

Figure V- 1. Structure of Fe-S cluster.

The study of mixed valence systems originated with the observation that mixing solutions of $Fe^{II}(aq)$ and $Fe^{III}(CN)_6^{3-}$ yielded the deep blue material known as Prussian blue.[6] The color of the $Fe^{II}[Fe^{III}(CN)_6^{4-}]$ salt was found to arise because visible light absorption induces electron transfer from Fe^{II} to Fe^{III}. Recent interest in mixed-valence materials is prompted in part by the synthesis of new conducting materials[7-8] and the occurrence of mixed-valence compounds in biology.[9]

The importance of metal ions in biology is now widely recognized. In many of these systems, several metal ions work together to perform a biological function that cannot be performed by a single metal center. The ability of these metal ions to assume more than one oxidation state in these systems is key to the functioning of these proteins. The best studied example of mixed-valence complexes in biology are the iron-sulfur

proteins, namely the ferredoxin and high potential iron proteins.[9] Both [2Fe-2S] and [4Fe-4S] ferredoxin contain iron in the formal 2+ and 3+ oxidation states that enables the protein to sustain reversible, one electron transfer processes.

Metal complexes with diatomic ions and molecules (O_2, CO, S_2, N_2, NO, H_2) have generated great interest. Complexes with S_2^{2-} units have been formed for many metals and have been reviewed extensively with other polysulfide complexes.[10]

Oxygen is a reactive molecule, and its essential chemical behavior is the oxidation of other molecules. Molecular-orbital rules dictate that molecular oxygen accept electron one at a time rather than in pairs.[11] This restriction ensures that oxygen does not react with most organic biomolecules, whereas it allows it to oxidize transition metals, which are good univalent electron donors.[12]

It has been known for years that *E. Coli* dihydroxy acid dehydratase is inactivated in cells treated with hyperbaric O_2. The finding of this enzyme containing a Fe-S cluster led to the hypothesis that the molecular basis for its inactivation was the oxidation and destruction of its Fe-S cluster by an oxygen species.[13] Series of studies suggest that a primary toxic act of O_2^- may be to destroy the Fe-S clusters of the hydrolyase class of enzymes. The one Fe^{2+} and three Fe^{3+} released from these clusters on complete destruction would be set free in the cell (**Scheme V-1**). The Fe^{3+} could be reduced by cellular reductants such as glutathione to Fe^{2+}. In A, the H_2O_2 leaves the active site before Fe^{+2} is released from the cluster, and in B, H_2O_2 remains in the active site until Fe^{+2} is released from the cluster. Hydroxyl radicals are formed in the active site.

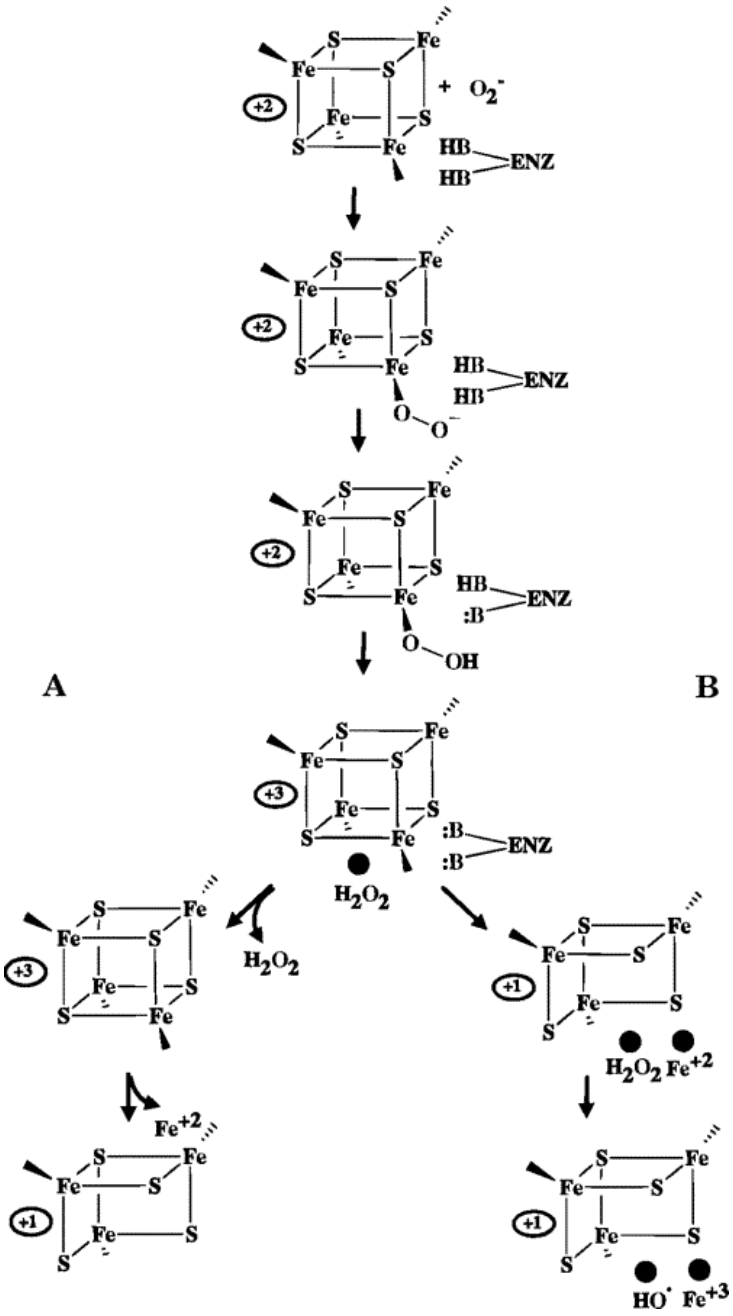

Scheme V- 1. (A) Reversible Inactivation Due to Cluster Degradation and (B) Irreversible Inactivation Due to Oxidation of Active Site Residue.[14]

Some of the Fe^{2+} could become associated with DNA and in reaction with hydrogen peroxide could generate hydroxyl radicals and damage the DNA.[15] The Fe protein of nitrogenase and the "archerase" enzymes that drive electrons onto flavin-

radical dehydratases also rely upon Fe-S clusters near the protein surface.[16] All these enzymes are rapidly inactivated by oxygen. While oxygen is not inherently a strong single electron oxidant (E_m= -0.16V), [4Fe-4S] clusters that operate with low +2/+2 midpoint potentials apparently also have low +3/+2 potentials that leave them vulnerable to over-oxidation, and enzymes that use these clusters are stable in anaerobic environments or if their clusters are deeply buried within the protein.[12]

2. RESULTS AND DISCUSSION

The ligands that we used for this series of complexes are: [tris(5-methyl-2-thio-phenyl) phosphine] (abbreviated H_3PS3'), and [tris(*ortho*-thio-phenyl)phosphine] (abbreviated H_3PS3). The **Scheme V-2** shows the structure of these ligands.

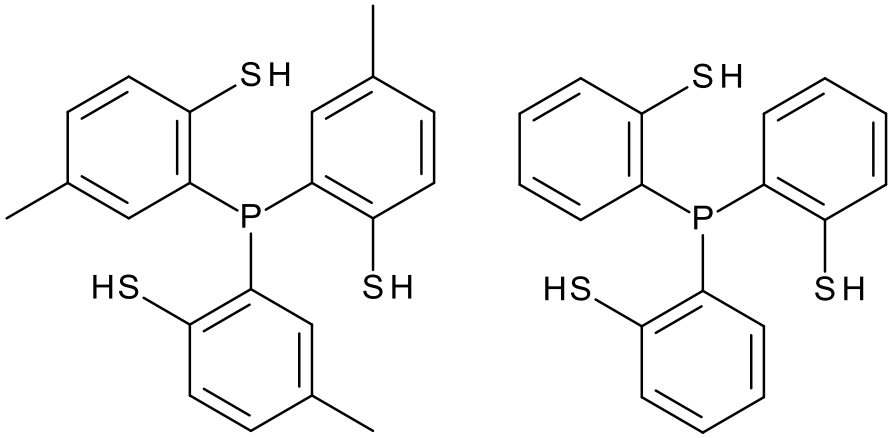

H_3PS3' H_3PS3

Scheme V- 2. Structure of ligands.

This chapter presents the attempts to isolate the product obtained from the reactions of Li_3PS3 or Li_3PS3' with Fe(II) in order to explore its possible reactivity with small molecules such as CO, N_2, H_2 and O_2.

$[Fe^{II}Fe^{III}(PS3)_2]^{2-}$

Previously Franolic[17] reported the reaction of $FeCl_2 \cdot 4H_2O$ and $Li_3(PS3)$ in methanol followed by the addition of a tetraalkylammonium cation produced the mixed-valent $Fe^{II}Fe^{III}$ complex, $[Fe^{II}Fe^{III}(PS3)_2]^{1-}$. The most notable observation was that starting from the Fe^{II} reactant, one electron was lost and the mixed-valent $Fe^{II}Fe^{III}$ complex was formed without an obvious oxidizing agent. The oxidation states of the mixed-valent compound were confirmed by the X-ray crystallography. I was able to reproduce this reaction and obtained $[(Pentyl)_4N][Fe^{II}Fe^{III}(PS3)_2]$ in 70% yield. Special precautions were taken to make sure that air was precluded from the reaction mixture. Franolic found that protons from the solvent and the reactants were reduced to H_2. The X-ray structure of $[(Pentyl)_4N][Fe^{II}Fe^{III}(PS3)_2]$, which I obtained from data collected at 100K, has a greater precision than the previously obtained room temperature structures studied by Franolic and Ai[18].

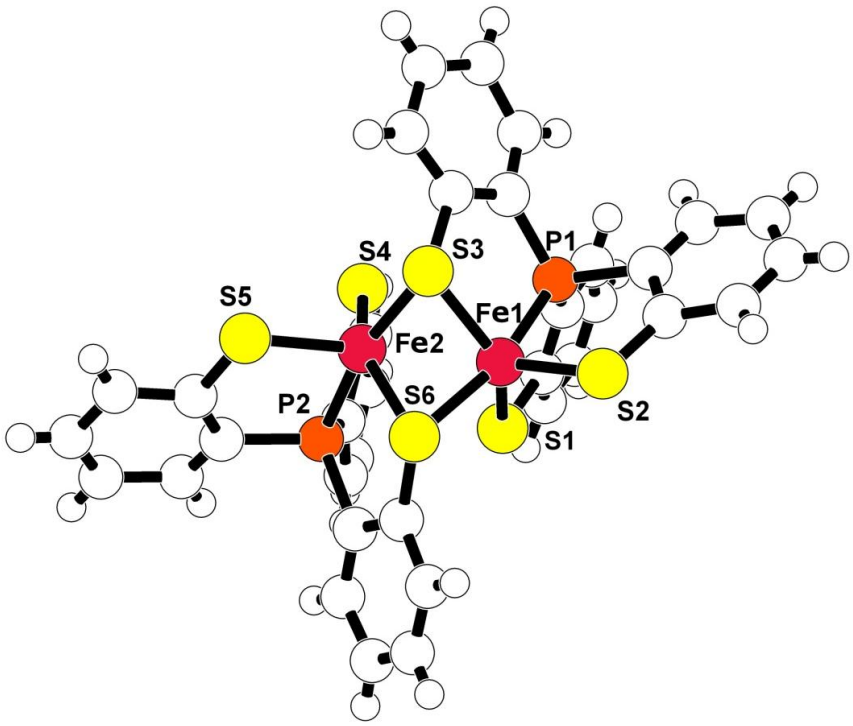

Figure V- 2. X-ray crystal structure of $[(Pentyl)_4N][Fe^{II}Fe^{III}(PS3)_2]$, Chem-Ray structure. The cations are omitted for clarity.

The X-ray crystal structure of $[Fe^{II}Fe^{III}(PS3)_2]^{1-}$ is shown in **Figure V-2**. The complex contains approximate C_2 symmetry and is composed of two, five-coordinate $[FeS_4P]$ units linked each other by two bridging thiolates from opposite ligands. The $[FeS_4P]$ coordination units do not rigorously conform to either the square pyramidal or trigonal bipyramidal limiting configuration, but do approach the square pyramidal structure somewhat more closely (**Figure V-3**). The Fe1 unit has P1, S3, S6 and S1 on the pyramidal base and S2 on the pyramidal top; whereas the Fe2 unit has P2, S6, S3 and S4 on the pyramidal base and S5 on the pyramidal top. Two Fe units share the pyramidal base edge.

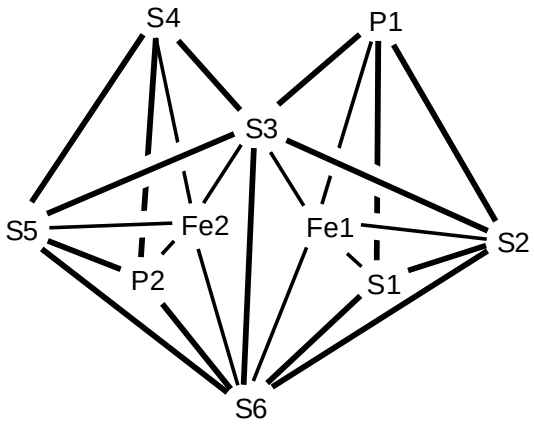

Figure V- 3. Geometry of $[(Pentyl)_4N][Fe^{II}Fe^{III}(PS3)_2]$.

The bond distances illustrate the presence of two non-equivalent iron sites (**Table V-1**). Overall, bond distances that involved with Fe2 are longer than the ones that involved with Fe1. This, along with the overall charge on the anion imply that it is a trapped-valence $Fe^{II}Fe^{III}$ dimer, with Fe1 in the +3 oxidation state and Fe2 in the +2 oxidation state. The Fe1-Fe2 distance of 2.592(4) indicates a substantial metal-metal interaction. It is notable that Fe2-S3 bond distance is shorter than expected, which is probably indicative of Fe(πd) –S(π*) overlap.

Bond length*(Å)*	**Fe1**		**Fe2**	
$Fe\text{-}S_{terminal}$	Fe1-S1	2.215(9)	Fe2-S4	2.292(10)
	Fe1-S2	2.249(8)	Fe2-S5	2.359(9)
$Fe\text{-}S_{bridging}$	Fe1-S3	2.298(7)	Fe2-S3	2.265(7)
	Fe1-S6	2.289(8)	Fe2-S6	2.326(8)
Fe-P	Fe-P1	2.081(9)	Fe2-P2	2.168(7)

Angle(°)	Fe1		Fe2	
S_t-Fe-S_t	S1-Fe1-S2	116.5(3)	S4-Fe1-S5	109.4(3)
S_t-Fe- S_b	S1-Fe1-S3	135.5(3)	S4-Fe2-S6	147.5(3)
	S1-Fe1-S6	91.1(3)	S4-Fe2-S3	99.1(3)
	S2-Fe1-S3	107.7(3)	S5-Fe2-S6	102.1(3)
	S2-Fe1-S6	105.4(4)	S5-Fe2-S3	100.4(3)
S_b-Fe- S_b	S3-Fe1-S6	82.3(3)	S3-Fe1-S6	82.2(3)
Fe-S_b-Fe	Fe1-S3-Fe2	69.2(2)	Fe1-S6-Fe2	68.4(3)
P-Fe-S_b	P1-Fe1-S6	165.7(3)	P2-Fe2-S3	167.0(3)
	P1-Fe1-S3	88.9(3)	P2-Fe2-S6	88.5(3)

Table V- 1. Selected bond distances and bond angles for $[(Pentyl)_4N][Fe^{II}Fe^{III}(PS3)_2]$.

The cyclic voltammogram of $[(Pentyl)_4N][Fe^{II}Fe^{III}(PS3)_2]$ (**Figure V-4**) shows that it is a central compound of a three-membered electron transfer series. The complex undergoes a one-electron reduction at -0.461V (ΔE= 136mV) (vs Ag/AgCl) to a $Fe^{II}Fe^{II}$ species, and a one-electron oxidation at +0.227 V (ΔE= 73mV) (vs Ag/AgCl) to a $Fe^{III}Fe^{III}$ species. Neither the $Fe^{II}Fe^{II}$ nor $Fe^{III}Fe^{III}$ species has been structurally characterized but it indicates that a $Fe^{II}Fe^{II}$ species is stable at least for the electrochemical time scale.

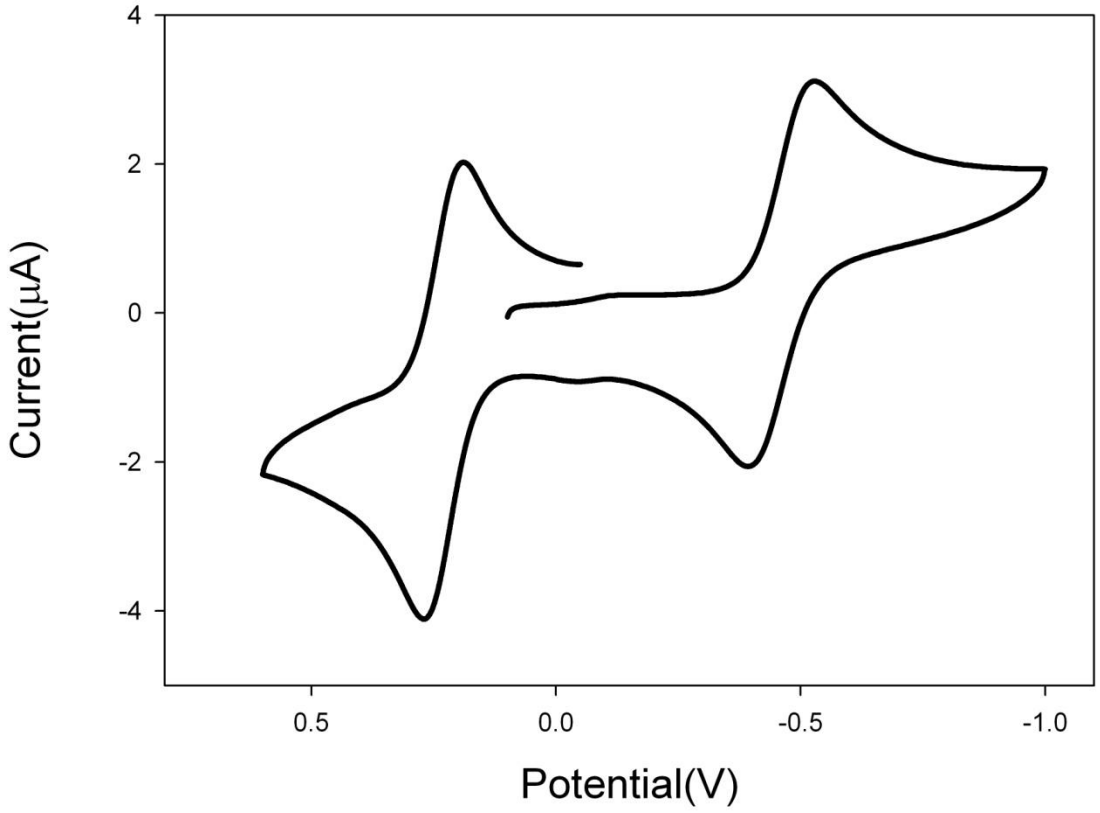

Figure V- 4. Cycle voltammetry of $[(Pentyl)_4N][Fe^{II}Fe^{III}(PS3)_2]$ in DMF (1.0mM), vs Ag/AgCl.

Considerable but unsuccessful attempts were made to isolate and structurally characterize the dimeric species $[Fe^{II}Fe^{II}(PS3)_2]^{2-}$ which was indicated by the electrochemical studies. An alternate structure for the initial product of the reaction of Fe(II) salts with $Li_3(PS3)$ would be a monomeric $[Fe^{II}(PS3)L]^{1-}$ complex where L is a molecule of solvent. Such complexes had been previously characterized for stronger binding ligands such as CO, PPh_3, pyridine, and N-methylimidazole. An $[Fe^{II}(PS3)L]^{1-}$ complex with an weakly binding L is highly desirable for an attempt to form complexes with weak ligands such as H_2 or N_2. Another synthetic goal was the isolation of an [Fe(PS3)] adduct with molecular oxygen. $[Fe^{II}(PS3)L]$ complexes with strongly bonded ligands such as cyanide, pyridine or N-methylimidazole had been previously observed to react with O_2 to just oxidize the metal to form the corresponding $[Fe^{III}(PS3)L]$ complex. Both a monomeric $[Fe(PS)_3(O_2)]^{1-}$ species or a dimer $[Fe(PS3)\text{-}OO\text{-}Fe(PS3)]^{2-}$ can be envisioned. The latter complex would be the analog to the previously characterized S_2 link dimer, $[Fe(PS3)\text{-}SS\text{-}Fe(PS3)]^{2-}$ complex.

$[Fe^{II}(PS3)(CO)_2]^{1-}$

In order to prevent or slow down the oxidation of solutions of Fe(II) complexes with $(PS3)^{3-}$ ligand, the reaction was performed in an aprotic solvent, acetonitrile or in MeOH at low temperature. Reactions were also attempted in propionitrile since it has a lower freezing point than CH_3CN. In none of these attempts was it possible to crystallize a $([Fe^{II}(PS3)]_n)^{n-}$ species. We used CO as a trapping or monitoring reagent to prove that we were able to generate $([Fe^{II}(PS3)]_n)^{n-}$ species and to monitor the stability of these

species in the Fe(II) oxidation state. The IR spectrum of the CO adduct, $[Fe^{II}(PS3)(CO)_2]^{1-}$ was used to monitor the reactions. $[Et_4N][Fe^{II}(PS3)(CO)_2]$ was isolated by bubbling CO into the synthetic reaction mixtures.

The crystal structure of $[Et_4N][Fe^{II}(PS3)(CO)_2]$ is shown in **Figure V-5**. By counting the cations, the overall charge of the anion part is -1, therefore the iron center was determined to be Fe(II). Since the complex was synthesized by bubbling CO to the synthetic mixture, the structure proved that the $[Fe^{II}Fe^{II}(PS3)_2]^{2-}$ complex or a Fe^{II} monomer actually existed before its oxidation to the $[Fe^{II}Fe^{III}(PS3)_2]^{1-}$ dimer.

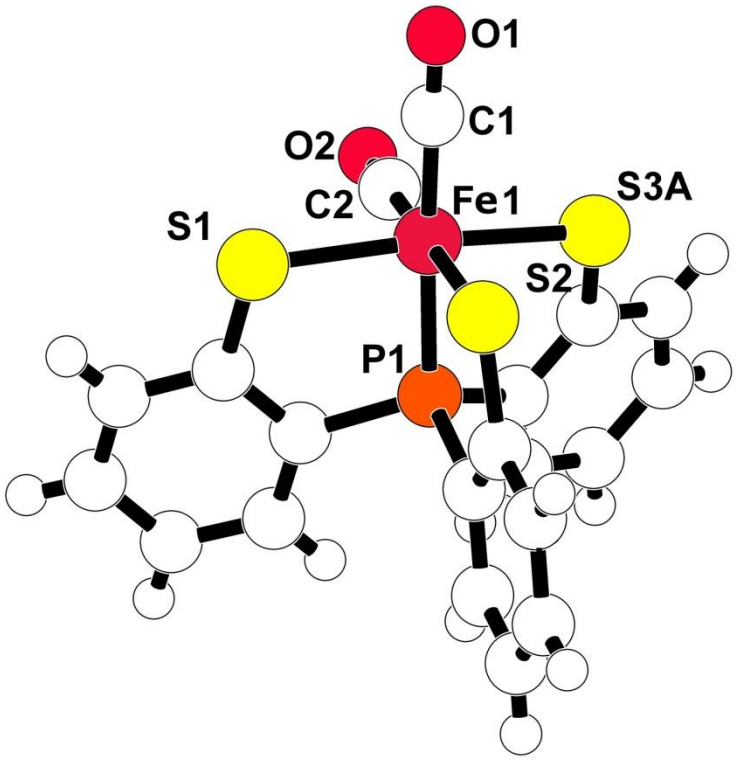

Figure V- 5. X-ray crystal structure of $[Et_4N][Fe^{II}(PS3)(CO)_2]$, Chem-Ray structure. The cations are omitted for clarity.

The crystal structure of $[Et_4N][Fe^{II}(PS3)(CO)_2]$ presents an octahedral geometry of the iron center. Carbon monoxide compounds usually have a low spin electronic state. Therefore a diamagnetic ground state d^6 is observed. The Fe-S2 bond distance is longer than the Fe-S1, which is probably resulted from the *trans*- effect of the carbon monoxide ligand (Fe1-S1= 2.2961(10) Å; Fe1-S2 = 2.3245(11) Å). Two Fe-CO bond distances are similar, with Fe-C1 (1.819(4) Å) slightly longer than the Fe-C2 (1.807(5)Å). This small difference in Fe-CO bond distance is probably resulted from *trans*- effect of phosphorus as well as a stronger π back bonding interaction with the CO which is *trans*- to the thiolate. This is consistent with the longer bond distance for C2-O2 (1.151(5) Å) than C1-O1(1.132(4)Å). There is some disorder in one of the thiolate ligands in the crystal structure as well, but the quality of the diffraction data allows us to model the disorder.

$[Fe^{II}Fe^{II}(OPS3)_2]^{2-}$

With exposure to the one equivalence of molecular oxygen at room temperature, $[(n\text{-}Pr)_4N]_2[Fe^{II}Fe^{II}(OPS3)_2]$ was isolated in high yield from an reaction mixture of $FeCl_2$ with $Li_3(PS3)$ in acetonitrile solution. $[(n\text{-}Pr)_4N]_2[Fe^{II}Fe^{II}(OPS3)_2]$ was previously characterized by Hua-Fen Hsu from the reaction of Fe(II) with the phosphine oxide thiolate ligand $(O{=}PS3)H_3$ ligand. But the observation of $[(n\text{-}Pr)_4N]_2[Fe^{II}Fe^{II}(OPS3)_2]$ prepared from $[Fe^{II}Fe^{II}(PS3)_2]^-$ solution confirms the existence of $[Fe^{II}Fe^{II}(PS3)_2]^-$ as well as indicates that phosphine is more readily oxidized than thiolate or the metal center at room temperature in acetonitrile solution.

The setup of bubbling quantitative amount molecular oxygen is shown in **Figure V-6** by practicing the following reaction:

$$2H_2O_2 \xrightarrow{FeCl_3} 2H_2O + O_2 \uparrow$$

Quantitative H_2O_2 gives off quantitative amount of molecular oxygen catalyzed by $FeCl_3$ quickly. The oxygen generated in the Schlenk tube is bubbled into the reaction mixture through cannula, and the pressure of the system is released by connecting the reaction Schlenk flask to an oil bubbler. By calculating the gas partial pressure, we are able to calculate the amount of H_2O_2 needed.

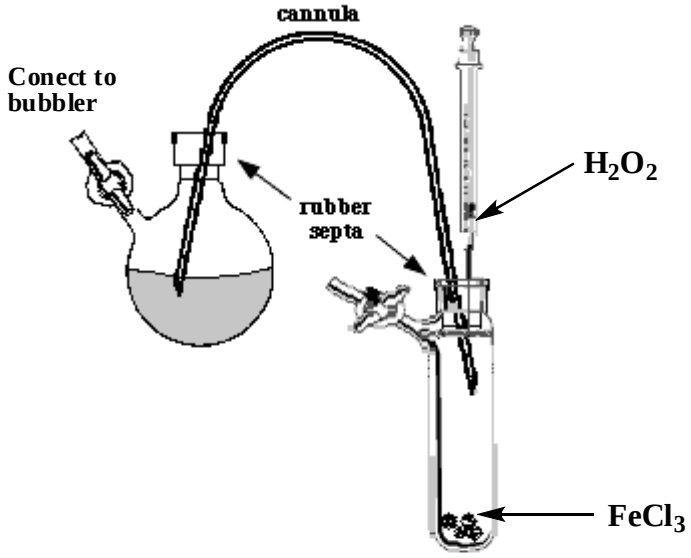

Figure V- 6. Setup for bubbling equivalent molecular O_2.

The crystal structure of $[(n\text{-Pr})_4N]_2[Fe^{II}Fe^{II}(OPS3)_2]$ is shown in **Figure V-7**. By counting the cations, the overall charge of the anions is -2, therefore both iron centers are determined to be Fe(II). The cycle voltammetry (**Figure V-8**) of the complex presents a reversible oxidation peak (+0.135V vs Ag/AgCl, ΔE= 60mV) and a quasi-reversible oxidation peak (+0.467V vs Ag/AgCl, ΔE= 76mV) in further positive region, which also supported the oxidation state assignment as Fe(II).

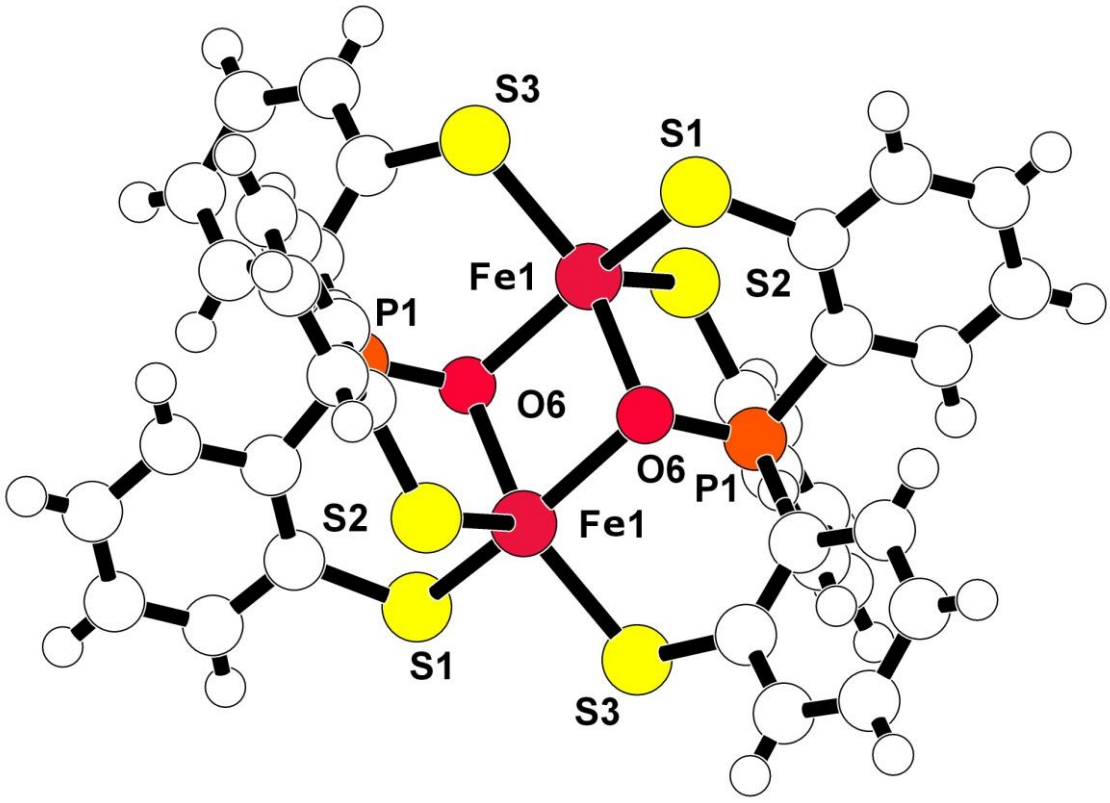

Figure V- 7. X-ray crystal structure of $[(n\text{-Pr})_4N]_2[Fe^{II}Fe^{II}(OPS3)_2]\bullet 1/2MeOH$, Chem-Ray structure. The cations and solvent molecules are omitted for clarity.

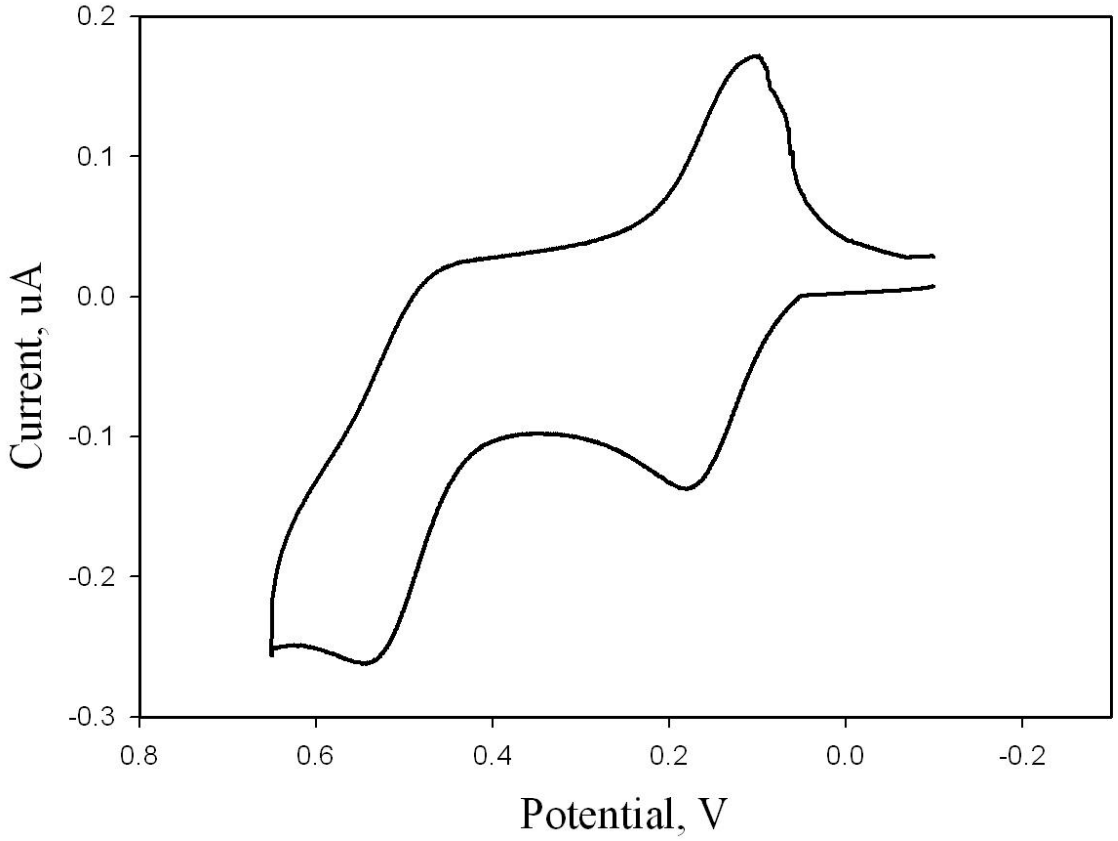

Figure V- 8. Cycle voltammetry of $[(n\text{-}Pr)_4N]_2[Fe^{II}Fe^{II}(OPS3)_2]$ in MeCN(1.0mM), vs Ag/AgCl.

The two iron centers in $[(n\text{-}Pr)_4N]_2[Fe^{II}Fe^{II}(OPS3)_2]$ are five coordinated and bridged by two oxygen atoms. The structure possesses a crystallographic center of inversion, which make the two iron centers indistinguishable. Therefore, it is rational to assign it to be $Fe^{II}Fe^{II}$ instead of $Fe^{I}Fe^{III}$.

The selected bond distances and angles are listed in **Table V-2**. The $(Fe\text{-}S)_{ave}$ bond distance is 2.425Å, which is much longer than the one in $[Et_4N][Fe^{II}(PS3)(CO)_2]$ (2.3103Å). This is consistent with the difference of the spin state of the compounds. The two iron centers are separated by 3.3455Å suggesting only limited interaction between

the metals. $[(n\text{-Pr})_4N]_2[Fe^{II}Fe^{II}(OPS3)_2]$ is one of few examples that oxo from phosphine oxide bridges two metals.

Bond length(Å)		**Angle(°)**	
Fe1-O6	2.1306(16)	P(1)-O(6)-Fe(1)	115.26(9)
Fe1*-O6	2.1699(17)	P(1)-O(6)-Fe(1)#1	123.13(9)
Fe1-S1	2.4022(8)	Fe(1)-O(6)-Fe(1)#1	105.57(7)
Fe1-S2	2.3782(7)	O(6)#1-Fe(1)-S(3)	91.87(4)
Fe1-S3	2.3450(7)	S(3)-Fe(1)-S(1)	91.28(3)

Table V- 2. Selected bond distances and bond angles for $[(n\text{-Pr})_4N]_2[Fe^{II}Fe^{II}(OPS3)_2]$

$[Fe^{II}Fe^{III}(PS3)(PS3O_2)]^{1-}$

The exposure of a half equivalence of molecular oxygen at -78℃ to a MeOH solution prepared by the reaction of Li_3PS3 with $FeCl_2$, resulted in the isolation of a bimetallic complex in which one of the RS- ligand was oxidized to a RSO_2- ligand. The crystal structure of $[(Pentyl)_4N][Fe^{II}Fe^{III}(PS3)(PS3O_2)]$ is shown in **Figure V-9**. Different from $[(n\text{-Pr})_4N]_2[Fe^{II}Fe^{II}(OPS3)_2]$, the resulting product at low temperature has the two oxygen atom added to a thiolate. The RSO_2- group provides one of the bridges with the S bound to one Fe and one of its oxygens bound to the second Fe; two thiolates complete the bridging unit. By counting the cations, the overall charge of the anion is -1; therefore, the iron centers are determined to be $Fe^{II}Fe^{III}$. The cyclic voltammetry (**Figure V-10**) of the complex shows that it is a central compound of a three-membered electron

transfer series, which present a quasi-reversible reduction peak (+0.518V vsAg/AgCl, ΔE= 82mV) and an irreversible oxidation peak (+0.692V vsAg/AgCl, ΔE= 122mV) in further positive region; the reduction peak is assigned to be the Fe^{II} Fe^{III}/ Fe^{II} Fe^{II} couple, while the oxidation peak belongs to $Fe^{III}Fe^{III}$/$Fe^{II}Fe^{III}$ couple. The rest potential falls between the reduction and oxidation peaks, which also supported the oxidation state assignment as $Fe^{II}Fe^{III}$.

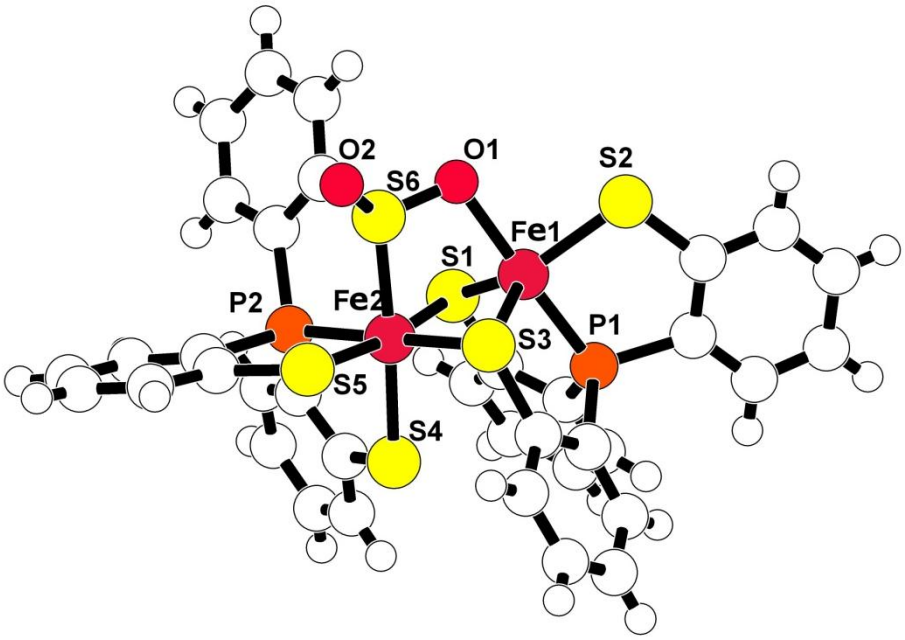

Figure V- 9. X-ray crystal structure of $[(Pentyl)_4N][Fe^{II}Fe^{III}(PS3)(PS3O_2)]$, Chem-Ray structure.

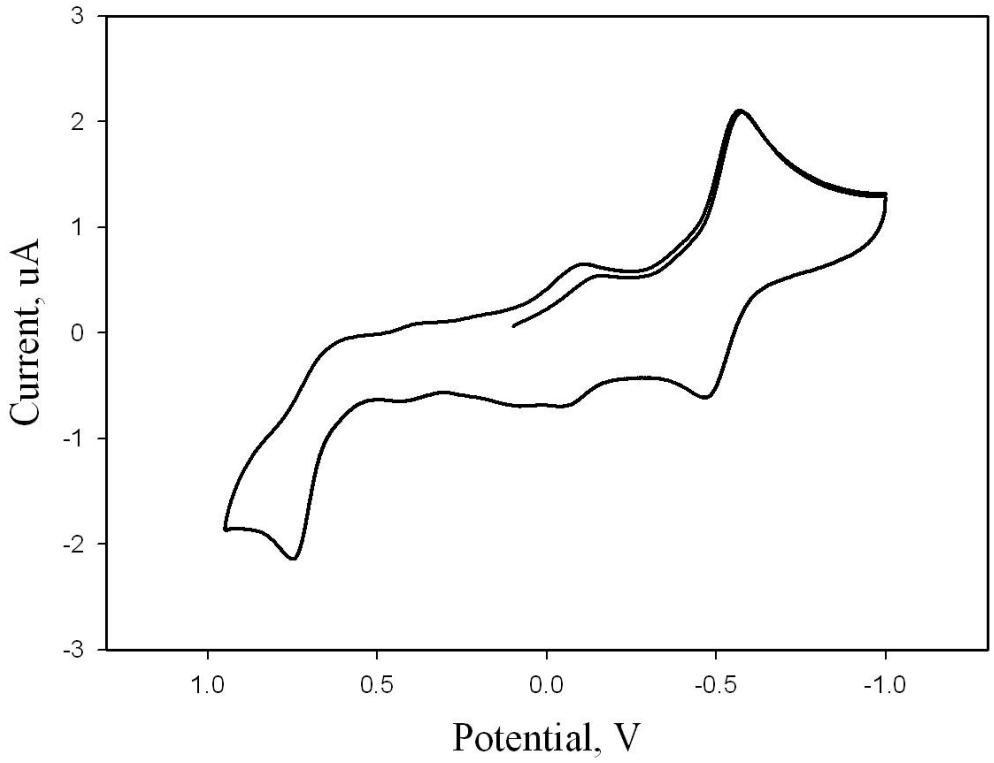

Figure V- 10. Cycle voltammetry of $[(Pentyl)_4N][Fe^{II}Fe^{III}(PS3)(PS3O_2)]$ in DMF(1.0mM), vs Ag/AgCl.

The Fe1 atom has a distorted trigonal bipyramidal geometry, with the two bridging thiolates and the terminal thiolate forming the trigonal plane and the phosphorus and oxygen atoms as the axial ligands. The Fe2 has an octahedral geometry, which share an edge with the Fe1 trigonal bipyramid.

Bond length(*Å*)	**Fe1**		**Fe2**	
$Fe\text{-}S_{bridging}$	Fe1-S1	2.188(2)	Fe2-S1	2.382(2)
	Fe1-S3	2.216(2)	Fe2-S3	2.301(2)
	Fe1-S6	2.796(5)	Fe2-S6	2.166(2)
$Fe\text{-}S_{terminal}$	Fe1-S2	2.193(3)	Fe2-S4	2.303(2)
			Fe2-S5	2.316(2)
Fe-P	Fe1-P1	2.119(3)	Fe2-P2	2.142(2)
	Fe-O1	2.039(6)	S6-O1	1.507(6)
			S6-O2	1.456(6)
	Fe1-Fe2	2.5941(15)		
Angle(°)				
	Fe1-S1-Fe2	69.02(7)	Fe1-S6-Fe2	61.45(6)
	Fe1-S3-Fe2	70.07(7)		
	P1-Fe1-S2	88.57(10)	P2-Fe2-S6	88.02(8)

Table V- 3. Selected bond distances and bond angles for of $[(Pentyl)_4N][Fe^{II}Fe^{III}(PS3)(PS3O_2)]$.

The selected bond distances and bond angles for $[(Pentyl)_4N][Fe^{II}Fe^{III}(PS3)(PS3O_2)]$ are shown in **Table V-3**. The average Fe-S bond distance for Fe1(2.199Å) is much shorter than that of Fe2(2.3255Å), as well as Fe-P bond distance. The Fe1-S distances are similar to those in the low spin monomeric complexes like $[Fe^{III}(PS3)(CN)]^{1-}$. The Fe2-S distances are similar to those in the low spin octahedral complex, $[Fe^{II}(PS3)(CO)_2]^{1-}$, which was described earlier in this chapter.

Therefore Fe2 and Fe1 are assigned as Fe^{2+} and Fe^{3+} respectively. The Fe1-Fe2 bond distance is almost identical (2.5941(15)Å) to the one in $[(Pentyl)_4N][Fe^{II}Fe^{III}(PS3)_2]$, indicates a substantial metal-metal interaction. There are several previous examples where a RSO_2- ligand bridges two metal centers with the S coordinated to one metal and an O bonding to the second metal.

The synthesis of $[(n\text{-}Pr)_4N]_2[Fe^{II}Fe^{II}(OPS3)_2]$ and $[(Pentyl)_4N][Fe^{II}Fe^{III}(PS3)(PS3O_2)]$ demonstrate that the reactivity of $[Fe^{II}Fe^{II}(PS3)_2]^{2-}$ with O_2 is dramatically dependent on the reaction conditions. With one equivalent of molecular oxygen at room temperature in acetonitrile, the phosphine is oxidized into phosphine oxide with the metal sites untouched; with a half equivalent of molecular oxygen at -78 ℃ in MeOH two oxygen atoms are added to a thiolate with the metal center being oxidized to a mixed valent $Fe^{II}Fe^{III}$ complex. The difference in the reactivity pattern may indicate that the different $[Fe^{II}(PS3)]_n^{n-}$ species are present under the different conditions of solvent and temperature.

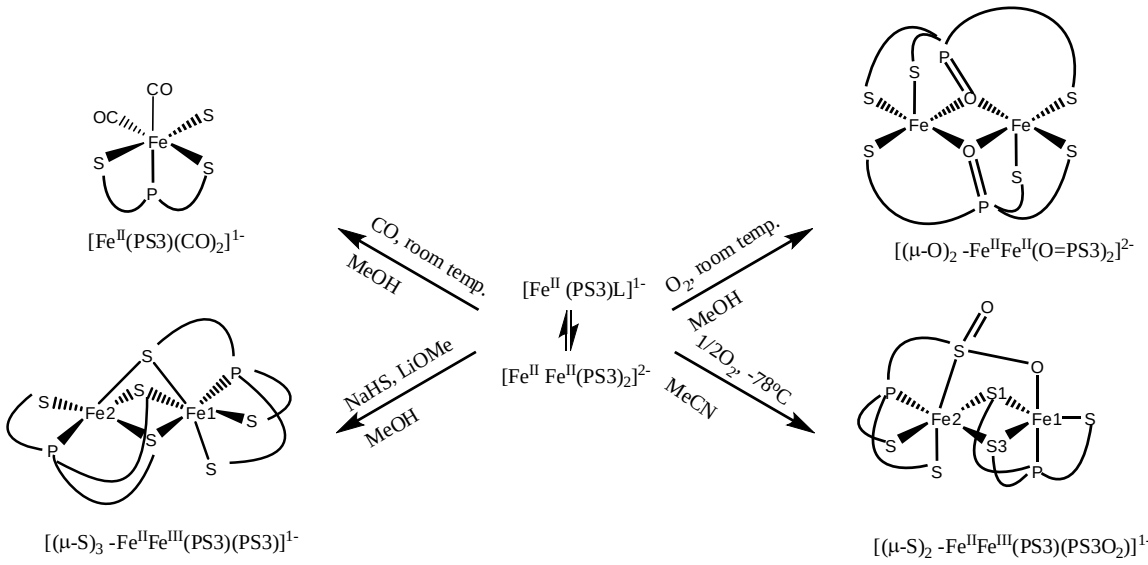

Scheme V- 3. Reactivity of $[Fe^{II}\ Fe^{II}(PS3)_2]^{2-}$ under different conditions.

The reactivity pattern of $[Fe^{II}(PS3)]_n$ species is summarized in **Scheme V-3**. It is possible the solution may be a mixture of a dimer, $[Fe^{II}Fe^{II}(PS3)_2]^{2-}$, and a dissociated monomer, $[Fe^{II}(PS3)L]^{-}$. Under CO atmosphere, the monomer was stabilized and isolated as $[Fe^{II}(PS3)(CO)_2]^{1-}$. Franolic[17] reported a unreproducible $(\mu\text{-}S)_3$-$[Fe^{II}Fe^{III}(PS3)2]^{1-}$ complex with NaHS and LiOMe in MeOH. It is clear that reactive O_2 adducts must be responsible for the phosphine and thiolate oxidations. In other Fe ligand systems it has been possible to characterize FeO_2 adducts and reactive Fe=O intermediates.[19]

3. CONCLUSIONS

$[(Pentyl)_4N][Fe^{II}Fe^{III}(PS3)_2]$ was synthesized and characterized by reacting $FeCl_2$ with lithium thiolate $P(o\text{-}C_6H_4SLi)_3$ in an alcoholic solvent. The oxidation state of the iron centers are assigned from both the crystallography data and cycle voltammetry.

It is predicted that $[Fe^{II}Fe^{II}(PS3)_2]^{2-}$ and/or $[Fe^{II}(PS3)(solvent)]^{1-}$ species exist as an intermediate, which is trapped by bubbling carbon monoxide into the system and yielding $[Et_4N][Fe^{II}(PS3)(CO)_2]$ as product.

The reactivity study of this $[Fe^{II}Fe^{II}(PS3)_2]^{2-}/[Fe^{II}(PS3)]^{1-}$ intermediate is conducted under different conditions. With 1 equivalent of molecular oxygen at room temperature in CH_3CN, the phosphine is oxidized into phosphine oxide with the metal sites not oxidized; with an half equivalent of molecular oxygen at -78 ℃, O_2 is added to thiolate with the metal center being oxidized to $Fe^{II}Fe^{III}$.

4. EXPERIMENTAL

Syntheses:

$[(Pentyl)_4N][Fe^{II}Fe^{III}(P(o\text{-}C_6H_4S)_3)_2]$, ($[(Pentyl)_4N][Fe^{II}Fe^{III}(PS3)_2]$):

The lithium thiolate $P(o\text{-}C_6H_4SLi)_3$ was generated in 20mL of methanol by the addition of lithium wire (0.0108g, 1.54mmole) to $P(o\text{-}C_6H_4SH)_3$ (0.1774g, 0.496mmole). $FeCl_2 \bullet 4H_2O$ (0.0985g, 0.495mmol) in 15mL methanol was added via cannula and produced a brown-green solution. The solution was stirred for 1 hour and filtered through Celite, after which addition of $(Pentyl)_4NBr$ (0.2015g, 0.533mmole) in 10 mL of methanol produced 0.3860g (yield 69.7%) of black solid. Alternatively, layering of the cation solution over the reaction mixture produced black, plate-like crystals suitable for X-ray crystallography.

CV: (1mM in DMF with 0.1M $[Bu4N][BF_4]$), vs Ag/AgCl: -0.461V (ΔE= 136mV), $Fe^{II}Fe^{III}$ /$Fe^{II}Fe^{II}$; and +0.227 V (ΔE= 73mV), $Fe^{III}Fe^{III}$/$Fe^{II}Fe^{III}$.

UV-Vis (10mM in DMF), λ_{max} (ε_m): 346(7442), 520(2456), 653(1384) nm ($M^{-1}cm^{-1}$).

Unit cell: (from MeOH) Monoclinic; $P2_1/n$; a = 16.338(4) Å ; b = 18.464(10) Å ; c = 18.828(3) Å ;α= 90°; β= 90.487(17)°; γ = 90°; 5679(4) $Å^3$.

$[Et_4N][Fe^{II}(PS3)(CO)_2]$ or $[Et_4N][Fe^{II}(P(o\text{-}C_6H_4S)_3)(CO)_2]$:

The lithium thiolate was generated by the addition of lithium wire (0.0106g, 1.51mmol) to PS3 (0.1789g, 0.500mmol) in 20mL of methanol. Once the lithium wire was consumed, a 10mL methanol solution of $FeCl_2 \cdot 4H_2O$ (0.0995g, 0.500mmol) was added and reaction mixture turned yellowish green immediately. Bubbling carbon monoxide through the solution caused a rapid change in color form green to red. The solution was stirred under a stream of carbon monoxide for 90mins and then filtered through Celite. Addition of Et_4NBr (0.1536g, 0.731mmole) in 10mL of methanol to the filtrate produced 0.2238g (yield 74.9%) of dark red solid. Alternatively, layering of the cation solution over the reaction mixture produced dark red needle crystals suitable for X-ray crystallography.

IR (in MeOH): ν_{CO} at 1946 and 2000 cm^{-1}

UV-Vis (10mM in DMF), λ_{max} (ε_m): 318(1410) nm ($M^{-1}cm^{-1}$).

Unit cell: (from MeOH) Monoclinic; Cc; a = 9.8191(3) Å ; b = 19.9044(11) Å ; c = 14.3261(4) Å ;α= 90°; β= 101.537(3) °; γ = 90 °; 2743.39(19) $Å^3$.

$[(n\text{-}Pr)_4N]_2[Fe^{II}Fe^{II}(O{=}PS3)_2]$ or $[(n\text{-}Pr)_4N]_2[Fe^{II}Fe^{II}(O{=}P(o\text{-}C_6H_4S)_3)_2]$:

The lithium thiolate was generated by the addition of lithium wire (0.0206g, 2.94mmol) to H_3PS3 (0.3407g, 0.952mmol) in 20mL of methanol. Once the lithium wire was consumed, the reaction mixture was dried under vacuum. On addition of a 25mL

acetonitrile solution of $FeCl_2 \cdot 4H_2O$ (0.1894g, 0.951mmol) into the dried lithium thiolate, the solution turns brown/green immediately. It is stirred for 10 minutes before bubbling a quantitative amount molecular oxygen (20.6ml, 0.952mmol generated from H_2O_2 and $FeCl_3$) into the system. The volume of the reaction mixture is reduced to around 15mL by vacuum and filtered under N_2, after which the addition of 15mL methanol solution of $[(n\text{-}Pr)_4N]Br$ (0.2812g, 1.03mmol) produced 0.3120g (yield 53.5%) of red solid. Alternatively, layering of the cation solution over the reaction mixture produced dark red crystals suitable for X-ray crystallography.

CV (1mM in MeCN with 0.1M [Bu4N][BF_4]), vs Ag/AgCl: +0.135V (ΔE= 60mV), $Fe^{II}Fe^{III}$ /$Fe^{II}Fe^{II}$; and +0.467 V (ΔE= 76mV), $Fe^{III}Fe^{III}$/$Fe^{II}Fe^{III}$.

UV-Vis (10mM in DMF), λ_{max} (ε_m): 491(6861) and 641(5127) nm ($M^{-1}cm^{-1}$).

Unit cell: (from MeOH/MeCN) Tetragonal; $P4_2/n$; a = 22.7909(3)Å ; b = 22.7909(3) Å ; c = 11.6984(3) Å ;α = 90°; β= 90 °; γ = 90°; 6076.44(19) $Å^3$.

$[(Pentyl)_4N][Fe^{II}Fe^{III}(PS3)(PS3O_2)]$ or $[(Pentyl)_4N][Fe^{II}Fe^{III}(P(o\text{-}C_6H_4S)_3)(P(o\text{-}C_6H_4S)_2(o\text{-}C_6H_4SO_2)]$:

The lithium thiolate was generated by the addition of lithium wire (0.0165g, 2.36mmol) to PS3 (0.2379g, 0.664mmol) in 15mL of methanol. Once the lithium wire was consumed, the reaction mixture was cooled to -78 ℃. On addition of a pre-cooled (-78 ℃) 20mL methanol solution of anhydrous $FeCl_2$ (0.0840g, 0.661mmol), the solution

turns light green immediately. At -78 ℃, it is stirred for 10 minutes before bubbling quantitative amount molecular oxygen (7.4ml, 0.331mmol generated from H_2O_2 and $FeCl_3$) into the system. The reaction mixture turned brown immediately. Addition of 15mL methanol solution of $[(Pentyl)_4N]Br$ (0.2670g, 0.706mmol) at -20 ℃ produced 0.190 g (yield 50.0%) of red solid. Alternatively, layering of the cation solution over the reaction mixture at -20 ℃ for 2days produced dark red crystals suitable for X-ray crystallography.

CV (1mM in DMF with 0.1M $[Bu_4N][BF_4]$), vs Ag/AgCl: -0.518V (ΔE= 82mV), $Fe^{II}Fe^{III}$ /$Fe^{II}Fe^{II}$; and +0.692 V (ΔE=122 mV), $Fe^{III}Fe^{III}$/$Fe^{II}Fe^{III}$.

Unit cell: (from MeOH/MeCN) Monoclinic; $P2_1/n$; a = 16.4855(5) Å ; b = 18.8099(5)Å ; c = 18.5607(6) Å ;α= 90°; β= 92.191(3) °; γ = 90°; 5751.3(3) $Å^3$.

X-ray Crystallography

$[(Pentyl)_4N][Fe^{II}Fe^{III}(PS3)_2]$:

A black crystal measuring 0.40 x 0.25 x 0.1 mm^3 was mounted on the nylon loop and centered on the X-ray beam under 100K. The accurate unit cell was obtained using reflection with 2θ= 2.94- 32.91 °. a = 16.338(4) Å ; b = 18.464(10) Å ; c = 18.828(3) Å ;α = 90°; β = 90.487(17)°; γ = 90°; V = 5679(4) $Å^3$. The structure was solved under the primitive monoclinic crystal system (space group $P2_1/n$) using 11862 reflections. The

asymmetric unit consist one molecule of the $Fe^{II}Fe^{III}$ dimer complex and one $(Pentyl)_4N^+$ cation. The data reduction was done with CrysAlis Pro and the structure refinement was done with SHELXL-97 (Sheldrick). All the non-hydrogen atoms were located by Direct Methods and were refined anisotropically by a full-matrix least-squares method. The positions of the hydrogen atoms were calculated.

The crystallographic parameters and atomic coordinates for this complex are located in **Table A-15**.

$[Et_4N][Fe^{II}(PS3)(CO)_2]$:

A black crystal measuring 0.60 x 0.1 x 0.03 mm^3 was mounted on the nylon loop and centered on the X-ray beam under 100K. The accurate unit cell was obtained using reflection with 2θ= 2.98- 31.99°. a = 9.8191(3) Å ; b = 19.9044(11) Å ; c = 14.3261(4) Å ;α = 90°; β = 101.537(3) °; γ = 90°; V = 2743.39(19) $Å^3$. The structure was solved under the C centered monoclinic crystal system (space group Cc) using 5884 reflections. The asymmetric unit consist one molecule of the Fe^{II}-CO monomer complex and one Et_4N^+ cation. The data reduction was done with CrysAlis Pro and the structure refinement was done with SHELXL-97 (Sheldrick). All the non-hydrogen atoms were located by Direct Methods and were refined anisotropically by a full-matrix least-squares method. The positions of the hydrogen atoms were calculated. S3 atom is disordered and was modeled as S3A and S3B.

The crystallographic parameters and atomic coordinates for this complex are located in **Table A-16**.

$[(n\text{-}Pr)_4N]_2[Fe^{II}Fe^{II}(O{=}PS3)_2]\bullet 1/2MeOH]$:

A red crystal measuring 0.10 x 0.1 x 0.2 mm^3 was mounted on the nylon loop and centered on the X-ray beam under 100K. The accurate unit cell was obtained using reflection with 2θ= 2.83- 29.61 º. a = 22.7909(3)Å ; b = 22.7909(3) Å ; c = 11.6984(3) Å ;α= 90°; β = 90 º; γ = 90°; V = 6076.44(19) $Å^3$ The structure was solved under the primitive tetragonal crystal system (space group $P4_2/n$) using 8223 reflections. The asymmetric unit consist half molecule of the $(\mu\text{-}O)_2Fe^{II}Fe^{II}$-PS2 dimer complex with inversion center, one $(Pentyl)_4N^+$ cation and one quarter molecule of methanol solvent molecules. The data reduction was done with CrysAlis Pro and the structure refinement was done with SHELXL-97 (Sheldrick). All the non-hydrogen atoms were located by Direct Methods and were refined anisotropically by a full-matrix least-squares method. The positions of the hydrogen atoms were calculated.

The crystallographic parameters and atomic coordinates for this complex are located in Table **A-17**.

$[(Pentyl)_4N][Fe^{II}Fe^{III}(PS3)(PS3O_2)]$:

A red crystal measuring 0.40 x 0.40 x 0.1 mm^3 mounted on the nylon loop and centered on the X-ray beam at 100K. The accurate unit cell was obtained using reflection with 2θ = 2.88- 32.98°: a = 16.4855(5) Å ; b = 18.8099(5)Å ; c = 18.5607(6) Å ;α = 90 °; β = 92.191(3) °; γ = 90°; V = 5751.3(3) $Å^3$. The structure was solved under the primitive monoclinic crystal system (space group $P2_1/n$) using 17525 reflections. The asymmetric unit consist one molecule of the $(\mu\text{-}S)_2Fe^{II}Fe^{II}\text{-}PSO_2$ dimer complex and one $(Pentyl)_4N^+$ cation. The data reduction was done with CrysAlis Pro and the structure refinement was done with SHELXL-97 (Sheldrick). All the non-hydrogen atoms were located by Direct Methods and were refined anisotropically by a full-matrix least-squares method. The positions of the hydrogen atoms were calculated.

The crystallographic parameters and atomic coordinates for this complex are located in **Table A-18**.

REFERENCE:

(1) Py, B.; Barras, F. *Nat. Rev. Microbiol.* **2010**, *8*, 436.

(2) Beinert, H. *J. Biol. Inorg. Chem.* **2000**, *5*, 2.

(3) Fontecave, M. *Nat. Chem. Biol.* **2006**, *2*, 171.

(4) Kiley, P. J.; Beinert, H. *Curr. Opin. Microbiol.* **2003**, *6*, 181.

(5) Kim, J. S.; Rees, D. C. *Nature* **1992**, *360*, 553.

(6) Woodward, J. *Philosophical Transactions* **1724**, *33*, 15.

(7) Marks, T. J. *Science* **1985**, *227*, 881.

(8) Walzer, K.; Maennig, B.; Pfeiffer, M.; Leo, K. *Chem. Rev.* **2007**, *107*, 1233.

(9) Berg, J. B.; Holm, R. H. *Metal Ions in Biology*; Wiley: New York, 1982; Vol. 4.

(10) Takeda, N.; Tokitoh, N.; Okazaki, R. In *Elemental Sulfur and Sulfur-Rich Compounds Ii*; Springer-Verlag Berlin: Berlin, 2003; Vol. 231, p 153.

(11) Naqui, A.; Chance, B.; Cadenas, E. *Annu. Rev. Biochem.* **1986**, *55*, 137.

(12) Imlay, J. A. *Molecular Microbiology* **2006**, *59*, 1073.

(13) Flint, D. H.; Smykrandall, E.; Tuminello, J. F.; Draczynskalusiak, B.; Brown, O. R. *J. Biol. Chem.* **1993**, *268*, 25547.

(14) Flint, D. H.; Allen, R. M. *Chem. Rev.* **1996**, *96*, 2315.

(15) Keyer, K.; Gort, A. S.; Imlay, J. A. *J. Bacteriol.* **1995**, *177*, 6782.

(16) Kim, J.; Hetzel, M.; Boiangiu, C. D.; Buckel, W. *Fems Microbiol. Rev.* **2004**, *28*, 455.

(17) Franolic, J. D., SUNY Stony Brook, 1993.

(18) Ai, K. S., SUNY Stony Brook, 1996.

(19) Frisch, J. R.; Vu, V. V.; Martinho, M.; Munck, E.; Que, L. *Inorg. Chem.* **2009**, *48*, 8325.

REFERENCES

(1) Adams, M. W. W. *Biochim. Biophys. Acta* **1990**, *1020*, 115.

(2) Adams, M. W. W.; Stiefel, E. I. *Science* **1998**, *282*, 1842.

(3) Ai, K. S., SUNY Stony Brook, 1996.

(4) Akitt, J. W. *NMR and Chemistry: An introduction to modern NMR spectroscopy* Third ed., 1992.

(5) Albracht, S. P. J.; Roseboom, W.; Hatchikian, E. C. *J. Biol. Inorg. Chem.* **2006**, *11*, 88.

(6) Anbalagan, V. *J. Coord. Chem.* **2003**, *56*, 161.

(7) Appleton, T. G.; Clark, H. C.; Manzer, L. E. *Coord. Chem. Rev.* **1973**, *10*, 335.

(8) Arendsen, A. F.; Lindley, P. F. In *Advances in Inorganic Chemistry, Vol 47*; Academic Press Inc: San Diego, 1999; Vol. 47, p 219.

(9) Arnold, D. P.; Bennett, M. A. *Inorg. Chem.* **1984**, *23*, 2117.

(10) Artero, V.; Fontecave, M. *Coord. Chem. Rev.* **2005**, *249*, 1518.

(11) Ballmann, J.; Dechert, S.; Bill, E.; Ryde, U.; Meyer, F. *Inorg. Chem.* **2008**, *47*, 1586.

(12) Barton, B. E.; Olsen, M. T.; Rauchfuss, T. B. *J. Am. Chem. Soc* **2008**, *130*, 16834.

(13) Barton, B. E.; Rauchfuss, T. B. *Inorg. Chem.* **2008**, *47*, 2261.

(14) Barton, B. E.; Zampella, G.; Justice, A. K.; De Gioia, L.; Rauchfuss, T. B.; Wilson, S. R. *Dalton Trans.* **2010**, *39*, 3011.

(15) Beinert, H. *J. Biol. Inorg. Chem.* **2000**, *5*, 2.

(16) Berg, J. B.; Holm, R. H. *Metal Ions in Biology*; Wiley: New York, 1982; Vol. 4.

(17) Blau, R. J.; Espenson, J. H. *Inorg. Chem.* **1986**, *25*, 878.

(18) Block, E.; Oforiokai, G.; Zubieta, J. *J. Am. Chem. Soc* **1989**, *111*, 2327.

(19) Bondin, M. I.; Borg, S. J.; Cheah, M. H.; Foran, G.; Best, S. P. *Aust. J. Chem.* **2006**, *59*, 263.

(20) Borg, S. J.; Ibrahim, S. K.; Pickett, C. J.; Best, S. P. *C. R. Chim.* **2008**, *11*, 852.

(21) Boyke, C. A.; Rauchfuss, T. B.; Wilson, S. R.; Rohmer, M. M.; Benard, M. *J. Am. Chem. Soc* **2004**, *126*, 15151.

(22) Brecht, M.; van Gastel, M.; Buhrke, T.; Friedrich, B.; Lubitz, W. *J. Am. Chem. Soc* **2003**, *125*, 13075.

(23) Briant, C. E.; Hughes, G. R.; Minshall, P. C.; Mingos, D. M. P. *J. Organomet. Chem.* **1980**, *202*, C18.

(24) Bruschi, M.; Fantucci, P.; De Gioia, L. *Inorg. Chem.* **2003**, *42*, 4773.

(25) Bruschi, M.; Greco, C.; Kaukonen, M.; Fantucci, P.; Ryde, U.; De Gioia, L. *Angew. Chem. Int. Edit.* **2009**, *48*, 3503.

(26) Buonomo, R. M.; Font, I.; Maguire, M. J.; Reibenspies, J. H.; Tuntulani, T.; Darensbourg, M. Y. *J. Am. Chem. Soc* **1995**, *117*, 963.

(27) Caldentey, X.; Pericas, M. A. *J. Org. Chem.* **2010**, *75*, 2628.

(28) Cammack, R. *Nature* **1999**, *397*, 214.

(29) Cammack, R.; Frey, M.; Robson, R. *Hydrogen as a fuel: Learning from Nature*; Tayor & Francis, 2001.

(30) Canaguier, S.; Artero, V.; Fontecave, M. *Dalton Trans.* **2008**, 315.

(31) Cao, Z. X.; Hall, M. B. *J. Am. Chem. Soc* **2001**, *123*, 3734.

(32) Capon, J. F.; Ezzaher, S.; Gloaguen, F.; Petillon, F. Y.; Schollhammer, P.; Talarmin, J. *Chem. Eur. J.* **2008**, *14*, 1954.

(33) Capon, J. F.; Ezzaher, S.; Gloaguen, F.; Petillon, F. Y.; Schollhammer, P.; Talarmin, J.; Davin, T. J.; McGrady, J. E.; Muir, K. W. *New J. Chem.* **2007**, *31*, 2052.

(34) Capon, J. F.; Gloaguen, F.; Petillon, F. Y.; Schollhammer, P.; Talarmin, J. *Eur. J. Inorg. Chem.* **2008**, 4671.

(35) Capon, J. F.; Gloaguen, F.; Petillon, F. Y.; Schollhammer, P.; Talarmin, J. *C. R. Chim.* **2008**, *11*, 842.

(36) Capon, J. F.; Gloaguen, F.; Petillon, F. Y.; Schollhammer, P.; Talarmin, J. *Coord. Chem. Rev.* **2009**, *253*, 1476.

(37) Capon, J. F.; Gloaguen, F.; Schollhammer, P.; Talarmin, J. *Coord. Chem. Rev.* **2005**, *249*, 1664.

(38) Carepo, M.; Tierney, D. L.; Brondino, C. D.; Yang, T. C.; Pamplona, A.; Telser, J.; Moura, I.; Moura, J. J. G.; Hoffman, B. M. *J. Am. Chem. Soc* **2002**, *124*, 281.

(39) Chakrabarti, M.; Deng, L.; Holm, R. H.; Munck, E.; Bominaar, E. L. *Inorg. Chem.* **2009**, *48*, 2735.

(40) Chan, K. H.-Y.; Chow, H.-S.; Wong, K. M.-C.; Yeung, M. C.-L.; Yam, V. W.-W. *Chemical Science* **2010**, *1*, 477.

(41) Chatt, J.; Mason, R.; Meek, D. W. *J. Am. Chem. Soc* **1975**, *97*, 3826.

(42) Chen, C. H.; Chang, Y. S.; Yang, C. Y.; Chen, T. N.; Lee, C. M.; Liaw, W. F. *Dalton Trans.* **2004**, 137.

(43) Chesters, M. A.; Packer, K. J.; Viner, H. E.; Wright, M. A. P. *J. Phys. Chem. B* **1997**, *101*, 9995.

(44) Chesters, M. A.; Packer, K. J.; Viner, H. E.; Wright, M. A. P.; Lennon, D. *J. Chem. Soc.-Faraday Trans.* **1996**, *92*, 4709.

(45) Chiarella, G. M. *Ph. D Dissertation*; State University of New York at Stony Brook, 2006.

(46) Chiarella, G. M.; Melgarejo, D. Y.; Koch, S. A. *J. Am. Chem. Soc* **2006**, *128*, 1416.

(47) Chikamoto, Y.; Hirotsu, M.; Kawamoto, T.; Konno, T. *Chem. Lett.* **2005**, *34*, 362.

(48) Chikamoto, Y.; Yoshinari, N.; Kawamoto, T.; Konno, T. *J. Organomet. Chem.* **2007**, *692*, 156.

(49) Chiou, T. W.; Liaw, W. F. *C. R. Chim.* **2008**, *11*, 818.

(50) Chong, D. S.; Georgakaki, I. P.; Mejia-Rodriguez, R.; Samabria-Chinchilla, J.; Soriaga, M. P.; Darensbourg, M. Y. *Dalton Trans.* **2003**, 4158.

(51) Chung, T. C. M.; Jeong, Y.; Kleinhammes, A.; Wu, Y. *ECS Transactions* **2009**, *19*, 57.

(52) Clemenson, P. I. *Coord. Chem. Rev.* **1990**, *106*, 171.

(53) Cohen, J. L.; Hoggard, P. E. *Inorg. React. Mech.* **2008**, *6*, 293.

(54) Contakes, S. M.; Hsu, S. C. N.; Rauchfuss, T. B.; Wilson, S. R. *Inorg. Chem.* **2002**, *41*, 4610.

(55) Cotton, F. A.; Eglin, J. L.; Hong, B.; James, C. A. *J. Am. Chem. Soc* **1992**, *114*, 4915.

(56) Crabtree, R. H. *The organometallic chemistry of the transition metals*; Wiley-Interscience, 2005.

(57) Darchen, A.; Mousser, H.; Patin, H. *J. Chem. Soc.-Chem. Commun.* **1988**, 968.

(58) Davies, S. C.; Evans, D. J.; Hughes, D. L.; Longhurst, S.; Sanders, J. R. *Chem. Commun.* **1999**, 1935.

(59) De Gioia, L.; Fantucci, P.; Guigliarelli, B.; Bertrand, P. *Int. J. Quantum Chem.* **1999**, *73*, 187.

(60) De Lacey, A. L.; Fernandez, V. M.; Rousset, M.; Cammack, R. *Chem. Rev.* **2007**, *107*, 4304.

(61) De Lacey, A. L.; Moiroux, J.; Bourdillon, C. *Eur. J. Biochem.* **2000**, *267*, 6560.

(62) De Lacey, A. L.; Stadler, C.; Cavazza, C.; Hatchikian, E. C.; Fernandez, V. M. *J. Am. Chem. Soc* **2000**, *122*, 11232.

(63) Dillon, K. B.; Goeta, A. E.; Monks, P. K.; Shepherd, H. J. *Polyhedron* **2010**, *29*, 606.

(64) Dilworth, J. R.; Wheatley, N. *Coord. Chem. Rev.* **2000**, *199*, 89.

(65) Domanska-Babul, W.; Chojnacki, J.; Matern, E.; Pikies, J. *Dalton Trans.* **2009**, 146.

(66) Dooley, D. M.; Patterson, B. M. *Inorg. Chem.* **1982**, *21*, 4330.

(67) Drew, M. G. B.; Wilkins, J. D. *Journal of the Chemical Society, Dalton Transactions* **1974**, 1973.

(68) Eilers, G.; Schwartz, L.; Stein, M.; Zampella, G.; de Gioia, L.; Ott, S.; Lomoth, R. *Chem. Eur. J.* **2007**, *13*, 7075.

(69) Ezzaher, S.; Orain, P. Y.; Capon, J. F.; Gloaguen, F.; Petillon, F. Y.; Roisnel, T.; Schollhammer, P.; Talarmin, J. *Chem. Commun.* **2008**, 2547.

(70) Fernandez, P.; Sousa-Pedrares, A.; Romero, J.; Duran, M. L.; Sousa, A.; Perez-Lourido, P.; Garcia-Vazquez, J. A. *Eur. J. Inorg. Chem.* **2010**, 814.

(71) Fernandez, P.; Sousa-Pedrares, A.; Romero, J.; Garcia-Vazquez, J. A.; Sousa, A.; Perez-Lourido, P. *Inorg. Chem.* **2008**, *47*, 2121.

(72) Fichtner, C.; van Gastel, M.; Lubitz, W. *Phys. Chem. Chem. Phys.* **2003**, *5*, 5507.

(73) Flint, D. H.; Allen, R. M. *Chem. Rev.* **1996**, *96*, 2315.

(74) Flint, D. H.; Smykrandall, E.; Tuminello, J. F.; Draczynskalusiak, B.; Brown, O. R. *J. Biol. Chem.* **1993**, *268*, 25547.

(75) Foerster, S.; Stein, M.; Brecht, M.; Ogata, H.; Higuchi, Y.; Lubitz, W. *J. Am. Chem. Soc* **2003**, *125*, 83.

(76) Foerster, S.; van Gastel, M.; Brecht, M.; Lubitz, W. *J. Biol. Inorg. Chem.* **2005**, *10*, 51.

(77) Fontecave, M. *Nat. Chem. Biol.* **2006**, *2*, 171.

(78) Fontecilla-Camps, J. C.; Volbeda, A.; Cavazza, C.; Nicolet, Y. *Chem. Rev.* **2007**, *107*, 4273.

(79) Franolic, J. D., SUNY Stony Brook, 1993.

(80) Franz, J. A.; Lee, S. J.; Bowden, T. A.; Alnajjar, M. S.; Appel, A. M.; Birnbaum, J. C.; Bitterwolf, T. E.; Dupuis, M. *J. Am. Chem. Soc* **2009**, *131*, 15212.

(81) Frey, M. *Chembiochem* **2002**, *3*, 153.

(82) Frisch, J. R.; Vu, V. V.; Martinho, M.; Munck, E.; Que, L. *Inorg. Chem.* **2009**, *48*, 8325.

(83) Fritz, G.; Griesshaber, D.; Seth, O.; Kroneck, P. M. H. *Biochemistry* **2001**, *40*, 1317.

(84) Fukuzumi, S. *Eur. J. Inorg. Chem.* **2008**, 1351.

(85) Galvez, C.; Ho, D. G.; Azod, A.; Selke, M. *J. Am. Chem. Soc* **2001**, *123*, 3381.

(86) Gao, S.; Fan, J. L.; Sun, S.; Peng, X. J.; Zhao, X.; Hou, J. *Dalton Trans.* **2008**, 2128.

(87) Garcin, E.; Vernede, X.; Hatchikian, E. C.; Volbeda, A.; Frey, M.; Fontecilla-Camps, J. C. *Structure* **1999**, *7*, 557.

(88) Georgakaki, I. P.; Miller, M. L.; Darensbourg, M. Y. *Inorg. Chem.* **2003**, *42*, 2489.

(89) George, S. J.; Cui, Z.; Razavet, M.; Pickett, C. J. *Chem. Eur. J.* **2002**, *8*, 4037.

(90) Gessner, C.; Trofanchuk, O.; Kawagoe, K.; Higuchi, Y.; Yasuoka, N.; Lubitz, W. *Chem. Phys. Lett.* **1996**, *256*, 518.

(91) Gloaguen, F.; Lawrence, J. D.; Rauchfuss, T. B. *Journal of the American Chemical Society* **2001**, *123*, 9476.

(92) Gloaguen, F.; Lawrence, J. D.; Rauchfuss, T. B.; Benard, M.; Rohmer, M. M. *Inorg. Chem.* **2002**, *41*, 6573.

(93) Gloaguen, F.; Lawrence, J. D.; Schmidt, M.; Wilson, S. R.; Rauchfuss, T. B. *J. Am. Chem. Soc* **2001**, *123*, 12518.

(94) Gloaguen, F.; Rauchfuss, T. B. *Chem. Soc. Rev.* **2009**, *38*, 100.

(95) Grapperhaus, C. A.; Darensbourg, M. Y. *Accounts Chem. Res.* **1998**, *31*, 451.

(96) Grapperhaus, C. A.; Maguire, M. J.; Tuntulani, T.; Darensbourg, M. Y. *Inorg. Chem.* **1997**, *36*, 1860.

(97) Grapperhaus, C. A.; Poturovic, S.; Mashuta, M. S. *Inorg. Chem.* **2002**, *41*, 4309.

(98) Greco, C.; Bruschi, M.; Fantucci, P.; De Gioia, L. *J. Organomet. Chem.* **2009**, *694*, 2846.

(99) Groysman, S.; Holm, R. H. *Biochemistry* **2009**, *48*, 2310.

(100) Gulea, M.; Kwiatkowska, M.; Lyzwa, P.; Legay, R.; Gaumont, A. C.; Kielbasinski, P. *Tetrahedron-Asymmetry* **2009**, *20*, 293.

(101) Halcrow, M. A.; Christou, G. *Chem. Rev.* **1994**, *94*, 2421.

(102) He, C.; Hus, J. C.; Sun, L. J.; Zhou, P.; Norman, D. P. G.; Dotsch, V.; Wei, H.; Gross, J. D.; Lane, W. S.; Wagner, G.; Verdine, G. L. *Mol. Cell* **2005**, *20*, 117.

(103) Heinekey, D. M. *J. Organomet. Chem.* **2009**, *694*, 2671.

(104) Higuchi, Y.; Ogata, H.; Miki, K.; Yasuoka, N.; Yagi, T. *Structure* **1999**, *7*, 549.

(105) Hiromoto, T.; Ataka, K.; Pilak, O.; Vogt, S.; Stagni, M. S.; Meyer-Klaucke, W.; Warkentin, E.; Thauer, R. K.; Shima, S.; Ermler, U. *FEBS Lett.* **2009**, *583*, 585.

(106) Hirotsu, M.; Kobayashi, A.; Yoshimura, T.; Konno, T. *J. Chem. Soc.-Dalton Trans.* **2002**, 878.

(107) Hoggard, P. E. *Coord. Chem. Rev.* **1997**, *159*, 235.

(108) Hoggard, P. E.; Bridgeman, A. J.; Kunkely, H.; Vogler, A. *Inorg. Chim. Acta* **2004**, *357*, 639.

(109) Hoggard, P. E.; Gruber, M.; Vogler, A. *Inorg. Chim. Acta* **2003**, *346*, 137.

(110) Hoggard, P. E.; Vogler, A. *Inorg. Chim. Acta* **2003**, *348*, 229.

(111) Holloway, C. E.; Melnik, M. *Rev. Inorg. Chem.* **2003**, *23*, 125.

(112) Holloway, C. E.; Melnik, M. *Rev. Inorg. Chem.* **2004**, *24*, 301.

(113) Holm, R. H.; Solomon, E. I. *Chem. Rev.* **2004**, *104*, 347.

(114) Hou, J.; Peng, X. J.; Liu, J. F.; Gao, Y. L.; Zhao, X.; Gao, S.; Han, K. L. *Eur. J. Inorg. Chem.* **2006**, 4679.

(115) Hu, J.; Xu, H.; Nguyen, M. H.; Yip, J. H. K. *Inorg. Chem.* **2009**, *48*, 9684.

(116) Hunter, C. A.; Sanders, J. K. M. *J. Am. Chem. Soc* **1990**, *112*, 5525.

(117) Imlay, J. A. *Molecular Microbiology* **2006**, *59*, 1073.

(118) Izutsu, K. In *Acid-Base Dissociation Constants in Dipolar Aprotic Solvents* Blackwell Science: 1990.
(119) Jaryszak, E. M.; Hoggard, P. E. *Inorg. Chim. Acta* **1998**, *282*, 217.
(120) Jiang, J. F.; Acunzo, A.; Koch, S. A. *J. Am. Chem. Soc* **2001**, *123*, 12109.
(121) Jiang, J. F.; Koch, S. A. *Angew. Chem. Int. Edit.* **2001**, *40*, 2629.
(122) Jiang, J. F.; Koch, S. A. *Inorg. Chem.* **2002**, *41*, 158.
(123) Jiang, S.; Liu, J. H.; Shi, Y.; Wang, Z.; Akermark, B.; Sun, L. C. *Dalton Trans.* **2007**, 896.
(124) Jiang, S.; Liu, J. H.; Sun, L. C. *Inorg. Chem. Commun.* **2006**, *9*, 290.
(125) Justice, A. K.; Zampella, G.; De Gioia, L.; Rauchfuss, T. B.; van der Vlugt, J. I.; Wilson, S. R. *Inorg. Chem.* **2007**, *46*, 1655.
(126) Kaesz, H. D.; Saillant, R. B. *Chem. Rev.* **1972**, *72*, 231.
(127) Kayal, A.; Rauchfuss, T. B. *Inorg. Chem.* **2003**, *42*, 5046.
(128) Keyer, K.; Gort, A. S.; Imlay, J. A. *J. Bacteriol.* **1995**, *177*, 6782.
(129) Kiley, P. J.; Beinert, H. *Curr. Opin. Microbiol.* **2003**, *6*, 181.
(130) Kim, J.; Hetzel, M.; Boiangiu, C. D.; Buckel, W. *Fems Microbiol. Rev.* **2004**, *28*, 455.
(131) Kim, J. S.; Rees, D. C. *Nature* **1992**, *360*, 553.
(132) Knoblauch, S.; Hartl, F.; Stufkens, D. J.; Hennig, H. *Eur. J. Inorg. Chem.* **1999**, 303.
(133) Krautscheid, H.; Matern, E.; Fritz, G.; Pikies, J. *Z. Anorg. Allg. Chem.* **1998**, *624*, 501.
(134) Kruger, H. J.; Holm, R. H. *Inorg. Chem.* **1987**, *26*, 3645.
(135) Kruger, H. J.; Peng, G.; Holm, R. H. *Inorg. Chem.* **1991**, *30*, 734.
(136) Lai, C. H.; Reibenspies, J. H.; Darensbourg, M. Y. *Angew. Chem. Int. Edit.* **1996**, *35*, 2390.
(137) Lamle, S. E.; Albracht, S. P. J.; Armstrong, F. A. *J. Am. Chem. Soc* **2004**, *126*, 14899.
(138) Lawrence, J. D.; Li, H. X.; Rauchfuss, T. B. *Chem. Commun.* **2001**, 1482.
(139) Lawrence, J. D.; Li, H. X.; Rauchfuss, T. B.; Benard, M.; Rohmer, M. M. *Angew. Chem. Int. Edit.* **2001**, *40*, 1768.
(140) Le Cloirec, A.; Best, S. P.; Borg, S.; Davies, S. C.; Evans, D. J.; Hughes, D. L.; Pickett, C. J. *Chem. Commun.* **1999**, 2285.
(141) Lee, S. C.; Holm, R. H. *Chem. Rev.* **2004**, *104*, 1135.
(142) Leger, C.; Jones, A. K.; Albracht, S. P. J.; Armstrong, F. A. *J. Phys. Chem. B* **2002**, *106*, 13058.
(143) Leger, C.; Jones, A. K.; Roseboom, W.; Albracht, S. P. J.; Armstrong, F. A. *Biochemistry* **2002**, *41*, 15736.
(144) Lemon, B. J.; Peters, J. W. *Biochemistry* **1999**, *38*, 12969.
(145) Leroux, F.; Dementin, S.; Burlatt, B.; Cournac, L.; Volbeda, A.; Champ, S.; Martin, L.; Guigliarelli, B.; Bertrand, P.; Fontecilla-Camps, J.; Rousset, M.; Leger, C. *Proc. Natl. Acad. Sci. U. S. A.* **2008**, *105*, 11188.
(146) Li, H. X.; Rauchfuss, T. B. *J. Am. Chem. Soc* **2002**, *124*, 726.
(147) Li, P.; Wang, M.; He, C.; Liu, X.; Jin, K.; Sun, L. *Eur. J. Inorg. Chem.* **2007**, 3718.
(148) Li, Z. L.; Ohki, Y.; Tatsumi, K. *J. Am. Chem. Soc* **2005**, *127*, 8950.

(149) Liaw, W. F.; Lee, J. H.; Gau, H. B.; Chen, C. H.; Jung, S. J.; Hung, C. H.; Chen, W. Y.; Hu, C. H.; Lee, G. H. *J. Am. Chem. Soc* **2002**, *124*, 1680.

(150) Liaw, W. F.; Lee, N. H.; Chen, C. H.; Lee, C. M.; Lee, G. H.; Peng, S. M. *J. Am. Chem. Soc* **2000**, *122*, 488.

(151) Lippard, S. J. *Principles of bioinorganic chemistry*; University Science Books: Mill Valley, Calif, 1994.

(152) Liu, T. B.; Darensbourg, M. Y. *J. Am. Chem. Soc* **2007**, *129*, 7008.

(153) Liu, T. B.; Wang, M.; Shi, Z.; Cui, H. G.; Dong, W. B.; Chen, J. S.; Akermark, B.; Sun, L. C. *Chem. Eur. J.* **2004**, *10*, 4474.

(154) Liu, Z. P.; Hu, P. *J. Am. Chem. Soc* **2002**, *124*, 5175.

(155) Loscher, S.; Burgdorf, T.; Zebger, I.; Hildebrandt, P.; Dau, H.; Friedrich, B.; Haumann, M. *Biochemistry* **2006**, *45*, 11658.

(156) Lounissi, S.; Capon, J. F.; Gloaguen, F.; Matoussi, F.; Petillon, F. Y.; Schollhammer, P.; Talarmin, J. *Organometallics* **2010**, *29*, 1296.

(157) Lubitz, W.; Reijerse, E.; van Gastel, M. *Chem. Rev.* **2007**, *107*, 4331.

(158) Lyne, P. D.; Mingos, D. M. P. *Journal of the Chemical Society, Dalton Transactions* **1995**, 1635.

(159) Lyon, E. J.; Georgakaki, I. P.; Reibenspies, J. H.; Darensbourg, M. Y. *Angew. Chem. Int. Edit.* **1999**, *38*, 3178.

(160) Lyon, E. J.; Georgakaki, I. P.; Reibenspies, J. H.; Darensbourg, M. Y. *J. Am. Chem. Soc* **2001**, *123*, 3268.

(161) Lyon, E. J.; Musie, G.; Reibenspies, J. H.; Darensbourg, M. Y. *Inorg. Chem.* **1998**, *37*, 6942.

(162) Lyon, E. J.; Shima, S.; Boecher, R.; Thauer, R. K.; Grevels, F. W.; Bill, E.; Roseboom, W.; Albracht, S. P. J. *J. Am. Chem. Soc* **2004**, *126*, 14239.

(163) Maier, L. *Helv. Chim. Acta.* **1969**, *52*, 827.

(164) Maier, L. *Helv. Chim. Acta.* **1971**, *54*, 1651.

(165) Malinak, S. M.; Coucouvanis, D. In *Progress in Inorganic Chemistry, Vol 49*; John Wiley & Sons Inc: New York, 2001; Vol. 49, p 599.

(166) Mann, K. R.; Gray, H. B. *J. Am. Chem. Soc* **1977**, *99*, 306.

(167) Mansy, S. S.; Cowan, J. A. *Accounts Chem. Res.* **2004**, *37*, 719.

(168) Marks, T. J. *Science* **1985**, *227*, 881.

(169) Matano, Y.; Miyajima, T.; Ochi, N.; Nakabuchi, T.; Shiro, M.; Nakao, Y.; Sakaki, S.; Imahori, H. *J. Am. Chem. Soc* **2008**, *130*, 990.

(170) Matern, E.; Pikies, J.; Fritz, G. *Z. Anorg. Allg. Chem.* **2000**, *626*, 2136.

(171) Matsumoto, T.; Ohki, Y.; Tatsumi, K. *J. Synth. Org. Chem. Jpn.* **2009**, *67*, 540.

(172) McGlynn, S. E.; Mulder, D. W.; Shepard, E. M.; Broderick, J. B.; Peters, J. W. *Dalton Trans.* **2009**, 4274.

(173) Mejia-Rodriguez, R.; Chong, D. S.; Reibenspies, J. H.; Soriaga, M. P.; Darensbourg, M. Y. *J. Am. Chem. Soc* **2004**, *126*, 12004.

(174) Morvan, D.; Capon, J. F.; Gloaguen, F.; Le Goff, A.; Marchivie, M.; Michaud, F.; Schollhammer, P.; Talarmin, J.; Yaouanc, J. J.; Pichon, R.; Kervarec, N. *Organometallics* **2007**, *26*, 2042.

(175) Morvan, D.; Capon, J. F.; Gloaguen, F.; Petillon, F. Y.; Schollhammer, P.; Talarmin, J.; Yaouanc, J. J.; Michaud, F.; Kervarec, N. *J. Organomet. Chem.* **2009**, *694*, 2801.

(176) Muller, A.; Jaegermann, W.; Enemark, J. H. *Coord. Chem. Rev.* **1982**, *46*, 245.

(177) Mullins, C. S.; Grapperhaus, C. A.; Frye, B. C.; Wood, L. H.; Hay, A. J.; Buchanan, R. M.; Mashuta, M. S. *Inorg. Chem.* **2009**, *48*, 9974.

(178) Murata, M.; Kojima, M.; Hioki, A.; Miyagawa, M.; Hirotsu, M.; Nakajima, K.; Kita, M.; Kashino, S.; Yoshikawa, Y. *Coord. Chem. Rev.* **1998**, *174*, 109.

(179) Musie, G.; Reibenspies, J. H.; Darensbourg, M. Y. *Inorg. Chem.* **1998**, *37*, 302.

(180) Myers, L. C.; Terranova, M. P.; Ferentz, A. E.; Wagner, G.; Verdine, G. L. *Science* **1993**, *261*, 1164.

(181) Naqui, A.; Chance, B.; Cadenas, E. *Annu. Rev. Biochem.* **1986**, *55*, 137.

(182) Nehring, J. L.; Heinekey, D. M. *Inorg. Chem.* **2003**, *42*, 4288.

(183) Ngu, T. T.; Stillman, M. J. *Dalton Trans.* **2009**, 5425.

(184) Nicolet, Y.; de Lacey, A. L.; Vernede, X.; Fernandez, V. M.; Hatchikian, E. C.; Fontecilla-Camps, J. C. *J. Am. Chem. Soc* **2001**, *123*, 1596.

(185) Nicolet, Y.; Lemon, B. J.; Fontecilla-Camps, J. C.; Peters, J. W. *Trends Biochem.Sci.* **2000**, *25*, 138.

(186) Nicolet, Y.; Piras, C.; Legrand, P.; Hatchikian, C. E.; Fontecilla-Camps, J. C. *Struct. Fold. Des.* **1999**, *7*, 13.

(187) Niu, S. Q.; Thomson, L. M.; Hall, M. B. *J. Am. Chem. Soc* **1999**, *121*, 4000.

(188) Nixcon, J. F.; Pidcock, A. *Annual Review of NMR Spectroscopy* **1969**, *2*, 345.

(189) Nova, A.; Gonzalez-Duarte, P.; Lledos, A.; Mas-Balleste, R.; Ujaque, G. *Inorg. Chim. Acta* **2006**, *359*, 3736.

(190) Ogata, H.; Hirota, S.; Nakahara, A.; Komori, H.; Shibata, N.; Kato, T.; Kano, K.; Higuchi, Y. *Structure* **2005**, *13*, 1635.

(191) Ogata, H.; Mizoguchi, Y.; Mizuno, N.; Miki, K.; Adachi, S.; Yasuoka, N.; Yagi, T.; Yamauchi, O.; Hirota, S.; Higuchi, Y. *J. Am. Chem. Soc* **2002**, *124*, 11628.

(192) Ohkubo, T.; Sakashita, H.; Sakuma, T.; Kainosho, M.; Sekiguchi, M.; Morikawa, K. *J. Am. Chem. Soc* **1994**, *116*, 6035.

(193) Okamoto, K.; Sasaki, C.; Yamada, Y.; Konno, T. *Bull. Chem. Soc. Jpn.* **1999**, *72*, 1685.

(194) Olsen, M. T.; Barton, B. E.; Rauchfuss, T. B. *Inorg. Chem.* **2009**, *48*, 7507.

(195) Oster, S. S.; Lachicotte, R. J.; Jones, W. D. *Inorg. Chim. Acta* **2002**, *330*, 118.

(196) Osterloh, F.; Saak, W.; Haase, D.; Pohl, S. *Chem. Commun.* **1997**, 979.

(197) Osz, J.; Bagyinka, C. *Biophys. J.* **2005**, *89*, 1984.

(198) Ott, S.; Borgstrom, M.; Kritikos, M.; Lomoth, R.; Bergquist, J.; Akermark, B.; Hammarstrom, L.; Sun, L. C. *Inorg. Chem.* **2004**, *43*, 4683.

(199) Otto, S.; Roodt, A. *Inorg. Chim. Acta* **2004**, *357*, 1.

(200) Pardo, A.; De Lacey, A. L.; Fernandez, V. M.; Fan, H. J.; Fan, Y. B.; Hall, M. B. *J. Biol. Inorg. Chem.* **2006**, *11*, 286.

(201) Pereira, A. S.; Tavares, P.; Moura, I.; Moura, J. J. G.; Huynh, B. H. *J. Am. Chem. Soc* **2001**, *123*, 2771.

(202) Perra, A.; Davies, E. S.; Hyde, J. R.; Wang, Q.; McMaster, J.; Schroder, M. *Chem. Commun.* **2006**, 1103.

(203) Peters, J. W.; Lanzilotta, W. N.; Lemon, B. J.; Seefeldt, L. C. *Science* **1998**, *282*, 1853.

(204) Petrov, K. A.; Parshina, V. A.; Gaidamak, V. A. *J.Gen.Chem.USSR (Engl.Transl.)* **1961**, *31*, 3180.

(205) Pham, K.; Henderson, W.; Nicholson, B. K.; Hor, T. S. A. *J. Organomet. Chem.* **2007**, *692*, 4933.

(206) Picot, D.; Ohanessian, G.; Frison, G. *Inorg. Chem.* **2008**, *47*, 8167.

(207) Picot, D.; Ohanessian, G.; Frison, G. *C. R. Chim.* **2009**, *12*, 546.

(208) Pidcock, A.; Richards, R. E.; Venanzi, L. M. *Journal of the Chemical Society a - Inorganic Physical Theoretical* **1966**, 1707.

(209) Popescu, C. V.; Munck, E. *J. Am. Chem. Soc* **1999**, *121*, 7877.

(210) Pratihar, P.; Mondal, T. K.; Patra, A. K.; Sinha, C. *Inorg. Chem.* **2009**, *48*, 2760.

(211) Py, B.; Barras, F. *Nat. Rev. Microbiol.* **2010**, *8*, 436.

(212) Rauchfuss, T. B. *Science* **2007**, *316*, 553.

(213) Rauchfuss, T. B.; Contakes, S. M.; Hsu, S. C. N.; Reynolds, M. A.; Wilson, S. R. *J. Am. Chem. Soc* **2001**, *123*, 6933.

(214) Razavet, M.; Borg, S. J.; George, S. J.; Best, S. P.; Fairhurst, S. A.; Pickett, C. J. *Chem. Commun.* **2002**, 700.

(215) Reihlen, H.; Friedolsheim, A. V.; Oswald, W. *Justus Liebigs Ann. Chem.* **1928**, *465*, 72.

(216) Rigamonti, L.; Forni, A.; Manassero, M.; Manassero, C.; Pasini, A. *Inorg Chem* **2010**, *49*, 123.

(217) Roodt, A.; Otto, S.; Steyl, G. *Coord. Chem. Rev.* **2003**, *245*, 121.

(218) Roseboom, W.; De Lacey, A. L.; Fernandez, V. M.; Hatchikian, E. C.; Albracht, S. P. J. *J. Biol. Inorg. Chem.* **2006**, *11*, 102.

(219) Roy, L. E.; Batista, E. R.; Hay, P. J. *Inorg. Chem.* **2008**, *47*, 9228.

(220) Royer, A. M.; Rauchfuss, T. B.; Wilson, S. R. *Inorg. Chem.* **2008**, *47*, 395.

(221) Ruegger, H.; Moskau, D. *Magn. Reson. Chem.* **1991**, *29*, S11.

(222) Ryde, U.; Greco, C.; De Gioia, L. *J. Am. Chem. Soc* **2010**, *132*, 4512.

(223) Salomone-Stagni, M.; Stellato, F.; Whaley, C. M.; Vogt, S.; Morante, S.; Shima, S.; Rauchfuss, T. B.; Meyer-Klaucke, W. *Dalton Trans.* **2010**, *39*, 3057.

(224) Sanderson, R. T. *Chemical Periodicity*; Reinhold: New York, USA, 1960.

(225) Schmidt, M.; Contakes, S. M.; Rauchfuss, T. B. *J. Am. Chem. Soc* **1999**, *121*, 9736.

(226) Schwartz, L.; Eilers, G.; Eriksson, L.; Gogoll, A.; Lomoth, R.; Ott, S. *Chem. Commun.* **2006**, 520.

(227) Sellmann, D.; Geipel, F.; Heinemann, F. W. *Chem. Eur. J.* **2002**, *8*, 958.

(228) Sellmann, D.; Geipel, F.; Lauderbach, F.; Heinemann, F. W. *Angew. Chem. Int. Edit.* **2002**, *41*, 632.

(229) Sellmann, D.; Haussinger, D.; Heinemann, F. W. *Eur. J. Inorg. Chem.* **1999**, 1715.

(230) Sellmann, D.; Prakash, R.; Geipel, F.; Heinemann, F. W. *Eur. J. Inorg. Chem.* **2002**, 2138.

(231) Sellmann, D.; Waeber, M.; Binder, H.; Boese, R. *Z.Naturforsch.(B)* **1986**, *41*, 1541.

(232) Seyferth, D.; Withers, H. P. *J. Organomet. Chem.* **1980**, *185*, C1.

(233) Shima, S.; Pilak, O.; Vogt, S.; Schick, M.; Stagni, M. S.; Meyer-Klaucke, W.; Warkentin, E.; Thauer, R. K.; Ermler, U. *Science* **2008**, *321*, 572.

(234) Siegbahn, P. E. M. In *Advances in Inorganic Chemistry - Including Bioinorganic Studies, Vol 56*; Elsevier Academic Press Inc: San Diego, 2004; Vol. 56, p 101.

(235) Siegbahn, P. E. M.; Tye, J. W.; Hall, M. B. *Chem. Rev.* **2007**, *107*, 4414.

(236) Silverstein, R. M.; Bassler, G. C.; Morrill, T. C. *Spectrometric Indentification of Organic Compounds*; 5th ed.; John Wiley & Sons, Inc.: New York, 1991.

(237) Singleton, M. L.; Bhuvanesh, N.; Reibenspies, J. H.; Darensbourg, M. Y. *Angew. Chem. Int. Edit.* **2008**, *47*, 9492.

(238) Slater, J. C. *J. Chem. Phys.* **1964**, *41*, 3199.

(239) Smee, J. J.; Miller, M. L.; Grapperhaus, C. A.; Reibenspies, J. H.; Darensbourg, M. Y. *Inorg. Chem.* **2001**, *40*, 3601.

(240) Smith, M. C.; Barclay, J. E.; Cramer, S. P.; Davies, S. C.; Gu, W. W.; Hughes, D. L.; Longhurst, S.; Evans, D. J. *J. Chem. Soc.-Dalton Trans.* **2002**, 3410.

(241) Song, L. C. *Accounts Chem. Res.* **2005**, *38*, 21.

(242) Song, L. C.; Cheng, J.; Yan, J.; Liu, C. R.; Hu, Q. M. *Organometallics* **2010**, *29*, 205.

(243) Song, L. C.; Gao, W.; Feng, C. P.; Wang, D. F.; Hu, Q. M. *Organometallics* **2009**, *28*, 6121.

(244) Song, L. C.; Luo, X.; Wang, Y. Z.; Gai, B.; Hu, Q. M. *J. Organomet. Chem.* **2009**, *694*, 103.

(245) Song, L. C.; Yang, Z. Y.; Bian, H. Z.; Hu, Q. M. *Organometallics* **2004**, *23*, 3082.

(246) Song, L. C.; Yang, Z. Y.; Bian, H. Z.; Liu, Y.; Wang, H. T.; Liu, X. F.; Hu, Q. M. *Organometallics* **2005**, *24*, 6126.

(247) Song, L. C.; Yang, Z. Y.; Hua, Y. J.; Wang, H. T.; Liu, Y.; Hu, Q. M. *Organometallics* **2007**, *26*, 2106.

(248) Song, L. C.; Yin, B. S.; Li, Y. L.; Zhao, L. Q.; Ge, J. H.; Yang, Z. Y.; Hu, Q. M. *Organometallics* **2007**, *26*, 4921.

(249) Stanley, J. L.; Rauchfuss, T. B.; Wilson, S. R. *Organometallics* **2007**, *26*, 1907.

(250) Stephenson, M.; Stickland, L. H. *Biochem. J.* **1931**, *25*, 205.

(251) Stripp, S. T.; Happe, T. *Dalton Trans.* **2009**, 9960.

(252) Sun, J. B.; Tessier, C.; Holm, R. H. *Inorg. Chem.* **2007**, *46*, 2691.

(253) Takeda, N.; Tokitoh, N.; Okazaki, R. In *Elemental Sulfur and Sulfur-Rich Compounds Ii*; Springer-Verlag Berlin: Berlin, 2003; Vol. 231, p 153.

(254) Takinowaki, H.; Matsuda, Y.; Yoshida, T.; Kobayashi, Y.; Ohkubo, T. *Protein Sci.* **2006**, *15*, 487.

(255) Tard, C.; Pickett, C. J. *Chem. Rev.* **2009**, *109*, 2245.

(256) Theil, E. C.; Goss, D. J. *Chem. Rev.* **2009**, *109*, 4568.

(257) Thomas, C. M.; Rudiger, O.; Liu, T.; Carson, C. E.; Hall, M. B.; Darensbourg, M. Y. *Organometallics* **2007**, *26*, 3976.

(258) Trofanchuk, O.; Stein, M.; Gessner, C.; Lendzian, F.; Higuchi, Y.; Lubitz, W. *J. Biol. Inorg. Chem.* **2000**, *5*, 36.

(259) Tye, J. W.; Darensbourg, M. Y.; Hall, M. B. *Inorg. Chem.* **2006**, *45*, 1552.

(260) van der Vlugt, J. I.; Rauchfuss, T. B.; Whaley, C. M.; Wilson, S. R. *J. Am. Chem. Soc* **2005**, *127*, 16012.

(261) Vanderzwaan, J. W.; Coremans, J.; Bouwens, E. C. M.; Albracht, S. P. J. *Biochim. Biophys. Acta* **1990**, *1041*, 101.

(262) Venanzi, L. M. *Chem. Br.* **1968**, *4*, 162.

(263) Venkateswara Rao, P.; Holm, R. H. *Chem. Rev.* **2004**, *104*, 527.

(264) Vetter, C.; Kaluderovic, G. N.; Paschke, R.; Gomez-Ruiz, S.; Steinborn, D. *Polyhedron* **2009**, *28*, 3699.

(265) Vignais, P. M. *Coord. Chem. Rev.* **2005**, *249*, 1677.

(266) Vignais, P. M.; Billoud, B. *Chem. Rev.* **2007**, *107*, 4206.

(267) Vignais, P. M.; Billoud, B.; Meyer, J. *Fems Microbiol. Rev.* **2001**, *25*, 455.

(268) Vincent, K. A.; Parkin, A.; Armstrong, F. A. *Chem. Rev.* **2007**, *107*, 4366.

(269) Volbeda, A.; Charon, M. H.; Piras, C.; Hatchikian, E. C.; Frey, M.; Fontecillacamps, J. C. *Nature* **1995**, *373*, 580.

(270) Volbeda, A.; Fontecilla-Camps, J. C. *Coord. Chem. Rev.* **2005**, *249*, 1609.

(271) Volbeda, A.; Garcin, E.; Piras, C.; deLacey, A. L.; Fernandez, V. M.; Hatchikian, E. C.; Frey, M.; FontecillaCamps, J. C. *J. Am. Chem. Soc* **1996**, *118*, 12989.

(272) Volbeda, A.; Martin, L.; Cavazza, C.; Matho, M.; Faber, B. W.; Roseboom, W.; Albracht, S. P. J.; Garcin, E.; Rousset, M.; Fontecilla-Camps, J. C. *J. Biol. Inorg. Chem.* **2005**, *10*, 239.

(273) Wackett, L. P.; Dodge, A. G.; Ellis, L. B. M. *Appl. Environ. Microbiol.* **2004**, *70*, 647.

(274) Walzer, K.; Maennig, B.; Pfeiffer, M.; Leo, K. *Chem. Rev.* **2007**, *107*, 1233.

(275) Wang, F. J.; Wang, M.; Liu, X. Y.; Jin, K.; Donga, W. B.; Sun, L. C. *Dalton Trans.* **2007**, 3812.

(276) Wang, W.-G.; Wang, H.-Y.; Si, G.; Tung, C.-H.; Wu, L.-Z. *Dalton Trans.* **2009**, 2712.

(277) Wang, W. M.; Zhao, C. Q. *Acta Crystallogr. Sect. E.-Struct Rep. Online* **2010**, *66*, O863.

(278) Wang, Z.; Liu, J. H.; He, C. J.; Jiang, S.; Akermark, B.; Sun, L. C. *J. Organomet. Chem.* **2007**, *692*, 5501.

(279) Whang, S.; Estrada, T.; Hoggard, P. E. *Photochem. Photobiol.* **2004**, *79*, 356.

(280) Windhager, J.; Rudolph, M.; Brautigam, S.; Gorls, H.; Weigand, W. *Eur. J. Inorg. Chem.* **2007**, 2748.

(281) Winter, A.; Zsolnai, L.; Huttner, G. *Z.Naturforsch.(B)* **1982**, *37*, 1430.

(282) Woodward, J. *Philosophical Transactions* **1724**, *33*, 15.

(283) Xu, F. F.; Tard, C.; Wang, X. F.; Ibrahim, S. K.; Hughes, D. L.; Zhong, W.; Zeng, X. R.; Luo, Q. Y.; Liu, X. M.; Pickett, C. J. *Chem. Commun.* **2008**, 606.

(284) Yakelis, N. A.; Bergman, R. G. *Organometallics* **2005**, *24*, 3579.

(285) Yamamura, T.; Tadokoro, M.; Nakamura, N.; Tanaka, K.; Asakura, K. *Bull. Chem. Soc. Jpn.* **1990**, *63*, 999.

(286) Yang, X. Z.; Hall, M. B. *J. Am. Chem. Soc* **2008**, *130*, 14036.

(287) Zhang, Y. H. P. *Energy Environ. Sci.* **2009**, *2*, 272.

(288) Zhao, X.; Georgakaki, I. P.; Miller, M. L.; Mejia-Rodriguez, R.; Chiang, C. Y.; Darensbourg, M. Y. *Inorg. Chem.* **2002**, *41*, 3917.

(289) Zhao, X.; Georgakaki, I. P.; Miller, M. L.; Yarbrough, J. C.; Darensbourg, M. Y. *J. Am. Chem. Soc* **2001**, *123*, 9710.

(290) Zhou, T. J.; Mo, Y. R.; Liu, A. M.; Zhou, Z. H.; Tsai, K. R. *Inorg. Chem.* **2004**, *43*, 923.

(291) Zhu, W. F.; Marr, A. C.; Wang, Q.; Neese, F.; Spencer, D. J. E.; Blake, A. J.; Cooke, P. A.; Wilson, C.; Schroder, M. *Proc. Natl. Acad. Sci. U. S. A.* **2005**, *102*, 18280.

Appendix

Table A- 1. Crystal data and structure refinement for $Ni^{II}_2(PS2)_2$

Identification code	$Ni^{II}_2(PS2)_2$	
Empirical formula	C72 H51 Ni4 P4 S8	
Formula weight	1531.33	
Temperature	100(2) K	
Wavelength	0.71073 Å	
Crystal system	Monoclinic	
Space group	$P\bar{1}$	
Unit cell dimensions	a = 16.6485(16) Å	a= 90 °.
	b = 11.0345(8) Å	b= 107.641(10) °.
	c = 18.2292(16) Å	g = 90 °.
Volume	3191.4(5) $Å^3$	
Z	2	
Density (calculated)	1.594 Mg/m^3	
Absorption coefficient	1.569 mm^{-1}	
F(000)	1566	
Crystal size	0.4 x 0.2x 0.05 mm^3	
Theta range for data collection	2.91 to 32.99 °.	
Index ranges	-24<=h<=23, -14<=k<=16, -26<=l<=26	
Reflections collected	16237	
Independent reflections	13097 [R(int) = 0.0986]	
Completeness to theta = 32.99 °	54.5 %	
Refinement method	Full-matrix least-squares on F^2	
Data / restraints / parameters	13097 / 0 / 694	
Goodness-of-fit on F^2	0.686	
Final R indices [I>2sigma(I)]	R1 = 0.0960, wR2 = 0.2411	
R indices (all data)	R1 = 0.2744, wR2 = 0.3099	
Extinction coefficient	0.0000(3)	
Largest diff. peak and hole	1.392 and -1.558 e.$Å^{-3}$	

Table A- 2. Crystal data and structure refinement for $[Ni^{II}(PS2'H)_2]\cdot 2CH_2Cl_2$.

Identification code	$Ni^{II}(PS2'H)_2$	
Empirical formula	C42 H40 Cl4 Ni P2 S4	
Formula weight	935.43	
Temperature	100(2) K	
Wavelength	0.71073 Å	
Crystal system	Orthorhombic	
Space group	Pbca	
Unit cell dimensions	a = 14.5328(2) Å	a= 90 °.
	b = 15.0982(2) Å	b= 90 °.
	c = 18.5622(2) Å	g = 90 °.
Volume	4072.90(9) $Å^3$	
Z	4	
Density (calculated)	1.526 Mg/m^3	
Absorption coefficient	1.055 mm^{-1}	
F(000)	1928	
Crystal size	0.20 x 0.20 x 0.15 mm^3	
Theta range for data collection	2.91 to 32.90 °.	
Index ranges	-15<=h<=20, -22<=k<=11, -15<=l<=26	
Reflections collected	17818	
Independent reflections	6842 [R(int) = 0.0221]	
Completeness to theta = 32.90 °	90.0 %	
Max. and min. transmission	0.8578 and 0.8168	
Refinement method	Full-matrix least-squares on F^2	
Data / restraints / parameters	6842 / 0 / 245	
Goodness-of-fit on F^2	0.946	
Final R indices [I>2sigma(I)]	R1 = 0.0255, wR2 = 0.0620	
R indices (all data)	R1 = 0.0408, wR2 = 0.0636	
Largest diff. peak and hole	0.441 and -0.389 $e.Å^{-3}$	

Table A- 3. Crystal data and structure refinement for [$Ni^{IV}(PS2)_2$]•1/2MeCN.

Identification code	$Ni^{IV}(PS2)_2$	
Empirical formula	C74 H55 N Ni2 P4 S8	
Formula weight	1455.97	
Temperature	100(2) K	
Wavelength	0.71073 Å	
Crystal system	Monoclinic	
Space group	$P2_1/n$	
Unit cell dimensions	a = 9.8947(6) Å	a= 90 °.
	b = 19.0213(8) Å	b= 93.547(8) °.
	c = 35.033(3) Å	g = 90 °.
Volume	6580.9(7) $Å^3$	
Z	4	
Density (calculated)	1.470 Mg/m^3	
Absorption coefficient	0.969 mm^{-1}	
F(000)	3000	
Crystal size	0.3 x 0.3x 0.5mm^3	
Theta range for data collection	2.97 to 32.96 °.	
Index ranges	-11<=h<=14, -21<=k<=28, -52<=l<=53	
Reflections collected	45830	
Independent reflections	22114 [R(int) = 0.0304]	
Completeness to theta = 32.96 °	89.4 %	
Refinement method	Full-matrix least-squares on F^2	
Data / restraints / parameters	22114 / 0 / 803	
Goodness-of-fit on F^2	0.942	
Final R indices [I>2sigma(I)]	R1 = 0.0393, wR2 = 0.0782	
R indices (all data)	R1 = 0.0727, wR2 = 0.0832	
Largest diff. peak and hole	0.652 and -0.477 e.$Å^{-3}$	

Table A- 4. Crystal data and structure refinement for $[Pd^{II}(PS2'H)_2]\cdot 2CH_2Cl_2$.

Identification code	$Pd^{II}(PS2'H)_2$	
Empirical formula	C42 H40 Cl4 P2 Pd S4	
Formula weight	983.12	
Temperature	100(2) K	
Wavelength	0.71073 Å	
Crystal system	Orthorhombic	
Space group	Pbca	
Unit cell dimensions	a = 14.3965(2) Å	a= 90 °.
	b = 15.17420(10) Å	b= 90 °.
	c = 18.8113(2) Å	g = 90 °.
Volume	4109.43(8) $Å^3$	
Z	4	
Density (calculated)	1.589 Mg/m^3	
Absorption coefficient	1.025 mm^{-1}	
F(000)	2000	
Crystal size	0.5 x 0.3 x 0.15 mm^3	
Theta range for data collection	3.22 to 32.92 °.	
Index ranges	-20<=h<=19, -22<=k<=23, -23<=l<=28	
Reflections collected	54274	
Independent reflections	7344 [R(int) = 0.0270]	
Completeness to theta = 32.92 °	95.6 %	
Refinement method	Full-matrix least-squares on F^2	
Data / restraints / parameters	7344 / 0 / 246	
Goodness-of-fit on F^2	1.093	
Final R indices [I>2sigma(I)]	R1 = 0.0243, wR2 = 0.0649	
R indices (all data)	R1 = 0.0360, wR2 = 0.0671	
Largest diff. peak and hole	0.482 and -0.765 e.$Å^{-3}$	

Table A- 5. Crystal data and structure refinement for $[Et4N]_2[Pd^{II}(PS2')_2]$•4MeOH.

Identification code	$[Pd^{II}(PS2')_2]^{2-}$	
Empirical formula	C30 H45 N O2 P Pd0.50 S2	
Formula weight	599.96	
Temperature	100(2) K	
Wavelength	0.71073 Å	
Crystal system	Monoclinic	
Space group	$P2_1/n$	
Unit cell dimensions	a = 14.1703(2) Å	a= 90 °.
	b = 15.1766(2) Å	b= 99.7320(10) °.
	c = 14.3726(2) Å	g = 90 °.
Volume	3046.45(7) $Å^3$	
Z	4	
Density (calculated)	1.308 Mg/m^3	
Absorption coefficient	0.540 mm^{-1}	
F(000)	1272	
Crystal size	0.4 x 0.3 x 0.25 mm^3	
Theta range for data collection	3.17 to 35.07 °.	
Index ranges	-22<=h<=21, -24<=k<=24, -22<=l<=23	
Reflections collected	65680	
Independent reflections	12811 [R(int) = 0.0286]	
Completeness to theta = 35.07 °	95.0 %	
Refinement method	Full-matrix least-squares on F^2	
Data / restraints / parameters	12811 / 2 / 339	
Goodness-of-fit on F^2	1.044	
Final R indices [I>2sigma(I)]	R1 = 0.0335, wR2 = 0.0873	
R indices (all data)	R1 = 0.0519, wR2 = 0.0939	
Largest diff. peak and hole	0.890 and -0.892 e.$Å^{-3}$	

Table A- 6. Crystal data and structure refinement for [Pd^{II}(PS2-CH_2-S2P)]•2CH_2Cl_2.

Identification code	Pd^{II}(PS2-CH_2-S2P).	
Empirical formula	C86 H80 Cl8 P4 Pd2 S8	
Formula weight	1990.26	
Temperature	100(2) K	
Wavelength	0.71073 Å	
Crystal system	Monoclinic	
Space group	C_2/c	
Unit cell dimensions	a = 39.0154(9) Å	a= 90°.
	b = 10.2450(2) Å	b= 98.231(2)°.
	c = 21.4837(4) Å	g= 90°.
Volume	8498.8(3) $Å^3$	
Z	4	
Density (calculated)	1.555 Mg/m^3	
Absorption coefficient	0.992 mm^{-1}	
F(000)	4048	
Crystal size	0.5 x 0.15 x 0.05 mm^3	
Theta range for data collection	3.17 to 31.42 °.	
Index ranges	-56<=h<=53, -14<=k<=14, -31<=l<=30	
Reflections collected	37599	
Independent reflections	12623 [R(int) = 0.0284]	
Completeness to theta = 31.42 °	89.9 %	
Refinement method	Full-matrix least-squares on F^2	
Data / restraints / parameters	12623 / 0 / 452	
Goodness-of-fit on F^2	0.906	
Final R indices [I>2sigma(I)]	R1 = 0.0317, wR2 = 0.0733	
R indices (all data)	R1 = 0.0541, wR2 = 0.0761	
Extinction coefficient	0.00000(2)	
Largest diff. peak and hole	1.269 and -1.026 e.$Å^{-3}$	

Table A- 7. Crystal data and structure refinement for $[Pd^{IV}(PS2')_2]\bullet CH_2Cl_2$.

Identification code	$Pd^{IV}(PS2')_2$	
Empirical formula	C41 H36 Cl2 P2 Pd S4	
Formula weight	896.18	
Temperature	100(2) K	
Wavelength	0.71069 Å	
Crystal system	Monoclinic	
Space group	$p2_1/c$	
Unit cell dimensions	a = 14.681(5) Å	a= 90 °.
	b = 15.094(4) Å	b= 92.270(5) °.
	c = 17.723(5) Å	g = 90 °.
Volume	3924(2) $Å^3$	
Z	4	
Density (calculated)	1.517 Mg/m^3	
Absorption coefficient	0.933 mm^{-1}	
F(000)	1824	
Crystal size	0.25 x 0.35 x 0.04 mm^3	
Theta range for data collection	3.23 to 32.89 °.	
Index ranges	-22<=h<=20, -21<=k<=13, -26<=l<=20	
Reflections collected	29148	
Independent reflections	13160 [R(int) = 0.0684]	
Completeness to theta = 32.89 °	89.6 %	
Refinement method	Full-matrix least-squares on F^2	
Data / restraints / parameters	13160 / 0 / 430	
Goodness-of-fit on F^2	0.836	
Final R indices [I>2sigma(I)]	R1 = 0.0576, wR2 = 0.1348	
R indices (all data)	R1 = 0.1062, wR2 = 0.1472	
Largest diff. peak and hole	1.988 and -2.219 e.$Å^{-3}$	

Table A- 8. Crystal data and structure refinement for *trans-anti*-$[Pt^{II}(PS2'H)_2]\cdot 2CH_2Cl_2$.

Identification code	*trans-anti*-$[Pt^{II}(PS2'H)_2]$	
Empirical formula	C42 H40 Cl4 P2 Pt S4	
Formula weight	1071.81	
Temperature	100(2) K	
Wavelength	0.71073 Å	
Crystal system	Orthorhombic	
Space group	Pbca	
Unit cell dimensions	a = 14.3769(2) Å	α= 90 °.
	b = 15.1969(2) Å	β= 90 °.
	c = 18.7966(3) Å	γ = 90 °.
Volume	4106.76(10) $Å^3$	
Z	4	
Density (calculated)	1.734 Mg/m^3	
Absorption coefficient	3.990 mm^{-1}	
F(000)	2128	
Crystal size	0.25 x 0.2 x 0.05 mm^3	
Theta range for data collection	3.22 to 32.96 °.	
Index ranges	-17<=h<=21, -22<=k<=21, -27<=l<=28	
Reflections collected	37678	
Independent reflections	7245 [R(int) = 0.0232]	
Completeness to theta = 32.96 °	94.0 %	
Refinement method	Full-matrix least-squares on F^2	
Data / restraints / parameters	7245 / 0 / 246	
Goodness-of-fit on F^2	1.024	
Final R indices [I>2sigma(I)]	R1 = 0.0191, wR2 = 0.0497	
R indices (all data)	R1 = 0.0365, wR2 = 0.0511	
Largest diff. peak and hole	0.727 and -0.701 e.$Å^{-3}$	

Table A- 9. Crystal data and structure refinement for *trans-anti*-$[Pt^{II}(PS2'H)_2]$•4$CHCl_3$.

Identification code	*trans-anti*-$[Pt^{II}(PS2'H)_2]$	
Empirical formula	C22 H20 Cl6 P Pt0.50 S2	
Formula weight	689.72	
Temperature	100(2) K	
Wavelength	0.71073 Å	
Crystal system	Triclinic	
Space group	$P\bar{1}$	
Unit cell dimensions	a = 9.2353(4) Å	α= 101.774(4) °.
	b = 11.9200(5) Å	β= 101.062(4) °.
	c = 13.1912(7) Å	γ = 107.236(4) °.
Volume	1307.38(11) $Å^3$	
Z	2	
Density (calculated)	1.752 Mg/m^3	
Absorption coefficient	3.550 mm^{-1}	
F(000)	680	
Crystal size	0.4 x 0.2 x 0.15 mm^3	
Theta range for data collection	3.25 to 29.60 °.	
Index ranges	-11<=h<=11, -16<=k<=16, -17<=l<=18	
Reflections collected	13428	
Independent reflections	6211 [R(int) = 0.0234]	
Completeness to theta = 29.60 °	84.5 %	
Refinement method	Full-matrix least-squares on F^2	
Data / restraints / parameters	6211 / 0 / 292	
Goodness-of-fit on F^2	0.990	
Final R indices [I>2sigma(I)]	R1 = 0.0227, wR2 = 0.0453	
R indices (all data)	R1 = 0.0248, wR2 = 0.0457	
Largest diff. peak and hole	0.787 and -0.658 e.$Å^{-3}$	

Table A- 10. Crystal data and structure refinement for *cis-anti*-[$Pt^{II}(PS2'H)_2$]•$CHCl_3$.

Identification code	*cis-anti*-[$Pt^{II}(PS2'H)_2$]	
Empirical formula	C41 H37 Cl3 P2 Pt S4	
Formula weight	1021.33	
Temperature	100(2) K	
Wavelength	0.71073 Å	
Crystal system	Triclinic	
Space group	P1	
Unit cell dimensions	a = 11.4230(3) Å	a= 76.8410(10) °.
	b = 13.4334(2) Å	b= 75.245(2) °.
	c = 14.7934(2) Å	g = 68.878(2) °.
Volume	2024.34(7) $Å^3$	
Z	2	
Density (calculated)	1.676 Mg/m^3	
Absorption coefficient	3.979 mm^{-1}	
F(000)	1012	
Crystal size	0.3 x 0.15 x 0.06 mm^3	
Theta range for data collection	3.16 to 30.49 °.	
Index ranges	-16<=h<=16, -18<=k<=18, -20<=l<=20	
Reflections collected	32691	
Independent reflections	10865 [R(int) = 0.0251]	
Completeness to theta = 30.49 °	88.1 %	
Refinement method	Full-matrix least-squares on F^2	
Data / restraints / parameters	10865 / 0 / 452	
Goodness-of-fit on F^2	1.009	
Final R indices [I>2sigma(I)]	R1 = 0.0226, wR2 = 0.0509	
R indices (all data)	R1 = 0.0281, wR2 = 0.0516	
Largest diff. peak and hole	1.526 and -1.489 e.$Å^{-3}$	

Table A- 11. Crystal data and structure refinement for *cis-syn*-[$Pt^{II}(PS2'H)_2$]•$CDCl_3$.

Identification code	*cis-syn*-[$Pt^{II}(PS2'H)_2$]	
Empirical formula	C41 H37 Cl3 P2 Pt S4	
Formula weight	1021.33	
Temperature	100(2) K	
Wavelength	0.71073 Å	
Crystal system	Triclinic	
Space group	P1	
Unit cell dimensions	a = 9.6006(3) Å	a= 100.997(3) °.
	b = 12.9302(4) Å	b= 101.740(3) °.
	c = 17.6838(6) Å	g = 108.856(3) °.
Volume	1954.45(11) $Å^3$	
Z	2	
Density (calculated)	1.735 Mg/m^3	
Absorption coefficient	4.122 mm^{-1}	
F(000)	1012	
Crystal size	0.1 x 0.1 x 0.05 mm^3	
Theta range for data collection	3.20 to 29.48 °.	
Index ranges	-13<=h<=13, -16<=k<=17, -23<=l<=21	
Reflections collected	17173	
Independent reflections	9092 [R(int) = 0.0515]	
Completeness to theta = 29.48 °	83.6 %	
Refinement method	Full-matrix least-squares on F^2	
Data / restraints / parameters	9092 / 1 / 435	
Goodness-of-fit on F^2	0.941	
Final R indices [I>2sigma(I)]	R1 = 0.0507, wR2 = 0.0940	
R indices (all data)	R1 = 0.0828, wR2 = 0.0995	
Largest diff. peak and hole	3.118 and -1.691 e.$Å^{-3}$	

Table A- 12. Crystal data and structure refinement for *cis*-[Pt^{II}(PS2'-CH_2-S2'P)]•2CH_2Cl_2.

Identification code	*cis*-[Pt^{II}(PS2-CH_2-S2P)]	
Empirical formula	C43 H40 Cl4 P2 Pt S4	
Formula weight	1083.82	
Temperature	293(2) K	
Wavelength	0.71073 Å	
Crystal system	Triclinic	
Space group	$P\bar{1}$	
Unit cell dimensions	a = 10.2541(3) Å	a= 87.306(2) °.
	b = 10.6811(3) Å	b= 77.159(2) °.
	c = 20.6573(4) Å	g = 74.299(2) °.
Volume	2123.39(10) $Å^3$	
Z	2	
Density (calculated)	1.695 Mg/m^3	
Absorption coefficient	3.860 mm^{-1}	
F(000)	1076	
Crystal size	0.4 x 0.4 x 0.2 mm^3	
Theta range for data collection	3.26 to 32.98 °.	
Index ranges	-15<=h<=15, -16<=k<=16, -31<=l<=31	
Reflections collected	38982	
Independent reflections	14423 [R(int) = 0.0244]	
Completeness to theta = 32.98 °	90.1 %	
Refinement method	Full-matrix least-squares on F^2	
Data / restraints / parameters	14423 / 0 / 474	
Goodness-of-fit on F^2	1.081	
Final R indices [I>2sigma(I)]	R1 = 0.0405, wR2 = 0.0898	
R indices (all data)	R1 = 0.0553, wR2 = 0.0948	
Largest diff. peak and hole	2.814 and -4.445 e.$Å^{-3}$	

Table A- 13. Crystal data and structure refinement for *cis*-[$Pt^{IV}(PS2')_2$]•CH_2Cl_2.

Identification code	*cis*-[$Pt^{IV}(PS2')_2$]	
Empirical formula	C41 H36 Cl2 P2 Pt S4	
Formula weight	984.87	
Temperature	100(2) K	
Wavelength	0.71073 Å	
Crystal system	Monoclinic	
Space group	$P2_1/c$	
Unit cell dimensions	a = 14.76440(10) Å	a= 90 °.
	b = 15.09140(10) Å	b= 92.3350(10) °.
	c = 17.73020(10) Å	g = 90 °.
Volume	3947.28(4) $Å^3$	
Z	4	
Density (calculated)	1.657 Mg/m^3	
Absorption coefficient	4.013 mm^{-1}	
F(000)	1952	
Crystal size	0.4 x 0.2 x 0.05 mm^3	
Theta range for data collection	3.22 to 32.93 °.	
Index ranges	-22<=h<=21, -22<=k<=23, -26<=l<=26	
Reflections collected	59160	
Independent reflections	13876 [R(int) = 0.0248]	
Completeness to theta = 32.93 °	93.7 %	
Refinement method	Full-matrix least-squares on F^2	
Data / restraints / parameters	13876 / 0 / 456	
Goodness-of-fit on F^2	0.958	
Final R indices [I>2sigma(I)]	R1 = 0.0192, wR2 = 0.0423	
R indices (all data)	R1 = 0.0279, wR2 = 0.0432	
Extinction coefficient	0.00000(3)	
Largest diff. peak and hole	2.369 and -1.270 e.$Å^{-3}$	

Table A- 14. Crystal data and structure refinement for *cis*-[$Pt^{IV}(PS2')_2$]•Et_2O.

Identification code	*cis*-[$Pt^{IV}(PS2')_2$]	
Empirical formula	C44 H44 O P2 Pt S4	
Formula weight	974.06	
Temperature	100(2) K	
Wavelength	0.71069 Å	
Crystal system	Monoclinic	
Space group	$P2_1/c$	
Unit cell dimensions	a = 15.000(5) Å	a= 90 °.
	b = 14.915(5) Å	b= 90.900(5) °.
	c = 18.036(5) Å	g = 90 °.
Volume	4035(2) $Å^3$	
Z	4	
Density (calculated)	1.604 Mg/m^3	
Absorption coefficient	3.799 mm^{-1}	
F(000)	1952	
Crystal size	0.2 x 0.1 x 0.1 mm^3	
Theta range for data collection	3.25 to 33.26 °.	
Index ranges	-21<=h<=22, -21<=k<=22, -25<=l<=27	
Reflections collected	24258	
Independent reflections	10949 [R(int) = 0.0532]	
Completeness to theta = 33.26 °	70.5 %	
Refinement method	Full-matrix least-squares on F^2	
Data / restraints / parameters	10949 / 0 / 455	
Goodness-of-fit on F^2	0.919	
Final R indices [I>2sigma(I)]	R1 = 0.0425, wR2 = 0.0905	
R indices (all data)	R1 = 0.0873, wR2 = 0.0971	
Largest diff. peak and hole	2.920 and -1.284 e.$Å^{-3}$	

Table A- 15. Crystal data and structure refinement for $[(Pentyl)_4N][Fe^{II}Fe^{III}(PS3)_2]$.

Identification code	$[(Pentyl)_4N][Fe^{II}Fe^{III}(PS3)_2]$	
Empirical formula	C56 H68 Fe2 N P2 S6	
Formula weight	1121.11	
Temperature	293(2) K	
Wavelength	0.71073 Å	
Crystal system	Monoclinic	
Space group	$P2_1/n$	
Unit cell dimensions	a = 16.338(4) Å	a= 90 °.
	b = 18.464(10) Å	b= 90.487(17) °.
	c = 18.828(3) Å	g = 90 °.
Volume	5679(4) $Å^3$	
Z	4	
Density (calculated)	1.311 Mg/m^3	
Absorption coefficient	0.824 mm^{-1}	
F(000)	2356	
Crystal size	0.4 x 0.25 x 0.1 mm^3	
Theta range for data collection	2.94 to 32.91 °.	
Index ranges	-14<=h<=24, -21<=k<=21, -25<=l<=26	
Reflections collected	20757	
Independent reflections	11862 [R(int) = 0.4692]	
Completeness to theta = 32.91 °	55.9 %	
Refinement method	Full-matrix least-squares on F^2	
Data / restraints / parameters	11862 / 0 / 320	
Goodness-of-fit on F^2	0.586	
Final R indices [I>2sigma(I)]	R1 = 0.1509, wR2 = 0.3245	
R indices (all data)	R1 = 0.5515, wR2 = 0.4983	
Extinction coefficient	0.0000(5)	
Largest diff. peak and hole	0.749 and -1.020 e.$Å^{-3}$	

Table A- 16. Crystal data and structure refinement for $[Et_4N][Fe^{II}(PS3)(CO)_2]$.

Identification code	$[Et_4N][Fe(II)(PS3)(CO)_2]$	
Empirical formula	C28 H32 Fe N O2 P S3	
Formula weight	597.55	
Temperature	100(2) K	
Wavelength	0.71073 Å	
Crystal system	Monoclinic	
Space group	Cc	
Unit cell dimensions	a = 9.8191(3) Å	a= 90 °.
	b = 19.9044(11) Å	b= 101.537(3) °.
	c = 14.3261(4) Å	g = 90 °.
Volume	2743.39(19) $Å^3$	
Z	4	
Density (calculated)	1.447 Mg/m^3	
Absorption coefficient	0.864 mm^{-1}	
F(000)	1248	
Crystal size	0.6 x0.1 x0.03 mm^3	
Theta range for data collection	2.98 to 31.99 °.	
Index ranges	-9<=h<=14, -17<=k<=28, -21<=l<=17	
Reflections collected	9160	
Independent reflections	5884 [R(int) = 0.0328]	
Completeness to theta = 31.99 °	88.1 %	
Refinement method	Full-matrix least-squares on F^2	
Data / restraints / parameters	5884 / 383 / 403	
Goodness-of-fit on F^2	0.918	
Final R indices [I>2sigma(I)]	R1 = 0.0405, wR2 = 0.0948	
R indices (all data)	R1 = 0.0549, wR2 = 0.1005	
Absolute structure parameter	0.015(16)	
Largest diff. peak and hole	0.860 and -0.748 e.$Å^{-3}$	

Table A- 17. Crystal data and structure refinement for [(n-Pr)$_4$N]$_2$[Fe^{II}Fe^{III}(O=PS3)$_2$]•1/2MeOH.

Identification code	[(n-Pr)$_4$N]$_2$[Fe(II)Fe(III)(O=PS3)$_2$]	
Empirical formula	C30.50 H41 Fe N O P S3	
Formula weight	620.64	
Temperature	100(2) K	
Wavelength	0.71073 Å	
Crystal system	Tetragonal	
Space group	P4$_2$/n	
Unit cell dimensions	a = 22.7909(3) Å	a= 90 °.
	b = 22.7909(3) Å	b= 90 °.
	c = 11.6984(3) Å	g = 90 °.
Volume	6076.44(19) Å^3	
Z	8	
Density (calculated)	1.357 Mg/m^3	
Absorption coefficient	0.780 mm^{-1}	
F(000)	2624	
Crystal size	0.1 x 0.1x 0.2 mm^3	
Theta range for data collection	2.83 to 29.61 °.	
Index ranges	-29<=h<=31, -31<=k<=31, -15<=l<=15	
Reflections collected	95544	
Independent reflections	8223 [R(int) = 0.1288]	
Completeness to theta = 29.61 °	96.0 %	
Refinement method	Full-matrix least-squares on F^2	
Data / restraints / parameters	8223 / 0 / 344	
Goodness-of-fit on F^2	0.903	
Final R indices [I>2sigma(I)]	R1 = 0.0461, wR2 = 0.0907	
R indices (all data)	R1 = 0.1084, wR2 = 0.0979	
Largest diff. peak and hole	0.507 and -0.477 e.Å^{-3}	

Table A- 18. Crystal data and structure refinement for $[(Pentyl)_4N][Fe^{II}Fe^{III}(PS3)(PS3O_2)]$.

Identification code	$[(Pentyl)_4N][Fe(II)Fe(III)(PS3)(PS3O_2)]$	
Empirical formula	C56 H68 Fe2 N O3 P2 S6	
Formula weight	1169.11	
Temperature	100(2) K	
Wavelength	0.71073 Å	
Crystal system	Monoclinic	
Space group	$P2_1/n$	
Unit cell dimensions	a = 16.4855(5) Å	a= 90 °.
	b = 18.8099(5) Å	b= 92.191(3) °.
	c = 18.5607(6) Å	g = 90 °.
Volume	5751.3(3) $Å^3$	
Z	4	
Density (calculated)	1.350 Mg/m^3	
Absorption coefficient	0.820 mm^{-1}	
F(000)	2452	
Crystal size	0.4 x 0.4 x 0.1 mm^3	
Theta range for data collection	2.88 to 32.98 °.	
Index ranges	-25<=h<=21, -28<=k<=25, -28<=l<=26	
Reflections collected	35521	
Independent reflections	17525 [R(int) = 0.0908]	
Completeness to theta = 32.98 °	80.9 %	
Refinement method	Full-matrix least-squares on F^2	
Data / restraints / parameters	17525 / 0 / 622	
Goodness-of-fit on F^2	0.951	
Final R indices [I>2sigma(I)]	R1 = 0.1314, wR2 = 0.2269	
R indices (all data)	R1 = 0.3027, wR2 = 0.2843	
Extinction coefficient	0.0000(3)	
Largest diff. peak and hole	0.886 and -0.526 $e.Å^{-3}$	